Analyse and modelling of nitrous oxide emissions from full-scale tertiary nitrifying biological aerated filters

Justine Fiat

Université Fédérale
Toulouse Midi-Pyrénées

THÈSE

En vue de l'obtention du

DOCTORAT DE L'UNIVERSITÉ DE TOULOUSE

Délivré par l'Institut National des Sciences Appliquées de Toulouse

---

Présentée et soutenue par

Justine FIAT

Le 29 mai 2019

Analyse et modélisation des émissions de protoxyde d'azote par les biofiltres nitrifiants tertiaires à échelle industrielle

---

Ecole doctorale : **MEGEP - Mécanique, Energétique, Génie civil, Procédés**

Spécialité : **Génie des Procédés et de l'Environnement**

Unité de recherche :
LISBP - Laboratoire d'Ingénierie des Systèmes Biologiques et des Procédés

Thèse dirigée par
Mathieu SPERANDIO et Sylvie GILLOT

Jury

M. Peter VANROLLEGHEM, Rapporteur
Mme Anna MIKOLA, Rapporteure
M. Kim SORENSEN, Examinateur
M. Julio PEREZ, Examinateur
M. Vincent ROCHER, Examinateur
Mme Ahlem FILALI, Examinatrice
M. Mathieu SPERANDIO, Co-directeur de thèse
Mme Sylvie GILLOT, Co-directrice de thèse

REMERCIEMENTS

La thèse s'est déroulée à Irstea, au sein de l'unité HBAN, dans le cadre du projet ANR N_2Otrack et du programme de recherche Mocopée. Je suis reconnaissante envers Nathalie Touze, directrice d'unité, pour m'avoir accueillie dans cette structure. Ces travaux ont vu le jour grâce à la présence de nombreuses personnes que je souhaite remercier ici.

Ma gratitude va avant tout à mes encadrants, sans qui ces travaux n'auraient jamais pu aboutir. Je suis très fière d'avoir été la première doctorante encadrée par Ahlem. Sa rigueur et sa passion pour la recherche auront été parfois terrifiantes, mais surtout très formatrices, et j'espère qu'elle a apprécié ces années à travailler ensemble autant que moi. Je remercie chaleureusement mes directeurs de thèse, Sylvie et Mathieu, pour leur confiance infaillible. J'ai souvent eu la sensation de ne pas en faire assez, mais leurs conseils et leur intérêt pour mes travaux m'ont toujours redonné confiance. A eux trois, ils m'ont permis de grandir professionnellement et personnellement, et j'espère sincèrement avoir l'occasion de collaborer avec eux dans des projets futurs.

Je tiens à remercier Anna Mikola et Peter Vanrolleghem d'avoir rapporté mes travaux, et les membres du jury, Kim Sorensen, Julio Perez et Vincent Rocher, pour la plupart venus de loin. Merci également à Diego Rosso, d'avoir pris le temps d'assister à ma soutenance pendant son été sabbatique. Je leur suis reconnaissante pour la pertinence de leurs questions, mais surtout pour leur bienveillance, qui me laissera un souvenir très positif de cette journée.

Je remercie les partenaires du projet et les membres du comité de pilotage. Un grand merci à Jean Bernier qui m'a formé à l'utilisation du modèle SimBio pendant plusieurs semaines et s'est toujours rendu disponible pour répondre à mes questions. Merci également aux autres membres du SIAAP, Sabrina Guérin, Sam Azimi et Rémi Coclès, qui ont contribué à ce travail, notamment en me fournissant les données d'exploitation indispensables à mon travail de modélisation. Merci à l'équipe Symbiose de l'INSA Toulouse pour son accueil pendant mon séjour toulousain, et pour son aide lors de la mise en place du réacteur. Une petite pensée pour Longqi Lang, qui m'a plusieurs fois sauvé la mise pendant ces manips et m'a fait découvrir un des meilleurs restaurants de la ville ! Merci à Mathieu Sébilo et Anniet Laverman pour leur collaboration sur ces expériences, et à Guillaume Humbert pour sa patience pendant ses maintes explications sur l'isotopie. Je n'oublie bien sûr pas Eveline Volcke, qui s'est jointe au comité de pilotage et a formulé des critiques très constructives sur mes travaux.

L'ambiance atypique qui règne dans l'équipe EPURE a rendu ces trois années très agréables, merci à eux pour leur bonne humeur au quotidien, les jeux de société et les soirées arrosées. Merci à Anne pour les conseils prodigués dans son bureau, les souvenirs de Bretagne et la rencontre avec le dieu Georges – élément indispensable au bon déroulement de toute thèse.

Merci à Elodie, mon ex-collègue du bureau de la « joie », pour les chocolats chauds et les conversations existentielles à n'en plus finir. Merci à Timo pour sa gentillesse et les pep-talks pendant les coups de mou, je lui souhaite de s'épanouir pendant sa thèse. Merci à Pierre, pour sa bonne humeur constante, les dégustations de chocolat et pour s'être rappelé de mon prénom rapidement, malgré le fait que j'ai passé 99% du temps devant un PC. Merci à Yannick pour sa jovialité et son implication plus que salvatrice dans la rédaction de l'article sur le transfert. Merci à Sylvain pour les blagues au quotidien, les vidéos pas toujours drôles et pour m'avoir adoptée en tant que membre de l'équipe malgré ma non-participation au frisbee ! Merci à Jean-Jacques pour tous ses conseils pendant la thèse. Merci aux stagiaires qui ont partagé le bureau, les jeux du midi et mon indignation face à la saison finale de Game of Thrones. Je pense aussi aux ex-collègues, David Delage et Sylvain Descloux, qui ont été de géniaux pet-sitters et partenaires de jeux de sociétés.

Merci également aux équipes supports d'Irstea, qui m'ont permis de partir en congrès en toute sérénité, de participer à des formations enrichissantes, et surtout d'obtenir une licence Simulink (dédicace spéciale à Roger) ! Plus généralement, merci à tous les collègues d'Irstea, je leur souhaite une très belle continuation au sein du futur INRAE.

Pour finir, je tiens à remercier mes proches, qui m'ont souvent fait l'effet d'une bouffée d'air frais. Merci à Brice, Savina, Aymeric, Katia et Margot pour les soirées, les vacances et la décompression plus qu'indispensable. Je remercie une fois de plus mon compagnon, Guillaume, pour avoir supporté mes plaintes et mes doutes, et partagé mes joies pendant ces trois ans de montagnes russes. Merci à ma famille d'avoir cru en moi, d'avoir été toujours répondu présente en cas de besoin.

Encore merci à tous et bonne lecture !

LIST OF PUBLICATIONS AND PROCEEDINGS

PEER-REVIEWED PUBLICATIONS

Considering the plug-flow behaviour of the gas phase in nitrifying BAF models significantly improves the prediction of N_2O emissions. Fiat Justine, Filali Ahlem, Fayolle Yannick, Bernier Jean, Rocher Vincent, Spérandio Mathieu, Gillot Sylvie. *In Water Research 156 (337-346).*

Isotopic evidence for alteration of nitrous oxide emissions and producing pathways contribution under nitrifying conditions. Humbert Guillaume, Sébilo Mathieu, Fiat Justine, Lang Longqi, Filali Ahlem, Vaury Véronique, Spérandio Mathieu, and Laverman Anniet. *In Biogeosciences (under review).*

CONFERENCE PROCEEDINGS

Modelling N_2O emissions in a tertiary nitrifying biofilter. Palermo, Italy, May 21st – 24th 2017. *Poster presentation.* Fiat Justine, Filali Ahlem, Gillot Sylvie, Spérandio Mathieu. *Frontiers International Conference on Wastewater Treatment.*

Modélisation des émissions de N_2O lors du traitement de l'azote par biofiltration : cas de la nitrification tertiaire. Colombes, France, November 21st 2017. *Oral communication.* Fiat Justine, Filali Ahlem, Fayolle Yannick, Bernier Jean, Rocher Vincent, Spérandio Mathieu, Gillot Sylvie. *Séminaire annuel Mocopée.*

Modelling N_2O emissions from a full-scale nitrifying BAF: impact of gas-liquid transfer hypotheses. Lac Beauport, Québec, March 10th – 14th 2018. *Poster.* Fiat Justine, Filali Ahlem, Fayolle Yannick, Bernier Jean, Rocher Vincent, Spérandio Mathieu, Gillot Sylvie. *6th IWA/WEF Water Resource Recovery Modelling Seminar.*

Modélisation des émissions de protoxyde d'azote par les biofiltres nitrifiants. Poitiers, France, October 9th – 11th 2018. *Oral communication.* Fiat Justine, Filali Ahlem, Gillot Sylvie, Bernier Jean, Rocher Vincent, Spérandio Mathieu. *23ème édition des Journées Information Eaux.*

TABLE OF CONTENTS

LIST OF FIGURES

LIST OF TABLES

Chapter I. Introduction

I.1 CONTEXT

Since the United Nations Framework Convention on Climate Change (UNFCCC) and the Kyoto protocol of 1997, numerous actions have been undertaken by public authorities and corporations to reduce their greenhouse gas (GHG) emissions and limit global warming. In France, Law 2015-992 of August 17, 2015, relative to the "Energy transition for green growth", targets a national reduction of the energy consumption by 50% in 2050 compared to 2012, and a 75% reduction of GHG emissions compared to 1990 levels. More recently, during the Conference of the parties (COP21) and the Paris Agreement on Climate of 2015, a common objective has been fixed to limit global warming beneath 2°C compared to pre-industrial era levels and to pursue efforts to limit it to 1.5°C by the end of the century.

The wastewater management sector is one of the sources of anthropogenic greenhouse gas emissions. Carbon dioxide (CO_2)[1], methane (CH_4) and nitrous oxide (N_2O) are all emitted during the treatment of wastewater. It also leads to indirect CO_2 emissions related to the plant's energy consumption; the dosing of fossil fuel derived chemicals and the treatment / transport of by-products of wastewater treatment. Although GHG emissions from municipal wastewater management represent less than 1% of the national emissions, the current actions involve every sector, whatever their emission volumes (ADEME, 2013). Indeed, since Law 2010-788 of July 12, 2010, known as "Grenelle II", French territorial municipalities of 50 000 inhabitants or more have to quantify their GHG emissions and to establish an action plan to reduce their emissions.

The main undertaken measures in wastewater resource recovery facilities (WRRFs) involved process optimization to reduce energy expanses or the consumption of reagents. Beyond the reduction of the plants' carbon footprint, these measures targeted a reduction of operational costs. Recent research progress highlighted the importance of considering the direct emissions of nitrous oxide (N_2O) during biological water treatment. N_2O is a potent

[1] In WRRFs, direct carbon dioxide emissions originate from the microbial respiration of organic matter. They are generally considered as biogenic, i.e. belonging to the short carbon cycle and thus not contributing to increased concentrations of CO_2 in the atmosphere. However, it was demonstrated that a substantial part of organic carbon in wastewater is of fossil origin GRIFFITH, D. R., BARNES, R. T. & RAYMOND, P. A. 2009. Inputs of Fossil Carbon from Wastewater Treatment Plants to U.S. Rivers and Oceans. *Environmental Science & Technology,* 43**,** 5647-5651..

GHG with a global warming potential that is 265 times higher than CO_2 on a 100-year horizon (IPCC, 2013). Since the Montreal Protocol (1987) which regulated the use of ozone-depleting substances, N_2O has become the primary ozone-depleting substance and should remain so throughout the 21st century (Ravishankara et al., 2009). In WRRFs, N_2O is mainly produced and released from bioreactors during nitrification and denitrification processes. Because of its high global warming potential, N_2O emissions can contribute significantly to the climate footprint of a WRRF and can even overcome the indirect CO_2 emissions (Daelman et al., 2013, Bollon et al., 2016b, Kosonen et al., 2016). Likewise, it was recently demonstrated that energy consumption should be put in perspective with GHG emissions when evaluating control/operational strategies in WRRFs (Flores-Alsina et al., 2014).

The current method to quantify N_2O emissions from WRRFs is based on the use of a fixed emission factor (EF) of 0.0032 kgN_2O/person/year (Eyring et al., 2007), corresponding to 0.035% of the nitrogen load for developed countries (Kampschreur et al., 2009). As a number of studies pointed out, this accounting approach lacks accuracy because it does not take into account the high temporal variability of emissions. Moreover, it was found to substantially underestimate the contribution of sewage management to the total anthropogenic N_2O emissions, currently estimated at 3.5% (IPCC, 2014). An alternative tool is therefore needed to quantify the contribution of N_2O emissions to the CO_2 balance of WRRFs, which requires understanding the triggers of N_2O emissions from full-scale WRRFs.

Over the past years, considerable efforts have been made in that sense. It has been shown that N_2O is an end-product of nitrification and an intermediate of denitrification, but the paths for N_2O production are numerous and impacted by many operating conditions, which complicate the identification of mitigation strategies. This led to the development of several mechanistic models (Ni and Yuan, 2015, Massara et al., 2017a). These have been mainly applied to conventional activated sludge plants and rarely to biofilm processes.

Among all biofilm reactors, biological aerated (or active) filters (BAF) are the main technologies applied in France. According to the French Ministry of Ecology's database of 2016, 20% of the national load is treated by BAFs. This figure goes up to 60% in the Parisian area, most of this load being treated in a single WRRF: Seine Aval (1 700 000 m^3/d, 5.5 million PE). At the outset of the study, Seine Aval included two BAF stages aiming at nitrifying an effluent from a high loaded activated sludge system and then at denitrifying the nitrate-enriched water using methanol as an external carbon source. Monitoring campaigns performed on site indicated that nitrification was the main source of N_2O, while denitrification could reduce a large proportion of residual N_2O (Bollon et al., 2016a, Bollon et al., 2016b). It also reported high emission factor values compared to French low loaded CAS

plants: a ratio of 10 to 200 times the CAS values was observed (Filali et al., 2017). There are therefore high stakes in better characterizing N_2O production from nitrifying BAFs.

I.2 SCOPE AND OBJECTIVES OF THE THESIS

This thesis focuses on the analysis of N_2O emissions from tertiary nitrifying BAFs. The final scientific objective is to contribute to a better understanding of the triggers of N_2O production pathways and emissions in such processes.

The first approach adopted consisted in analysing the full-scale production of N_2O along with dynamic changes of operating conditions through the development of a dynamic model, based on data from the Seine Aval WRRF. The second approach adopted consisted in lab-scale analysis of N_2O emissions and production pathways under controlled conditions. From an operational perspective, the objectives were: 1) to develop and calibrate a model able of describing N_2O emission dynamics from the tertiary nitrifying BAFs of Seine Aval WRRF along with operating conditions, 2) to propose an alternative methodology to quantify N_2O emission factors based on few operating conditions typically monitored on WRRFs and 3) to identify mitigation strategies in order to reduce N_2O emissions from the tertiary nitrifying BAFs of the Seine Aval WRRF.

The presented work was carried out within the framework of the "N_2OTrack" project[2] (2015-2019) that aims at quantifying, modelling and mitigating N_2O emissions from French WRRFs, with a focus on biofilm reactors. It is funded by the French Research Agency and brings together several academic and operational partners. The thesis mostly contributed to the work package dedicated to the development of dynamic models and confrontation to full-scale data (WP3). It is also part of the research program "Mocopée[3]" which aims at improving operation and maintenance practices of WRRFs, notably through the development of innovative metrological tools and models.

[2] http://n2otrack.insa-toulouse.fr/

[3] http://www.mocopee.com/

I.3 STRUCTURE OF THE MANUSCRIPT

The document is structured in eight chapters, including this introduction. Their outlines and main objectives are presented thereafter.

Chapter II - State of the art

This chapter is dedicated to a literature review. It provides an overview of the main N_2O production mechanisms during nitrification and denitrification processes, and the associated models that have been proposed. Biofilm systems are presented in terms of models and N_2O production and a focus is made on the specific biofilm reactor type studied in this project. Finally, this chapter presents the selected BAF and biokinetic models chosen in this thesis.

Chapter III - Material and methods

This chapter presents the experimental and modelling material and methods of the thesis. In a first part, full-scale datasets from the Seine Aval WRRF are presented and associated to the modelling objectives. In a second part, the base tertiary nitrifying BAF model is presented, along with the successive extensions made to include N_2O production pathways. In a last part, the lab-scale experimental set-up, tested operating conditions and analysis methods are presented, preceded by a brief description of the Seine Centre WRRF, on which colonized materials were collected.

Chapter IV - Considering the plug-flow behaviour of the gas phase in nitrifying BAF models significantly improves the prediction of N_2O emissions

This chapter aims at extending the gas/liquid transfer representation of the BAF model, to better describe N_2O emissions. It presents the initial predictions of the tertiary nitrifying BAF model after including biological N_2O production pathways. It defines the step-by-step modifications of the gas/liquid transfer representation and their impacts on the prediction of nitrification performances and N_2O fluxes. Results are discussed along with the comprehension of oxygen transfer in full-scale colonized fixed-bed reactors.

Chapter V - Predicting N_2O emissions from a full-scale tertiary nitrifying BAF: model calibration

In this chapter the extended model is calibrated based on the prediction of long-term nitrification performances from the Seine Aval WRRF, and the prediction of N_2O fluxes measured at two periods on a given nitrifying BAF. A preliminary sensitivity analysis is

performed, to assess the impact of model parameters on N_2O production and identify the main parameters to calibrate. The large differences in terms of N_2O fluxes observed over the two periods is discussed based on simulations.

Chapter VI - Model-based evaluation of long-term N_2O emissions in a nitrifying BAF

This chapter is meant to answer the operational objectives of the thesis. The calibrated model is used to investigate N_2O production and emissions from the Seine Aval WRRF over two years: quantification of the emission factor and evaluation of the dynamics of N_2O production and emission rates along with operating conditions. A simplified model is finally proposed, to predict the daily emission factor from tertiary nitrifying BAFs of the Seine Aval WRRF, and mitigation strategies are discussed.

Chapter VII - N_2O emissions from a nitrifying BAF: a lab-scale study

This chapter aims at identifying the single impact of the main operating conditions – identified in chapter VI– on N_2O emissions and production pathways. The experiments are performed on a lab-scale reactor filled with colonized Biostyrene® removed from Seine Centre nitrifying BAFs. This is a collaborative work between most of the N_2OTrack partners. The iEES-Paris and Ecobio performed isotopic analyses to estimate the respective contributions of N_2O production pathways (WP2 of N_2OTrack). These results are mentioned, but not presented in details, as they will be included in a research paper in preparation. Pilot-scale results are discussed along with model results from full-scale nitrifying BAFs.

Chapter VIII - Conclusion and perspectives

This chapter aims at summarizing the main results and advancements made in this thesis. A number of perspectives are suggested in terms of experimental work to further validate some of the present results and to go deeper in the understanding of N_2O production at the micro-scale. Suggestions are made in terms of modelling work to extrapolate the present results to other plants operating nitrifying BAFs.

Chapter II. State of the art

RÉSUMÉ

Ces deux dernières décennies, plusieurs études ont été dédiées à l'étude des émissions de protoxyde d'azote (N_2O, puissant gaz à effet de serre et destructeur de la couche d'ozone) lors du traitement biologique des eaux usées en station d'épuration. Il s'agit d'un sous-produit de la nitrification et un intermédiaire réactionnel de la dénitrification hétérotrophe. Lors de la nitrification, il a été observé que les conditions de faibles concentrations en oxygène dissous couplées à la présence de nitrite favorisent la génération et l'émission du N_2O. Tandis que la dénitrification hétérotrophe a principalement été démontrée comme jouant un rôle clé dans la réduction de N_2O, elle peut dans certaines conditions en produire d'importantes proportions.

Ces observations ont conduit au développement de nombreux modèles mécanistes, du plus simple considérant une seule voie de production de N_2O, aux plus complexes couplant plusieurs voies par les micro-organismes autotrophes et hétérotrophes. En effet, les bactéries autotrophes et hétérotrophes coexistent généralement dans les procédés de traitement biologique et contribuent à la production nette de N_2O dans des proportions variables. Une difficulté réside dans l'identification des paramètres de tels modèles car la nitrification et la dénitrification partagent un certain nombre d'intermédiaires réactionnels. Actuellement, le modèle développé par le LISBP (Pocquet et al., 2016) et le modèle ASMN (Hiatt and Grady, 2008) sont les modèles les plus propices pour décrire respectivement la production de N_2O lors des processus de nitrification et dénitrification.

La plupart des études ont été dédiées aux systèmes à biomasse en suspension, et très peu aux procédés basés sur le développement de biofilms, pourtant de plus en plus populaires pour leur efficacité de traitement et leur compacité. En France, c'est le procédé de biofiltration qui est le plus répandu, particulièrement dans les grandes agglomérations. La station d'épuration de Seine Aval (Achères) admet environ 40% de la charge parisienne et traite la pollution azotée par deux étages de biofiltration. De récentes campagnes de mesures réalisées sur cette station ont rapporté des facteurs d'émission bien supérieurs à ceux mesurés sur les procédés conventionnels de boues activées. Ces mesures révèlent que l'étage de nitrification est la principale source de production et d'émission de N_2O. Elles soulignent également la forte variabilité temporelle et saisonnière des émissions, en lien avec les conditions environnementales et opératoires appliquées.

Le développement de modèles dynamiques constitue une perspective essentielle pour comprendre les mécanismes de production de N_2O, affiner l'estimation de ses émissions et proposer des voies de réduction. A ce jour, peu de modèles de biofiltration ont été

développés et encore moins dans le cas de la nitrification tertiaire (Bernier et al. 2014; Vigne et al. 2010; Viotti et al. 2002). Cela s'explique probablement par la multitude et la complexité des mécanismes à représenter pour simuler leur fonctionnement. Le modèle proposé par Bernier et al. (2014), qui décrit le fonctionnement des unités de biofiltration en nitrification tertiaire de la station Seine Aval, compte parmi les modèles les plus complets et c'est également le seul à avoir été calé et validé sur des données long-terme à échelle réelle. Cependant, il ne permet pas la description des émissions de N_2O et de leur impact sur l'empreinte environnementale des installations.

Dans ce travail, les voies de production de N_2O -lors des processus de nitrification et dénitrification- ont été intégrées au modèle de biofiltration en nitrifiante tertiaire de la station de Seine Aval. L'objectif final étant que cet outil permette, à terme, d'orienter les choix et modes d'exploitation des biofiltres sur des critères environnementaux incluant l'impact climatique. Les paramètres du modèle ont été calés sur les données de campagnes de mesure réalisées sur site. De plus, des expériences laboratoires -en conditions contrôlées- ont été entreprises pour déterminer la contribution respective des différentes voies de production de N_2O et discuter des résultats au regard du ceux du modèle. Enfin, sur la base des résultats de simulation, un modèle statistique a été proposé comme outil de quantification des émissions à partir d'un nombre réduit de paramètres opératoires.

II.1 N_2O EMISSIONS FROM WRRFS

II.1.1 N_2O PRODUCTION PATHWAYS

The earliest and still the most applied biological process for nitrogen removal from wastewater is the coupled nitrification-denitrification, as presented in Figure II.1-1. Nitrification is usually viewed as two successive steps, both requiring oxygen as the terminal electron acceptor. Nitritation is the oxidation of ammonia (NH_3) to nitrite (NO_2^-), performed by ammonia oxidizing bacteria (AOB) and/or archaea (AOA), while nitratation is the oxidation of NO_2^- to nitrate (NO_3^-) by nitrite oxidizing bacteria (NOB). Heterotrophic denitrification is the anoxic reduction of NO_3^- to dinitrogen (N_2) by ordinary heterotrophic organisms (OHO) requiring organic carbon as electron donor.

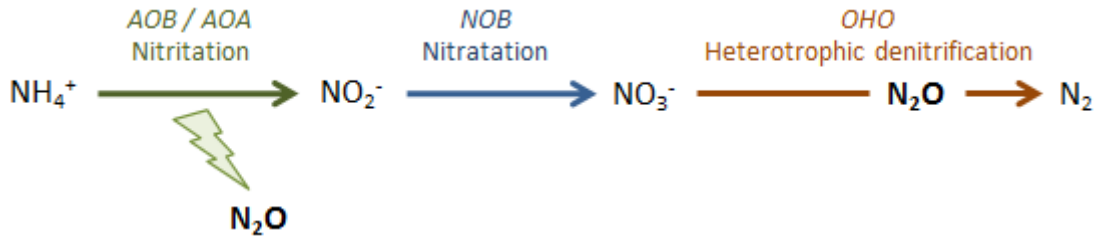

Figure II.1-1. Simplified representation of nitrification-denitrification processes.

Depending on process operating conditions, high or low amounts of N_2O can be produced during nitrogen removal, as an intermediate product in the heterotrophic denitrification chain, and a by-product of nitrification (Kampschreur et al., 2009, Chandran et al., 2011, Law et al., 2012b). Biological and abiotic reactions leading to N_2O formation in natural and engineered microbial communities are many, as described by Duan et al. (2017) and Schreiber et al. (2012).

However, in WRRFs, N_2O is believed to be mainly produced *via* three biological pathways (Ni and Yuan, 2015, Massara et al., 2017a): during the incomplete oxidation of hydroxylamine (NH_2OH) by AOB (called nitrifier nitrification, or "NN"), through the reduction of nitrite (NO_2^-) by AOB (called nitrifier denitrification, or "ND"), and during heterotrophic denitrification (called "HD"). Recently, it was demonstrated that abiotic reactions can also form N_2O (Harper et al., 2015, Soler-Jofra et al., 2016). The possible chemical reactions to produce nitrogen oxides are numerous and with a rather complex chemistry (Soler-Jofra et al., 2016). However, these were shown in conditions of high concentrations of NH_2OH and/or NO_2^- concentrations corresponding to those of partial nitrification processes. Since these conditions are not encountered in the studied BAF, they will not be discussed hereinafter.

II.1.1.1 DURING NITRIFICATION

Complete nitrification and its two sequential processes (nitritation and nitratation), are described by equations Eq.1, Eq.2 and Eq.3, respectively.

Eq.1 $$NH_3 + 2O_2 \rightarrow NO_3^- + H_2O + H^+$$

Eq.2 $$NH_3 + 1.5O_2 \rightarrow NO_2^- + H_2O + H^+$$

Eq.3 $$NO_2^- + 0.5O_2 \rightarrow NO_3^-$$

Nitratation by NOB catalysed by nitrite oxidoreductase (NXR) has not been reported to be involved in N_2O production (Colliver and Stephenson, 2000). Furthermore, Shiskowski et al. (2004) found that OHO did not generate, or very little, N_2O under aerobic conditions, making AOB and AOA the only source of N_2O during nitrification. In fact, nitritation involves several reaction intermediates, which are precursors to N_2O production. These are presented on Figure II.1-2, along with the main associated N_2O production pathways.

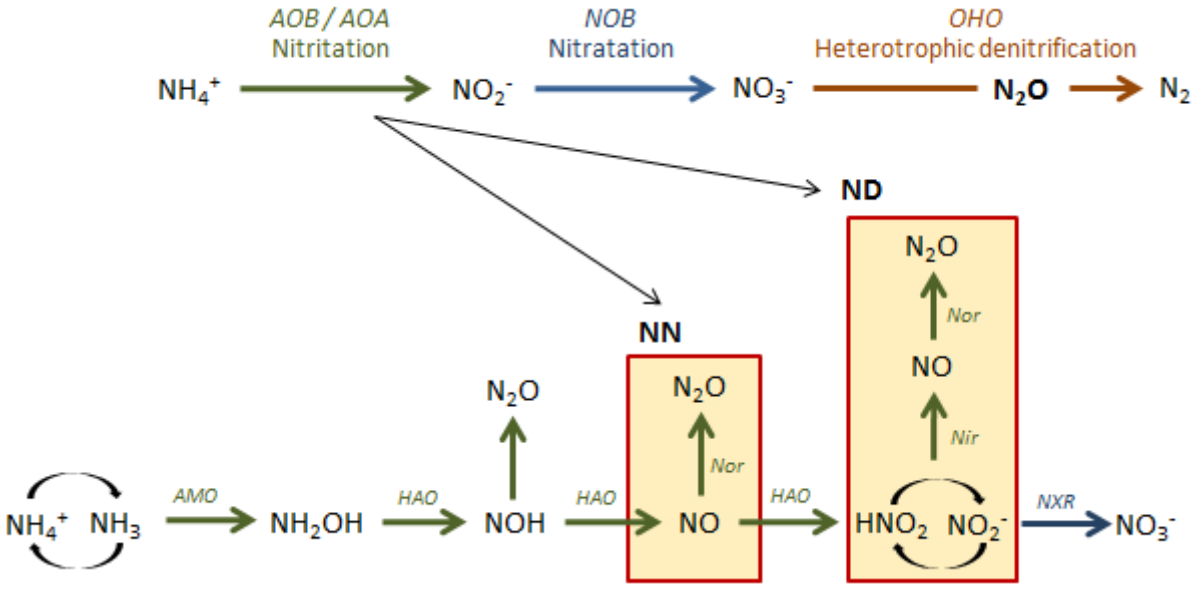

Figure II.1-2. Biological N_2O pathways related to nitrification. Acronyms AMO, HAO, NXR, Nir and Nor stand for the enzymes ammonium monooxygenase, hydroxylamine oxidoreductase, nitrite oxidoreductase, nitrite reductase, and NO reductase.

Hydroxylamine (NH_2OH) is a well-known intermediate produced by ammonia oxidation (Eq.4); mediated by the enzyme ammonia monooxygenase (AMO) using NH_3 rather than NH_4^+ as substrate (Suzuki et al., 1974). NH_2OH is further oxidized to nitroxyl (NOH) by the enzyme hydroxylamine oxidoreductase (HAO), releasing two electrons (Eq.5). NOH is converted to nitric oxide -NO (Eq.6), releasing one electron, further converted to NO_2^- (Eq.7),

releasing another electron (Poughon et al., 2001). In total, NH_2OH oxidation to NO_2^- releases two pairs of electrons, the first one being used by AOB to oxidize NH_3 (Eq.4), and the remaining two being supplied for energy production.

Eq.4 $$NH_3 + O_2 + 2e^- + 2H^+ \rightarrow NH_2OH + H_2O$$

Eq.5 $$NH_2OH \rightarrow NOH + 2e^- + 2H^+$$

Eq.6 $$NOH \rightarrow NO + e^- + H^+$$

Eq.7 $$NO + H_2O \rightarrow NO_2^- + e^- + 2H^+$$

N_2O can be a by-product of NH_2OH oxidation, either *via* the biological reduction of NO (Eq.8) through nitric oxide reductase (Nor), referred as the "NN" pathway, or *via* the non-enzymatic disintegration of NOH (Eq.9), also named chemical breakdown.

Eq.8 $$2NO + 2e^- + 2H^+ \rightarrow N_2O + H_2O$$

Eq.9 $$2NOH \rightarrow N_2O + H_2O$$

The second biological N_2O production pathway related to nitrification, referred as the "ND" pathway, occurs when AOB use nitrite as electron acceptor instead of oxygen. Nitrite is reduced to NO by the enzyme Nir, and further to N_2O by the enzyme Nor. Beaumont et al. (2002) showed that Nir was expressed by AOB to counteract the toxic effect of nitrite on AOB cells. In fact, AOB use free nitrous acid (HNO_2) as the true substrate, which is at equilibrium with NO_2^- (Eq.10) (Shiskowski and Mavinic, 2006). In modelling studies, several authors considered NH_2OH to be the electron donor during ND, but hydrogen, pyruvate and ammonia have also been reported to be electron donors under anoxic conditions (Bock et al., 1995). Equations Eq.11 and Eq.12 represent the reduction of HNO_2 to NO and NO to N_2O, respectively.

Eq.10 $$HNO_2 \rightarrow NO_2^- + H^+$$

Eq.11 $$HNO_2 + e^- + H^+ \rightarrow NO + H_2O$$

Eq.12 $$NO + e^- + H^+ \rightarrow 0.5N_2O + 0.5H_2O$$

II.1.1.2 DURING HETEROTROPHIC DENITRIFICATION

Heterotrophic denitrification is the reduction of NO_3^- to N_2 by various groups of heterotrophs, using nitrogen oxides as electron acceptors and organic matter as both carbon source and electron donor (Ahn, 2006). It is a 4-step process (Figure II.1-3): reduction of NO_3^- to NO_2^- by nitrate reductase (Nar), reduction of NO_2^- to NO by nitrite reductase (Nir), reduction of NO to N_2O by NO reductase (Nor), and reduction of N_2O to N_2 by N_2O reductase (Nos). Most heterotrophs are facultative aerobic bacteria preferring free molecular oxygen to nitrogen oxides as electron acceptors. Not all of them can perform complete denitrification by reducing NO_3^- to N_2 as some of them can lack one or several critical enzymes. So, in WRRFs, complete denitrification is likely achieved by cooperation of denitrifying bacteria with different nitrogen oxide reduction capabilities (Ni et al., 2016).

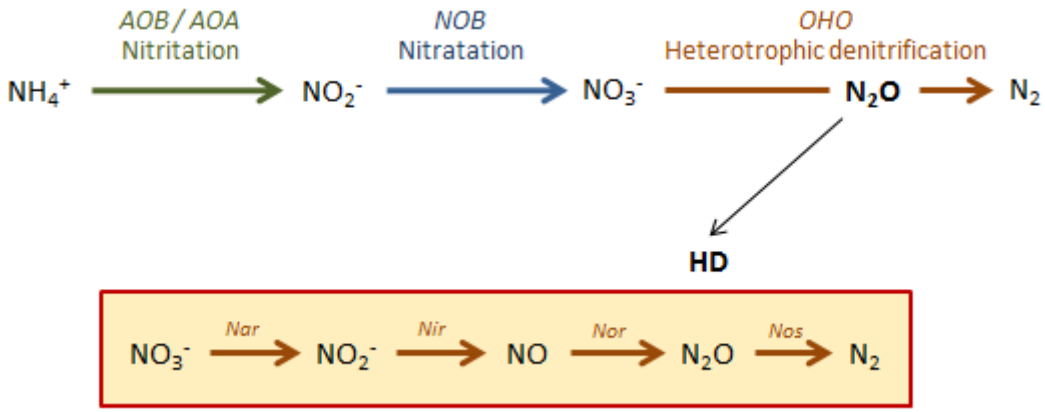

Figure II.1-3. Biological pathways related to heterotrophic denitrification.

Most reactions involved in ND are similar to HD, but those two processes are distinct in terms of microorganisms involved and electron donors (Wrage et al., 2001): presumably NH_2OH for ND, and organic carbon for HD. While most OHO have the gene encoding N_2O reductase (Nos), it was not identified, so far, in pure cultures of AOB (Schmidt et al., 2004, Casciotti and Ward, 2005, Shaw et al., 2006).

Regardless of the biological nitrogen removal technology, HD was found to be a source (Ni et al., 2011, Hanaki et al., 1992, Wicht, 1996, Eldyasti et al., 2014, Domingo-Felez et al., 2017) or a sink of N_2O (Guo, 2014, Bollon et al., 2016a, Conthe et al., 2019, Vieira et al., 2019). Its accumulation is thought to result from an unbalance of its production and consumption rates (Pan et al., 2013b, Conthe et al., 2019), depending on the applied operating conditions (presented in section II.1.2). However, it should be noted that recent findings suggested a link between N_2O emissions and microbial community profile and function in WRRFs (Vieira et al., 2019). In fact, recently a new cluster of atypical nosZ genes called “clade II nosZ” was identified. Interestingly, many clade II nosZ genes were found on genomes lacking the nirS

and/or nirK gene, which provides them the capacity of reducing N_2O production and its subsequent emission (Jones et al., 2012). These observations should be confirmed by further measurements on full-scale BNR systems.

II.1.1.3 IDENTIFICATION OF N_2O PATHWAYS

Nitrification and HD have been presented as distinct processes, but nitrifying and denitrifying organisms most often cohabit in wastewater treatment processes as both are required to achieve complete nitrogen removal. They share several reaction intermediates (Figure II.1-4), which means that the N_2O production rate, for instance, is governed by both nitrification and denitrification rates. Measurements performed on full-scale WRRFs reported that nitrification rather than HD was the main source of N_2O (Ahn et al., 2010, Foley et al., 2010, Bollon et al., 2016a, Bollon et al., 2016b). This is owing to the fact that N_2O is a by-product of nitrification whereas it is an intermediate product of HD, which moreover, has been evidenced as a potential strategy to reduce N_2O emissions (Guo and Vanrolleghem, 2014, Conthe et al., 2019). The enhanced gas-liquid transfer in aerobic reactors or zones is an additional explanation for the higher emissions during nitrification.

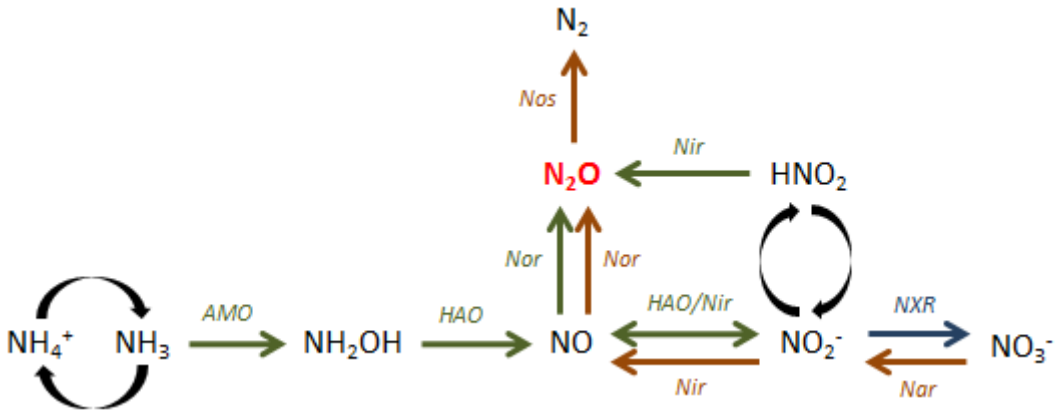

Figure II.1-4. Main biological pathways involved in coupled nitrification-denitrification.

For the last decade, isotopic analyses have been used to identify the respective contribution of N_2O production pathways in natural environments, and during wastewater treatment (Duan et al.). Such analyses are based on the determination of natural stable isotopes of the central (N_α) and terminal (N_β) nitrogen atoms (^{14}N and ^{15}N), and oxygen atom (^{16}O, ^{17}O and ^{18}O), by isotope ratio mass spectrometry (IRMS) or laser spectroscopy. The most promising method is the calculation of the site-preference (SP) value, which is based on the distribution of ^{15}N on the central or terminal position of the N_2O molecule (Figure II.1-5). Typical SP values range from 28.4 to 36.6‰ for NN, -10.7 to 0.1‰ for ND, and -5.1 to -0.5‰ for HD (Wunderlin et al., 2013, Duan et al., 2017), which mainly allow a distinction between N_2O production from NH_2OH oxidation and NO_2^- reduction. When N_2O reduction occurs, the SP

value significantly increases, which complicates the distinction between nitrification and denitrification pathways in mixed cultures. Toyoda et al. (2011) proposed a method, based on the combined calculation of SP and $\delta^{15}N$, to better distinguish pathways.

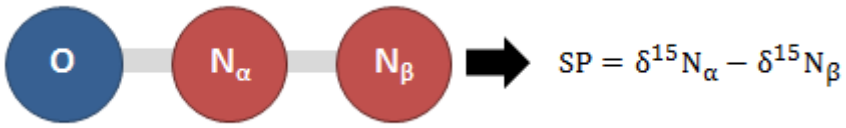

Figure II.1-5. Calculation of the site-preference (SP) value.

These methods have been applied to BNR systems to quantify the respective contributions of NN and ND to N_2O production, along with applied conditions. The effect of operating conditions on N_2O production –and emissions– in BNR systems were extensively reviewed by Law et al. (2012b) and Massara et al. (2017a), and briefly presented in the next section, along with the results of isotopic studies.

II.1.2 INFLUENCE OF OPERATING CONDITIONS

II.1.2.1 DISSOLVED OXYGEN AND NITRITE CONCENTRATIONS

II.1.2.1.1 DURING NITRIFICATION

Dissolved oxygen (DO) and NO_2^- (or associated HNO_2) concentrations are important parameters controlling N_2O production from AOB (Kampschreur et al., 2009). Several full-scale studies reported high N_2O emissions at low DO and high NO_2^- concentrations (Kampschreur et al., 2008b, Foley et al., 2010, Aboobakar et al., 2013, Bollon et al., 2016b), which were found to favour N_2O production by ND, based on isotopic analyses (Wunderlin et al., 2013, Peng et al., 2014, Tumendelger et al., 2014).

The combined effect of DO and NO_2^- on AOB activity solely was studied through lab-scale experiments. Peng et al. (2015) showed that at fixed DO level, the N_2O production rate and the emissions factor (EF) increased with the NO_2^- concentration. At fixed NO_2^- concentration, even as low as 3 mgN/L, the N_2O-EF decreased with increasing DO level while the production rate increased to reach a maximum at 0.85 mgO_2/L. Based on a batch study of N_2O emissions on activated sludge, Tallec et al. (2006a) reported the highest N_2O emission rate and factor at DO around 1 mgO_2/L. Batch-test experiments on enriched AOB cultures showed that the N_2O production rate reached its maximum at a NO_2^- concentration of 50 mgN/L, but started decreasing above this value to reach its slowest rate for NO_2^- concentrations above 500 mgN/L, suggesting that the ND pathway could be inhibited by high NO_2^- concentrations (Law et al., 2013). This was not verified so far, other studies even showing contradictory results

(Castro-Barros et al., 2016). Furthermore, this situation is not encountered in conventional low-loaded BNR systems, with nitrite concentrations far below this range of values.

The relative importance of NN and ND for N_2O production is likely dependent on operating conditions and in particular DO and NO_2^- concentrations. Peng et al. (2014) investigated the contributions of ND and NN pathways using isotopic measurements in a mixed AOB / NOB culture. They found that ND was the main contributor to N_2O production in all situations (66 to 95%). The N_2O-EF decreased with increasing DO concentration, which was related to a lower contribution of ND: the latest decreased from 95 to 70% as DO passed from 0.5 to 1.5 mgO_2/L. Another lab-scale study showed that the contribution of the ND pathway is dominant in nitrifying systems, except during NH_2OH pulses, and reaches 100% during NO_2^- pulses (Wunderlin et al., 2013). Based on samples from a full-scale conventional activated sludge (CAS), Tumendelger et al. (2014) found contrasted contributions of NN and ND. Under limited aeration conditions, ND was the dominant pathway, while NN and ND contributed almost equally to N_2O production in other conditions. However, it was suspected that a reduction of N_2O by heterotrophs occurred, which may have conducted to an overestimation of the NN contribution (increased SP, section II.1.1.3).

II.1.2.1.2 DURING HETEROTROPHIC DENITRIFICATION

Tallec et al. (2008) investigated the impact of DO on N_2O production in denitrifying activated sludge at lab-scale. In anoxic conditions (below 0.3 mgO_2/L), heterotrophic denitrification was found to be the only source of N_2O. From 0.3 to 1.1 mgO_2/L, total N_2O emissions were higher and originated from both heterotrophic denitrification and ND pathway, the latest contributing to 60%. Furthermore, oxygen is an inhibitor for nitrogen reductases, among which N_2O reductase (Nos) is the most affected (Knowles, 1982). In this case, incomplete denitrification leads to N_2O accumulation during the anoxic phase. Indeed, Wunderlin et al. (2012) observed an accumulation of N_2O during denitrification even at low levels of oxygen (0.1 – 0.2 mgO_2/L). In the light of these observations, it is recommended to operate heterotrophic denitrification in strict anoxia. Nitrite (or HNO_2) is also known to inhibit the activity of N_2O reductase and was reported to trigger N_2O production for concentrations as low as 1-2 mgN/L (von Schulthess et al., 1994, Zeng et al., 2003).

II.1.2.2 AMMONIA LOADING AND OXIDATION RATES

It is known that increasing ammonium load results in increasing ammonium oxidation rate, therefore N_2O production, since N_2O is a by-product of nitrification (Law et al., 2012a, Daelman et al., 2015, Ali et al., 2014). Through experiments in a batch reactor performing nitritation and fed with a nitrogen-rich synthetic solution, Law et al. (2012b) found, for

specific ammonium oxidation rates (AOR) below 150 mgNH_4-N/h/gVSS, a positive linear correlation between the specific N_2O emission rate and AOR and an exponential relation above this value. Based on model verification, authors concluded that under such operating conditions, N_2O production was mainly related to the chemical decomposition of NOH (Eq.9). Under low AOR, however, the model based on the NN pathway could describe the N_2O production rate. Based on isotope analyses, Wunderlin et al. (2013) did report an increase of the NN contribution to N_2O production (from 3 to 10% of the total N_2O production) with increasing influent ammonium concentration (from 9 to 15 mgN/L). This contribution increased when the system was submitted to NH_4^+ pulses (10 – 25%) and became most important when submitted to NH_2OH pulses (100%). The fact that the NN contribution is lower under NH_4^+ than NH_2OH pulses can be explained by the fact that the NH_4^+ oxidation to NH_2OH is the limiting step. It can also indicate that the ammonium loading rate not only favours N_2O production by NN, but also by ND, which can be explained by transient NO_2^- accumulation or/and low DO concentrations due to increased nitrifier activity.

II.1.2.3 GAS-LIQUID MASS TRANSFER CONDITIONS

Compared to oxygen, N_2O is more than 10 times more soluble in water: 2.4 10^{-4} mol/m^3/Pa at 25°C, against 1.3 10^{-5} mol/m^3/Pa for O_2 (Sander, 2015). Thus, it can accumulate at relatively high levels in the liquid phase during non-aerated periods, and be released to the atmosphere through stripping when active aeration takes place. Indeed, several full-scale studies reported that N_2O emissions mainly originate from the aerobic tanks (Ahn et al., 2010, Foley et al., 2010). Aeration also has an effect on DO levels, which impacts N_2O production rates, as discussed in section II.1.2.1.

II.1.2.4 TRANSIENT CONDITIONS

II.1.2.4.1 DURING NITRIFICATION

In BNR systems, microbial populations can be subjected to transient conditions in terms of aeration with cyclic aerobic-anoxic conditions to sustain nitrification and denitrification for efficient nitrogen removal. It is also subjected to variation of the nitrogen load with influent flow and ammonium concentration changing diurnally. Such transient conditions were reported to be associated with high N_2O emissions, as they lead to transient accumulation of reaction intermediates (Chandran et al., 2011, Massara et al., 2017a). Rassamee et al. (2011) showed that N_2O production is enhanced by abrupt process changes like transient anoxia. Lab-scale experiments on AOB cultures demonstrated that the gene expression of AOB was impacted by anoxic-aerobic transition, and that N_2O production takes place during recovery from, rather than imposition of anoxia in presence of ammonia (Yu et al., 2010). According

to Chandran et al. (2011), the increased N_2O production during the recovery from anoxic conditions is owing to a shift in metabolism from a low hydroxylamine oxidation activity towards the maximum activity (due to the accumulation of ammonia during the non-aerated phase) inducing transient accumulation of NO further reduced to N_2O through the NN pathway. This would also explain the positive relationship found at full-scale plants between influent ammonium concentrations and N_2O emissions (Kampschreur et al., 2008a, Ahn et al., 2010, Bollon et al., 2016b). It has to be noted that these transient conditions are generally associated with periods of intermediate DO concentrations (short term period when aeration is switched on and varying duration in case of an overloading). Such limited DO conditions can enhance N_2O production by AOB through the ND pathway in case of nitrite accumulation (Peng et al., 2015).

II.1.2.4.2 DURING HETEROTROPHIC DENITRIFICATION

Transition from anoxic to aerobic conditions is also suspected to enhance N_2O production from heterotrophs as O_2 can inhibit the last step of the denitrification chain, the most sensitive to oxygen (Otte et al., 1996). It was observed that the production of N_2O from heterotrophs can continue several hours after the recovery of the anoxic conditions because the synthesis of the N_2O reductase has a longer lag-phase compared with the NO_2^- reductase synthesis (Otte et al., 1996).

II.1.2.5 TEMPERATURE

II.1.2.5.1 DURING NITRIFICATION

So far, it remains unclear whether temperature has a direct negative or positive effect on N_2O emissions. Temperature is supposed to enhance biological reactions, leading to higher N_2O production during nitrification (Guo and Vanrolleghem, 2014). In contrast, full-scale campaigns have shown higher emissions at low temperatures (Daelman et al., 2015, Bollon et al., 2016b). However, both studies were more likely to correlate these emissions to the high NO_2^- concentration occurring simultaneously, which is well-known to trigger N_2O production. Bao et al. (2018) and Reino et al. (2017) investigated N_2O emissions from partial nitrification reactors under various temperature conditions (10 to 30°C). Both studies reported an increase of the N_2O-EF with increasing temperature from 10 to 20°C. However, these studies were performed on AOB-enriched cultures (80% to 90% of the biomass composed of AOB). Nitrification therefore induced direct accumulation of NO_2^- and further production of N_2O.

Kim et al. (2006) studied the effect of temperature on nitrification performance in a biofilm airlift reactor inoculated with sludge from a full-scale contact aeration basin. At constant NH_4^+ load (1.0 kgN/m^3/d) and increasing temperature from 12 to 33°C, the authors observed a decrease of the NO_2^- concentration with increasing ammonium oxidation rate. Although N_2O was not measured in this study, one can imagine that the associated N_2O production by ND would have decreased. Specific studies of N_2O emissions with temperature in mixed AOB/NOB (and AOB/NOB/OHO) cultures would be needed, preferably coupled with isotopic analyses to distinguish the N_2O production pathways.

II.1.2.5.2 DURING HETEROTROPHIC DENITRIFICATION

Once again, there is no consensus on the effect of temperature on N_2O production during HD. Lab-experiments in denitrifying conditions showed higher N_2O and NO_2^- production with temperature. It is hypothesized that enhanced reaction rates promote electron competition, which disfavours N_2O reductase (Pan et al., 2013a). In parallel, N_2O solubility decreases with temperature, leading to higher N_2O accumulation in the gas phase, which is not available for denitrification (Poh et al., 2015). On the other hand, Hu et al. (2011) found an increase of N_2O emissions with decreasing temperature from 30 to 15°C in an anoxic/aerobic sequencing batch reactor. The authors attributed these results to a contrasted effect of temperature on enzymes of the denitrification chain. Indeed, it was reported that low temperatures affect N_2O reductase more than NO_3^-, NO_2^- and NO reductases in soils (Avalakki et al., 1995, Holtan-Hartwig et al., 2002). In a denitrifying batch reactor fed with 40 mgNO_3-N/L (at a fixed COD/N ratio of 3 and a pH of 7), the N_2O-EF increased from 13 to 40 and 82 % of the denitrified nitrogen when temperature decreased from 20 to 10 and 5 °C (Adouani et al., 2015).

II.1.2.5.3 EFFECT OF TEMPERATURE ON N_2O STRIPPING

Besides its effects on biokinetic reactions, temperature is also known to affect gas-liquid mass transfer, since it has a positive effect on the volumetric transfer coefficient, k_La (NFEN-12255-15, 2004). Moreover, temperature decreases the solubility of N_2O in water (Sander, 2015). Overall, a temperature increase would therefore result in an increase of N_2O stripping. For example, Bollon et al. (2016b) measured a decrease of the emitted fraction of N_2O from 72 to 43%, associated to a decrease of the water temperature from 15.7 to 12.8°C.

II.1.2.6 PH

Low pH values (< 5-6) were reported to induce partial inhibition of the HAO with subsequent release of NO (Jiang and Bakken, 1999) and also affect the activity of N_2O reductase (Hanaki

et al., 1992, Schreiber et al., 2012). In most conventional BNR systems, the pH is generally between 7 and 8 meaning that the direct pH effect is expected to play a minor role (Kampschreur et al., 2009). However, it may indirectly affect N_2O production from AOB and heterotrophs through controlling the partitioning of NO_2^- and HNO_2.

II.1.2.7 COD/N RATIO

Substrate availability for HD is often expressed as the chemical or biological oxygen demand (COD and BOD respectively) to nitrate ratio. Several lab-scale studies demonstrated that low COD/NO_3-N ratios (< 3.5) lead to high N_2O emissions during heterotrophic denitrification (Hanaki et al., 1992, Itokawa et al., 2001). It was confirmed in a full-scale denitrifying BAF, that peaks of N_2O are recorded during low BOD/NO_3-N events (Bollon et al., 2016a). The combination of various methanol loading rates and electron acceptors on denitrifying cultures highlighted the electron competition between denitrification stages under both limiting and non-limiting carbon condition. The percentage of electrons distributed to N_2O reductase decreased with decreasing carbon loading rate (Pan et al., 2013a). The mechanisms responsible for N_2O accumulation at low C/N ratio were investigated on a molecular level through gene quantification. High nitrogen removal and low N_2O accumulation occurred at a C/N ratio of 3, the highest N_2O accumulation being found at 1, which corresponded to the highest Nor/Nir ratio (Zhang et al., 2016). Finally, increased N_2O emissions at low C/N ratio can also be caused by the indirect effect of NO_2^- and/or NO accumulation (Hanaki et al., 1992, von Schulthess et al., 1995, Itokawa et al., 2001).

He et al. (2017a) studied the effect of the C/N ratio on N_2O production in up-flow lab-scale nitrifying BAFs. At similar applied NH_4^+ concentrations (24 to 30 mgN/L), three separate reactors were supplied with glucose to maintain C/N ratios of 2, 5 and 8. The steady state concentrations of DO, N_2O, NH_4^+, NO_2^- and NO_3^- within the biofilm were measured by micro-electrodes. The increased C/N ratio was associated to increased biofilm thickness (210 to 375 µm), higher NH_4^+ removal, lower NO_2^- and NO_3^- production and lower DO concentration in the biofilm. Authors recorded the highest N_2O production rates (and NO_2^- concentration in the biofilm) at the lowest C/N ratio, while the lowest production (and NO_2^- concentration) was associated to a C/N ratio of 5, and therefore recommended to operate nitrifying BAFs at a C/N ratio of 5 to minimize N_2O emissions. Although the contributions of N_2O pathways were not investigated, one can assume that their contributions changed with the C/N ratio. The high N_2O production at the lowest C/N ratio could be attributed to a higher inhibition of N_2O reductase by O_2. On the other hand, higher N_2O production at a C/N ratio of 8 compared to 5 could be due to an increase of N_2O production by ND due to low DO concentrations.

- N_2O is an end-product of nitrification, mainly produced by the NN and ND pathways;
- N_2O is a reaction intermediate of HD, which can act as a sink of N_2O;
- The contributions of N_2O pathways are influenced by several conditions, in particular DO and NO_2^- concentrations, NH_4^+ peaks and COD/N ratio;
- The influence of temperature on N_2O production during nitrification and denitrification remains controversial, while it is known to increase N_2O stripping.

II.2 N_2O BIOKINETIC MODELS

As discussed in section II.1, significant efforts have been made to identify the conditions favouring N_2O production/consumption in WRRFs. This better understanding of N_2O production pathways led to the development of several mechanistic models, which have been recently reviewed by Ni and Yuan (2015) and Massara et al. (2017a). A brief summary is given in this section, the focus being made on models coupling multiple pathways.

II.2.1 HETEROTROPHIC DENITRIFICATION MODELS

Two models have been proposed to describe four-step HD: the ASMN (Hiatt and Grady, 2008) and the ASM-ICE (Pan et al., 2013b). Similarly to AOB-pathway models, they are different in the sense that the second model is based on electron carriers as the Ni et al. (2014) model. The ASMN describes HD by four reduction reactions with different specific growth rates. Equal affinity constants for the carbon substrate and inhibition constant for oxygen are used for each step (K_S = 20 mgCOD/L and $K_{I,O,H}$ = 0.1 mgO_2/L), except for the last step for which a K_s of 40 mgCOD/L was considered. On the other hand, a lower inhibition constant for NO is considered for N_2O reduction (0.75 against 0.5 and 0.3 mgN/L for NO_2^- and NO reduction rates, respectively). Pan et al. (2013b) investigated the electron distribution among the nitrogen oxide reduction reactions under different carbon loading rates. This study revealed that electron competition can occur at each step of denitrification under limited as well as abundant carbon loads, with less electrons distributed to N_2O reductase at decreasing carbon loading rates. Those observations led to a model of denitrification based on electron competition. Basically, the model considers one reaction linked to the carbon oxidation process, instead of two reactions in the original version, and a 4-step denitrification with electron carriers. As previously stated, this model seems less applicable to full-scale studies, since some parameters related to electron carriers cannot be measured. On the other hand, the model by Hiatt and Grady (2008) was not calibrated on

NO nor N_2O concentrations in the original publication; their parameters therefore lack reliability.

II.2.2 NITRIFICATION MODELS

In the early stage of N_2O modelling in BNR systems, several single-pathway models have been proposed, describing either NN, NOH decomposition or ND pathways. These models have been tested against four long-term data sets collected from different BNR processes (Spérandio et al., 2016). Models based on the NN or NOH pathway (Law et al., 2012a, Ni et al., 2013) could describe most of the data except in case of high nitrite variations, while models based on the ND pathway (Ni et al., 2011, Mampaey et al., 2013, Guo and Vanrolleghem, 2014) could describe most of the data, as ND is a main source of N_2O. In conclusion, none of the models was able to describe all the data with the same parameter set, sometimes leading to controversial values during calibration. In the light of these results, it appeared that single-pathway models cannot claim to be robust. Indeed, they are not capable to describe N_2O emissions under different operating conditions, since a regulation between pathways has been observed depending on operating conditions, especially NO_2^- accumulation and low DO levels (II.1.2.1). To fill this gap, multiple-pathway models have been proposed (Ni et al., 2014, Domingo-Felez and Smets, 2016, Pocquet et al., 2016). These models differ in the number of pathways considered and their representation, which are summarized in Table II.2-1.

Table II.2-1. Comparison of multiple AOB-pathway models developed in recent years.

	Ni et al. (2014)	Pocquet et al. (2016)	Domingo-Felez and Smets (2016)
Biological pathways	NN + ND	NN + ND	NN + ND
Abiotic pathways	None	None	2 reactions
DO effect on ND	None	Haldane term	Inhibition term
Number of parameters	19	13	13
Calibration on	Enriched-AOB lab-scale reactor	Lab-scale SBR performing nitritation and denitrification	Respirometric assays

The first and second models to consider both NN and ND pathways have been developed by Ni et al. (2014) and Pocquet et al. (2016), respectively. The same biological reactions are considered in these models (Figure II.2-1 and Figure II.2-2). Both models considered NO as an intermediate of the NN pathway only. It was not considered an intermediate of ND to avoid its consumption by NN, which would eliminate the ND-related N_2O production. The hypothesis, verified using lab-scale experiments, was that the reduction of NO to N_2O has a

much higher rate than NO_2^- reduction to NO (Ni et al., 2014). The main difference between these models is the inclusion of two intracellular state variables representing electron carriers in their oxidized and reduced forms by Ni et al. (2014). The model of Pocquet et al. (2016) also considers pH influence on NO_2^-/HNO_2 equilibrium, and DO inhibition in the ND pathway with the Haldane term suggested by Guo and Vanrolleghem (2014) to take into account that maximum N_2O production occurs at around 0.8 – 1.0 mgO_2/L.

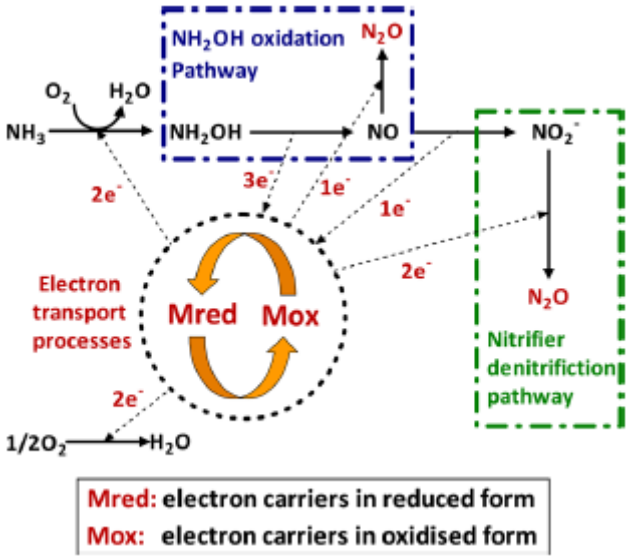

Figure II.2-1. AOB production pathways described by Ni et al. (2014).

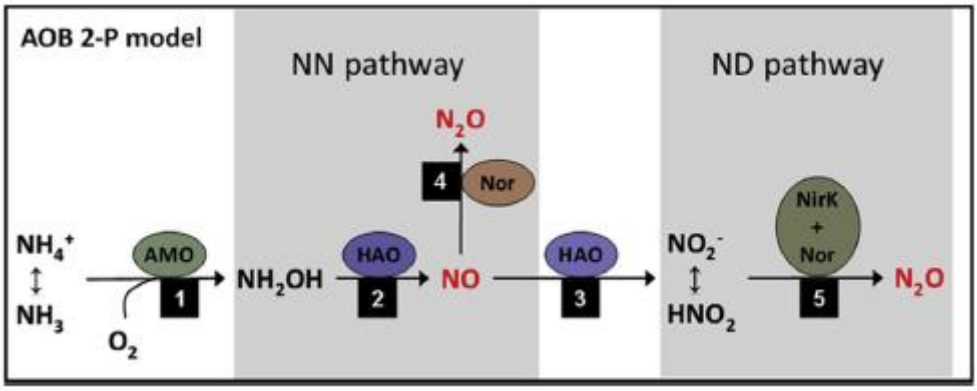

Figure II.2-2. AOB production pathways described by Pocquet et al. (2016).

The third model was developed by Domingo-Felez and Smets (2016). A key difference with previous models is that NO is produced in parallel by NN and ND pathways, but is consumed by a single reduction to N_2O, which avoids the NO loop (Figure II.2-3). In addition, the model includes two abiotic reactions and four-step heterotrophic denitrification. Recent studies suggested that abiotic reactions could produce substantial amounts of N_2O in systems prone to high NO_2^- levels (Harper et al., 2015, Soler-Jofra et al., 2016). These experiments were performed on NO_2^- rich cultures (50 – 650 mgN/L) to get close to conditions found in partial

nitritation systems. This model was presented as a theoretical one in the original publication. It was calibrated in further work, based on respirometric assays (Domingo-Félez et al., 2017).

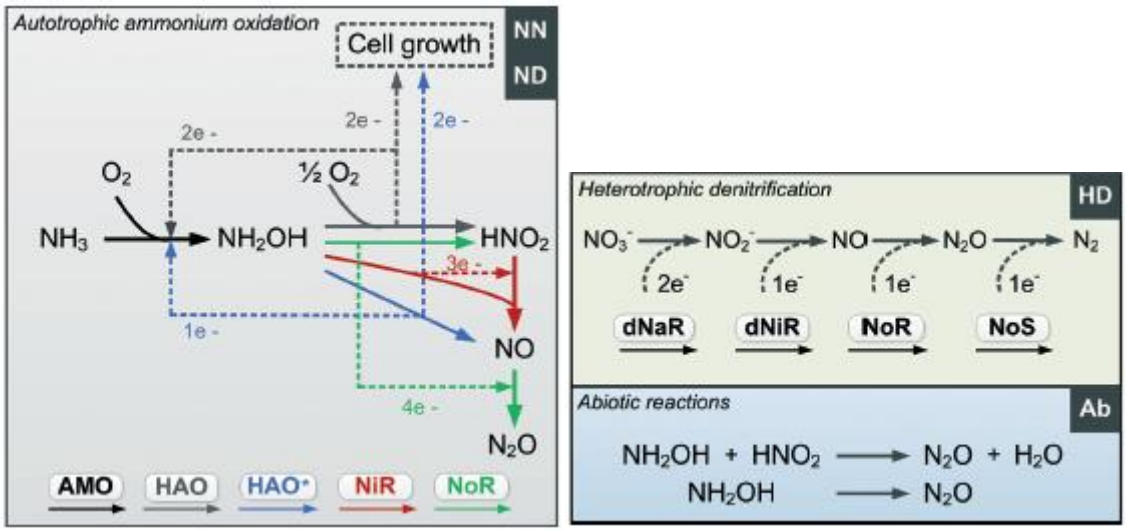

Figure II.2-3. AOB production pathways described by Domingo-Felez and Smets (2016).

The effectiveness and applicability of the first two-pathway models have been compared by Lang et al. (2016), using three lab-scale data sets with contrasted operating conditions (applied NH_4^+, NO_2^- and DO conditions range from: 10 to 20 mgN/L, 1 to 123 mgN/L and 0.2 to 4.5 mgO_2/L, respectively). Both models were able to predict N_2O production in all DO and NO_2^- conditions. They both reported a major contribution of ND to N_2O production and a decrease of this contribution with increasing DO and decreasing NO_2^- concentrations. The predicted contribution of ND was, however, more important with the model of Pocquet et al. (2016) compared to the other one (70 to 95% against 40 to 90%). This study was not able to identify the best model, since no isotopic analysis was performed to estimate NN and ND contributions to N_2O production. However, the model of Ni et al. (2014) involves parameters that are not measurable (those related to the electron carriers).

II.2.3 COUPLED NITRIFICATION-DENITRIFICATION MODELS

Recent models including N_2O pathways by both AOB and OHO are summarized in Table II.2-2. Please mind that this review may not be complete, but allows identifying the main issues and advantages of modelling coupled nitrification-denitrification. In all these studies, NO_2^- oxidation to NO_3^- by NOB was also included and HD was modelled as a four-step process according to Hiatt and Grady (2008). Moreover, NO was included as a state variable and a precursor to N_2O production in these models, but was never measured. The differences were in the representation of N_2O production pathways by AOB and in the objectives of the studies.

Ni et al. (2011) applied a model coupling N_2O production by ND and HD to four datasets obtained in contrasted nitrifying and denitrifying conditions in previous studies characterized by large differences in N_2O-EF (0 to 25 % of the applied nitrogen load). Parameter values related to HD were taken from von Schulthess and Gujer (1996), who also studied heterotrophic denitrification rates. The model was able to predict effluent N_2O concentrations with moderate calibration of AOB-related parameters (8 out of 12; close to their reference values). One parameter related to HD (K_{SH3}, substrate affinity constant for NO reduction by heterotrophs) was reduced by a factor four to predict N_2O production from an anoxic lab-scale reactor. In all conditions, HD was a source of N_2O, never a sink. In this model, the oxygen inhibition coefficient on N_2O reduction was set 2.8, 3.2 and 2.1 times lower than those on NO_3^-, NO_2^- and NO reduction, respectively, which explained that N_2O reduction remained lower than its production.

In her PhD thesis, Guo (2014) extended the ASM2d to include N_2O production by HD (Hiatt and Grady, 2008) and ND (Mampaey et al., 2013). It was calibrated on data from a one-month measuring campaign on a plant operating anaerobic/anoxic/aerobic tanks (A^2/O). The model was able to predict N_2O emissions, except under wet-weather conditions (which may be related to the non-inclusion of the NN pathway according to the author). The model predicted that ND was the main source of N_2O, while HD denitrified on average 2/3 of the produced N_2O.

In a further study, Ni et al. (2015) applied the 2-pathway model of Ni et al. (2014) coupled to the HD model of Hiatt and Grady (2008) to full-scale data from a plug-flow reactor. Again, the model was able to predict N_2O emissions with only few calibrated parameters (5 related to AOB and 1 related to OHO). The respective contributions predicted by the model were quantified for different locations of the reactor. In the anoxic zone, HD contributed to 100% of the produced N_2O, which was only observed at high NO_3^- levels and NO_2^- accumulation. In all aerobic zones, N_2O production was mainly attributed to AOB. Close to the anoxic zone, the contribution of ND was maximum (80 to 100%) and decreased along the plug-flow with increasing DO concentration, while the NN contribution increased, up to 70%. Once again, HD was only identified as a source of N_2O.

Massara et al. (2017b) and Mannina et al. (2018) both coupled the 2-pathway model of Pocquet et al. (2016) to the HD model according to Hiatt and Grady (2008). In the first study, the model was applied to full-scale data from a WRRF operating A^2/O; in the second to a pilot-scale A^2/O followed by a membrane bioreactor (MBR). Massara et al. (2017b) did not calibrate the model but performed a sensitivity analysis on the predicted N_2O-EF for two distinct conditions: high and low DO concentrations in the tank (3 and 1 mgO_2/L,

respectively). Although NOB are not directly responsible for N_2O production, the N_2O-EF was found most sensitive to parameters related to NOB in non-limiting DO conditions. An increase of NOB activity decreased NO_2^- accumulation, therefore N_2O production. In low DO conditions, the N_2O-EF was mainly sensitive to AOB parameters, but insensitive to NOB parameters, as NOB activity was always limited by O_2. The anoxic growth factor of heterotrophs (η_G) had a strong positive impact on the N_2O-EF (ranked 2nd most influencing parameter in both conditions). These results highlighted important contributions of ND and HD to the net N_2O production, which is in agreement with the modelling studies of Domingo-Felez et al. (2017) and Mannina et al. (2018).

Indeed, Mannina et al. (2018) also highlighted a high impact of ND and HD parameters on the predicted N_2O based on a global sensitivity analysis. In anaerobic and anoxic tanks, effluent N_2O was mainly affected by anoxic growth factors on NO_3^- reduction to NO_2^- (η_{H1}) and NO reduction to N_2O (η_{H3}). In the aerated tank and MBR, it was mainly affected by parameters regulating N_2O production by ND: the reduction factor for ND (η_{ND}) and the inhibition constant of O_2 ($K_{I,O2,AOB}$). In batch experiments on a nitrifying activated sludge, Domingo-Felez et al. (2017) found a better description of N_2O production with the model coupling ND and HD than with NN and HD. Interestingly, the prediction with the model describing HD only was almost as correct as the one with coupled ND-HD. Based on these results, coupling HD to multiple AOB-pathway models seems essential to predict N_2O production, even in BNR systems performing nitrification. However, such consideration leads to a higher complexity in parameter identification, due to common reaction intermediates between nitrification and denitrification processes (Domingo-Felez et al., 2017).

- Considering both NN and ND production pathways by AOB increases the robustness of N_2O models;
- These multiple AOB-pathway models were coupled to four-step HD in a few occasions. Results reported a large contribution of denitrification by nitrifiers and/or heterotrophic denitrifiers to the net N_2O production, even in nitrifying BNR systems;
- Coupled nitrification-denitrification should therefore be included in further models, which, however, calls for dedicated work to identify parameters.

Table II.2-2. Applications of models coupling N_2O production pathways by AOB and OHO and including nitratation by NOB. [1] Hiatt and Grady (2008); [2] Ni et al. (2014); [3] Pocquet et al. (2016); [4] Mampaey et al. (2013).

Study	N_2O pathways	Application	Sensitivity analysis / calibration
Ni et al. (2011)	ND + HD[1]	Four lab- and pilot-scale case studies for various NH_4^+ (17-54 mgN/L) and DO (0.1-6.2 mgO_2/L) conditions (aerobic and anoxic)	✓ Calibration on dissolved N_2O concentrations ✓ Similar calibrated parameter values for AOB in each case ✗ Different parameters sets for HD between cases (K_{SH3})
Guo (2014)	ND[4] + HD[1]	Full-scale N_2O emissions from anaerobic/anoxic/aerobic tanks (A^2/O)	✓ Calibration on N_2O emissions ✓ Good fit except under wet-weather conditions, which were associated to unstable conditions ✗ Including the NN path may have increased model accuracy
Ni et al. (2015)	NN[2] + ND[2] + HD[1]	Full-scale data from a plug-flow reactor (anoxic + aerobic zones)	✓ Calibration on N_2O emissions ✓ Good fit after calibration of six parameters for AOB-related N_2O pathways (one for HD)
Domingo-Felez et al. (2017)	NN + HD[1] ND + HD[1]	Batch tests on aerated CAS submitted to NH_4^+ loadings and anaerobic CAS submitted to NO_3^- loadings	✓ Best fit with ND + HD model ✗ Difficulty to discriminate between pathways based on bulk and off-gas N_2O concentrations only
Massara et al. (2017b)	NN[3] + ND[3] + HD[1]	Full-scale data from different locations of A^2/O	✗ No calibration ✓ High sensitivity to NOB parameters at non-limiting DO concentrations ✓ High sensitivity to AOB parameters at low DO concentrations, insensitivity to NOB (limited activity)
Mannina et al. (2018)	NN[3] + ND[3] + HD[1]	Data from different locations of a pilot A^2/O + membrane bioreactor (MBR) plant	✓ High sensitivity to HD parameters in anaerobic/anoxic tanks and to ND parameters in the aerobic tank ✗ Overestimation of dissolved and gaseous N_2O concentrations in the aerated tanks ✓ Better fit for non-aerated tanks

II.3 BAF OPERATION AND MODELS FOR WASTEWATER TREATMENT

Previous sections presented N_2O production pathways and associated models, which were mainly applied to conventional activated sludge systems (CAS). In this section, N_2O production and modelling in biofilm reactors, and more specifically nitrifying BAFs, are discussed.

II.3.1 DESCRIPTION OF BIOFILM SYSTEMS

Biofilms are dynamic and heterogeneous structures which develop on the surface of inert supports in regular contact of aqueous environments (Morgenroth, 2008). They are composed of microorganism aggregates encased in a matrix of extracellular polymeric substances (EPS), which enable biofilm adhesion to the substratum (or media) and protect the bacteria from external aggressions (Boltz et al., 2017). A biofilm system is composed of: the support media on which the biofilm develops, the biofilm itself (10 to 200 µm), an external mass-transfer boundary layer (20 to 1 500 µm) and the aqueous phase (Rittmann et al., 2018) (Figure II.3-1).

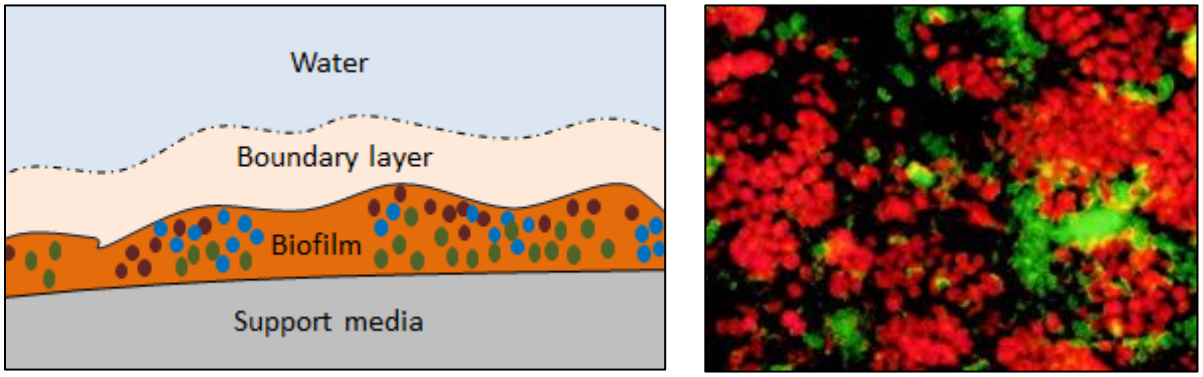

Figure II.3-1. Schematic representation of a biofilm system and visualization of a nitrifying biofilm by fluorescence in situ hybridization (FISH), taken from (Kindaichi et al., 2004).

Biofilms are known for their detrimental effects (for example for dental hygiene or water contamination) but also for their beneficial applications, when properly controlled. They are notably used for biological wastewater treatment (organic matter, phosphorous and/or nitrogen species). A review of existing biofilm reactors applied in WRRFs has been proposed by Morgenroth (2008). Biofilm reactors are characterized by higher biomass concentrations, which imply that a lower reactor volume is necessary for a given loading rate. While the biological reactions involved in biofilm and CAS systems are similar, there are several differences in their functioning. In particular, mass transport within the biofilm is limited by diffusion; the competition between autotrophic and heterotrophic biomasses is therefore

not only related to substrate availability in water but also to their gradients within the biofilm, which create zones suitable for specific populations (Zhang et al., 1995).

Controlling the biofilm thickness is a key element when operating biofilm reactors: the biofilm growth (due to biomass activity and/or filtration of particles) must be compensated by biofilm detachment (due to abrasion, erosion, sloughing and/or predator grazing), while maintaining sufficient active biomass to achieve biological conversions (Boltz and Daigger, 2010). In submerged fixed-bed reactors, such as biological aerated filters (BAFs), detachment is dominated by regular backwashing events which prevent clogging of the media bed by removing excess biomass (Morgenroth and Wilderer, 2000). In nitrogen elimination systems, heterotrophic and autotrophic biomasses coexist within the biofilm and compete for their common substrates (oxygen and nitrogen species), which impact process performances. For example, when submitted to frequent detachment events, mainly fast-growing heterotrophs –located at the surface of the biofilm– are eliminated, which favours the growth of autotrophs, characterized by more cohesive clusters (Derlon, 2008). To conclude, biofilms are highly heterogeneous systems, which compositions depend on many factors, in particular internal and external mass-transfer limitations and biomass competition.

II.3.2 BIOLOGICAL WASTEWATER TREATMENT USING BAFS

Biofilm systems are becoming increasingly popular for their performance and compactness (Sabba et al., 2018). In particular, BAFs are being widely used in large urbanized areas, where space is limited (Mendoza-Espinosa and Stephenson, 1999a). BAFs are submerged fixed-bed reactors in which nitrogen and/or carbon pollution is treated by passing the water through the bed in continuous up-flow or down-flow mode (Figure II.3-2).

The bed is composed of small-size support media (2 – 4 mm) to maximize the specific surface area for biofilm growth (1 000 – 3 000 m^2/m^3). This media can be denser than water, therefore supported by a floor (Biofor® process for example), or lighter than water, in this case retained by a grid (Biostyr®). Owing to the small pore spaces within the media bed, these processes combine biological treatment to solids removal by deep-bed filtration. The continuous feeding induces bacterial growth and particle deposit, which generate a gradual reduction of the bed porosity. The latter results in an increase of the reactor head loss, associated to a decrease in reactor performance. Regular backwashing is therefore performed, every 24 to 36 hours, resulting in a temporary expansion of the bed, which facilitates the removal of excess biomass (Morgenroth, 2008).

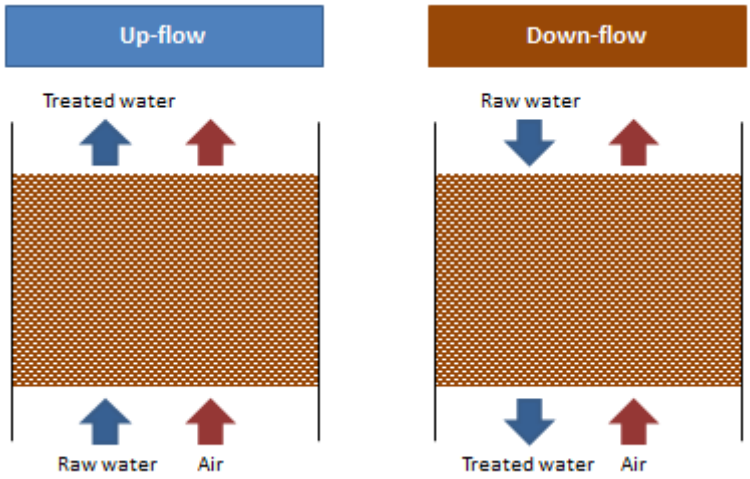

Figure II.3-2. Schematic representation of up-flow and down-flow fixed-bed reactors.

The use of biofilm reactors in France was evaluated based on the French database of residual urban wastewater (http://assainissement.developpement-durable.gouv.fr/, 2016). Process data are provided in nominal biological oxygen demand (BOD) loads. These numbers do not quantify the exact partition between biofilm reactors and CAS (different treated against applied loads) but identify the main trends. About 90% of the total BOD pollution is treated by WRRFs with a capacity above 2 000 PE and 95% of them use intensive processes, mainly CAS and BAFs (Figure II.3-3). The latter are biofilm reactors, used in a few plants compared to CAS (3% in France). Despite their small number, WRRFs operating BAFs receive 20% of the nominal organic load over the country and more than 60% in the Parisian area. Moreover, 40% of the Parisian load is treated by a single WRRF operating BAFs, Seine Aval.

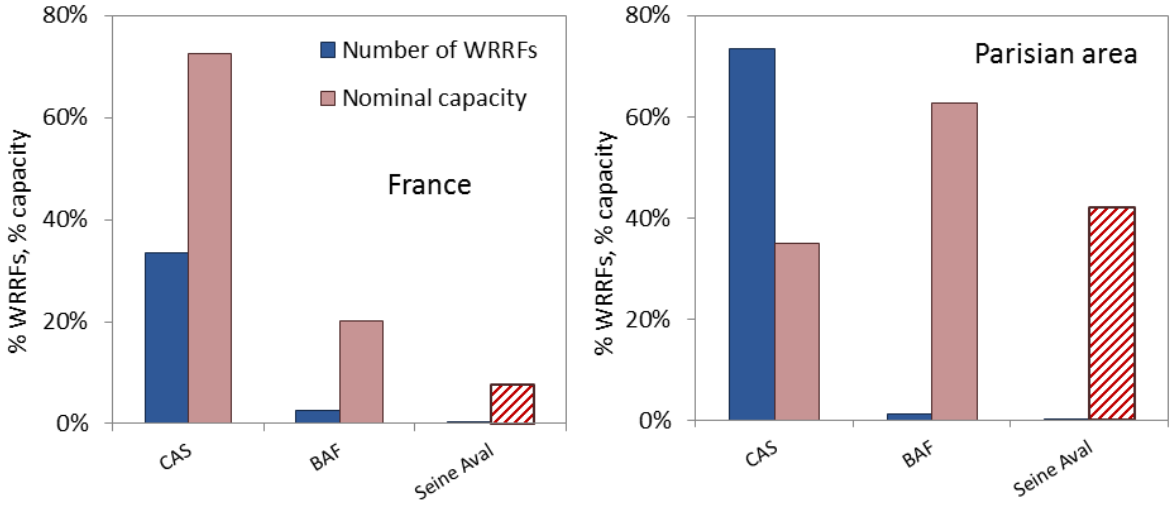

Figure II.3-3. WRRFs and nominal capacities treated by CAS and BAFs in France (left) and in the Parisian area (right). Dashed red bars correspond to Seine Aval WRRF only.

Nitrogen removal performance of tertiary nitrifying and denitrifying BAFs in France were reviewed by Rocher et al. (2012), based on 10 years of data from Seine Aval and Seine Centre WRRFs. The ammonium removal rate (AUR) is plotted against the ammonium load on Figure II.3-4.

According to this review, tertiary nitrifying BAFs were able to remove up to 100% of the applied load for ammonium loading rates below 1.1 – 1.2 kgN/m^3/d, resulting in low residual NH_4^+ concentrations. Aeration was around 100 – 150 $Nm^3/kgNH_4\text{-}N_{applied}$ to ensure proper nitrification. Based on Eq.1, the AUR corresponds to the nitrate production rate when there is limited accumulation of reaction intermediates. The nitrate removal efficiency in post-denitrifying BAF was almost higher that 85% for an applied nitrate load of 4 - 5 kgN/m^3/d, but was associated with nitrite accumulation (3 - 4 mgN/L). To ensure efficient removal and limited effluent NO_2^- concentration, it was suggested to limit the load to 2.5 kgN/m^3/d. These results were obtained under optimum denitrification conditions: the applied BOD to NO_3-N ratio was higher than 3.

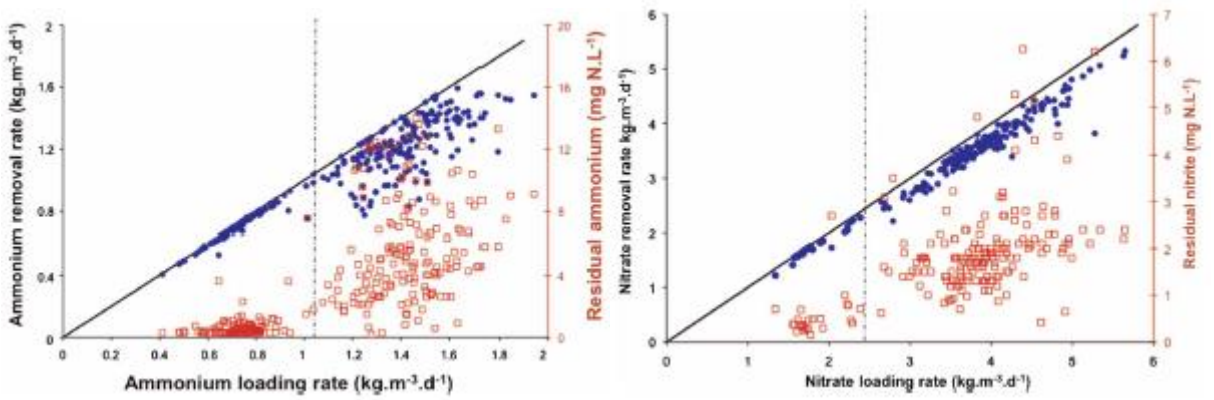

Figure II.3-4. Ammonium and nitrate removal rates against applied rates in Seine Centre and Seine Aval nitrifying and denitrifying BAFs, respectively. Source: Rocher et al. (2012).

II.3.3 N_2O EMISSIONS FROM NITRIFYING AND DENITRIFYING BAFS

N_2O emissions from BAFs have been investigated only recently based on full-scale monitoring (Bollon et al., 2016a, Bollon et al., 2016b, Wang et al., 2016) and controlled experiments (He et al., 2017a, He et al., 2017b).

Wang et al. (2016) monitored N_2O emissions from a full-scale nitrifying BAF in China over 12 months. The nitrifying BAFs were preceded by A^2/O tanks and a secondary clarifier, which provided low nitrogen concentrations at the inlet of the nitrification stage (approximately 0 – 6 $mgNH_4$-N/L, 5 – 15 $mgNO_3$-N/L and 0 – 0.8 $mgNO_2$-N/L). Low N_2O-EF (0.017 – 0.828% of the influent nitrogen load) were reported and explained by the very low ammonium load

applied (0.004 – 0.05 kgN/m^3/d). The authors mainly related N_2O emissions to high influent nitrite concentration events, and statistically demonstrated an absence of effect of other conditions (pH, temperature, influent NH_4^+, NO_3^- and DO) on N_2O emissions. Therefore, N_2O production was attributed to the ND pathway and the contribution of HD was considered negligible considering the high in-situ DO concentrations (> 6.9 mgO_2/L).

Nitrifying (Bollon et al., 2016b) and post-denitrifying (Bollon et al., 2016a) BAFs of the Seine Aval WRRF were monitored during two measuring campaigns: one week in summer (September 2014) and two weeks in winter (January/February 2015). The N_2O production factor of the nitrifying BAFs was twice as high in winter (4.86% of the NH_4-$N_{removed}$) compared to summer (2.26%). N_2O emissions were also highly dynamic over the campaigns: the daily average N_2O-EF fluctuated from 1.31 to 3.76% of the NH_4-$N_{removed}$. Based on a statistical analysis, N_2O production was negatively correlated to the influent temperature and positively to the influent NH_4^+ and NO_3^- concentrations, the influent flow rate, the filtration time and the airflow. However, the authors suggested that the negative influence of temperature was due to the higher nitrite concentration in the biofilm in winter, which is one of the main triggers of N_2O production (section II.1.2.1). Only 78% (in summer) and 64% (in winter) of the N_2O production was emitted in the system, which means that significant fractions of N_2O remained dissolved and entered the post-denitrification stage. Under non-limiting carbon addition (BOD/N ratio 3) conditions, the denitrifying BAFs consumed 93% of the influent N_2O flux, while net production of N_2O was observed during methanol dosage failures, i.e. at low BOD/N ratios.

Whereas the latter campaigns revealed that a large proportion of N_2O produced in nitrifying BAFs was reduced in subsequent denitrifying BAFs, it did not give any information on a possible contribution of HD to the net N_2O production within the nitrifying BAFs themselves. As mentioned in section II.1.2.7, He et al. (2017a) investigated N_2O emissions from lab-scale nitrifying BAFs submitted to different C/N ratios. The C/N ratio significantly impacted the biofilm composition: its thickness increased with increasing C/N. Moreover, DO concentrations –measured in the biofilm with micro-sensors– decreased with increasing thickness, due to diffusion limitations and possibly higher HD activity. The largest biofilm thickness also induced the largest DO concentration gradients within the biofilm. Nitrite and N_2O concentrations in the biofilm were highest for the lowest C/N ratio (2), which was expected. On the other hand, the high C/N ratio (8) did not result in the lowest NO_2^- and N_2O concentrations in the biofilm. These results suggest that both nitrifying and denitrifying biomasses can impact the net production of N_2O in nitrifying BAFs. This was, however, never investigated by isotopic analyses or demonstrated *via* modelling tools.

He et al. (2017b) investigated the impact of DO concentrations on N_2O production in a pilot aerated BAF fed with synthetic water (45 – 55 mgNH_4-N/L, 0 – 15 mgNO_3-N/L and 0 – 0.25 mgNO_2-N/L). DO was controlled at 2, 4 and 6 mgO_2/L in the bulk liquid of three separate reactors. The N_2O EFs varied between 1.14 and 2.56%, 0.41 and 1.33% and 0.24 and 0.71% at 2, 4 and 6 mgO_2/L, respectively. Based on micro-sensor measurements of nitrogen and DO concentrations within the biofilm, the authors revealed that the lowest applied DO induced the lowest NH_4^+ removal rate, the highest NH_4^+, NO_2^- (0.6 against 0.4 and 0.2 mgN/L) and lowest DO and NO_3^- concentrations in the biofilm. Moreover, the dissolved N_2O concentration increased over the biofilm depth (from 0.02 mgN/L at 0 µm to 0.10 mgN/L at 600 µm). Interestingly, at the highest applied DO concentration, dissolved N_2O was maximal at 0 µm (0.05 mgN/L) and decreased with biofilm depth (0.02 mgN/L at 500 µm). Based on these results, the increase of N_2O production with decreasing DO concentration in nitrifying BAFs was likely to be due to triggered ND. Again, no experimental evidence of the pathways contributions was proposed.

In lights of these results, modelling N_2O production from tertiary nitrifying BAFs would be of high interest to understand the effect of operating conditions on the respective contributions of N_2O production pathways and on possible interactions between nitrifying and denitrifying biomasses.

II.3.4 BAF MODELS FOR TERTIARY NITRIFICATION

II.3.4.1 PRESENTATION OF EXISTING MODELS

Nitrifying BAFs are submitted to contrasted conditions: continuous feeding with varying characteristics during the filtration cycle and intermittent liquid and air pulses during backwash events. Hydraulics, generally considered to be plug-flows (Mendoza-Espinosa and Stephenson, 1999a) lead to high concentration gradients over the bed height in the water phase, but also within the biofilm. The difficulty in modelling the functioning of nitrifying BAFs –and biofilm reactors in general– therefore comes from the combination of physical mechanisms (detachment, filtration, gas/liquid exchanges) and biological mechanisms, which conduct to large heterogeneities in such systems. Still, a few models have been proposed to describe the behaviour of pilot or full-scale nitrifying BAFs.

These models differ in their level of complexity and in modelling objectives, as summarized in Table II.3-1. These models are based on a one-dimensional description of the biofilm, either homogenous or heterogeneous (Figure II.3-5). Such simplified representation of the biofilm was found sufficient to answer most engineering questions (Boltz et al., 2010). The main issue so far was the prediction of nitrification and/or filtration performance. None of

the proposed models so far considered N_2O production during nitrification. Only the last model, developed by Bernier et al. (2014), was calibrated and validated on long-term data from full-scale nitrifying BAFs (Seine Aval WRRF). Moreover, this model is the most complete in terms of mechanisms included. In this model, the biofilm is considered heterogeneous, but discretized in two layers only, and its thickness varies with biomass growth and decay, filtration of solids and continuous detachment. The liquid phase behaviour is represented as a plug-flow: the reactor height is divided into seven reactors in series and exchanges between liquid compartments are convectional, while exchanges between biofilm layers are diffusional. This is a classical way to describe hydraulics in such systems (Mendoza-Espinosa and Stephenson, 1999a, Boltz and Daigger, 2010).

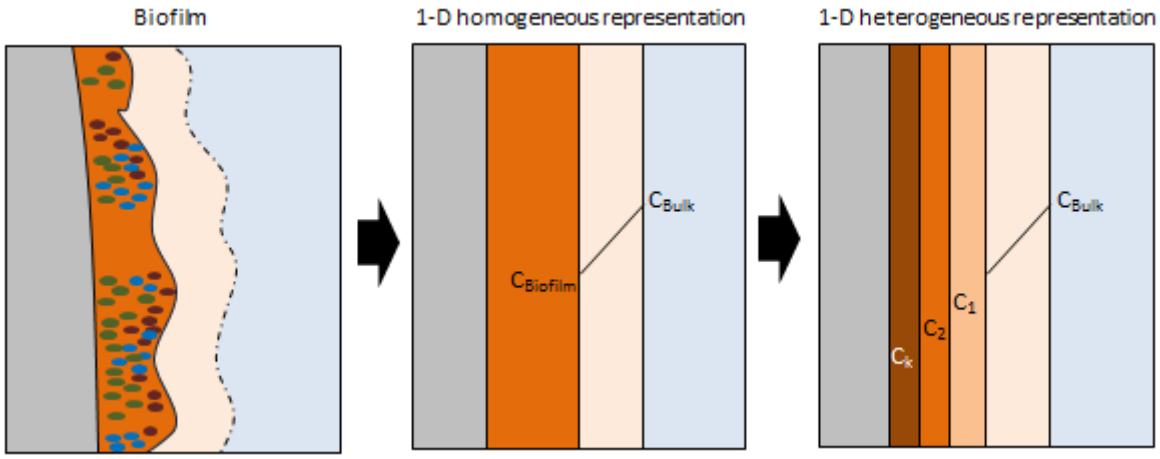

Figure II.3-5. A biofilm and its 1-D homogeneous and heterogeneous representation (Boltz and Daigger, 2010).

The mass transfer resistance between the bulk liquid and the biofilm is modelled by an external resistance L_L/D_W, where L_L is the liquid film thickness and D_W the diffusion coefficient of a given component in water. Although L_L was found to impact biofilm model predictions significantly, no consensus was found on its calculation (Boltz et al., 2010). Its value can be estimated based on empirical relations, applied by (Viotti et al., 2002) and (Vigne, 2007), but Bernier et al. (2014) used a constant value, which was justified by the fact that the actual value cannot be verified experimentally. Typical ranges of L_L estimated for BAFs were 75 – 140 µm depending on superficial liquid velocity and diffusion coefficients (Vigne, 2007, Rittmann et al., 2018). In some models, oxygen supply was represented in a simplified manner, assuming a constant and high DO concentration in the filter (Viotti et al., 2002, Vigne et al., 2010); in others the transfer model was considered to predict the variation of DO in the bulk liquid with the airflow rate (Bernier et al., 2014, Behrendt, 1999). Some simplifications were also considered by Bernier et al. (2014): the evolution of the gas phase composition was neglected, as it was not included as a proper compartment of the model.

II.3.4.2 PREDICTION OF N_2O EMISSIONS FROM NITRIFYING BIOFILMS

So far, N_2O production pathways were never included in a tertiary nitrifying BAF model, only in a post-denitrifying BAF model (Samie et al., 2011). However, N_2O production in nitrifying biofilms was evaluated in theoretical studies (Sabba et al., 2015, Sabba et al., 2017).

The biological mechanisms leading to N_2O production from biofilm systems are similar to suspended biomass reactors (low DO and high NO_2^- concentrations in particular) but the heterogeneous composition of the biofilm can lead to different N_2O production over the reactor for identical applied conditions (Sabba et al., 2018). Sabba et al. (2015) included the multiple-pathway model of Ni et al. (2014) to describe N_2O production by AOB in a pure AOB biofilm. Different biofilm thicknesses have been tested, the lowest (2 µm) meant to represent a suspended growth system, and different bulk DO conditions tested (0 – 4 mgO_2/L). For the same conditions applied, N_2O production from the 2-µm biofilm plateaued at a low value compared to other thicknesses tested. Thicker biofilms were moreover associated to higher N_2O production rates.

Considering a 100-µm biofilm, authors investigated the triggers of such N_2O production rates. They revealed that NH_2OH, produced in the outer zones of the biofilm were oxygen is available, could diffuse into deeper biofilm layers. Such zones are characterized by low DO concentrations; therefore, in the presence of NH_2OH, NO_2^- becomes the sole electron acceptor (instead of oxygen in the outer zones), producing high amounts of N_2O by ND (Figure II.3-6). In a complementary study coupling AOB and NOB, Sabba et al. (2017) suggested that the presence of NOB would increase competition for O_2, leading to O_2 gradients in the biofilm, inducing higher N_2O production rates. However, the authors did not include heterotrophic bacteria, which could reduce N_2O in such anoxic zones.

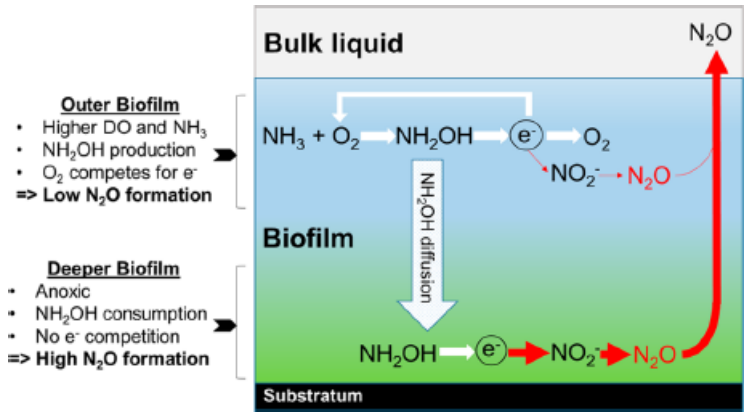

Figure II.3-6. N_2O production in a nitrifying biofilm. Source: Sabba et al. (2015).

Table II.3-1. Summary of nitrifying BAF models developed at pilot and full-scales.

Study	Objective	Mechanisms	Biofilm model	Calibration / validation
Behrendt (1999)	Describe nitrification in a pilot BAF	✓ 2-step nitrification ✓ Gas-liquid transfer	✓ 1-D heterogeneous	✓ NH_4^+ concentration gradients ✓ Effluent ammonium concentrations
Le Tallec et al. (1999)	Describe TSS removal and headloss from pilot and full-scale BAFs	✓ Headloss	✓ 1-D homogeneous ✓ Filtration	✓ Effluent TSS concentration ✓ Headloss
Viotti et al. (2002)	Describe nitrification and headloss in a full-scale BAF	✓ COD and ammonium removal ✓ Headloss ✓ Gas-liquid transfer ✗ Constant liquid DO	✓ 1-D homogeneous ✓ Biomass growth	✓ NH_4^+ and COD concentration gradients ✓ Effluent NH_4^+ and COD concentrations ✓ Headloss
Vigne et al. (2007)	Describe nitrification and headloss from a pilot tertiary nitrifying BAF	✓ 1-step nitrification + 1-step HD ✓ Backwashing ✓ Headloss ✗ No gas-liquid exchanges	✓ 1-D heterogeneous ✓ Filtration + detachment ✓ Biomass growth	✓ Effluent NH_4^+, NO_3^- and TSS concentrations ✓ Headloss
Bernier et al. (2014)	Describe nitrification and headloss from full-scale tertiary nitrifying BAFs of Seine Aval WRRF	✓ 2-step nitrification + 2-step HD ✓ Backwashing ✓ Headloss ✓ Gas-liquid exchanges of O_2 ✗ Constant gas composition	✓ 1-D heterogeneous ✓ Filtration + detachment ✓ Biomass growth	✓ Concentration gradients ✓ Long-term effluent concentrations ✓ Long-term headloss

N_2O emissions from biofilm reactors have been reviewed by Todt and Dorsch (2016) and Sabba et al. (2018). According to these studies, the main conditions leading to N_2O production are: deep anaerobic zones where low DO concentrations trigger N_2O production by ND or incomplete HD, especially if reaction intermediates are present (NH_2OH, NO_2^-); conditions leading to high reaction rates, which induce transient accumulation of reaction intermediates, which can moreover diffuse to low DO zones; limiting electron donors for HD, which favour N_2O production over its reduction. On the other hand, low DO zones where carbon is non-limiting for HD can act like sinks of N_2O produced by AOB.

- Biofilm systems are characterized by high biomass concentrations and stratifications;
- N_2O emissions measured on nitrifying BAFs are high compared to French CAS processes;
- If a few nitrifying BAF models have been developed, N_2O production pathways and emissions were never included;
- A correct prediction of N_2O from these systems will require a proper prediction of biological pathways, but also of the biofilm representation and mass transfer conditions.

II.4 SYNTHESIS OF THE BIBLIOGRAPHIC STUDY

Studies dedicated to N_2O production from WRRFs have proliferated these last 20 years, as BNR systems have been found hotspots of N_2O emissions, a powerful greenhouse gas and an ozone depleting substance. It is a by-product of nitrification and an intermediate of heterotrophic denitrification, mainly produced and emitted in aerated zones in low DO and/or high nitrite conditions. While heterotrophic denitrification was reported to act like a sink of N_2O in optimum COD/N conditions, it can also produce N_2O in large amounts in case of DO control or carbon dosage failures. Such observations led to the development of numerous models, from the simplest ones considering only one production pathways, to more complex ones coupling multiple nitrification pathways and heterotrophic denitrification. Indeed, nitrifying and denitrifying bacteria generally cohabit in BNR systems and contribute in various proportions to the net N_2O production. One remaining issue is the identification of model parameters, as nitrification and denitrification share several reaction intermediates.

Most studies so far were dedicated to suspended-growth systems and very little to biofilm systems, while these are becoming increasingly popular for their reliability and compactness. In France, one type of biofilm systems, BAF, is widely used and treats an important fraction

of the total load of French WRRFs. More specifically, the Seine Aval WRRF treats 40% of the Parisian load and operates nitrifying and denitrifying BAFs. Recent measuring campaigns on this plant reported high N_2O emission factors compared to conventional low loaded suspended growth systems. These emissions were highly variable seasonally and diurnally in relation to applied conditions. Developing models to understand the triggers of N_2O production from such systems and define mitigation strategies is therefore needed. However, biofilm reactors are complex systems submitted to high concentration gradients and models describing the functioning of nitrifying BAFs are still scarce. In fact, N_2O production from tertiary nitrifying BAF was never simulated, let alone at full-scale.

In this work, N_2O production pathways by AOB and OHO will be included in a tertiary nitrifying BAF model to describe N_2O production and emission from the Seine Aval WRRF. The model developed by Bernier et al. (2014) was chosen to implement N_2O production pathways according to Pocquet et al. (2016) and Hiatt and Grady (2008). According to previous modelling studies, heterotrophic denitrification can affect the net N_2O production even in apparent nitrifying conditions, which is why it was included. This model will be calibrated on data from the Seine Aval WRRF and used to get an insight into the triggers of N_2O production in full-scale nitrifying BAF. Lab-scale experiments will moreover be performed to assess the respective contributions of N_2O production pathways and possibly validate model predictions. Finally, the current method to quantify N_2O emissions from full-scale WRRFs lacks accuracy and possibly underestimates the contribution of WRRF to the global carbon balance. This model could serve as an alternative tool to estimate N_2O emissions from nitrifying BAFs.

Chapter III. Material and methods

III.1 GENERAL PRESENTATION

The material and methods presented here and their associated thesis chapters are presented in Figure III.1-1. They can be divided into two main objectives:

1- The development of the tertiary nitrifying BAF model able to describe N_2O production in the full-scale BAFs of the Seine Aval WRRF;
2- The better understanding of the N_2O production from nitrifying BAFs through interpretation of modelling results and lab-scale experiments.

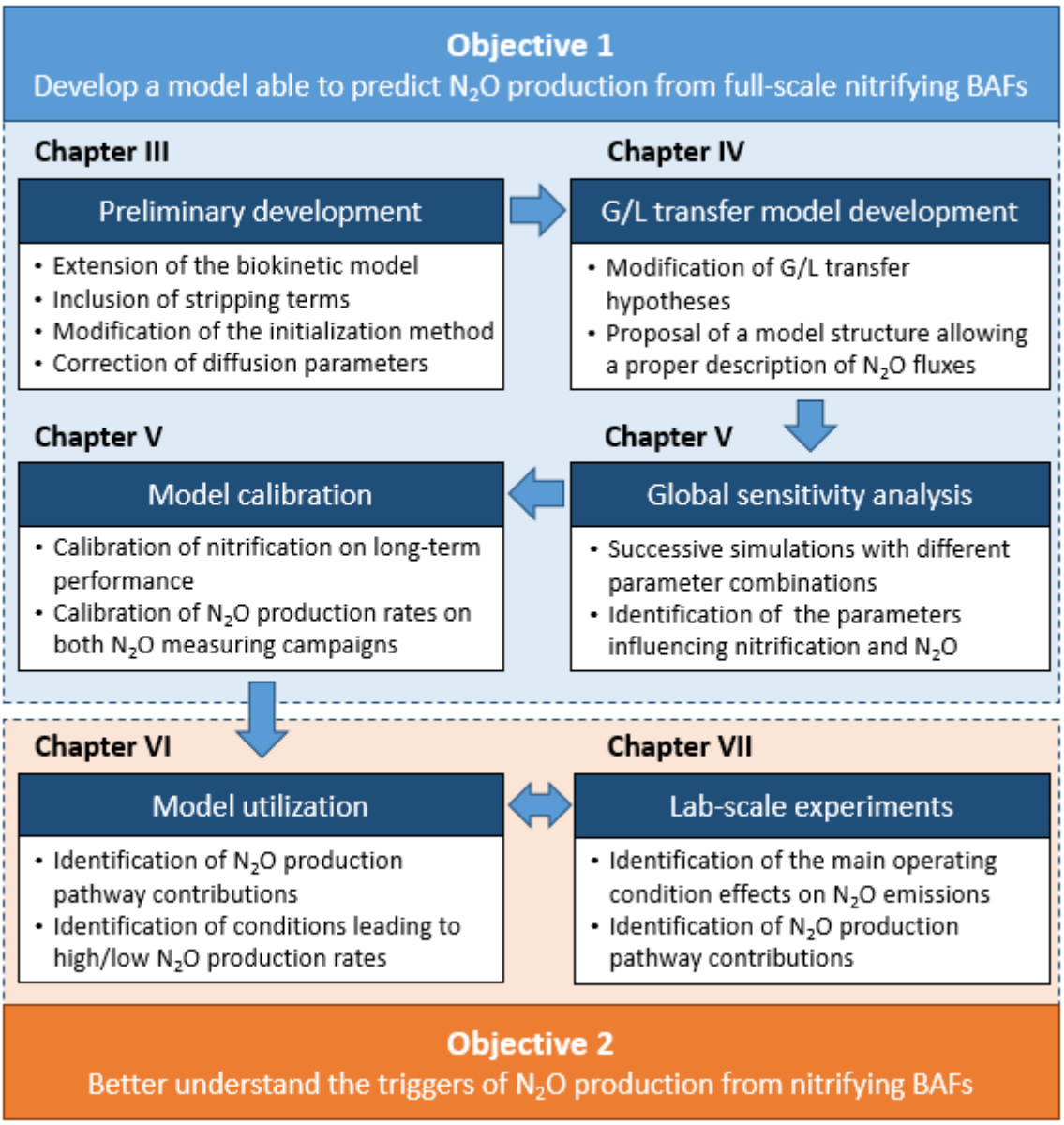

Figure III.1-1. General presentation of the methods and associated objectives.

III.2 FULL-SCALE DATA FROM SEINE AVAL NITRIFYING BAFS

III.2.1 DESCRIPTION OF THE SEINE AVAL WRRF AND ITS NITRIFYING BAFS

The Seine Aval wastewater resource recovery facility (WRRF), which is the largest plant in Europe, is managed by the French Interdepartmental Syndicate for Sanitation of the Paris conurbation (SIAAP). Seine Aval WRRF is situated in the municipality of Achères (Yvelines department - 78) and was designed to treat about 1 700 000 m^3/d, which corresponds to approximately 5.5 million people equivalents (PE).

The layout of the water line during the simulated period is schematized on Figure III.2-1. The arriving flow undergoes conventional initial treatment phases, with a pre-treatment stage comprising screening, grit and oil removal. It is followed by primary settlement to remove suspended solids before entering the secondary treatment stage. The latter is designed for carbon removal and is composed of high loaded conventional activated sludge lines (9 aerated biological reactors combined with 25 secondary settling tanks). Then, the water enters a coagulation / flocculation process with lamella settling to mainly remove suspended solids and phosphorus. Finally, nitrogen is eliminated in the tertiary treatment stage which is composed of 84 nitrifying Biostyr® filters and 18 Biostyr® and 12 Biofor® post-denitrifying filters using methanol as external carbon source.

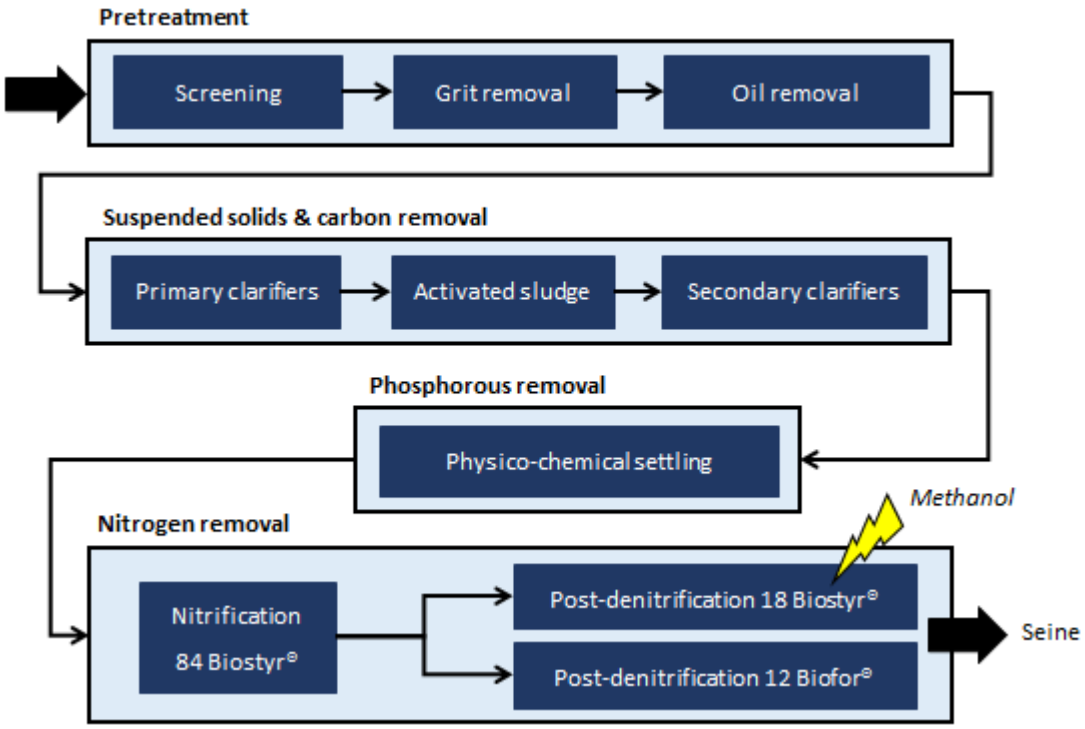

Figure III.2-1. Layout of Seine Aval WRRF water line during the simulated period.

Nitrification is performed in 84 Biostyr® units (Veolia Water Technology), which are divided into six batteries (A1, A2, B1, B2, C1, and C2). During wastewater treatment, these units are operated in co-current upflow configuration (Figure III.2-2). They are filled with 4-mm polystyrene beads on which the biofilm develops. A single filter is characterized by its 173 m^3 surface and its maximum 3.5 m bed height. Some beads can leave the filter during backwash events, resulting in a regular decrease of the bed height, which calls for occasional refilling of the filter. During the campaigns performed by Irstea (section III.2.2), the measured bed height of the studied filter was 2.95 m in summer (and evaluated to be 3.35 m in winter). The maximum active volume of a filter, located between two water zones, is 606 m^3.

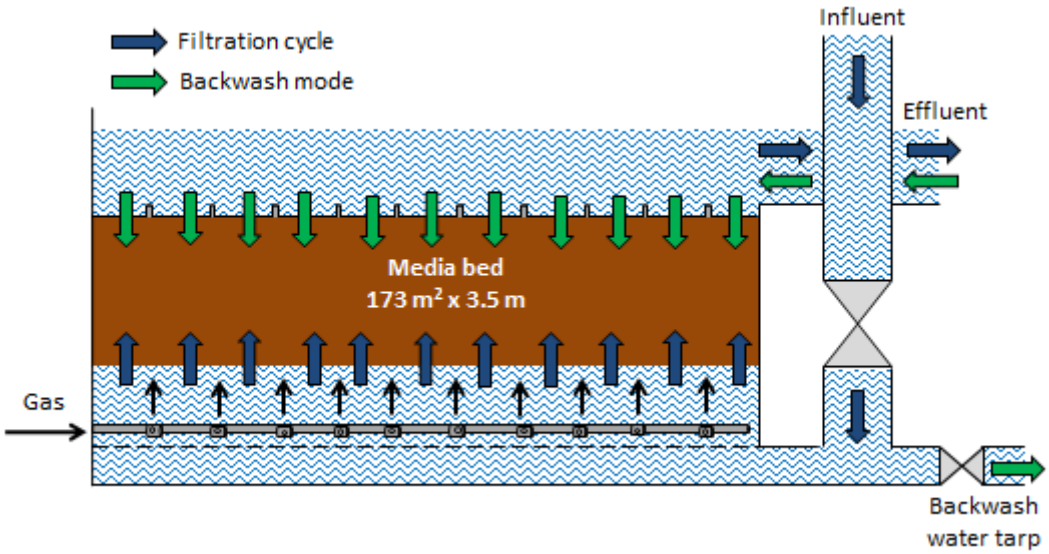

Figure III.2-2. Schematic representation of a nitrifying filter of Seine Aval WRRF.

Aeration is controlled on each battery based on three measurements: the influent and effluent ammonium (NH_4^+) concentrations, and the influent flowrate. It is automatically controlled in order to supply sufficient oxygen for nitrification, in practice between 100 and 150 $Nm^3/kgNH_4\text{-}N_{applied}$ (Rocher et al., 2012). Over a filtration cycle, the filtering bed gets clogged by suspended solids and the biofilm growth, which results in an increase of headloss. In Seine Aval, a filter goes to backwash mode every 24 h on average (23.6 and 21.1 h during the summer and winter campaigns presented in section III.2.2). It consists in successive air and water pulses in counter-current direction. Water first drops from the effluent channel to expand the media bed and is extracted in a common water tarp for all BAFs of the battery. Air is then pulsed, in cycles, at high rates to loosen the bed and to remove particles accumulated in the media. It also helps to partially mix the filter media (Vigne et al., 2011). These cycles last 30 minutes and enable a return to the initial headloss of a filter. A filter can also be stopped during maintenance, or when the influent flow rate reaches a given set-point below which the low velocity causes faster clogging.

III.2.2 DATA COLLECTION AND PROCESSING

III.2.2.1 DATA COLLECTION

The data used for modelling combined supervision and operational data over three years (2014 to 2016, 1 095 days) provided by the SIAAP, and data measured by Irstea on a single filter (called "JNB27" of battery B2) over two campaigns in 2014 and 2015. The locations of flow meters, sensors and samplers are schematized on Figure III.2-3.

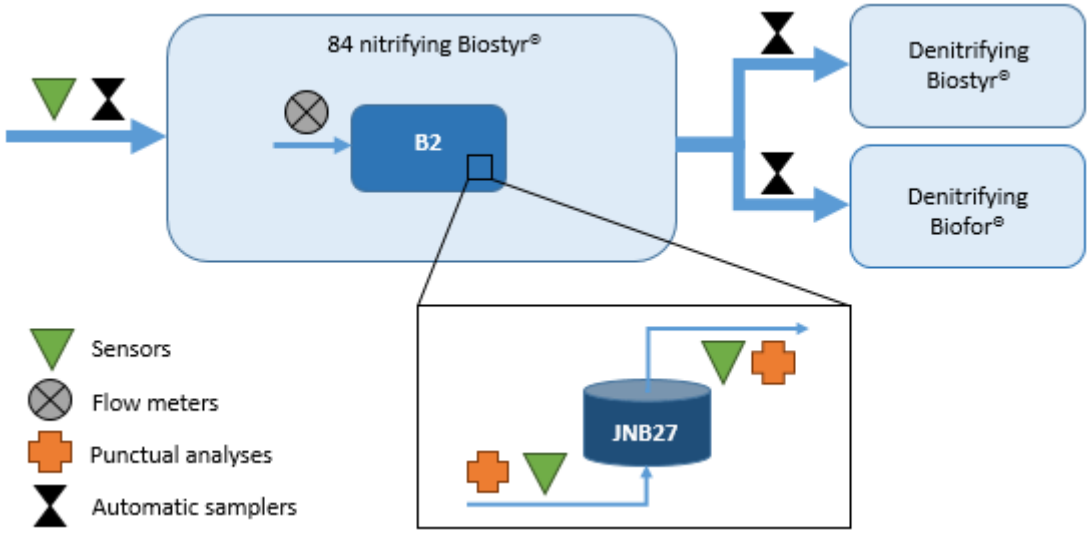

Figure III.2-3. Schematic representation of all data collected for the modelling work.

Data used in the thesis are summarized in Table III.2-1. Different datasets were used according to the modelling objectives. To ensure the proper functioning of the nitrifying BAFs, water characteristics are analysed on a daily basis at Seine Aval. Refrigerated automatic samplers are installed at the inlet of the nitrification stage and at the inlet of each denitrification line. Temperature and pH sensors are also installed at the inlet of the nitrification stage. Liquid and air flow rates are measured by flow meters at the inlet of each battery.

The N_2O measuring campaigns were performed by Irstea in a previous project (Bollon et al., 2016b). Gaseous samples were collected in the middle of the overflow of a single filter of the battery B2 (JNB27) over two periods. The first, later called "summer campaign", occurred in September 2014 (days 257 to 264). The second, called "winter campaign", occurred in January / February 2015 (days 390 to 404). Data used for modelling included: online measurements of inlet NH_4^+ and NO_3^-, outlet NH_4^+, NO_3^-, DO, pH, temperature, and outlet dissolved N_2O (measured every minute in the water zone above the media, called the overflow). One-off measures of effluent NO_2^- concentration were also performed to assess

its variability. For information on the analysers and sensors, please refer to Bernier et al. (2014) and Bollon et al. (2016b).

Table III.2-1. Type of data used for modelling, frequency of measurements.

	Measurement	Type / frequency	Duration (days)
Nitrification	Influent composition (NH_4^+, NO_3^-, NO_2^-, TSS, COD, PO_4^{3-})	Automatic sampler (24 h)	1 095
	Influent pH and temperature	Sensor (24 h)	1 095
	Influent and air flow rates Number of filters in activity	Flow meter (24 h)	1 095
Denitrification lines	Influent composition (NH_4^+, NO_3^-, NO_2^-, TSS, COD, PO_4^{3-}, DO)	Automatic sampler (24 h)	1 095
Battery B2	Influent and air flow rates Number of filters in activity	Flow meter (24 h)	1 095
	Influent and air flow rates Number of filters in activity	Flow meter (1 min)	21
Filter JNB27	Influent composition (NH_4^+ and NO_3^-) pH and temperature	Sensor (1 min)	21
	Effluent composition (NH_4^+, NO_3^-, DO, N_2O)	Sensor (1 min)	21
	Influent & effluent compositions (NO_2^-, TSS, COD, PO_4^{3-}, N_2O)	Automatic sampler (24 h)	21
	Off-gas N_2O concentration	(1 min)	21
	Filtration time, backwash activation time	(1 min)	21

III.2.2.2 DATA ANALYSIS AND PROCESSING

III.2.2.2.1 DATA FROM 2014 - 2016

Wastewater characteristics measured at the inlet of the nitrification stage, from January 1st 2014 to December 31th 2016, are summarized in Table III.2-2 (daily average concentrations). The nitrification stage stopped functioning from October 20th to December 7th 2015 (with no filter in activity), which explained most missing values (14%). The rest of the missing values were due to occasional lack of measurements. Missing values generated computational issues on the used Matlab scripts. They were therefore replaced by the average of the previous and following days. Influent characteristics considered for modelling (processed data) are presented in Table III.2-2.

Table III.2-2. Raw and processed influent composition of the nitrification stage in 2014-2016.

n = 1095		NH_4^+ mgN/L	NO_3^- mgN/L	NO_2^- mgN/L	TSS mg/L	COD Nm/L	PO_4^{3-} mgP/L
Raw data	Mean	30.4	5.4	0.78	41	77	0.58
	St. dev	6.4	2.1	0.61	18	18	0.42
Processed data	Mean	29.6	5.6	0.79	39	75	0.60
	St. dev	6.1	2.0	0.51	15	17	0.41

Effluent characteristics of the nitrification stage are summarized in Table III.2-3. Only characteristics of the Biostyr® denitrification line were used because they were more frequent. Raw data are directly presented, as no outlier was detected. Moreover, missing values due to the stop of the nitrification stage or absence of measurements (14%) do not cause problem as they were not used in Matlab scripts (outlet data).

Table III.2-3. Effluent characteristics of the nitrification stage in 2014-2016.

n = 1095	NH_4^+ mgN/L	NO_3^- mgN/L	NO_2^- mgN/L	TSS mg/L	COD mg/L	PO_4^{3-} mgP/L
Mean	4.3	29.3	0.67	13	47	0.59
St. dev	1.9	5.6	0.28	5	8	0.43

Liquid and air flow rates (Q_L and Q_G) were calculated for a given filter of the nitrification stage in operation and of battery B2. Basically, they were estimated by dividing the corresponding flow rate (either at the inlet of the nitrification stage or at the inlet of the battery B2) by the number of active filters. Flow rates calculated from the raw data are presented in Table III.2-4. Data from battery B2 were only used from January 1st 2014 to October 6th, i.e. before the nitrification stage stop. Consequently, average flow rates of battery B2 were calculated on this period only (n = 643). Only few missing values were observed for liquid and air flow rates (0 – 7%, respectively). To avoid computational issues on Matlab, an interpolation based on the data from the previous and following days was used to replace these missing values. Values after processing are presented in Table III.2-4.

Table III.2-4. Raw and processed liquid and air flow rates data of nitrification and battery B2.

		Nitrification (n = 1095)			Battery B2 (n = 643)		
		Q_L m^3/d	Q_G Nm^3/d	Filters in activity	Q_L m^3/d	Q_G Nm^3/d	Filters in activity
Raw data	Mean	23 055	57 900	59	21 969	55 977	10
	St. dev	5 745	17 298	18	7 980	19 932	4
Processed data	Mean	23 403	60 057	-	23 653	60 502	-
	St. dev	4 873	10 470	-	5249	13 379	-

III.2.2.2.2 DATA FROM N_2O MEASURING CAMPAIGNS

Data from the N_2O measuring campaigns presented in this work are different from the original publication (Bollon et al., 2016b) for three reasons:

1- Influent interruptions during backwashing periods were not considered, in order to avoid computational issues. During these 30 min backwash events, the filter was considered to be operated at average influent flow rates and concentrations from the previous hour.
2- During both campaigns, emitted N_2O fluxes were measured at the centre of the filter. Occasional measurements of the airflow rate at different positions of the filter's surface revealed that its value was on average 1.147 and 1.085 times the airflow rate applied to the reactor (Figure III.2-4), revealing a heterogeneous axial distribution of the air. Thus, the measured gas N_2O concentrations and fluxes were recalculated to correspond to reactor values (multiplied by 1.147 and 1.085 in summer and winter, respectively).
3- The summer campaign was marked by a filter stop of five hours. To avoid computational issues, liquid and air flows were calculated as an interpolation between previous and following values.

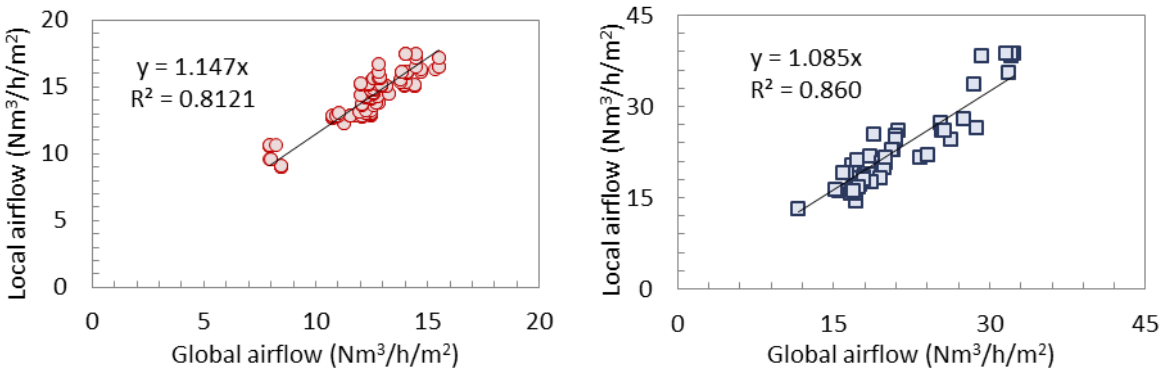

Figure III.2-4. Superficial gas velocity measured by Irstea under the floating hood against exploitation data in summer (left) and winter (right).

Influent & effluent compositions and N_2O measurements of the filter JNB27 over the two campaigns are presented in Table III.2-5 and Table III.2-6 respectively (10-min averages, except for influent and effluent NO_2^-, PO_4^{3-}, TSS and COD concentrations).

The ammonium uptake rate (AUR, kgN/d) was calculated from the effluent and influent NH_4^+ concentrations multiplied by the liquid flowrate (Eq.13). The N_2O production rate (N_2O-PR, kgN/d) was the sum of dissolved and gaseous N_2O production rates (Eq.14), while the N_2O emission rate (N_2O-ER, kgN/d) was only the gaseous part of it (Eq.15). The N_2O production and emission factors (N_2O-PF and N_2O-EF) were respectively the N_2O production and emission rates divided by the AUR (Eq.16 and Eq.17).

Eq.13 $$\mathrm{AUR} = (\mathrm{C}_{\mathrm{NH}_4^+,\mathrm{L,in}} - \mathrm{C}_{\mathrm{NH}_4^+,\mathrm{L,out}})\mathrm{Q}_\mathrm{L}/1000$$

Eq.14 $$\mathrm{N_2O-PR} = (\mathrm{C}_{\mathrm{N_2O,G,out}}\mathrm{Q}_\mathrm{G} + \mathrm{C}_{\mathrm{N_2O,L,out}}\mathrm{Q}_\mathrm{L})/1000$$

Eq.15 $$\mathrm{N_2O-ER} = \left(\mathrm{C}_{\mathrm{N_2O,G,out}}\mathrm{Q}_\mathrm{G}\right)/1000$$

Eq.16 $$\mathrm{N_2O-PF} = \mathrm{N_2O-PR/AUR}$$

Eq.17 $$\mathrm{N_2O-EF} = \mathrm{N_2O-ER/AUR}$$

Where $C_{NH4+,L,in}$ and $C_{NH4+,L,out}$ are the influent and effluent ammonium concentrations, respectively (gN/m^3), Q_L the influent flowrate (m^3/d), Q_G the air flowrate (Nm^3/d), $C_{N2O,G,out}$ and $C_{N2O,L,out}$ the effluent gaseous and dissolved N_2O concentrations, respectively (gN/m^3).

Table III.2-5. Influent composition at the inlet of the filter JNB27 in summer and winter campaigns (10-min averages).

	Q_L	Q_G	NH_4^+	NO_3^-	T	pH	NO_2^-	PO_4^{3-}	TSS	COD	U_G	U_L	Applied NH_4^+ load
	m^3/d	Nm^3/d	mgN/L		°C	-	mgN/L	mgP/L	mg/L	mg/L	Nm^3/h	m^3/h	$kgN/m^3/d$
Summer campaign (n = 1 008)													
Mean	19 613	50 139	38.1	1.4	22.5	7.0	0.56	0.83	43	99	13.7	4.8	1.25
St. dev.	5 318	15 461	3.3	0.7	0.4	0.1	0.27	0.28	19	43	4.1	1.3	0.36
Winter campaign (n = 2 016)													
Mean	20 157	51 333	34.8	2.5	14.5	7.5	0.19	0.51	35	107	12.4	4.9	1.14
St. dev.	4 919	15 309	5.1	0.5	0.9	0.4	0.04	0.17	8	13	3.7	1.2	0.25

Table III.2-6. N_2O emissions and effluent composition at the outlet of the filter JNB27 in winter campaign.

	NH_4^+	NO_3^-	NO_2^-	COD	TSS	PO_4^{3-}	DO	N_2O-PR	N_2O-ER	N_2O-PF	N_2O-EF	Emitted / produced N_2O
	mgN/L	mgN/L	mgN/L	mg/L	mg/L	mgP/L	mgO_2/L	kgN/h	kgN/h	%	%	%
Summer campaign (n = 1 008)												
Mean	5.6	29.2	0.25	48	13	0.93	5.6	0.72	0.61	2.7	2.3	82
St. dev.	3.0	3.9	0.09	7	6	0.34	0.5	0.25	0.23	0.8	0.8	4
Winter campaign (n = 2 016)												
Mean	5.7	27.7	0.64	56	14	0.48	7.1	1.26	0.84	5.4	3.6	66
St. dev.	2.2	4.8	0.24	12	4	0.18	0.6	0.24	0.20	0.8	0.8	9

III.2.2.3 DATA USED FOR MODELLING

The different modelling steps and associated datasets are summarized on Figure III.2-5. The operating conditions of the nitrifying BAFs during the winter campaign, used for gas-liquid mass transfer model development (Chapter IV), were already described in the previous section (III.2.2.3.3). In this section, the data used for preliminary model development, sensitivity analysis and model calibration are presented.

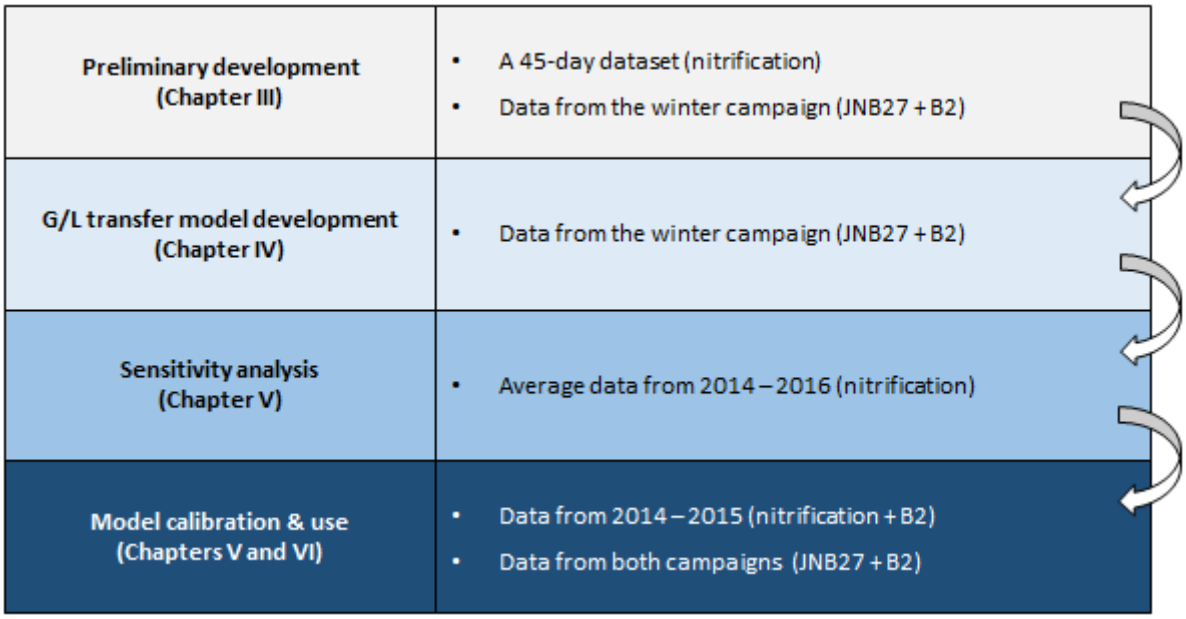

Figure III.2-5. Modelling steps and associated datasets used to compute/evaluate the model.

III.2.2.3.1 PRELIMINARY DEVELOPMENT ON A 45-DAY DATASET

A 45-day dataset from the Seine Aval nitrifying BAFs was furnished by the SIAAP for preliminary model development. It was used to compare the predictions of the extended model (extended biokinetic model, gas stripping added for N_2O, NO and N_2, explained in section III.3) to the initial model. Input and output characteristics (daily averages) are presented in Table III.2-7 and Table III.2-8.

Table III.2-7. Daily average inputs of the 45-day dataset (n = 45).

	Q_L	Q_G	NH_4^+	NO_3^-	NO_2^-	COD	TSS	PO_4^{3-}	T
	m^3/d	Nm^3/d	mgN/L	mgN/L	mgN/L	mg/L	mg/L	mgP/L	°C
Mean	25 273	78 012	35.4	4.6	0.66	77	31	0.49	17.3
St. dev.	5 347	17 816	6.6	1.2	0.45	10	14	0.20	0.8

Table III.2-8. Daily average outputs of the 45-day dataset (n = 45).

	NH_4^+ mgN/L	NO_3^- mgN/L	NO_2^- mgN/L	COD mg/L	TSS mg/L	PO_4^{3-} mgP/L
Mean	5.1	32.3	0.59	61	19	0.47
St. dev.	2.2	5.6	0.23	11	7	0.19

III.2.2.3.2 SENSITIVITY ANALYSIS: DATA FROM 2014-2016

The global sensitivity analysis was performed with average input data of the nitrification stage in 2014-2016 (Table III.2-2 and Table III.2-4). The objective was to assess the sensitivity of nitrification and N_2O predictions to model parameters under average operating conditions. It should be noted that the influent NH_4^+ concentration was lower than during the measuring campaigns, but the influent flow rate was higher, resulting in similar loads. The air supply was slightly higher (84 $Nm^3/kgNH_4\text{-}N_{applied}$ against 67 in summer and 74 in winter). However, these values remained within the usual operational range observed in 2014 and 2016.

III.2.2.3.3 CALIBRATION: DATA FROM 2014-2015 AND N_2O CAMPAIGNS

Model calibration was performed for the long-term prediction of nitrification over 2014-2015 and the prediction of N_2O fluxes during both campaigns. Data from 2016 were not simulated, because of the long nitrification stop. Therefore, the long-term dataset only included data from January 1st 2014 to October 6th 2015 (643 days). Since the campaigns were performed during these two years, their data were directly included in the long-term dataset (Figure III.2-6). During the campaign periods, input data were averaged over 10 minutes (presented in Table III.2-5); otherwise, they were daily data.

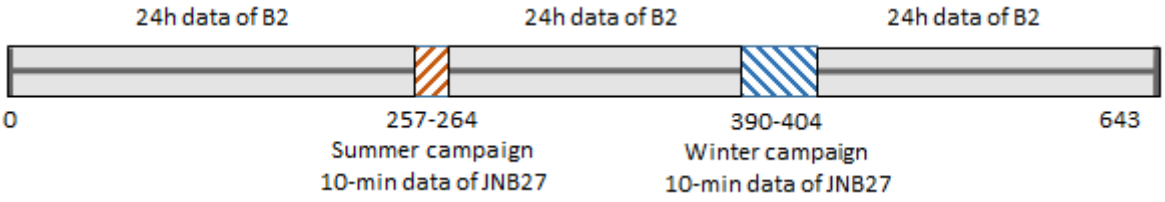

Figure III.2-6. Data used for model calibration.

To ensure consistency in the origin of the data between the 2014-2015 period and the N_2O measuring periods, it was decided to use liquid and air flow rates of battery B2 to simulate the functioning of the nitrification stage (using output data from the nitrification stage). Thus, a similar air and water distribution among all batteries was assumed.

This was verified by comparing the specific functioning of battery B2 to that of the nitrification stage in 2014-2015 (Figure III.2-7). On average, influent and air flow rates of an active filter of B2 were 23 653 ± 5 249 m^3/d and 60 502 ± 13 379 Nm^3/d, respectively. These are similar to the rates of an active filter of the nitrification stage (23 641 ± 5 175 m^3/d and 61 084 ± 11 189 Nm^3/d). Consequently, it was concluded that flow rates from battery B2 could be used to simulate the long-term period.

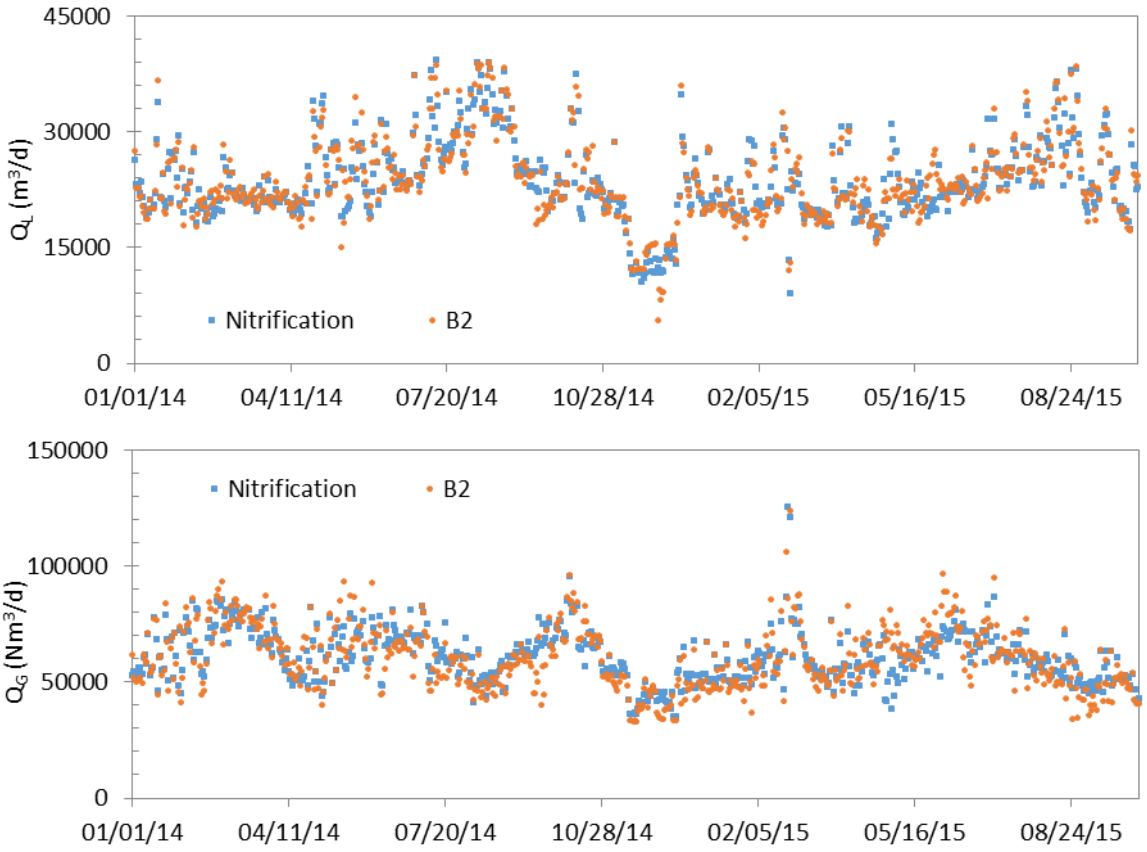

Figure III.2-7. Daily variations of liquid (Q_L) and air (Q_G) flow rates for an active filter of the nitrification stage and of battery B2 over 2014-2015.

The daily average influent and effluent characteristics of the nitrifying BAFs over 2014-2015 are presented in Table III.2-9 and Table III.2-10, respectively. Influent water was supposed to be homogeneous, and therefore the characteristics measured at the inlet of the nitrification stage were supposed to be those of a given filter.

Table III.2-9. Daily average inputs of nitrifying BAFs in 2014-2015 (n = 643).

	Q_L	Q_G	NH_4^+	NO_3^-	NO_2^-	COD	TSS	PO_4^{3-}	T
	m^3/d	Nm^3/d	mgN/L	mgN/L	mgN/L	mg/L	mg/L	mgP/L	°C
Mean	23 653	60 502	30.1	5.6	0.75	75	39	0.68	19.2
St. dev.	5 249	13 379	6.5	2.0	0.49	16	16	0.44	2.9

Table III.2-10. Daily average outputs of nitrifying BAFs in 2014-2015 (n = 643).

	NH_4^+	NO_3^-	NO_2^-	COD	TSS	PO_4^{3-}
	mgN/L	mgN/L	mgN/L	mg/L	mg/L	mgP/L
Mean	4.2	29.6	0.65	48	13	0.69
St. dev.	1.8	5.7	0.26	8	5	0.46

Concentrations measured at the inlet of the Biofor® and Biostyr® post-denitrification lines were compared (nitrogen concentration are represented on Figure III.2-8). They were very similar, except for the NO_2^- concentrations. Since more data were available for the Biostyr® line, these water characteristics were used as effluent data to evaluate model predictions of the nitrification stage.

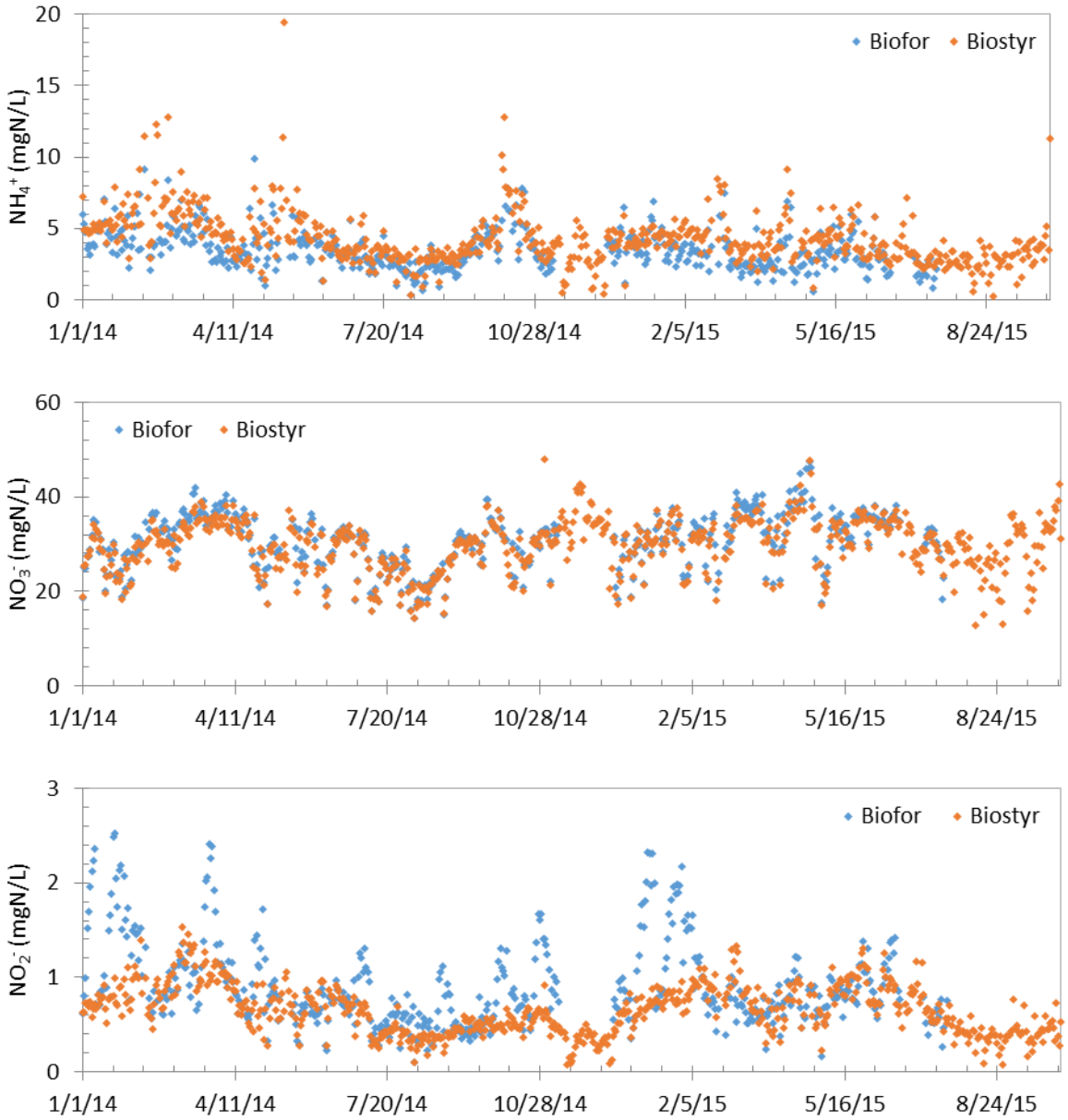

Figure III.2-8. Daily average nitrogen concentrations measured at the inlet of each denitrification line.

Effluent NO_2^- concentrations measured on the filter JNB27 and measured at the effluent of the nitrification stage (Biostyr® denitrification line) were compared (Figure III.2-9). Concentrations measured on the filter were lower than those measured on the nitrification stage (0.25 ± 0.09 against 0.46 ± 0.05 mgN/L in summer, 0.64 ± 0.24 against 0.83 ± 0.12 mgN/L in winter) but remained in the same order of magnitude. Moreover, they agreed on the observed increase of effluent NO_2^- concentrations between summer and winter.

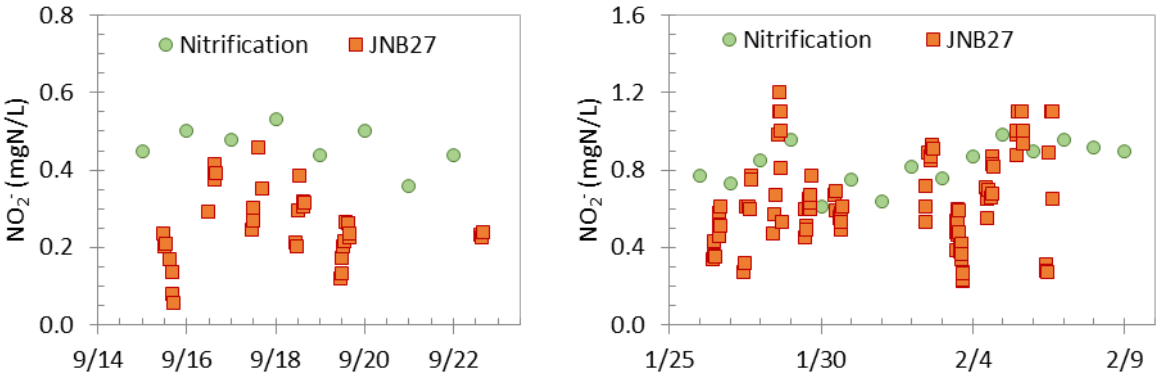

Figure III.2-9. NO_2^- concentrations measured at the outlet of the filter JNB27 and daily samplings of the inlet of post-denitrifying Biostyr® in summer (left) and winter (right).

III.3 MODEL DEVELOPMENT

III.3.1 PRESENTATION OF THE BASE MODEL

The model developed in the thesis was based on an existing one, built on the Simulink toolbox of Matlab (Bernier et al., 2014). It was designed to describe the long-term nitrification performance of tertiary nitrifying Biostyr® filters of the Seine Aval WRRF. Using data from 2009 to 2010, the model was calibrated and validated on: (1) effluent NH_4^+, NO_3^-, NO_2^-, COD, TSS concentrations of the nitrification stage and head loss data, (2) nutrient concentration gradients within the filters' height (Bernier et al., 2014).

Briefly, hydrodynamics was described by a series of seven CSTR (continuously stirred-tank reactors) of equal volume, representing the "active zone" where biological conversions occurred (Figure III.3-1). Each given reactor is composed of a biologically inactive bulk liquid compartment, an inert media volume, and two biofilm layers. The biofilm model included soluble material diffusion, biofilm growth and particulates exchange between biofilm layers as well as attachment and detachment. On top of the active zone, an additional CSTR representing the overflow was implemented. Because it has low biomass concentrations (only resulting from the detachment of particles), it was considered as "passive".

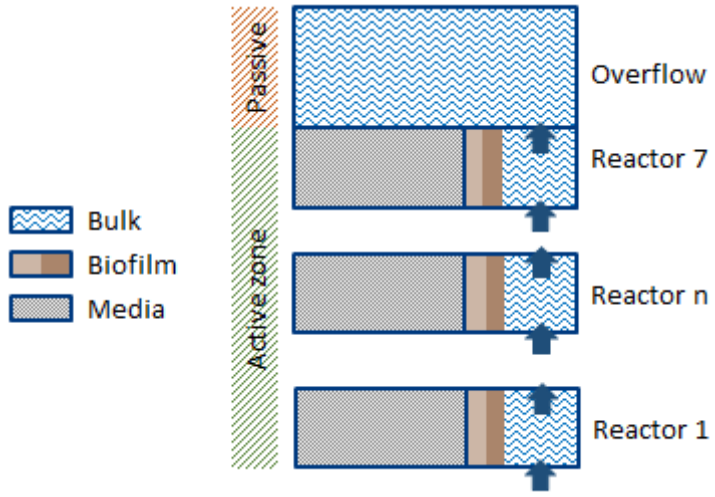

Figure III.3-1. Simplified representation of the BAF model compartments.

Biokinetic reactions were computed within the two biofilm layers. A simplified representation of nitrification-denitrification reactions considered in the base model is displayed on Figure III.3-2. The initial biokinetic sub-model was a modified version of the Activated Sludge Model n°1 (ASM1) proposed by (Henze et al., 1987). Nitrification was described as a two-step reaction: the oxidation of NH_4^+ to NO_2^- by ammonium oxidizing bacteria (AOB), followed by the oxidation of NO_2^- to NO_3^- by nitrite oxidizing bacteria (NOB). Heterotrophic denitrification (HD) was a modified version of the ASMN (Hiatt and Grady, 2008). It described HD as a two-step reaction performed by heterotrophic bacteria (OHO): the reduction of NO_3^- to NO_2^- followed by the reduction of NO_2^- to nitrogen gas (N_2). The limitation of biomass growth by PO_4^{3-} was taken into account in the model.

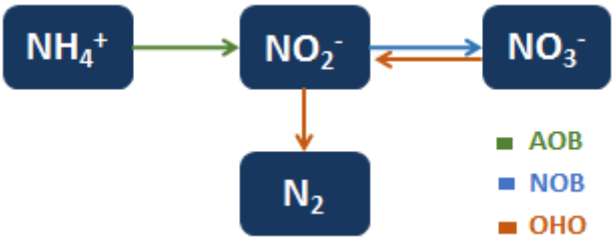

Figure III.3-2. Intermediate compounds considered in the initial biokinetic model.

III.3.2 MODIFICATIONS MADE TO THE BASE MODEL

The base model was developed to predict the performance of the nitrification stage of Seine Aval. In this thesis, it was extended to describe N_2O fluxes. To this end, several modifications were made (Figure III.3-3). The main modifications to the model structure are presented in detail in Chapters IV and V, and briefly explained here. Intermediate modifications of the base model are presented with their impact on model predictions.

The final model structure can be found in Annex 1.

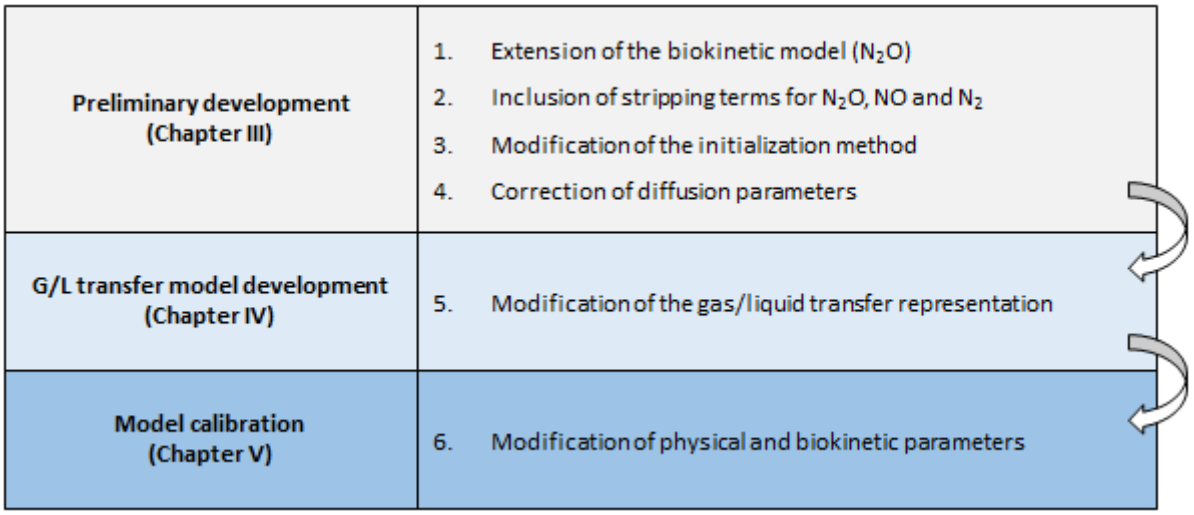

Figure III.3-3. Order of modifications made to the base model.

III.3.2.1 MODEL PREDICTIONS AFTER INCLUSION OF N_2O PATHWAYS

The first modification of the BAF model was the extension of the biokinetic model to include the N_2O production pathways by AOB (Pocquet et al., 2016) and four-step heterotrophic denitrification (Hiatt and Grady, 2008). The reactions involved in nitrification-denitrification are schematized on Figure III.3-4. Then, gas/liquid transfer terms were added for N_2O, NO and N_2 (already included for O_2 in the base model).

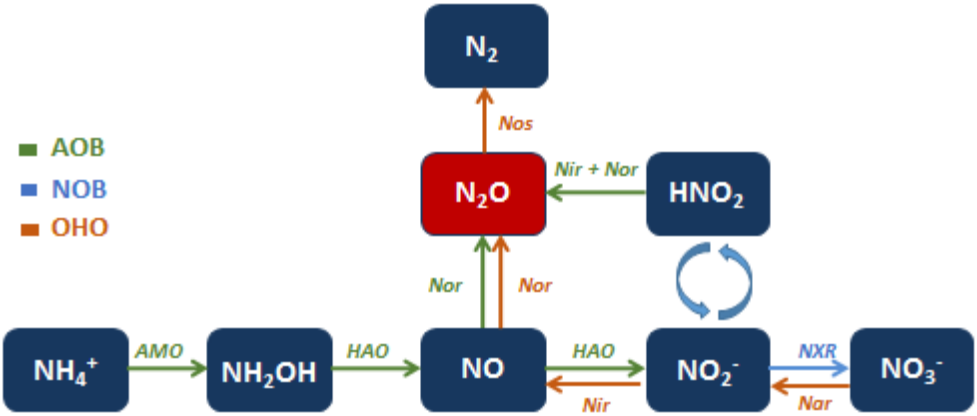

Figure III.3-4. Schematic representation of the N_2O biological pathways included in the modified BAF model. AMO, HAO, NXR, Nar, Nir, Nor and Nos stand for the enzymes ammonium monooxygenase, hydroxylamine oxidoreductase, nitrite oxidoreductase, nitrate reductase, nitrite reductase, and NO reductase and N_2 synthase.

At this point, predictions of the modified model were compared to those of the initial one. Data presented in Table III.2-7 were used as model inputs. Model predictions were only evaluated on the last 35 days, as the 10 first were used to stabilize the system (see section III.3.2.2). The predictions of effluent NH_4^+, NO_3^- and NO_2^- concentrations are presented on Figure III.3-5.

Effluent NH_4^+ concentration predicted by the modified model followed the same dynamics as the base model, but its mean value was 26% lower (6.3 ± 2.1 mgN/L against 5.0 ± 1.8 mgN/L). Consequently, the predicted effluent NO_3^- was 5% lower (31.4 ± 5.3 mgN/L against 32.8 ± 5.8 mgN/L). Effluent NO_2^- concentrations predicted by the modified model were 59% lower (0.24 ± 0.04 mgN/L against 0.58 ± 0.20 mgN/L), due to a higher fraction of NO_2^- consumed by heterotrophs in the modified model (mass balance not shown). No calibration was performed at this point, as predictions remained in good agreement with experimental data.

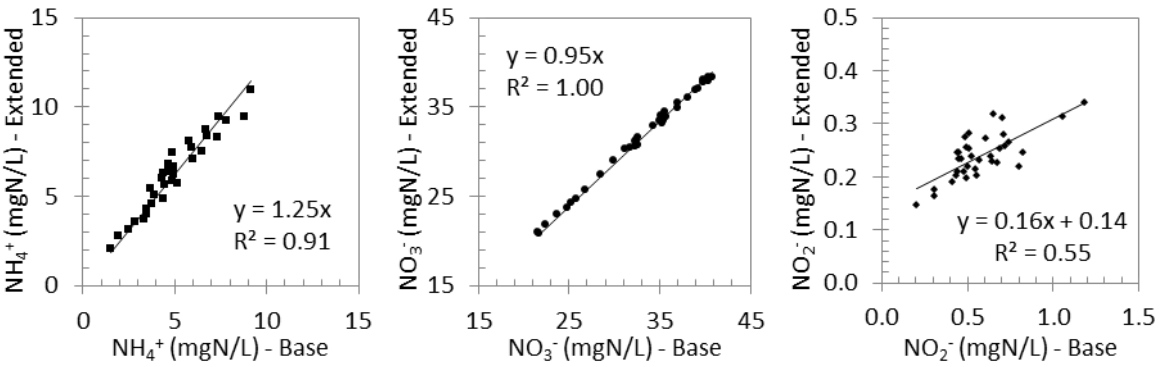

Figure III.3-5. Effluent $NH4^+$, NO_3^- and NO_2^- concentrations predicted by the modified and base models.

III.3.2.2 MODIFICATION OF THE INITIALISATION METHOD

Before any dynamic simulation was made, the model was initialized. To this end, a simulation was performed on a long-enough timespan to get the stabilization of the system. Ideally, a few months of data prior to the studied period are simulated, final values being used as initial state variables. In the base model, each state variable was initialized at the same value for each of the eight liquid compartments, and for each of the 14 biofilm compartments. This was not representative of the real state of the system since it did not consider the concentration gradients along the BAF height and along the biofilm thickness. Consequently, another period of time was needed at the beginning of dynamic simulations to stabilize the entire system. To avoid this “second initialization”, the modified model considered a dataset of initial conditions for each compartment of the BAF (i.e. 22 sets of initial concentrations).

The initialization can be referred as a "pseudo steady-state", since backwash events were still implemented every 24 hours. A 100-day time was found sufficient to reach stabilization of the system, in particular to stabilize the biomasses within the biofilm (Figure III.3-6). The observed short-term variations are related to the regular increase of biomass concentrations over a filtration cycle (biomass growth), and their decrease due to backwashing.

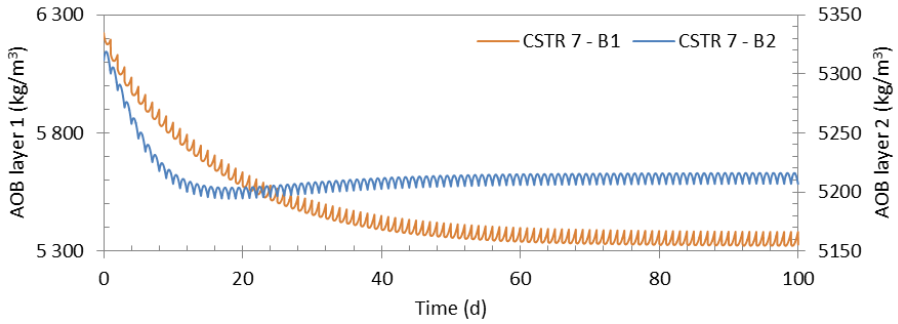

Figure III.3-6. Evolution of the AOB concentration in two biofilm compartments of CTSR 7 during a 100-day initialization.

III.3.2.3 CORRECTION OF DIFFUSION PARAMETERS

In the base model, diffusion coefficients of soluble compounds were reduced by a factor 10 compared to literature values. To compensate, the liquid film –which represents the resistance to diffusion between the bulk liquid and the biofilm- was thinner than literature values: 10 µm against 50 – 150 µm (Rittmann et al., 2018). In this work, literature values for diffusion coefficients were re-established (Vigne, 2007). These values are reported in Table III.3-1. They were used to estimate the liquid film thickness during the winter and summer campaigns, for each soluble compound (Eq.18 to Eq.21).

Eq.18 $$L_f = \frac{d_{eq}}{Sh}$$

Eq.19 $$Sh = 2 + 0.51 * \left(4.23 Re^{5/6}\right)^{0.6} Sc^{1/3}$$

Eq.20 $$Re = \frac{U_L d_{eq}}{\nu \varepsilon_0}$$

Eq.21 $$Sc = \frac{\nu}{D_i}$$

Where ν is the kinetic viscosity of water (m^2/s), d_{eq} the average diameter of the media beads (m), Sh, Sc and Re the Sherwood, Schmidt and Reynolds numbers (adimensional), U_L the superficial liquid velocity ($m^3/m^2/d$).

Table III.3-1. Average liquid film thickness calculated for each soluble component.

S_i	D_i (m^2/d)	Sc (-)	Sh (-)	L_f (µm)
S_{alk}	1.73E-04	654	38	106
S_S	8.64E-05	1307	47	85
S_i	8.64E-05	1307	47	85
S_{no3}	1.73E-04	654	38	106
S_{n2}	1.64E-04	688	38	104
S_{nd}	8.64E-05	1307	47	85
S_{nh}	2.16E-04	523	35	114
S_{po}	2.16E-04	523	35	114
S_{no2}	1.81E-04	623	37	107
S_o	2.16E-04	523	35	114
S_{nh2oh}	1.87E-04	605	37	108
S_{no}	1.91E-04	591	37	109
S_{n2o}	2.22E-04	509	35	115

Since the average U_L was very similar between the measuring campaigns (4.8 ± 1.3 $m^3/m^2/h$ in summer, 4.9 ± 1.2 $m^3/m^2/h$ in winter), only the average liquid film thicknesses calculated in winter are presented. They varied between 85 and 115 µm. An average value of 100 µm was therefore chosen, which lies within literature ranges.

The modified model was launched with and without these corrections to see their single impacts on model predictions. Simulations were performed on the winter campaign dataset. Each simulation was preceded by a 100-day pseudo-steady-state simulation with average influent conditions measured during the winter campaign. The average DO concentration, AUR and N_2O-PR predicted before and after correction are presented on Figure III.3-7.

DO concentration in the biofilm was reduced by 27% (0.56 against 0.77 mgO_2/L), resulting in a reduction of the AUR from 611 to 588 kgN/d. On the other hand, it resulted in a higher accumulation of NO_2^- (1.20 against 1.07 mgN/L), and higher N_2O production (38 against 34 kgN/d). These modifications were not homogeneous over the biofilm thickness. The DO concentration was significantly reduced in the surface layer (-40%), but mostly increased in the deep layer (+63%). The AUR increased by 242% in the deep layer, as it was highly limited before ($K_{O,AOB,2}$ = 0.30 mgO_2/L). This increased the accumulation of NO_2^- in this zone (1.19 against 1.01 mgN/L). On the other hand, N_2O production mostly increased in the deep layer, from a small consumption (-0.29 kgN/d), to a significant production (13.38 kgN/d). This modified model was used as the reference one (#0) in Chapter IV.

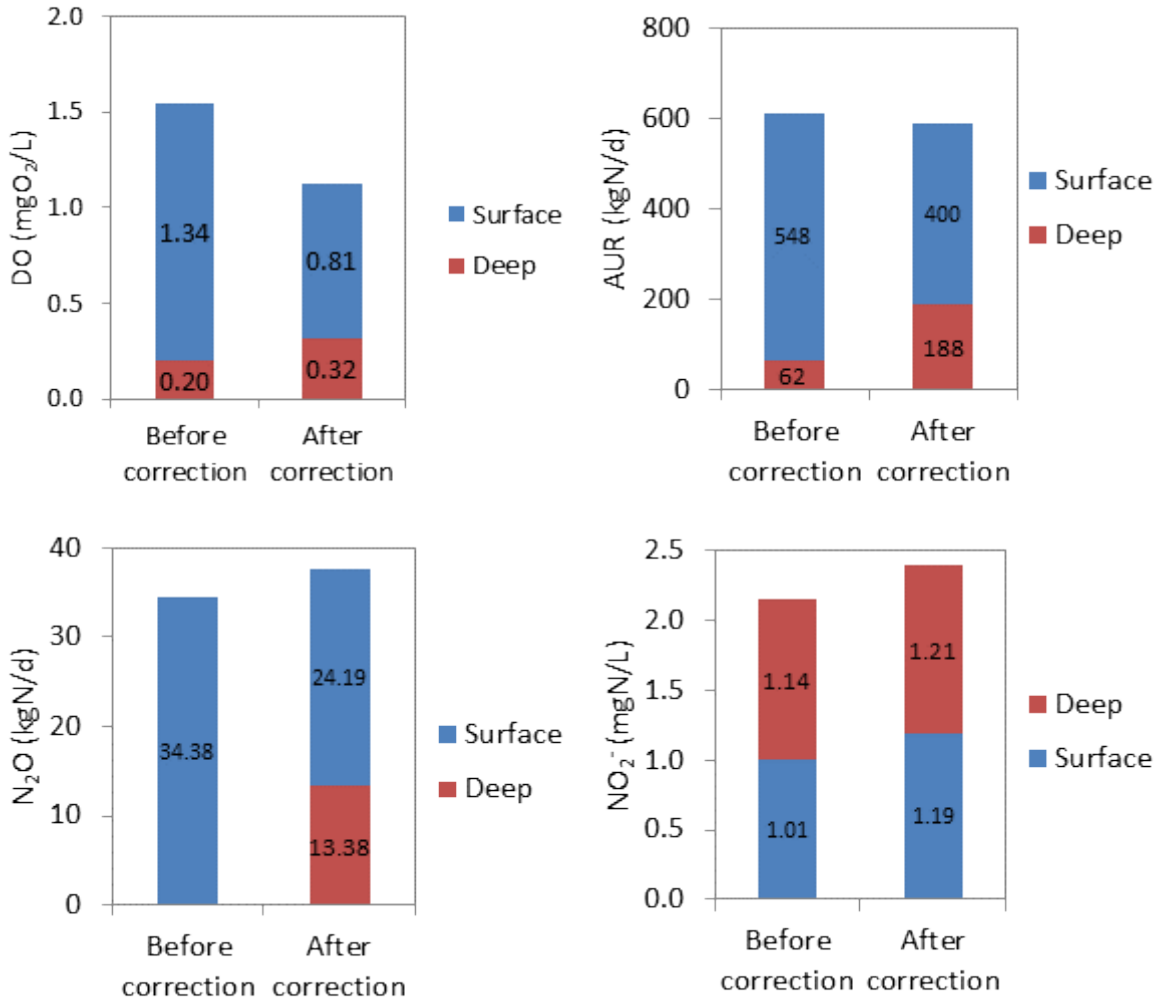

Figure III.3-7. Partition of DO concentration (top left), AUR (top right), N_2O production rate (bottom left) and NO_2^- concentration (bottom right) between biofilm layers before and after correction of the diffusion coefficients.

III.3.3 DESCRIPTION OF THE GLOBAL SENSITIVITY ANALYSIS

Global sensitivity analysis have been successfully applied to wastewater treatment models, including biofilm reactors, to identify parameters most affecting model outputs (Bernier, 2013, Cosenza et al., 2013, Sin et al., 2011, Brockmann et al., 2008). The method is based on the simultaneous variation of all model parameters in a defined range, around their reference values. In this work, it was performed with the BAF model after modification of its gas-liquid transfer structure. It can be described by three successive steps: the creation of the matrix of parameters, the simulation runs, and the statistical analysis of the results (standardized regression coefficient –SRC– method). The procedure is analogous to the one used by Bernier (2013) in his thesis.

III.3.3.1 LATIN HYPERCUBE SAMPLING

To avoid a time consuming manual modification of model parameters, a matrix of combinations was created to assign a vector of values to each parameter (Figure III.3-8). The matrix dimensions were p x n, where p is the number of parameters, and n the number of combinations. The matrix was created by Latin hypercube sampling (LHS), which consisted in creating a near-random sample of parameters. Each parameter range was divided into n intervals of equal length. A random value was then created in each interval.

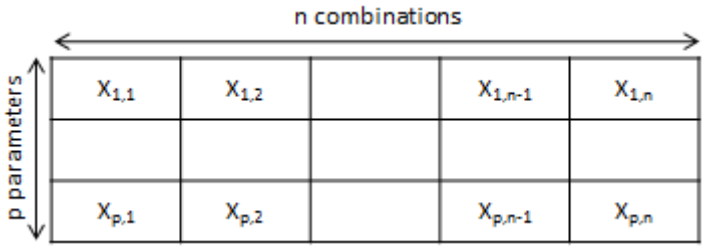

Figure III.3-8. Matrix of parameters used for the sensitivity analysis.

The parameters used for the sensitivity analysis, as well as their reference values and variation ranges are presented in Annex 2. The number of parameters p was 90, which included all model parameters except those set to zero (inert, AOB and NOB fractions of influent particular COD), those related to transfer efficiency (fouling of diffusers F, aeration efficiency compared to clean water α and salinity factor β_0), and diffusion coefficients. As recommended by Vigne (2007), different variation ranges were attributed. They were set to ± 10-100% around the reference values. Most parameter ranges were set to ± 20%, except for:

- N_2O-related parameters for AOB (± 100%), as we have little insight in their values in biofilm reactors;
- Gas-liquid transfer coefficients (± 50%), as we lack information about their values in full-scale BAFs;
- The liquid film thickness (± 50%), as it was reported to be a crucial parameter in the modelling of biofilm reactors (Rittmann et al., 2018, Boltz et al., 2011);
- Affinity constants related to AOB and NOB (± 50%), since the biokinetic model structure was modified;
- Inhibition constants of NO on heterotrophic denitrification (± 50%), since the NO concentration is typically not measured;
- Temperature parameters and nitrogen and phosphorus fractions of COD (± 10%).

III.3.3.2 SIMULATIONS

The large number of model parameters required a large number of combinations. Preliminary analyses were performed with 100, 300 and 450 combinations. They are called preliminary because the model structure was not definitive, and input data were averaged on 2014 only. The following results are therefore only presented as an example. Standardized coefficients of 30 parameters on the simulated effluent NH_4^+ concentrations are presented on Figure III.2-9.

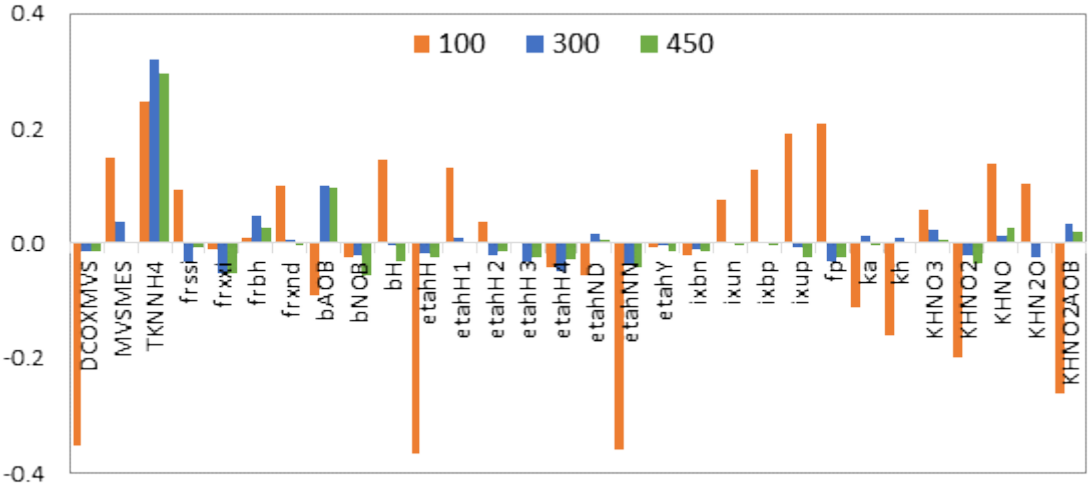

Figure III.3-9. Standardized coefficients of 30 parameters for effluent NH_4^+ concentration obtained with 100, 300 and 450 successive simulations (preliminary simulations).

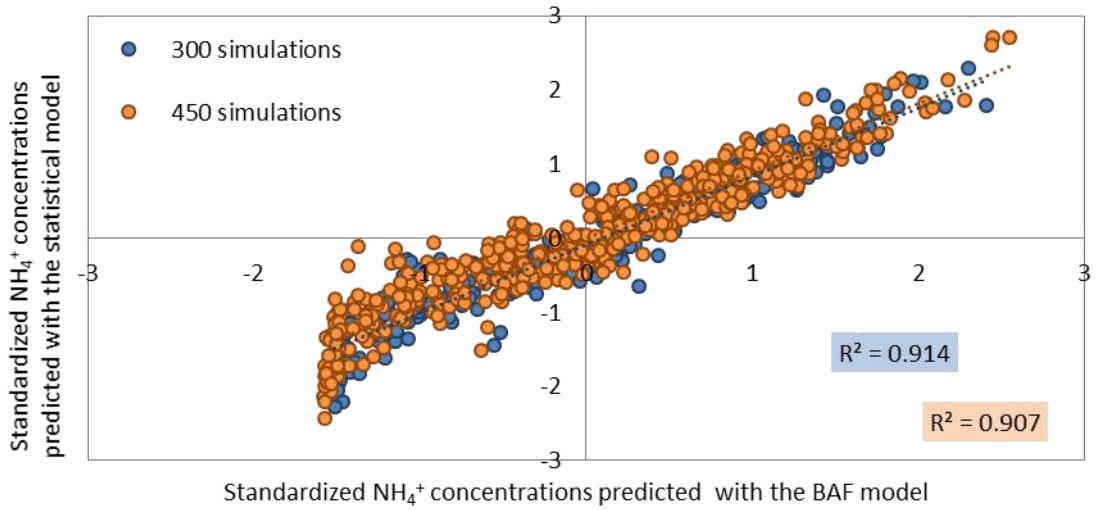

Figure III.3-10. Statistical versus BAF model predictions of effluent NH_4^+ concentration (standardized).

A hundred combinations were not sufficient to give reliable information on effluent NH_4^+ concentration sensitivity to the model parameters (R^2 = 0.78). Results with 300 and 450 gave similar estimations of the correlation coefficients and were able to describe effluent NH_4^+

(Figure III.3-10) with high precision (R^2 = 0.92 and 0.91, respectively). The highest number of combinations was chosen, which corresponds to five times the number of parameters, and lies within literature recommendations (Sin et al., 2011, Saltelli et al., 2008).

As presented on Figure III.3-6, 100 days were necessary to initialize the model. Each combination was therefore simulated for this duration: the first 99 days were used to reach stabilization and effluent concentrations predicted on the last day were used as the output variables. Data used to implement the model were average characteristics of the nitrification stage in 2014-2016 (Table III.2-2 and Table III.2-4).

III.3.3.3 STATISTICAL DATA ANALYSIS

Data processing was done on average outputs of the last day of each simulation. The outputs of interest were: effluent NH_4^+, NO_3^-, NO_2^-, DO, dissolved and gaseous N_2O concentrations. A parameter classification was obtained by the standardized regression coefficient (SRC) method, which is considered relevant for regression coefficient $R^2 > 0.7$ (Cosenza et al., 2013, Saltelli et al., 2008). It consisted in creating a multiple linear regression between input parameters and each output variable. All inputs and outputs were standardized using the "zscore" function of Matlab. This function centred all parameter combinations and averaged outputs on 0 and set their standard variation to 1.

Finally, the effect of a standardized parameter p_i on a given standardized output Y was given by its standardized coefficient β_i of the regression ($Y = b_0 + \sum \beta_i p_i$). The closer to zero the value of β_i, the lower its impact on a given output. The impact of parameters on model outputs was defined as: highly negative for standardized coefficient $\beta i < -0.3$, moderately negative for $-0.3 < \beta i < -0.2$, slightly negative for $-0.2 < \beta i < -0.1$, insignificant for ($-0.1 < \beta i < 0.1$, slightly positive for $0.1 < \beta i < 0.2$, moderately positive for $0.2 < \beta i < 0.3$, and highly positive for $0.3 < \beta i$.

III.4 LABORATORY EXPERIMENTS

III.4.1 PRESENTATION OF THE SEINE CENTRE WRRF

Laboratory experiments were carried out in a reactor filled with colonized polystyrene beads sampled from the tertiary nitrification stage of the Seine Centre WRRF. Like in Seine Aval, nitrification is performed by Biostyr® type filters. The influent flow rate of the Seine Centre WRRF is, however, much lower (240 000 m^3/d, or 900 000 PE). Wastewater passes through a pre-treatment stage, followed by a physiochemical sedimentation, and tertiary biological

treatment. The latter is composed of three biofiltration stages: carbon elimination (24 Biofor®), nitrification (29 Biostyr®), and post-denitrification (12 Biofor®). The unitary surface and filter bed of the nitrifying BAFs are lower than those of Seine Aval (111 against 173 m^2 and 3.0 against 3.5 m, respectively). The functioning of the nitrification stage of the Seine Centre WRRF between July 2017 and June 2018 is presented in Table III.4-1 and Table III.4-2. The nitrifying BAFs were designed to receive 0.7 $kgN/m^3/d$ but they only received 0.44 ± 0.18 $kgN/m^3/d$ in 2017-2018. The aeration intensity was high (169 ± 105 Nm^3/kgN), resulting in high NH_4^+ uptake (97 ± 8% of the applied load). The lower NH_4^+ load compared to the Seine Aval WRRF was due to lower influent flow rates, but also lower influent NH_4^+ concentrations.

Table III.4-1. Influent characteristics of the Seine Centre nitrifying BAFs in 2017-2018 (n = 365).

	Q_L	Q_G	NH_4^+	NO_3^-	NO_2^-	COD	TSS	PO_4^{3-}	T
	m^3/d	Nm^3/d	mgN/L	mgN/L	mgN/L	mg/L	mg/L	mgP/L	°C
Mean	8 469	19 803	16.2	7.2	0.53	38	9	0.26	19.0
St. dev.	1 944	4 219	5.9	1.9	0.17	13	4	0.15	3.2

Table III.4-2. Effluent characteristics of the Seine Centre nitrifying BAFs in 2017-2018 (n = 365).

	NH_4^+	NO_3^-	NO_2^-	COD	TSS	PO_4^{3-}
	mgN/L	mgN/L	mgN/L	mg/L	mg/L	mgP/L
Mean	0.5	21.1	0.04	20	4	0.23
St. dev.	0.7	3.7	0.04	4	2	0.14

The media was sampled on January 29th 2018 in the water tarp of the nitrification stage, where backwash water is collected. Unfortunately, a disruption of Seine Centre WRRF was caused by the River Seine overflow at this period (Figure III.4-1).The filters were functioning at decreasing NH_4^+ loads before this disruption, as influent NH_4^+ concentrations decreased from 27 to 7 mgN/L between November 11th 2017 and January 21st 2018.

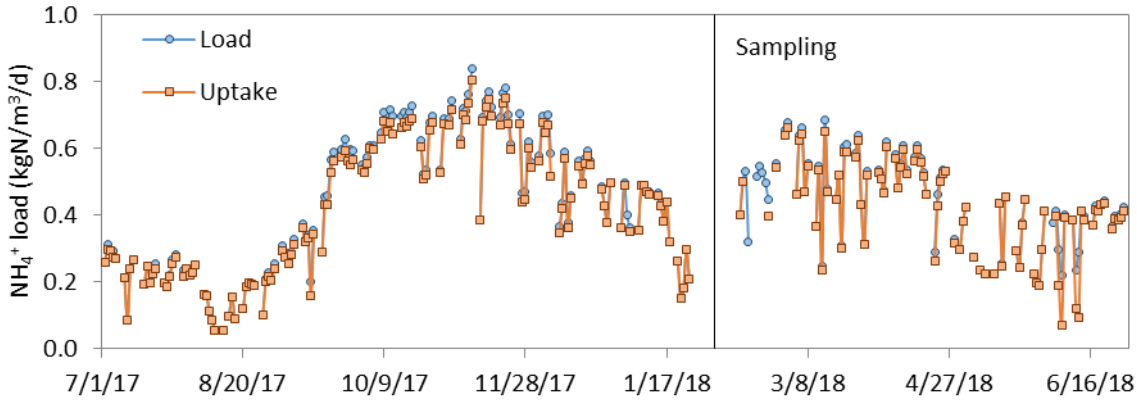

Figure III.4-1. Influent and uptake NH_4^+ loads of Seine Centre nitrifying BAFs in 2017-2018.

III.4.2 REACTOR SET-UP

A lab-scale reactor was filled with the colonized media samples (Figure III.4-2). The light media (density < 1) was retained by a metal grid. The gas was distributed from the bottom of the reactor through a pierced coiled pipe, and controlled by mass flow meters. Initially, a volume of water was supposed to be present under the bed zone, similarly to full-scale conditions. However, the gas was poorly distributed within the media bed, as large gas pockets formed underneath the bed were noticed. Therefore, it was chosen to put the media bed directly in contact to the coiled pipe (Figure III.4-2). This; however, imposed to feed the reactor from the top, which means that the reactor was functioning in a down-flow counter-current mode. The reactor was filled up in order to maintain a small water lamina on top the metal grid (5 cm), where DO, pH and temperature sensors were located.

Figure III.4-2. Image of colonized polystyrene beads (left) and reactor set-up (right).

The feeding solution was introduced by a peristaltic pump from a feeding tank into the reactor. It was synthetic water composed of ammonium chloride (NH_4Cl) as substrate, monobasic potassium phosphate (KH_2PO_4) as phosphorus source for bacterial growth, and sodium bicarbonate ($NaHCO_3$) as pH buffer and inorganic carbon source (2.5 mol HCO_3^-/mol N) in 100 or 150 L of tap water that was dechlorinated overnight.

The dimensions of the reactor are given in Table III.4-3. The total working and water volumes were measured (11.36 and 5.20 L, respectively). The overflow volume was 1.42 L, which resulted in a bed volume of 9.94 L. The latter was used to calculate the volumetric NH_4^+ loads (applied and eliminated). Note that the colonized media volume was only measured once, on April the 24th 2018. The volume of biofilm may have changed between the first experiments (on January 30th) due to biomass growth and decay, but, for simplification, it

was considered to be representative of the conditions during the entire experimental period. This assumption was, however, not verified during these experiments.

Table III.4-3. Dimensions of the lab-scale reactor.

	Value	Origin
Total working volume V_T	11.36 L	Measured
Total liquid volume V_L	5.20 L	Measured
Colonized media volume V_{CM}	6.16 L	Calculated: V_T - V_L
Overflow volume V_O	1.42 L	Measured
Interstitial volume V_I	3.78 L	Calculated: V_L - V_O

III.4.3 REACTOR MONITORING

III.4.3.1 CONTINUOUS MEASUREMENTS

A summary of all measurements and analyses is given in Table III.4-4.

Table III.4-4. Analyses performed on influent/effluent water during the experiments.

	Measurement	Type/method	Frequency
NH_4^+ load tests			
Influent	DO, temperature, pH	Sensor	1 minute
	NH_4^+	Nessler photometry	3 samples
	NO_3^-, NO_2^-, SO_4^{2-}, PO_4^{3-}, Mg, Ca, K	Ion chromatography	
Effluent	Off-gas N_2O, NO, CO_2	Spectroscopy	1 minute
	NH_4^+	Nessler photometry	1 sample / HRT
	NO_3^-, NO_2^-, SO_4^{2-}, PO_4^{3-}, Mg, Ca, K	Ion chromatography	
Aeration tests			
Influent	DO, temperature, pH	Sensor	1 minute
	NH_4^+, NO_3^-	Smartchem photometry	2-3 samples
Effluent	Off-gas N_2O, NO, CO_2	Spectroscopy	1 minute
	NH_4^+, NO_3^-, NO_2^-	Smartchem photometry	1 sample / HRT
Temperature tests			
Influent	DO, temperature, pH	Sensor	1 minute
	NH_4^+, NO_3^-	Smartchem photometry	2-3 samples
Effluent	Off-gas N_2O, NO, CO_2	Spectroscopy	1 minute
	NH_4^+, NO_3^-, NO_2^-	Smartchem photometry	1 sample / HRT

DO, pH and temperature were continuously measured by sensors in the top water zone of the reactor. The characteristics of this top water zone were supposed to be those of the feeding tank, as the solution was fed in down-flow mode. However, it was likely that the up-flow gas injection induced exchanges from the bed to the top water zone. It would be recommended to perform a tracer test to verify this assumption in further work, in particular if a modelling of the system is intended. The off-gas was continuously pumped at 0.06 L/min and was analysed for N_2O (X-STREAM X2GP, Emerson) and NO (NGA 2000 CLD, Emerson) concentrations. The NO concentration was always null and therefore not presented. The dissolved N_2O concentration was monitored (N_2O sensors, Unisense, limit of detection: 10^{-3} mgN/L) in preliminary recirculation experiments. It remained null, even at high NH_4^+ loads. We made the assumption that all N_2O produced was transferred to the gas phase and thus it was not possible to measure dissolved N_2O concentrations during the experiments.

III.4.3.2 ANALYSES OF INFLUENT/EFFLUENT CHARACTERISTICS

The reactor performance was regularly evaluated. For each condition tested, the synthetic solution was sampled in duplicates or triplicates (on a single sampling volume of 20 mL). The maximum and minimum tank volumes when influent was sampled were 150 and 18 L. Therefore, these samples had no significant effect on the tank volume. The number of samples was highly fluctuating between experiments. Effluent was generally sampled after one HRT, when the system reached stabilization. Liquid samples were immediately filtered through a 0.2 µm syringe filter and stored at 4 °C until their analysis within five days. During NH_4^+ load tests, NH_4^+ concentrations were measured photometrically according to the Nessler method (AFNOR NFT 90-015). NO_2^- and NO_3^- concentrations were determined by ion chromatography. During aeration and temperature tests, NO_3^- concentrations were analysed photometrically (SMARTCHEM200, AMS). The same procedure was applied to effluent samples, with the additional analysis of NO_2^- concentrations (SMARTCHEM200, AMS).

III.4.4 EXPERIMENTAL CONDITIONS TESTED

Average conditions were chosen to be representative of those observed in the Seine Centre WRRF in terms of applied NH_4^+ load, HRT and air supply. Influent was pumped at 0.20 L/min, in order to maintain the HRT at 20.1 ± 0.4 min, which is close to the estimated value of a full-scale BAF of Seine Centre WRRF (19 min in the active zone, considering a bed porosity of 0.34). The standard influent NH_4^+ concentration was 26 ± 6 mgN/L, which corresponded to an applied NH_4^+ load of 0.7 ± 0.2 kgN/m^3/d. Mass flow meters maintained the gas flow rate at 0.5 L/min, which corresponded to 105 Nm^3/kgN. Except during specific experiments dedicated to temperature, temperature was controlled at 19.9 ± 0.6 °C (with a cryogenic regulator and a water jacket).

The effect of three main operating conditions was tested in a series of experiments: NH_4^+ load, oxygenation and temperature. To avoid modifying the reactor hydraulics, NH_4^+ load was tested by modifying the influent NH_4^+ concentration only, and the aeration was tested by modifying the fraction of oxygen in the influent gas. Twenty-one experiments were performed. Seven nitrogen load tests were performed by increasing (6.2, 28.6 and 62.1 mgN/L) and decreasing (56.1, 42.9, 42.7 and 20.2 mgN/L) the NH_4^+ concentration. Eight aeration tests were performed by mixing compressed air and pure nitrogen gas to reach 0 (pure N_2) to 21 % O_2 in the gas mix. Finally, six temperature tests were conducted by cooling the influent directly in the feeding tank (22.3 to 13.5 °C). For all experiments, the pH was 7.8 ± 0.3. A complete description of all experiments is given in Table III.4-5. For the additional experiments that were conducted, information is presented in Annex 3.

Table III.4-5. Influent conditions during the 21 experiments performed in the lab-scale reactor.

Test #	$[NH_4^+]_{in}$	Q_L	Q_G	% air	Temperature	pH
NH_4^+ load tests						
#1	6.2 ± 0.1 mgN/L	0.19 L/min	0.50 L/min	100	19.7 ± 0.1 °C	7.4 ± 0.0
#2	28.6 ± 0.5 mgN/L	0.18 L/min			19.6 ± 0.1°C	7.4 ± 0.0
#3	62.1 ± 0.4 mgN/L	0.18 L/min			19.8 ± 0.0°C	7.4 ± 0.0
#4	56.1 ± 0.3 mgN/L	0.19 L/min			18.9 ± 0.1°C	7.9 ± 0.0
#5	42.9 mgN/L (single sample)	0.19 L/min			19.0 ± 0.1°C	7.9 ± 0.0
#6	42.7 ± 1.0 mgN/L	0.19 L/min			19.4 ± 0.4°C	7.6 ± 0.2
#7	20.2 ± 0.5 mgN/L	0.18 L/min			19.6 ± 0.1°C	7.9 ± 0.0
Aeration tests						
#8	25.1 ± 0.5 mgN/L	0.19 L/min	0.57 L/min	100	19.4 ± 0.1°C	7.8 ± 0.0
#9		0.19 L/min	0.40 L/min	0	19.2 ± 0.1°C	8.1 ± 0.0
#10		0.19 L/min	0.53 L/min	20	19.2 ± 0.1°C	8.2 ± 0.0
#11		0.18 L/min	0.51 L/min	50	19.2 ± 0.1°C	8.2 ± 0.0
#12		0.18 L/min	0.50 L/min	80	19.3 ± 0.1°C	8.2 ± 0.0
#13	23.4 ± 0.6 mgN/L	0.19 L/min	0.53 L/min	20	19.9 ± 0.1°C	7.9 ± 0.0
#14		0.19 L/min	0.51 L/min	50	20.1 ± 0.1°C	8.1 ± 0.0
#15		0.18 L/min	0.50 L/min	80	20.0 ± 0.1°C	8.2 ± 0.0
Temperature tests						
#16	20.8 ± 0.8 mgN/L	0.20 L/min	0.50 L/min	100	20.3 ± 0.1 °C	7.5 ± 0.0
#17		0.19 L/min			16.4 ± 0.3 °C	7.7 ± 0.0
#18		0.19 L/min			15.5 ± 0.1 °C	7.7 ± 0.0
#19	20.1 ± 0.3 mgN/L	0.19 L/min			22.3 ± 0.1 °C	7.6 ± 0.0
#20		0.19 L/min			18.2 ± 0.1 °C	7.9 ± 0.0
#21		0.19 L/min			13.4 ± 0.2 °C	7.7 ± 0.0

III.4.5 DATA PROCESSING

III.4.5.1 CORRECTION OF THE LIQUID FLOW RATE

The liquid flow rate (Q_L) was fixed at 0.20 L/min. However, a decrease of Q_L was observed along with the gradual emptying of the feeding tank. The correlation between Q_L and the tank volume is presented on Figure III.4-3. The tank volume was estimated continuously, and used to calculate the actual flow rate during all experiments.

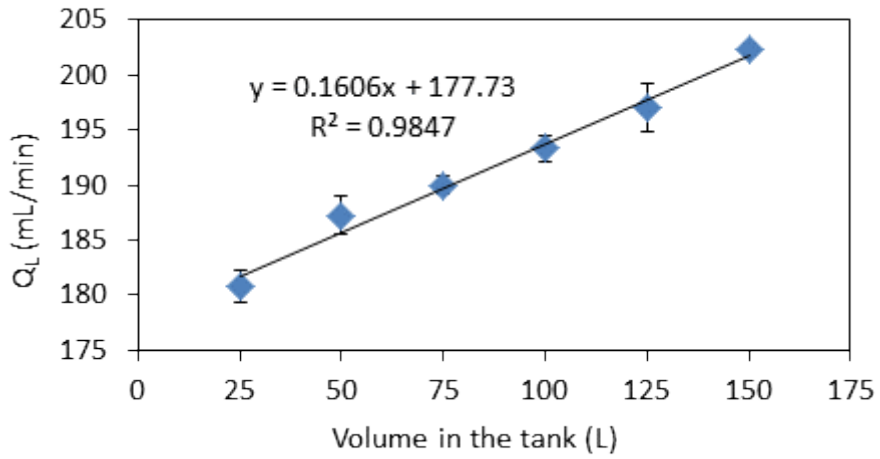

Figure III.4-3. Observed correlation between the liquid flow rate and the tank volume.

III.4.5.2 REACTOR PERFORMANCES

The ammonium elimination rate, N_2O emission rate and N_2O emission factor were calculated according to equations Eq.13, Eq.15 and Eq.17, respectively. They were only calculated when a stable functioning of the reactor was reached.

The off-gas N_2O concentration was measured in parts per million (ppm), which were converted to mgN/L according to Eq.22.

Eq.22
$$C_{N_2O,G,out} = (C_{N_2O,G,out})_{ppm} * \frac{2 * M_N * 10^{-3}}{R * (T + 273.15)}$$

Where $C_{N2O,G,out}$ and $(C_{N2O,G,out})_{ppm}$ are the off-gas N_2O concentrations in mgN/L and ppm respectively, M_N the nitrogen molar mass (g/mol), R the ideal gas constant (L atm mol^{-1} K^{-1}) and T the water temperature (°C).

Chapter IV. Considering the plug-flow behavior of the gas phase in nitrifying BAF models significantly improves the prediction of N_2O emissions[4]

[4] This work was published in Water Research. Only a few editorial changes were done to assure consistency with the rest of the manuscript. Please refer to: J. Fiat, A. Filali, Y. Fayolle, J. Bernier, V. Rocher, M. Sperandio, and S. Gillot. 2019. Considering the plug-flow behavior of the gas phase in nitrifying BAF models significantly improves the prediction of N_2O emissions. *Water Res* 156:337-346.

RESUME

Les biofiltres nitrifiants ont été identifiés comme de forts émetteurs de protoxyde d'azote (N_2O), un puissant gaz à effet de serre contribuant à la destruction de la couche d'ozone. Alors que de récents modèles ont grandement amélioré notre compréhension des mécanismes d'émissions de N_2O dans les procédés à biomasse en suspension, nous en savons bien moins sur les procédés à biofilm.

Les biofiltres nitrifiants tertiaires ont été modélisés à quelques occasions, mais en considérant d'importantes simplifications de la représentation des échanges gaz/liquide, qui ne sont pas appropriées pour la prédiction du N_2O. Dans ce chapitre, un modèle de biofiltration nitrifiante incluant les principales voies biologiques du N_2O a été développé et confronté à des données mesurées sur la station Seine Aval, la plus grande station de traitement des eaux usées d'Europe. Un bilan de masse sur la phase gazeuse a été inclus pour décrire correctement la répartition des flux de N_2O entre les phases gazeuse et liquide, et ainsi les émissions de N_2O. Des modifications préliminaires ont été apportées à la structure du modèle pour inclure la phase gazeuse en tant que compartiment du modèle, ce qui a significativement affecté la prédiction de la nitrification. En particulier, la prise en compte d'une rétention gazeuse a impacté la prédiction du temps de séjour hydraulique, et ainsi les performances : une fraction de gaz de 3.5% du volume de réacteur a induit une diminution de l'abattement de l'ammonium de 13% car le volume de liquide, très faible dans ce type de systèmes, est sensible à la présence de gaz. Finalement, la valeur du coefficient de transfert d'oxygène a été augmentée pour prédire correctement à la fois la nitrification et les émissions de N_2O.

Mots-clés : biofilm, modélisation, nitrification, N_2O, pleine échelle, transfert gaz/liquide

ABSTRACT

Nitrifying biologically active filters (BAFs) have been found to be high emitters of nitrous oxide (N_2O), a powerful greenhouse gas contributing to ozone layer depletion. While recent models have greatly improved our understanding of the triggers of N_2O emissions from suspended-growth processes, less is known about N_2O emissions from full-scale biofilm processes.

Tertiary nitrifying BAFs have been modelled at some occasions but considering strong simplifications on the description of gas-liquid exchanges which are not appropriate for N_2O prediction. In this work, a tertiary nitrifying BAF model including the main N_2O biological pathways was developed and confronted to full-scale data from Seine Aval, the largest wastewater resource recovery facility in Europe. A mass balance on the gaseous compounds was included in order to correctly describe the N_2O gas-liquid partition, thus N_2O emissions. Preliminary modifications of the model structure were made to include the gas phase as a compartment of the model, which significantly affected the prediction of nitrification. In particular, considering gas hold-up influenced the prediction of the hydraulic retention time, thus nitrification performances: a 3.5% gas fraction reduced ammonium removal by 13%, as the liquid volume, small in such systems, is highly sensitive to the gas presence. Finally, the value of the volumetric oxygen transfer coefficient was adjusted to successfully predict both nitrification and N_2O emissions.

Keywords: Biofilm, Full-scale, Gas-liquid transfer, Modelling, Nitrification, N_2O

IV.1 INTRODUCTION

Biological active filters (BAFs) are submerged fixed-bed biofilm reactors combining solids removal by filtration with the biological conversion of carbon, ammonium and/or nitrate. Since the early eighties, they have been successfully used to treat a variety of urban and industrial wastewaters. Owing to their compactness, flexibility and reliability, BAFs have been widely developed in Europe, especially in large urbanized areas where available space is scarce (Mendoza-Espinosa and Stephenson, 1999b). Recent monitoring campaigns suggest that nitrifying BAFs are important sources of nitrous oxide (N_2O), a potent greenhouse gas contributing to global warming and ozone depletion. In China, Wang et al. (2016) monitored nitrifying BAFs over a period of 12 months and reported emissions ranging from 0.02 to 1.26 % of influent total nitrogen load. In France, the two monitoring campaigns performed in tertiary nitrifying BAFs of the Seine Aval plant (the largest plant in Europe) reported higher emission factor values: 1.77% of $N\text{-}NH_4^+$ removed in summer and 3.11% in winter (Bollon et al., 2016b). Based on the results of the winter campaign, authors estimated that N_2O emissions contributed to almost 80% of the carbon footprint of the biological nitrogen removal stage of the plant (Filali et al., 2017).

Modelling may represent a very useful tool in view of a better understanding of N_2O production mechanisms and can serve to comprehend the effect of different operational conditions and define mitigation strategies. To this end, existing activated sludge models (ASM) were extended to include NO and N_2O formation during autotrophic nitrification and heterotrophic denitrification. N_2O is an obligate intermediate of the heterotrophic denitrification, and the end product of two main biological pathways by ammonium oxidizing bacteria (AOB) and archaea (AOA) (Schreiber et al., 2012). In the first pathway (nitrifier nitrification, or NN pathway), N_2O is generated as a by-product of incomplete oxidation of hydroxylamine (NH_2OH) to nitrite (NO_2^-). In the second pathway (nitrifier denitrification, or ND pathway), N_2O is generated upon the reduction of NO_2^-. Several models have been proposed to describe either one of these pathways, but failed to predict N_2O emissions in contrasted conditions, especially when transient conditions of dissolved oxygen (DO) or NO_2^- occurred (Spérandio et al., 2016). Hence, recent models coupling multiple N_2O pathways were proposed to describe and extrapolate the emissions for a wide broad of operating conditions. A detailed review of these models can be found in the literature (Massara et al., 2017a, Ni and Yuan, 2015). Among them, the model of Pocquet et al. (2016), which couples the two N_2O biological production pathways by AOBs, has been validated on extensive lab-scale datasets. It was found able to predict N_2O emissions for contrasted DO and NO_2^- conditions, and also the respective contributions of NN and ND pathways to the total production of N_2O (Lang et al., 2016).

On the other hand, few models have been proposed to describe the behaviour of nitrifying BAFs (Bernier et al., 2014, Vigne et al., 2010, Hidaka and Tsuno, 2004, Behrendt, 1999, Viotti et al., 2002). They are mainly one dimensional and differ in the number of mechanisms simulated and in the level of complexity considered in their description. Gas-liquid mass transfer of oxygen is one of the mechanisms that received the least attention, probably because of the difficulty to obtain experimental data and of the lack of standardized measurement methods. Biofilm reactors being mass-transfer limited, a good representation of oxygen gas-liquid mass transfer is usually essential to correctly predict nitrification performances. However, little is known about gas-liquid mass transfer in fixed-bed reactors. Some studies investigated the impact of operating conditions and media properties on oxygen transfer, and mostly at lab or pilot scales, and with a clean media bed (Maldonado et al., 2008, Leung et al., 2006, Pérez et al., 2006, Gillot et al., 2005, Behrendt, 1999, Deront et al., 1998). In some occasions, oxygen supply in BAFs was described in a simplified manner, i.e. assuming a constant non-limiting DO concentration through the filter height (Vigne et al., 2010, Viotti et al., 2002); whereas, in others an aeration model was considered to predict the oxygen supply variation with the airflow rate and the profiles of DO throughout the filter (Bernier et al., 2014, Hidaka and Tsuno, 2004). However, several simplifications were made: the gas phase was not considered as a compartment of the reactor, i.e. the gas volume was not included in the calculation of the working volume and the evolution of the gas phase composition was neglected. If this representation of gas-liquid exchanges was found sufficient to describe nitrification performances, it may not be appropriate for NO and N_2O prediction. It has to be noted that few modelling studies considered the gas phase as a compartment when describing nitrification in lab-scale (Poughon et al., 1999) and pilot-scale (Behrendt, 1999) fixed-bed reactors. Both studies included oxygen transfer as their final objective was to investigate nitrification but provided little information about this parameter. Moreover, N_2O was not adressed in these studies, and N_2O emissions from full-scale nitrifying BAFs were never modelled so far. The increasing concern about greenhouse gas emissions and the sensivity of plant's carbon footprint to N_2O emissions call for an upgrade of full-plant BAF models to include N_2O production pathways.

To this aim, the model proposed by Bernier et al. (2014), calibrated and validated on long term data from full-scale tertiary nitrifying BAFs of the Seine Aval plant, was extended to describe N_2O emissions monitored on this site. Beforehand, it was necessary to assess the relevance of gas-liquid transfer hypotheses for N_2O prediction. In this paper, different successive options related to gas-liquid transfer hypotheses are considered and implemented for a better description of physical characteristics of BAFs and associated mass transfer: gas-hold up was included to estimate a gas volume, the working volume was

estimated considering the gas volume and a mass balance was added on the gas phase to describe the evolution of the gas phase composition. Their relevance is discussed and the newly developed model is evaluated by comparing modelling results with experimental data. Finally, recommendations of experiments are provided in order to better characterize gas-liquid mass transfer in full-scale BAFs.

IV.2 MATERIAL AND METHODS

IV.2.1 EXPERIMENTAL DATA

Data were collected during a 14-day measuring campaign, in winter 2015, on a Biostyr® unit of the tertiary nitrification stage of the Seine Aval plant (Bollon et al., 2016b). The unitary surface was 173 m^2, and the media bed - composed of 4 mm polystyrene beads – was 3.5 m high. Data used for modelling included: online measurements of inlet NH_4^+ and NO_3^-, outlet NH_4^+, NO_3^-, DO, pH, temperature, and outlet dissolved N_2O (measured in the water zone above the media, called the overflow). One-off measures of effluent NO_2^- were also performed. Gas emissions were collected in the middle of the overflow with a floating hood. The main operating conditions of the BAF are displayed in Table IV.2-1, with the estimated N_2O production and emission rates. The winter period was preferred to the summer period for the following reasons: (i) the duration of the monitoring was longer; (ii) it is characterized by a higher variability of the loading rate, the temperature and the N_2O gas-liquid partition. More details about the measurement procedure and the results can be found in Bollon et al. (2016b).

Table IV.2-1. Daily average operating conditions in the studied filtration unit (n = 14).

	Applied NH_4^+ load	Removed NH_4^+ load	Gas velocity	Liquid velocity	Dissolved N_2O	Emitted N_2O	Emitted / total N_2O
	kgN/d		$m^3/m^2/d$		kgN/d		%
Mean	692	571	299	116	10.0	20.0	65
St. dev.	74	55	88	29	1.6	3.2	6

Average values presented in Table IV.2-1 are slightly different from the original publication, as influent interruptions occurring during backwashing periods were not considered, in order to avoid computational issues. During these 30 min backwashing events, the filter was considered to be operated at usual influent flow and concentration conditions, but was

characterized by a higher detachment rate of particles. A detailed description of the BAF reactor and model inputs are provided in Chapter III.

IV.2.2 MATHEMATICAL MODEL

Preliminary modifications made to the model proposed by Bernier et al. (2014) –referred as the "base" model– were related to: (i) the biokinetic model, and (ii) the gas-liquid transfer representation. The biokinetic model was extended in order to include the main biological N_2O production and consumption pathways related to nitrification and denitrification. A stripping term was added on N_2O and other nitrogen compounds. These preliminary modifications are presented thereafter, followed by the modifications made to assess the model sensitivity to gas-liquid transfer hypotheses.

IV.2.2.1 BIOCHEMICAL AND BIOFILM MODEL

The proposed model is based on an existing co-current up-flow filter model built on the Simulink toolbox of Matlab (Mathworks) to describe the functioning of tertiary nitrifying Biostyr® filters of the Seine Aval plant (Bernier et al., 2014). The main features of the base model are recalled hereafter. A detailed description is provided in Annex 1.

Hydrodynamics in the BAF are described by a series of seven reactors of equal volume, representing the "active zone" where biological conversions occur. Each reactor is composed of a biologically inactive bulk zone, composed of a gas and a liquid compartment, an inert media volume, and two biofilm layers (Figure IV.2-1). It should be noted that the gas compartment was not included in the base model. The biofilm model includes soluble material diffusion, biofilm growth and particular exchange between biofilm layers as well as attachment and detachment. On top of this zone, an additional CSTR representing the overflow is implemented. Because it has low biomass concentrations in comparison with the underneath zone (only resulting from the detachment, no biofilm layer), it is considered "passive". For simplification, the 1.4 m water zone beneath the media bed was not represented in the model because: (i) the concentration of biomass is low and (ii) oxygen gas/liquid transfer is low considering that the influent entering this zone has a DO concentration of 8 mgO_2/L.

Biokinetic reactions are computed within the two biofilm layers. The model, previously describing nitrification and heterotrophic denitrification as two-step reactions, was extended to include the main N_2O pathways. NO and N_2O were added as intermediates of heterotrophic denitrification, with parameters from the original publication of Hiatt and Grady (2008). The two-pathway model proposed by Pocquet et al. (2016) was included to

describe N_2O production by AOBs. Sets of parameters were taken from the second case study of Lang et al. (2016), who worked at NH_4^+ and NO_2^-concentrations close to the ones measured on the Seine Aval plant. The Gujer matrix of the extended model and the list of parameters are given in Annex 1.

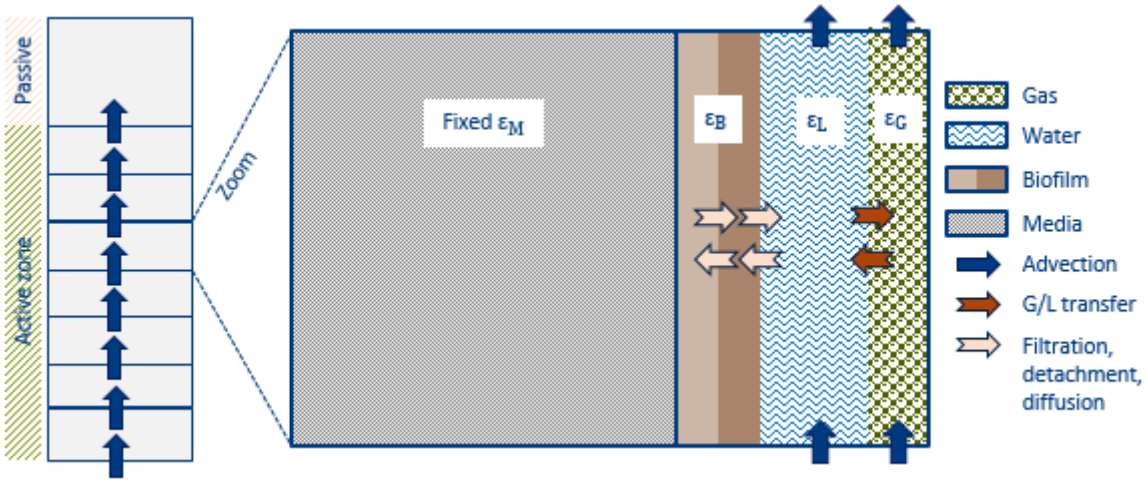

Figure IV.2-1. Schematic representation of the BAF model. Each compartment on the left side is a CSTR. ε_M is fixed (0.64), ε_G only depends on superficial gas velocity, ε_B varies with filtration, detachment and biomass growth, and ε_L is deduced from the other fractions.

IV.2.2.2 GAS-LIQUID MASS TRANSFER MODEL

IV.2.2.2.1 GENERAL DESCRIPTION OF GAS-LIQUID MASS TRANSFER

The base model included a gas-liquid transfer equation for oxygen in each reactor. In this study, it was implemented for all gases considered (i: O_2, N_2O, NO and N_2) according to Eq.23. Mass transfer limitations being localized at the liquid side for all gases (all having a low solubility), their volumetric transfer coefficient was estimated from the one of oxygen (Eq.24), in application of the penetration theory (Higbie, 1935), as done in other studies (Lizarralde et al., 2018, Vaneeckhaute et al., 2018).

The volumetric oxygen transfer coefficient was defined as a function of the superficial gas velocity and temperature (Maldonado et al., 2008, Pérez et al., 2006, Gillot et al., 2005, Fujie et al., 1992) (Eq.25). The equilibrium concentration with the gas phase was estimated from the partial pressure of the compound i, calculated itself considering its gas molar fraction, the corresponding Henry's law constant and the total pressure in the reactor (Eq.26).

Eq.23
$$F_{i,G\rightarrow L,n} = \alpha F V_{L,n} k_L a_i (\beta C^*_{i,L,n} - C_{i,L,n})$$

Eq.24 $$k_L a_i = k_L a_{O2} \sqrt{\frac{D_i}{D_{O2}}}$$

Eq.25 $$k_L a_{O2} = A * U_G^B \theta^{T-293.15}$$

Eq.26 $$C^*_{i,L,n} = K_{H,i} y_{i,n} P_{total,n}$$

Where $F_{G \to L}$ is the flux transferred from the gas to the liquid phase (g/d), α, F and β parameters that respectively account for the impact of wastewater characteristics, fouling of diffusers, and the effect of wastewater salinity on the saturation concentration, V_L the liquid volume (m^3), $k_L a$ the liquid side volumetric transfer coefficient (d^{-1}), C^*_L and C_L the equilibrium and the liquid concentrations respectively (g/m^3), D the diffusion coefficient in water (m^2/d), θ the Arrhenius coefficient describing temperature effect on $k_L a$, T the working water temperature (K), K_H the Henry's law constant ($g/m^3/atm$), y the molar fraction in the gas phase (mol/mol), and P_{total} the pressure in a given reactor (atm). Indices i and n stand for the compound and the reactor in series, respectively.

The transfer rate in the passive zone was reduced by a factor (F_R) compared to the rate in the active zone. The value of this factor, used in the present model, was calibrated in previous work to 0.032 to adjust the simulated effluent DO concentration with the measured one. The value lies within ranges proposed by Amiel (2002), which is 0.008 to 0.04 of the total mass of oxygen transferred in the reactor.

IV.2.2.2.2 IMPLEMENTATION OF A MASS BALANCE ON THE GAS PHASE

The base model assumed the same gas composition over the BAF height with O_2 molar fraction set to 0.21 in all reactors (atmospheric value). In this study, a mass balance on the gas phase was added to describe the evolution of the gas composition (Eq.27). Its implementation required several modifications of the model: inclusion of a gas volume, first to calculate the actual air/water proportion employed for total pressure estimation (set arbitrarily to 5/95% in the base model), then to estimate the working volume, and modification of $k_L a_{O2}$ accordingly (modification of $k_L a_{O2}$ calculation to make it consistent with the gas hold-up). Therefore, preliminary simulations were performed (simulations #1 to #3) to assess their impact on nitrification and N_2O predictions; which are described in the next sections. Mass balance was first added on O_2 only to assess its single impact on simulation results (simulation #4), and then it was implemented for all gases (simulation #5).

Eq.27 $$V_{G,n}\frac{\partial C_{i,G,n}}{\partial t} = \left(Q_{G,n-1}C_{i,G,n-1} - Q_{G,n}C_{i,G,n}\right) - V_{L,n}\alpha F k_L a_i(\beta C^*_{i,L,n} - C_{i,L,n})$$

Where Q_G is the air flow rate (Nm^3/d), C_G the concentration in the gas phase (g/m^3), and V_G the gas volume (m^3).

IV.2.2.2.3 EVOLUTION OF THE VOLUMETRIC OXYGEN TRANSFER RATE WITH THE SUPERFICIAL GAS VELOCITY

The base model of Bernier et al. (2014) used k_La_{O2} values and airflow evolution curves taken from the experiments of Gillot et al. (2005), who investigated oxygen transfer in a pilot-scale biofilter operated in similar conditions as those simulated (for more details see Section 4.3). The main difference being that the pilot-scale study was performed in clean water and with unseeded media. The application of the correlation proposed by Gillot et al. (2005) resulted in severe underestimation of nitrification. Consequently, authors increased k_La_{O2} values to meet effluent ammonium concentration.

In this study, we decided to get back to the correlation from Gillot et al. (2005) because it quantified the effect of increased superficial gas velocity both on gas hold-up and oxygen transfer rate evolution (both parameters being considered in our model). A first simulation was performed using these data (#1), and results were compared to the base model predictions (#0).

IV.2.2.2.4 MODIFICATION OF THE PRESSURE CALCULATION CONSIDERING A VARIABLE GAS HOLD-UP

In the base model, pressure inside the BAF was calculated considering the pressure exerted by a 5/95% air/water volume. In this work, the partition between mobile phases was calculated from their actual fractions in the BAF, according to Eq.28.

For the gas fraction, the relation from Gillot et al. (2005), which positively correlates the gas hold-up to the superficial gas velocity (Eq.29), was chosen, as it was obtained under similar operating conditions. The gas hold-up was considered as homogenous in the BAF for simplification.

The liquid fraction was deduced from the others, the sum of air, liquid, media and biofilm fractions being equal to one (Eq.30). The biofilm fraction was estimated from the biofilm thickness according to Eq.31. The latter is a function of filtration, detachment and biomass growth. Consequently, the biofilm fraction varies with time and along the BAF height. The

media fraction is a fixed value, equal to 0.64, which was considered homogeneous in the BAF for simplification.

Eq.28 $$P_{total,n} = gh_n \left(\frac{\varepsilon_G}{\varepsilon_G + \varepsilon_{L,n}} \rho_G + \frac{\varepsilon_{L,n}}{\varepsilon_G + \varepsilon_{L,n}} \rho_L \right) * (10^{-3}/101325)$$

Eq.29 $$\varepsilon_G = 2.9\ 10^{-2} - 4.1\ 10^{-4} U_G + 6.8\ 10^{-5} U_G^2$$

Eq.30 $$\varepsilon_{L,n} = 1 - \varepsilon_G - \varepsilon_M - \varepsilon_{B,n}$$

Eq.31 $$\varepsilon_{B,n} = Z_n a_a$$

Where g is the gravitational constant (m/s^2), ε_G, ε_L, ε_M, and ε_B the gas, liquid, media and biofilm fractions respectively, ρ_G, ρ_L, ρ_M and ρ_B the associated densities at working temperature (g/m^3), Z the biofilm thickness (m) and a_a the media specific area (m^2/m^3). The multiplication by 10^{-3}/101325 is used to convert pressure from Pa to atm.

IV.2.2.2.5 MODIFICATION OF THE WORKING VOLUME CALCULATION CONSIDERING THE GAS VOLUME

The liquid volume (i.e. the working volume) is commonly assumed to be the interstitial volume due to the reactor porosity. In BAFs, this working volume is actually occupied by an air/water mixture as both are injected into the system. Consequently, the liquid volume should be calculated considering the gas volume (Eq.32), which is deduced from the gas hold-up (Eq.33).

Eq.32 $$V_{L,n} = V_{R,n} - V_{M,n} - V_{B,n} - V_{G,n}$$

Eq.33 $$V_{G,n} = \varepsilon_G V_{R,n}$$

Where V_R, V_M and V_B are the total, media and biofilm volumes (m^3).

IV.2.2.3 SYNTHESIS OF THE PERFORMED SIMULATIONS

The impact of each hypothesis on the prediction of nitrification performances and N_2O gas-liquid partition was tested in a series of simulations. Modifications were implemented step by step, as described in Table IV.2-2. An additional simulation (#6) was performed after calibrating the K_La_{O2} value while keeping biokinetic parameters unchanged. It has to be noted that this paper is not intended to discuss into details the mechanisms of N_2O production in BAFs. It is focused on the evaluation of the impact of gas-liquid mass transfer representation on N_2O gas-liquid partition, thus on predicted off-gas N_2O concentrations.

Table IV.2-2. Series of simulations performed and the associated gas-liquid transfer hypotheses.

#	k_La_{O2}	ε_G	V_L =	Mass balance C_G	Remark
0	$17*U_G^{0.85}$	0.05	$V_R–V_M–V_B$	-	Base model
1	$43*U_G^{0.63}$	0.05	$V_R–V_M–V_B$	-	Using k_La to U_G curve from [a]
2	$43*U_G^{0.63}$	$f(U_G)$[a]	$V_R–V_M–V_B$	-	Considering variable ε_G from [a] to calculate pressure
3	$43*U_G^{0.63}$	$f(U_G)$[a]	$V_R–V_M–V_B–V_G$	-	Considering V_G to calculate V_L
4	$43*U_G^{0.63}$	$f(U_G)$[a]	$V_R–V_M–V_B–V_G$	O_2	Considering gas O_2 depletion
5	$43*U_G^{0.63}$	$f(U_G)$[a]	$V_R–V_M–V_B–V_G$	Complete	Considering gas N_2O and NO enrichment
6	$81*U_G^{0.63}$	$f(U_G)$[a]	$V_R–V_M–V_B–V_G$	Complete	Final calibration of the transfer model

[a] Gillot et al. (2005)

Each dynamic simulation was preceded by a 100-day pseudo-steady-state using average constant inputs from Table IV.2-1 and data describing the influent composition (more details can be found in Chapter III). Only dynamic predictions are presented in the paper. If "average" is indicated, it stands for an average of the dynamic simulation outputs for the period. Model outputs were compared to effluent characteristics measured on the studied BAF over 14 days.

IV.2.3 CALCULATION OF N_2O EMISSIONS AND FACTORS

The N_2O production rate was calculated considering the sum of the production rate by AOBs and the net production rate by heterotrophs. The N_2O emission rate is calculated as the sum of fluxes stripped in each reactor (Eq.34). As long as the mass balance on gaseous N_2O had not been added (simulations #0 to #4), it was the only way to calculate this emission rate. Afterwards, it could also be calculated as the product of the off-gas N_2O concentration and the airflow rate. Both calculations gave the exact same result for a given simulation (verified on simulations #5 and #6). The N_2O emission and production factors are respectively calculated by dividing the emission and production rates by the ammonium removal rate according to Eq.35 and Eq.36.

Eq.34
$$\mathrm{F_{N2O,G}} = -\sum_{n=1}^{8} \mathrm{F_{N2O,G\rightarrow L,n}}$$

Eq.35
$$\mathrm{N_2O - EF} = \frac{\mathrm{F_{N2O,G}}}{\mathrm{F_{NH4\ removed}}}$$

Eq.36
$$\mathrm{N_2O - PF} = \frac{\mathrm{F_{N2O}}}{\mathrm{F_{NH4\ removed}}}$$

Where F_{N2O} and $F_{N2O,G}$ are respectively the N_2O production and emission rates (gN/d), $F_{N2O,G\rightarrow L}$ the N_2O flux transferred from the gas to the liquid phase (gN/d), $N_2O - PF$ and $N_2O - EF$ the production and emission factors respectively (% of N-NH_4^+ removed), and $F_{NH4\ removed}$ the ammonium removal rate (gN/d).

IV.3 RESULTS

IV.3.1 SIMULATION RESULTS OBTAINED WITH THE BASE MODEL

A simulation run was performed with the base model (simulation #0, Table 2), for which the results are presented in Annex 4.

On average, predicted and observed effluent NH_4^+ and NO_3^- concentrations were 4.9 and 28.0 mgN/L, against 5.7 and 27.7 mgN/L. Nitrite concentration was correctly predicted (0.65 against 0.64 mgN/L measured), as well as effluent DO concentration (7.3 against 7.1 mgO_2/L measured). In addition, the model was also found able to catch the main dynamics of effluent concentrations (DO, ammonium, nitrate and nitrite).

N_2O production was overestimated by 30% (39.1 against 30.0 kgN/d), but most importantly the model was not able to describe the partition of N_2O between the gas and liquid phases. N_2O emission rate was overestimated by 89%, while the dissolved N_2O was underestimated by 88%. All in all, the emitted to produced N_2O ratio was 97%, while the measured one was 65%, questioning the performance of the gas-liquid transfer model. On the other hand, the oxygen transfer prediction was satisfying as nitrification rate was correctly predicted as well as effluent DO concentration.

IV.3.2 IMPACT OF GAS-LIQUID TRANSFER HYPOTHESES IMPLEMENTATION

Table IV.3-1 presents a summary of model predictions in terms of nitrification performance, N_2O production rate and its gas-liquid partition for each simulation. Results are detailed in the following sections.

Table IV.3-1. Summary of modelling results for each gas-liquid hypothesis.

#	NH_4^+ removal (%)	N_2O-PR (kgN/d)	N_2O-PF (% of N-NH_4^+ removed)	N_2O-EF (% of N-NH_4^+ removed)	Emitted / total (%)
Data	83	30.0	5.3	3.5	65
0	85	39.1	6.7	6.4	97
1	65	34.1	7.6	7.1	93
2	64	34.0	7.7	7.1	93
3	56	30.6	7.8	7.2	92
4	52	28.0	7.8	7.2	92
5	52	26.3	7.3	5.2	71
6	83	34.8	6.1	4.5	74

IV.3.2.1 EVOLUTION OF THE VOLUMETRIC OXYGEN TRANSFER RATE WITH THE SUPERFICIAL GAS VELOCITY

For an average superficial gas velocity of 299 $Nm^3/m^2/d$, the k_La_{O2} was 91 h^{-1} with the initial model. After modifying the k_La_{O2} to U_G's correlation (Eq.25), it decreased to 65 h^{-1}. Consequently, the mass of O_2 transferred to the liquid phase dropped substantially which negatively impacted nitrification performances (ammonium removal rate passed from 587 to 449 kgN/d).

N_2O production rate decreased in a lower extent (from 39.1 to 34.1 kgN/d), resulting in an increase of predicted N_2O production factor from 6.7 to 7.6%. According to the model, the net N_2O production by AOBs decreased by 11 kgN/d, and its proportion consumed by heterotrophic bacteria remained constant (53%, i.e. 6 kgN/d), resulting in a lower net N_2O production rate. The emitted to produced N_2O ratio decreased from 97 to 93% as k_La_{N2O} decreased with k_La_{O2}, reducing N_2O transfer to the gas phase.

IV.3.2.2 MODIFICATION OF THE PRESSURE CALCULATION CONSIDERING A VARIABLE GAS HOLD-UP

In simulation #2, the gas hold-up was estimated according to Eq.29. The gas hold-up was used to calculate the gas saturation, i.e. the proportion of gas in the gas/liquid mixture, and the reactor pressure according to Eq.28. A 5% gas saturation was set arbitrarily in simulations #0 and #1.

Depending on the superficial gas velocity, the gas hold-up was 3.5% on average during the 14-day period. This resulted in a mean gas saturation of 13% in the active zone (Figure IV.3-1), which was about three times higher than the previously imposed value. The

decrease of gas saturation over the filter height was related to the thinner biofilm, which induced higher liquid volume, while gas hold-up was considered as homogeneous in the BAF. In the passive zone, gas saturation was directly equal to gas hold-up, since there was no media. Consequently, gas saturation considered in simulations #0 and #1 was higher in this zone. The modifications did not significantly affect pressure values in the BAF (-1% on average), which resulted in similar nitrification performance (444 and 449 kgN/d after and before modification, respectively) and N_2O production rates (34.0 and 34.1 kgN/d respectively). Likewise emitted to total N_2O ratio was similar (93.0 against 93.1%).

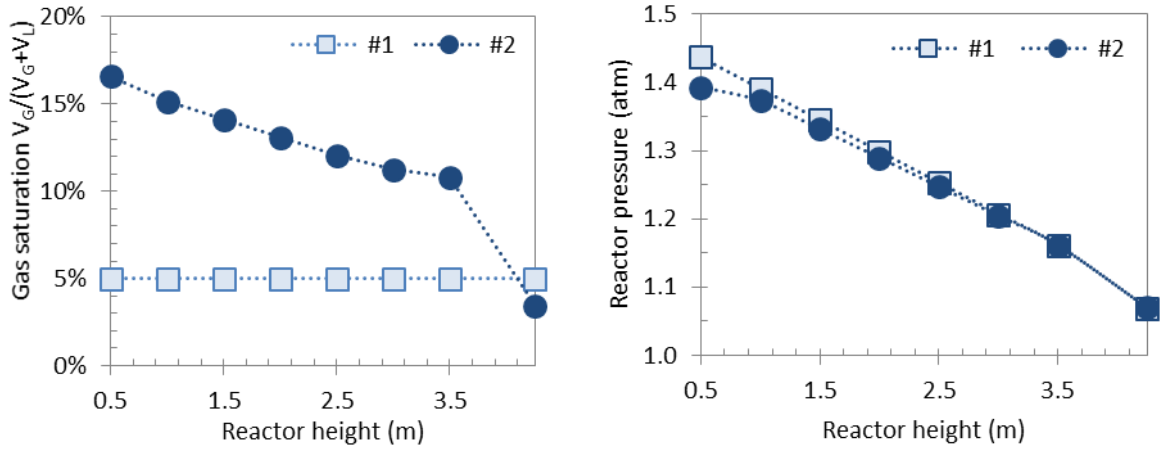

Figure IV.3-1. Evolution of air/liquid proportion (left) and pressure (right) over the BAF height before (#1) and after (#2) including a variable gas hold-up to calculate pressure.

IV.3.2.3 MODIFICATION OF THE WORKING VOLUME CALCULATION CONSIDERING THE GAS VOLUME

The repartition of media, biofilm, liquid and gas volumes in the active zone is presented on Figure IV.3-2 (left panel); whereas the evolution of the hydraulic retention time (HRT) is presented on the right panel.

Accounting for the gas volume (21 m^3 on average) reduced the liquid volume from 160 to 140 m^3. The HRT was therefore reduced in the same proportion (13%), which resulted in lower mass of autotrophic biomass stabilized in the BAF and reduced nitrification performances (ammonium removal rate passed from 444 to 390 kgN/d). Total HRT in the BAF was 29.9 and 27.9 min before (#2) and after (#3) including gas hold-up to calculate the remaining liquid volume.

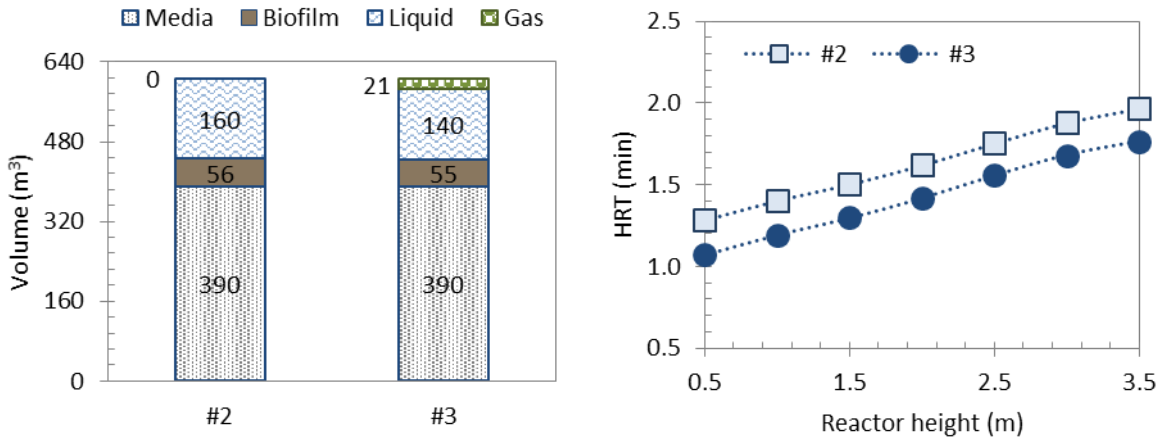

Figure IV.3-2. Prediction of compartment volumes in the active zone of the BAF (left) and evolution of HRT over the BAF height (right) before (#2) and after (#3) including gas hold-up to calculate V_L.

For simplification, gas hold-up was considered homogeneous over space. On the other hand, the biofilm fraction was not homogeneously distributed. In agreement with experimental observations (Azimi et al., 2010, Vigne, 2007), the model predicted a decrease of the biofilm thickness over the height that followed the evolution of nitrogen removal. Consequently, the volume available for water, thus NH_4^+ removal, was more affected at the bottom of the reactor (ammonium removal rate -21% and -8% at the bottom and the top of the BAF, respectively).

IV.3.2.4 IMPLEMENTATION OF A MASS BALANCE ON THE GAS PHASE

Figure IV.3-3 displays the evolution of O_2 (left panel), NO and N_2O (right panel) gas molar fractions over the BAF height.

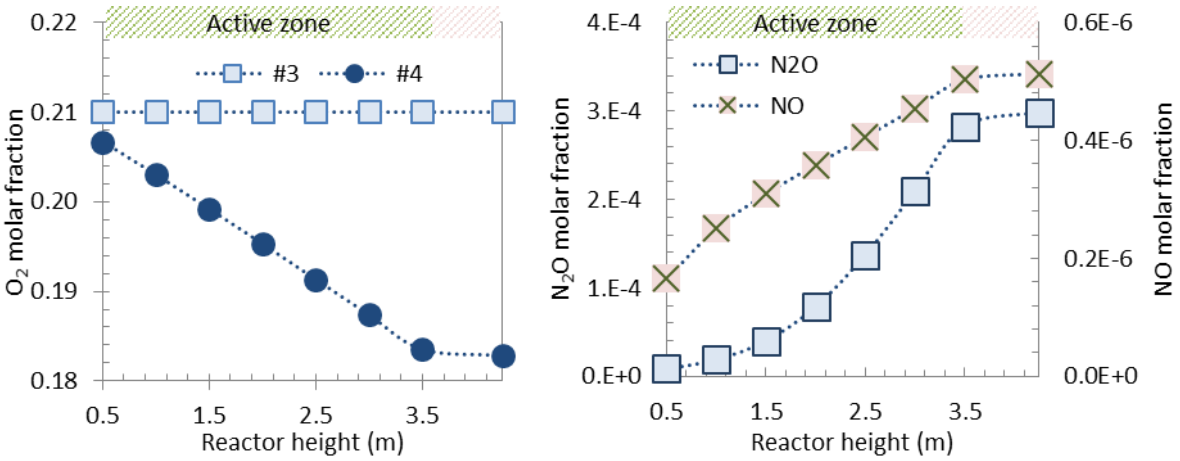

Figure IV.3-3**.** Gas molar fraction of O_2 before (#3) and after (#4) including a mass balance (left); Gas molar fractions of NO and N_2O after including a mass balance (right).

Simulation results indicated a depletion of O_2, as it was transferred to the liquid phase: O_2 gas fraction decreased from 0.21 to 0.18 on average. This reduced the concentration gradient at the gas-liquid interface by 8% on average in the active zone, lowering the O_2 transfer rate. Consequently, ammonium removal rate was reduced from 390 to 359 kgN/d (-8%). At the contrary, the N_2O gas molar fraction increased over the BAF height as it got stripped from the liquid. On average, its fraction increased from 3 10^{-7} to 1.3 10^{-4} and its concentration in the off-gas was 298 ppm, i.e. almost 10^3 times the atmospheric concentration (~ 328 ppb). This enrichment decreased the gradient concentration at the gas-liquid interface for stripping and the associated total N_2O flux from liquid to gas. The results were similar for NO in a lower extent (5 ppm in the off-gas). Models #1 to #4 highly overestimated the emitted to produced N_2O ratio (over 90% predicted against 65% measured). After integrating the gas enrichment in NO and N_2O, the predicted ratio for simulation #5 (71%) was closer to full-scale data.

The NO and N_2O gas fraction profiles were related to their production within the filter. The latter increased over the reactor height, as NO and N_2O were produced during nitrification. The associated transfer rates from the bulk to the gas phase therefore increased over the BAF height, which explained the accumulation of NO and N_2O in the gas phase. Finally, their small evolutions between 3.5 and 4.25 meters were due to the lower gas-liquid transfer rates in the passive zone.

The same net N_2O production by AOBs was modelled in simulations #4 and #5. However, the available dissolved N_2O to be reduced by heterotrophs was higher in simulation #5, which induced a higher consumption rate, i.e. a lower net N_2O production. Consequently, the net N_2O production rate was 26.3 against 28.0 kgN/d in simulation #4.

IV.3.3 SIMULTANEOUS PREDICTION OF NITRIFICATION PERFORMANCES AND N_2O EMISSIONS

In order to recover nitrification performances, k_La_{O2} values were increased from 65 to 117 h^{-1} on average, by increasing the A constant of Eq.25 from 43 to 81 (simulation #6). Figure IV.3-4 represents measured and predicted effluent NH_4^+, NO_3^-, DO concentrations, emitted to produced N_2O ratio, as well as airflow rate and effluent temperature. Predicted and measured average effluent concentrations were very similar: 5.4 vs. 5.7 mgN/L for NH_4^+, 27.6 vs. 27.7 mgN/L for NO_3^-, 6.5 vs. 7.1 mg/L for DO, and 0.71 vs. 0.64 mgN/L for NO_2^- (not shown on Figure 5), respectively. Their dynamics were also well described by the model.

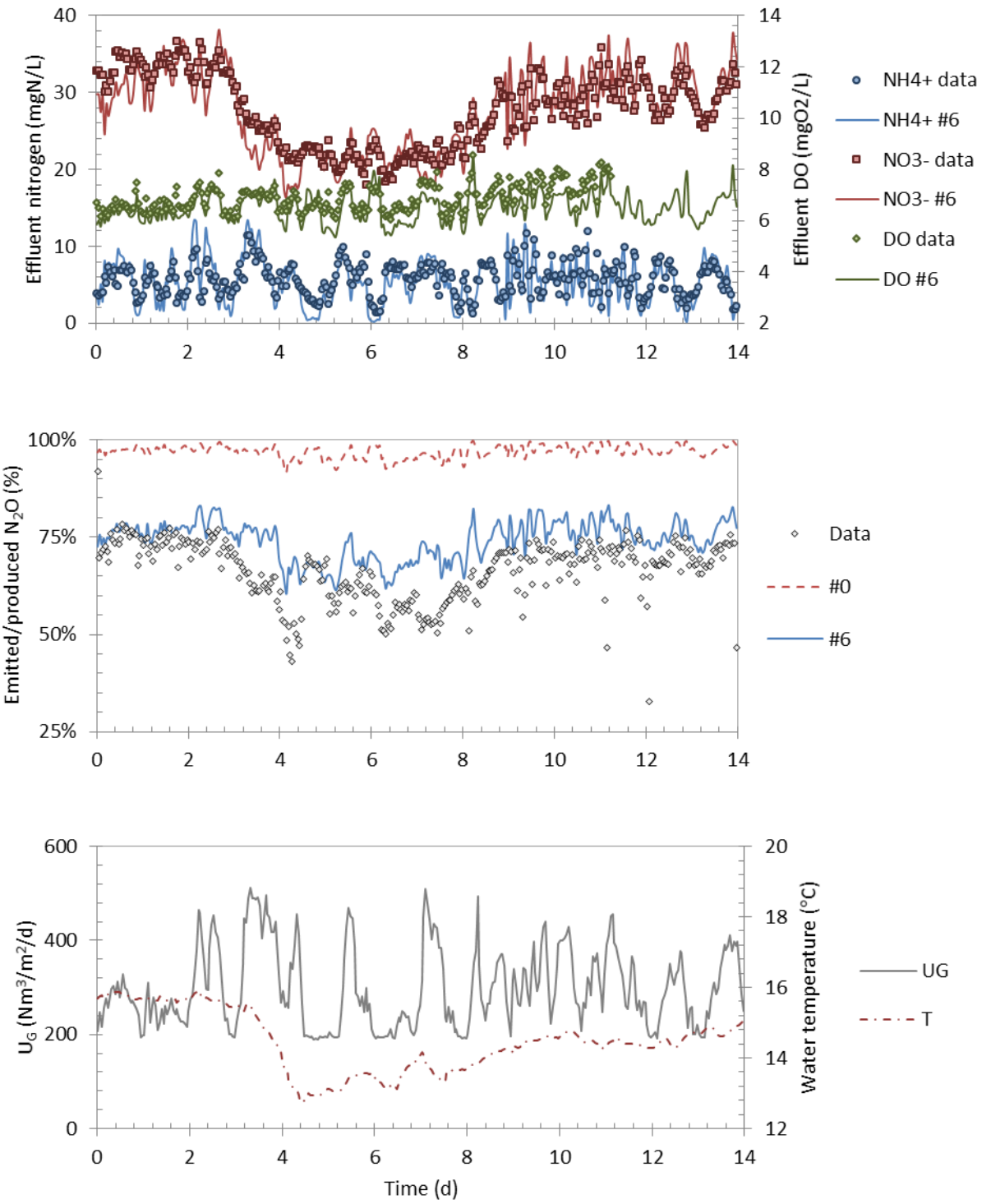

Figure IV.3-4. One-hour averaged predicted and measured effluent NH_4^+, NO_3^- and DO (top), emitted to produced N_2O predicted before (#0) and after (#6) including the mass balance on NO and N_2O (middle), superficial gas velocity and effluent temperature (bottom).

The modification of k_La_{O2} increased k_La_{N2O} (Eq.24), thus increasing the emitted to produced N_2O ratio from 71 to 74%. The N_2O emission factor was however closer to experimental data (4.5% vs. 5.2% before calibration), as the NH_4^+ removal rate was better described (Table 3). The predicted ratio followed the main trends as experimental data. Its value is well predicted

from days 0 to 3 and days 8 to 14. The drop from day 3 to day 8 was due to an increase of the airflow rate - related to a peak of ammonium load - and to a decrease of temperature. Measures reported a drop of the emitted to produced N_2O ratio more pronounced than model predictions. The effect of temperature on Henry's constants was included in the model, according to the literature (Sander, 2015). The difference of the emitted to produced N_2O ratio between observations and model predictions is due to an overestimation of N_2O production which is much more pronounced at this period (+44%) compared to the rest of the period (+4%). Model results suggested an increase of N_2O production by AOBs, and a decrease of N_2O consumption by heterotrophs, related to high O_2 transfer rates.

After calibrating k_La_{O2} value, and without any calibration of N_2O parameters, simulation results were closer to experimental data than predictions from the initial model. N_2O concentrations were 407 ppm and 0.44 mgN/L in the off-gas and the effluent respectively, against 318 ppm and 0.50 mgN/L measured.

IV.4 DISCUSSION

IV.4.1 CONSIDERING GAS ENRICHMENT IS ESSENTIAL TO PREDICT N_2O EMISSIONS

Whereas the plug flow behaviour of the liquid phase is usually considered in BAF models, it has rarely been taken into account for the gas phase (Bernier et al., 2014, Vigne et al., 2010, Hidaka and Tsuno, 2004, Viotti et al., 2002), with the exception of some studies performed at small-scale on oxygen gas-liquid mass transfer (Cruvellier et al., 2017, Poughon et al., 1999). To our best knowledge, the BAF model developed in this study is to date the only one describing both oxygen and N_2O gas-liquid mass transfer and moreover at full-scale.

Results of this study highlighted significant differences in model predictions when considering a constant (well-mixed hypothesis) or a variable gas composition. With a constant gas composition corresponding to that of ambient air (simulation #0), the model was able to predict nitrification performances but failed to describe the emitted to produced N_2O ratio as it overestimated N_2O stripping (see Table 3). It was only when a mass balance on the gas phase was included, that the model correctly described the emitted to produced N_2O ratio. Gas enrichment along the BAF height (from bottom to top: 300 ppb to 298 ppm, in simulation #5) highly decreased the driven potential of N_2O transfer [Eq.1], allowing a larger fraction of N_2O to remain soluble.

The inclusion of this mass balance impacted much more NO and N_2O than O_2 transfer (simulation #4). It induced gas depletion in O_2 by 8% only, lowering nitrification

performances to a small extend (-8% between simulations #3 and #4). Even when k_La_{O2} and k_La_{N2O} were increased by the same proportion in simulation #6, the impact was more pronounced for N_2O outflow molar fraction (+36%) compared to the one of O_2 (-7%). This result is explained by the fact that oxygen is respectively 2 and 19 times less soluble than NO and N_2O ($K_{H,O2}$ = 1.5 10^{-5} ; $K_{H,NO}$ = 2.3 10^{-5} ; $K_{H,N2O}$ = 2.8 10^{-4} mol/m^3/atm at 15°C) and its content in the ambient air is much higher.

In sum, modelling the gas-phase as a plug-flow reactor, similarly to the liquid phase, appears to be essential to model gas-liquid N_2O exchanges. Otherwise, predicted N_2O off-gas concentration would be highly underestimated and N_2O stripping overestimated. If dissolved N_2O concentration is not measured (which is often the case), this could lead to unnecessary calibration of the biokinetic model parameters to fit measured off-gas N_2O concentration. This result is in accordance with other studies dealing with gases of higher solubility than O_2 like CO_2 (Sperandio and Paul, 1997). This recommendation stands not only for BAFs but also for any process having a plug-flow behaviour of the gas phase, such as activated sludge processes with bubble aeration.

IV.4.2 CONSIDERING GAS HOLD-UP LARGELY IMPACTED NITRIFICATION PREDICTION

Modifications have been made to the initial BAF model to take into account the minimum physical phenomena that allow a proper description of N_2O emissions. These affected predictions of nitrification performances, in particular the consideration of the gas phase as a compartment of the model.

The gas phase was added as a compartment of the BAF by including gas hold-up according to Eq.30, which was 3.5% of the active volume on average. Results indicated that it highly decreased nitrification performances when considered to calculate the working volume (-13%). This result may seem surprising given the small gas fraction. However, it should be reminded that the BAF system is mostly filled with polystyrene materials (64% of the reactor volume in the active zone). Unlike suspended growth systems, such as conventional activated sludge, the working volume in BAFs cannot be considered to be the reactor volume. The volume available for water is relatively small (about 26% of the active zone, considering that 10% is occupied by the biofilm on average), making the liquid fraction very sensitive to gas variations. Such feature could help improving the prediction of nitrogen removal in case of hydraulic peak-loads or episodes of high aeration rates, both operational parameters reported as requiring additional calibration of the BAF model parameters (Vigne et al., 2010).

The sum of all modifications resulted in a large underestimation of ammonium removal rate (-39%), which required a calibration. Given the capacity of the initial model to describe nitrification with biokinetic parameters from the literature (simulation #0), it seemed more adapted to calibrate transfer model parameters only.

IV.4.3 CALIBRATION PROCEDURE AND RECOMMENDATIONS

The extended model was calibrated after modification of the gas-liquid transfer coefficient to recover average nitrification performances. Similarly to Bernier et al. (2014), our approach was to increase k_La_{O2}, considering that gas-liquid exchanges should be higher in a functioning BAF compared to a clean media bed (unseeded and working with clean water), which has been observed in previous studies (Reiber and Stensel, 1985, Stenstrom et al., 2008). We did not, however, modify the correlation between gas hold-up and superficial gas velocity [Eq.6]. The main elements supporting these assumptions are the differences in terms of fixed-bed properties and hydraulics. This is discussed hereinafter with our current understanding of the physical mechanisms involved in such systems, and supported by simulation results and a literature review.

IV.4.3.1 SLIGHT EVOLUTION OF GLOBAL GAS HOLD-UP

A functioning BAF differs from a clean media bed by the effluent composition which could affect the surface tension (Gunde et al., 1992, Sridhar and Rami Reddy, 1984); but also by lower bed porosity due to the development of the biofilm on the media (increasing particle size) and within the media bed interstices. Likewise, based on a set point value of the headloss, BAFs are regularly backwashed to avoid too much biofilm and particles accumulation (Bernier et al., 2016).

In a pilot BAF study, Stenstrom et al. (2008) attributed the higher oxygen transfer efficiency observed in process water to an increase of gas hold-up. This assumption was based on a naked eye observation through an observation port on the column, which revealed that gas bubbles were retained by the media for a few seconds before being washed away. Previous work on lab-scale fixed-beds –operated in co-current upflow mode and in clean conditions– has shown that gas hold-up was negatively correlated with packing size (Collins et al., 2017, Maldonado et al., 2008, Kies et al., 2005) and negatively with bed porosity (Collins et al., 2017, Maldonado et al., 2008). According to Collins et al. (2017), and Maldonado et al. (2008), the increase of gas hold-up is mainly due to a higher static gas fraction (also called stagnant gas hold-up); which is attributed to increased gas to particles contact area and higher surface tension forces.

However, it is likely that the increase of the static gas fraction is less pronounced in a functioning backed bed system compared to a clean water system due to the lower liquid surface tension and associated capillarity forces. This latter is expected to favour the deformation of bubbles and their breakup. Considering that bubbles size was found to be calibrated by the pores size (Chen et al., 2017, Bordas et al., 2006), a distribution with lower bubble sizes is to be found in a functioning BAF. Thanks to their reduced size, bubbles should have the ability to evolve more easily within the bed (Deshpande et al., 2018), thus reducing the static gas fraction and compensating the increase of the dynamic gas hold-up.

To evaluate the hypothesis based on a slight evolution of global gas hold-up, an additional simulation was performed (results not shown) by increasing gas hold-up along with k_La_{O2}. This led to a severe reduction of ammonium removal rate, as the HRT highly decreased (see Section 4.2). In order to achieve correct ammonium removal (81%), k_La_{O2} had to be increased to 162 h^{-1}, which corresponded to an average gas hold-up of 8.6%. These high values –far beyond literature ranges in clean systems– increased the emitted to produced N_2O ratio from 74 to 75%, moving it further away from experimental data (65%).

This result supports the hypothesis of a less pronounced evolution of global gas hold-up in a functioning BAF compared to a clean media bed. However, experimental validation is necessary. It would require characterizing the evolution of the different gas fractions (static and dynamic) and bubbles size with water composition (such as surface tension) and backed bed properties (such as bed porosity). Application of new characterization methods such as tomography could be very useful (Collins et al., 2017, Chen et al., 2017).

IV.4.3.2 EVOLUTION OF OXYGEN TRANSFER COEFFICIENT

The main elements supporting a higher gas/liquid transfer rate in a functioning BAF compared to a clean media bed are:

- As mentioned above, a slight evolution of gas hold-up coupled with a reduction of the distribution of bubbles size would increase the interfacial area ;
- The decrease of the bed porosity due to the biofilm coupled with a slight evolution of gas hold up would increase the gas to liquid volume ratio. According to the present model, the biofilm fills about 9% of the active zone. This would theoretically increase the gas to liquid volume ratio from 0.097 to 0.130 ;
- The reduced liquid volume would induce a higher local liquid velocity in the bed, therefore increasing the slip velocity between liquid and bubbles and consequently the liquid side mass transfer coefficient k_L (Maldonado et al., 2008) ;

- Lower bed porosity is expected to influence bubbles movement in the void fraction inducing increased turbulence in the bubble wake and consequently increased k_L (Kherbeche et al., 2013).

In summary, the mechanisms affecting mass transfer parameters in full-scale BAFs are not fully understood, especially the combined effect of bed porosity and particle size changes in the gas hold-up and oxygen transfer needs to be evaluated. In this study, k_La_{O2} and gas hold-up were both found to highly impact nitrification performances and gas to liquid partition of N_2O. It was chosen to partially decorrelate those parameters as we kept the gas hold-up corresponding to that of a clean media bed (Gillot et al., 2005) while increasing the value of k_La_{O2}. This way, it was possible to correctly predict both the mass transfer of oxygen (with nitrification performances and effluent DO concentration being well predicted) and N_2O (as its gas to liquid partition was well predicted). However, experiments are necessary to validate these hypotheses. Gas-liquid transfer measurements with a clean media bed against a colonized one at different colonization degrees (i.e. progressive reduction of the bed porosity), would provide useful information for model calibration. The experimental design should also evaluate the evolution of bubble's size and shape for dissociating the impact of the presence of the biofilm on the liquid side mass transfer coefficient (k_L) and on the interfacial area (a). Furthermore, experiments should also be performed in full-scale BAFs to assess the gas distribution within the media bed and global k_La_{O2} for various superficial gas velocities.

IV.5 CONCLUSION

In this work, a tertiary nitrifying BAF model, previously validated on long-term data of the Seine Aval plant, was extended to include the main biological production and consumption pathways of N_2O. Hypotheses related to gas-liquid exchanges were successively implemented in the model, in order to assess their relevance to describe nitrification and N_2O emissions. Model predictions were confronted to experimental data from a 14-day measuring campaign on Seine Aval. The main conclusions are:

- Without considering the mass balance on the gas phase, the model was able to successfully describe nitrification and the order of magnitude of N_2O production rate. It was, however, unable to predict the N_2O gas-liquid partition, highly overestimating the emitted to produced N_2O ratio (over 90%, against 65%);
- Including the mass balance for the gas phase, allowed the model to describe N_2O emissions, predicting gas enrichment over the BAF height (300 ppb to 298 ppm);
- Preliminary modifications of the model heavily impacted the prediction of nitrifying performances. In particular, the inclusion of a gas compartment decreased the liquid volume, i.e. the HRT, and consequently ammonium removal by 13%;
- In the absence of experimental data on gas-liquid transfer in full-scale BAFs, the model was calibrated by increasing k_La_{O2} from 65 to 117 h^{-1};
- The calibrated model successfully described nitrification and N_2O production and emissions.

In future work, the extended model will be confronted to a second dataset and evaluated on its ability to predict nitrification and N_2O emissions for contrasted operating conditions. After validation, it will be used to get a further insight into the mechanisms leading to high N_2O emissions in full-scale nitrifying BAFs.

Chapter V. Predicting N_2O emissions from a full-scale tertiary nitrifying BAF: model calibration

ERRATUM

In chapters V and VI, the solid fraction was included in the calculation of the total pressure (Eq.28), which is an error. This induced an underestimation of pressure by 8% (1.19 against 1.29 atm) in the filter bed, which affected slightly the prediction of nitrification and N_2O production.

More importantly, it is not expected to significantly alter any of the results from the following chapters nor their messages. Only a small modification of the calibrated parameters may be required, which will be verified in further work.

RESUME

Dans le chapitre précédent, l'influence des mécanismes de transfert gaz/liquide sur la prédiction des performances de nitrification et la répartition gaz/liquide des flux de NO et N_2O a été évaluée. Ce travail a été fait sans calage préalable des paramètres du modèle décrivant les mécanismes biologiques de production et de consommation de N_2O et sur la base des résultats obtenus lors de la campagne hivernale. Dans ce chapitre, les mécanismes biologiques de production de N_2O vont être investigués, via une analyse de sensibilité et le calage des paramètres des modèles biocinétiques et de transfert gaz/liquide, sur la base d'un jeu de données long-terme incluant les deux campagnes de mesure (hivernale et estivale).

Un modèle décrivant le fonctionnement de biofiltres nitrifiants de la station de Seine Aval et incluant les principales voies biologiques de production/consommation de N_2O a été calé. Le jeu de données considéré inclut deux ans de données de fonctionnement des biofiltres (2014-2015) et deux périodes pour lesquelles les flux de N_2O gazeux et dissous ont été mesurés (septembre 2014 et janvier/février 2015). Une analyse de sensibilité a montré que seuls 19 des 90 paramètres du modèle ont une influence significative sur les performances de nitrification et sur la production de N_2O. Alors que l'activité de nitrification est principalement sensible aux paramètres régissant le transfert d'oxygène, les concentrations en N_2O gazeux et dissous sont fortement et positivement corrélées aux paramètres induisant une accumulation de nitrites, révélant une contribution forte de la voie de dénitrification par les bactéries nitritantes (ND) à la production de N_2O en cas d'accumulation importante des nitrites. Avec une modification de seulement cinq paramètres (la porosité initiale du lit filtrant ε_0, la constante d'affinité des bactéries nitratantes pour l'oxygène $K_{O,NOB}$, et les paramètres liés à la voie ND : $K_{O,AOB,ND}$, $K_{I,O,AOB}$ et η_{ND}), le modèle est capable de décrire les performances de nitrification sur l'ensemble de la période d'étude, mais aussi l'ordre de grandeur et les principales évolutions dynamiques des flux de N_2O gazeux et dissous, et ce, lors des deux campagnes de mesure. En revanche, le modèle montre une tendance à surestimer la production de N_2O pour les forts débits d'air (>100 $Nm^3/kgN\text{-}NH_4$). Finalement, le modèle calé a été employé pour comprendre les raisons pour lesquelles le facteur d'émission observé lors de la période hivernale était deux fois plus élevé qu'en période estivale. Le modèle indique une forte influence de la dénitrification hétérotrophe sur la production globale. En effet, celle-ci agit comme un puits de N_2O, consommant 77% du N_2O produit en été, et 58% en hiver. La plus faible consommation hivernale est, selon le modèle, liée à une concentration en oxygène dissous plus élevée au sein du biofilm, induisant une inhibition plus importante de l'étape de réduction du N_2O en N_2 par les hétérotrophes.

Mots-clés : analyse de sensibilité, biofilm, diffusion, nitrification, oxygène, protoxyde d'azote

ABSTRACT

In the previous chapter, the influence of gas-liquid transfer mechanisms on the prediction of nitrification performance and the partitioning of gas-liquid NO and N_2O fluxes was evaluated. This work was done without any preliminary calibration of the N_2O model, and was based on experimental data collected during the winter campaign. In the present chapter, the biological N_2O production mechanisms will be investigated, with the help of a global sensitivity analysis and the calibration of model parameters using a long-term dataset including both N_2O measuring campaigns (performed in winter and in summer).

A model describing the functioning of nitrifying BAFs of the Seine Aval WRRF, and including the main biological N_2O production and consumption pathways, was calibrated. The experimental dataset combined two years of operational conditions of the biofilters (2014-2015), and two periods during which emitted and liquid N_2O fluxes were measured (September 2014 and January/February 2015). A global sensitivity analysis revealed that only 19 out of 90 parameters had a significant influence on the prediction of nitrification performance and N_2O production. While the nitrifying activity was mainly dependent on gas-liquid oxygen transfer parameters, dissolved and off-gas N_2O concentrations were highly and positively correlated to the parameters which induced nitrite accumulation. This suggests a potentially high production of N_2O by the nitrifier denitrification pathway (ND) in case of important nitrite accumulation. By modifying five parameters only (initial porosity of the bed ε_0, affinity constant of nitrite oxidizing bacteria to oxygen $K_{O,NOB}$, parameters related to ND: $K_{O,AOB,ND}$, $K_{I,O,AOB}$ et η_{ND}), the model was able to describe nitrification performance over the long-term study, but also the order of magnitude and the main trends of N_2O fluxes during both measuring campaigns. The model, however, shows a tendency to overestimate N_2O production at high aeration rates (>100 $Nm^3/kgNH_4\text{-}N_{applied}$). The calibrated model was finally used to understand the reason behind the higher N_2O emission factor in the winter period compared to the summer period. Modelling results highlighted the significant influence of heterotrophic denitrification on the overall N_2O production. Indeed, heterotrophic denitrification was found to act as a sink of N_2O, consuming 77% of the N_2O produced by nitrification in summer, and 58% in winter. The lower consumption predicted in winter was due to higher concentration of dissolved oxygen in the biofilm, which induced a higher inhibition of the heterotrophic N_2O reduction step.

Keywords: biofilm, diffusion, nitrification, nitrous oxide, oxygen, sensitivity analysis

V.1 INTRODUCTION

Nitrous oxide (N_2O) is a potent greenhouse gas, about 300 times more powerful than carbon dioxide (CO_2), and the most important ozone depleting substance of the 21st century (Ravishankara et al., 2009). Wastewater resource recovery facilities (WRRFs) have received increasing attention for their role as point source of N_2O emissions. N_2O is mainly produced and released from bioreactors during nitrification and denitrification reactions, which have been recently described in several models, reviewed by Ni and Yuan (2015) and Massara et al. (2017a).

Nitrification transforms ammonium (NH_4^+) into nitrate (NO_3^-) under aerobic conditions. It is the successive oxidation of NH_4^+ to nitrite (NO_2^-) by ammonium oxidizing bacteria (AOB) and archaea (AOA), and oxidation of NO_2^- to NO_3^- by nitrite oxidizing bacteria (NOB). NH_4^+ oxidation to NO_2^- is divided into the oxidation to hydroxylamine (NH_2OH), followed by the oxidation of NH_2OH to nitric oxide (NO), and further oxidized to NO_2^-. N_2O is mainly produced *via* two biological routes: nitrifier nitrification (NN), which is the reduction of NO to N_2O during NH_2OH oxidation, and nitrifier denitrification (ND), which is the reduction of NO_2^- to NO, further reduced to N_2O (Kampschreur et al., 2009, Schreiber et al., 2012). Ordinary heterotrophic organisms (OHO) transform NO_3^- to nitrogen gas (N_2) under anoxic conditions during heterotrophic denitrification (HD), NO_2^-, NO and N_2O being the successive reaction intermediates. Nitrification and HD thus share common intermediates but only HD is known to reduce N_2O. For more details, please see Chapter III.

N_2O production related to AOB and OHO individually has been largely investigated and reviewed (Kampschreur et al., 2009, Law et al., 2012b, Schreiber et al., 2012, Massara et al., 2017a). In particular ND is known to be enhanced by low DO concentrations and NO_2^- accumulation (Peng et al., 2015, Kampschreur et al., 2009). HD can act as a source or a sink of N_2O, depending mainly on DO levels and the availability of an electron donor (Pan et al., 2013a). However, autotrophic and heterotrophic micro-organisms can cohabit, notably in biofilm systems when exposed to ammoniac (NH_3) and low organic carbon concentrations (Derlon, 2008, Henze et al., 2008, Sabba et al., 2018). Biofilms are subject to mass transfer resistance, represented by a liquid film between the bulk liquid and the biofilm, which leads to contrasted concentrations of substrate between the bulk and the biofilm, and substrate gradients and biomass stratification within the biofilm (Boltz et al., 2010, Sabba et al., 2018). The conditions affecting N_2O in biofilm systems have been poorly documented so far, while such processes are growing in popularity (Todt and Dorsch, 2016, Sabba et al., 2018).

Sabba et al. (2017) investigated N_2O production from nitrifying and denitrifying biofilms in a modelling study. According to their results, a spatial distribution of N_2O pathways is to be found in the biofilm depending on operating conditions. In the outer part of the biofilm, usually well oxygenated, the NH_4^+ oxidation rate is high and NN is likely to dominate N_2O production. The produced NH_2OH can diffuse in the inner parts of the biofilm, where O_2 is limited. In these conditions, NO_2^- being the sole electron acceptor, it will form N_2O *via* ND. Authors also highlighted that the inner regions of denitrifying biofilms can act as a sink of N_2O, in excess electron donor conditions, which was also reported by Read-Daily et al. (2016). Nitrification and HD were not simulated simultaneously in these studies, but we can assume that N_2O formed in the outer layers of the biofilm may be consumed in the inner layers. In fact, the capability of HD to consume N_2O produced by nitrification was reported in several studies (Guo and Vanrolleghem, 2014, Bollon et al., 2016a, Conthe et al., 2019).

Tertiary nitrifying biological active filters (BAFs) of the Seine Aval WRRF were found to produce large fractions of N_2O during two periods: 2.3% of the eliminated NH_4^+ load in summer 2014 and 4.9% in winter 2015 (Bollon et al., 2016b). The authors assumed that the higher N_2O production in winter was related to a thicker biofilm, higher effluent NO_2^- concentrations, and therefore higher production by ND. Tertiary nitrifying BAFs are complex systems, as they combine autotrophic and heterotrophic biomasses and are designed to work with a plug flow behaviour of the liquid phase leading to gradients of microbial activities (Zhang et al., 1995). Understanding the triggers of N_2O production in such complex systems requires the development of mechanistic models coupling a proper description of mass transfer mechanisms with a proper representation of biological conversion processes.

A BAF model describing the functioning of the tertiary nitrifying BAFs of the Seine Aval WRRF was developed by Bernier et al. (2014) and updated by Fiat et al. (2019) to include N_2O pathways and emissions. Hydraulics is described as a plug-flow and the biofilm by a 1-D heterogeneous model, which leads to spatial gradients over the filter height and moderate gradients within the biofilm. Although this model was successfully applied to the data of the winter campaign, it was not confronted to the data of the summer campaign, nor calibrated on long-term data. In this work, simulation results obtained using the BAF model were confronted to long-term data and to N_2O data from the two distinct measuring campaigns performed on the Seine Aval WRRF. The objective were: (1) to calibrate the model for long-term prediction of nitrification, (2) to investigate the interactions between autotrophic and heterotrophic biomasses, and (3) to explore the mechanisms leading to higher N_2O production observed during the winter campaign in comparison to the summer campaign.

V.2 MATERIAL AND METHODS

V.2.1 EXPERIMENTAL DATA

Datasets used in this work were collected on the Seine Aval WRRF between January 2014 and December 2016 (Chapter III). During that period, the plant was designed to receive a nominal flow of 1.7 million m^3/d (5.5 million PE). The pre-treatment stage included screening, grit/oil removal and primary clarifiers. The secondary biological treatment was performed by high load activated sludge tanks followed by secondary clarifiers and ballasted flocculation units to mainly remove suspended solids and phosphorus. Nitrogen removal was performed in a biofiltration stage composed of 84 Biostyr® filters for nitrification (divided into six batteries) followed by 18 Biostyr® and 12 Biofor® filters for post-denitrification using methanol as an external carbon source. Tertiary nitrifying filters were characterized by a section of 173 m^2 and a design media bed height of 3.5 m composed of 4 mm polystyrene beads.

The long-term dataset consisted in operational data monitored on a daily basis, provided by the plant's operator (SIAAP). It included 24-hour composite samples collected at the inlet and outlet of the nitrification stage. They were analysed to determine NH_4^+, NO_3^-, NO_2^-, PO_4^{3-}, TSS, and COD concentrations. Model inputs also included the daily average influent and air flows of the battery "B2" on which N_2O measurements were performed. It has to be noted that a preliminary simulation was performed using influent and air flow data of the nitrification stage. It showed only a slight difference with the results obtained using data of the battery B2 (Annex 5). Finally, measurements of pH and temperature performed at the inlet of the nitrification stage were used. The main operating conditions and nitrification performance over the simulated period are recalled in Table V.2-1.

High-frequency data (10 min average) from the two measuring campaigns were inserted in the long-term dataset. The summer campaign was 7 days long and was carried out in September 2014 (days 257.5 to 264.5). The winter campaign was 14 days long and was carried out in January/February 2015 (days 390.5 to 404.5). These campaigns corresponded approximately to the maximum and minimum influent temperatures in 2014-2015 (22.5°C and 14.5°C). Data used for modelling included: online measurements of inlet NH_4^+ and NO_3^-, outlet NH_4^+, NO_3^-, DO, pH, temperature, and outlet dissolved N_2O (measured in the water zone above the media). Effluent NO_2^- concentrations were also occasionally measured in grab samples. N_2O emissions were collected in the middle of the tank surface area using a floating hood (Bollon et al., 2016b). Average operating conditions, nitrification performance, N_2O production rates (N_2O-PR) and N_2O emission factors (N_2O-EF) are presented in Table

V.2-1. The calculations of the ammonium uptake rate (AUR), N_2O-PR and N_2O-EF were given in Eq.III.1, Eq.III.3 and Eq.III.5, respectively.

Table V.2-1. Main operating conditions and performances of the nitrification stage (n = 643), and the studied Biostyr filter during the summer (n = 7) and winter (n = 14) campaigns.

	NH_4^+ load	AUR	Aeration	Temperature	N_2O-PR	N_2O-EF
	$kgN/m^3/d$		$Nm^3/kgNH_4\text{-}N_{applied}$	°C	kgN/h	%
Nitrification	1.14 ± 0.22	0.98 ± 0.18	91 ± 27	19.2 ± 2.9	*N.D.*	*N.D.*
Summer	1.25 ± 0.05	1.05 ± 0.20	67 ± 10	22.5 ± 0.3	0.72 ± 0.24	2.3 ± 0.7
Winter	1.14 ± 0.24	0.94 ± 0.16	75 ± 12	14.5 ± 0.9	1.26 ± 0.23	3.6 ± 0.8

During the winter campaign, the specific effect of the air flowrate on NH_4^+ removal and N_2O production rates was experimentally tested. At fairly constant NH_4^+ load (618 ± 28 kgN/d on a 10 min average basis), the air flowrate was increased gradually: 34 866, 49 807, 64 672 and 84 781 Nm^3/d, which corresponded to aeration loads of 57, 81, 106 and 131 $Nm^3/kgNH_4\text{-}N_{applied}$. Experimental data showed a gradual increase of the AUR from 491 to 623 kgN/d, while the N_2O-PR remained relatively constant (1.12, 1.14, 1.12 and 1.13 kgN/h respectively), which resulted in a decrease of the N_2O production factor. The simulation results were confronted to these data to: (i) verify the ability of the model to predict the observed tendencies, (ii) analyse the mechanisms behind the constant N_2O-PR observed despite the changing aeration conditions.

V.2.2 MODEL SET-UP

A detailed description of the BAF model is provided in Annex 1, together with the Gujer matrix of the model and parameter values. Briefly, its development was based on an existing co-current up-flow filter model, built on the Simulink toolbox of Matlab (Mathworks) to describe the functioning of tertiary nitrifying Biostyr® filters of the Seine Aval plant (Bernier et al., 2014). It was previously extended to consider the main N_2O production and consumption pathways and a plug-flow evolution of the gas phase, necessary to describe the partitioning of N_2O fluxes (Chapter IV).

The biokinetic model is recalled on Figure V.2-1. It describes the oxidation of NH_4^+ to NO_2^- according to Pocquet et al. (2016), which combines N_2O production by NN and ND; the oxidation of NO_2^- to NO_3^- by NOB; and HD as a four-step process, in which N_2O is an intermediate product (Hiatt and Grady, 2008). The reference parameter set came from (Lang et al., 2016) for AOB reactions, (Bernier et al., 2014) for NOB and physical reactions, and (Hiatt and Grady, 2008) for OHO reactions.

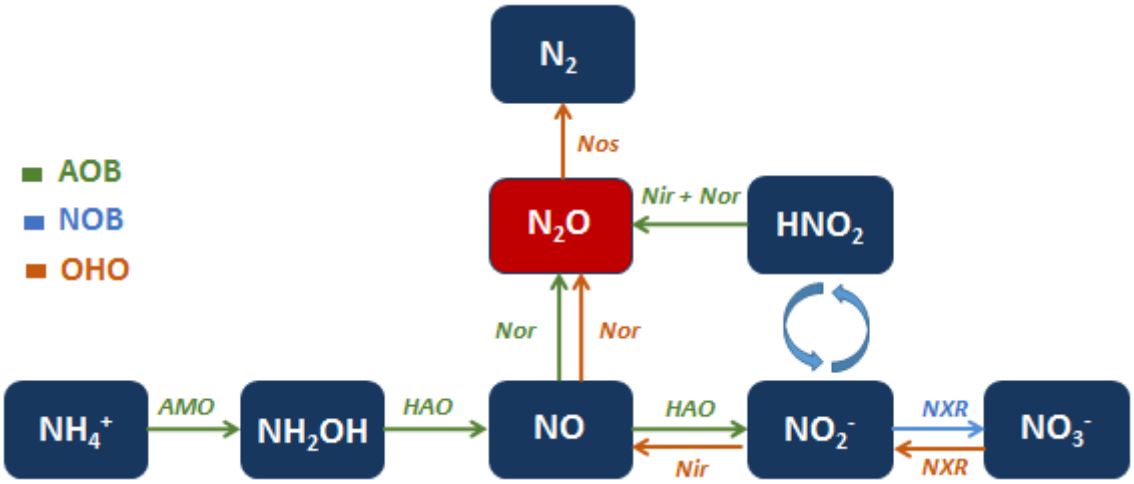

Figure V.2-1. Schematic representation of the N_2O biological pathways included in the modified BAF model. AMO, HAO, NXR, Nar, Nir, Nor and Nos stand for the enzymes ammonium monooxygenase, hydroxylamine oxidoreductase, nitrite oxidoreductase, nitrate reductase, nitrite reductase, and NO reductase and N_2 synthase.

Preliminary modifications were made compared to the model presented in Chapter IV:

- The Arrhenius coefficient describing the temperature effect on the oxygen volumetric transfer coefficient (θ_{kLa}) was modified from 1.005 to 1.024 according to literature (NFEN-12255-15, 2004);
- The evolution of gas hold-up with superficial gas velocity was changed from a polynomial to a power law ($0.0145*U_G^{0.3564}$), based on experimental results from Gillot et al. (2005);
- Nitrous acid (HNO_2) was previously calculated according to Eq.37. Small variations of pH induced high variations of HNO_2 and its associated Monod term on ND (Annex 6). In order to provide a model easily usable in practice, whose N_2O predictions do not largely depend on the reliability and/or availability of pH measurements, NO_2^- was therefore considered the true substrate of ND instead of HNO_2. The affinity constant of ND for NO_2^- was calculated from the one of HNO_2, considering an average pH of 7 and temperature of 20°C. Model results before/after modification are presented in Annex 6. All in all, the effect of pH on biokinetics was not considered.

Eq.37
$$[HNO_2] = \frac{[NO_2^-]}{1 + e^{-2300/(273+T)} 10^{pH}}$$

V.2.3 GLOBAL SENSITIVITY ANALYSIS

A global sensitivity analysis was performed in order to prioritize parameters for wastewater treatment models, including the biofilm reactor models (Brockmann et al., 2008, Sin et al., 2011, Cosenza et al., 2013). The method is provided in details in Chapter III.

Briefly, a global sensitivity analysis is based on the simultaneous variation of all parameters (90 parameters in this analysis, see Annex 2). Some parameters were intentionally discarded: parameters related to oxygen transfer efficiency (fouling of diffusers F, aeration efficiency compared to clean water α and salinity factor β_0) and the diffusion coefficients. The variation ranges of the considered parameters were set to ± 10 - 100% around their reference values, according to the current knowledge on these parameters. The larger the number of parameter combinations n, the more accurate the results. In this study, it was set to five times the number of parameters, i.e. 450, which lies at the lower end of the literature recommendation range (Saltelli et al., 2008, Sin et al., 2011).

A Latin Hypercube Sampling (LHS) was performed to obtain a matrix of 450 combinations of parameters. Each was simulated for 100 days: the first 99 were used to stabilize the system and the last one to analyse the results. Data used to implement the model were the average conditions of the global nitrification stage during the entire 2014 to 2016 years (1095 days). Average liquid and gas flowrates were 23 403 m^3/d and 60 057 Nm^3/d; influent NH_4^+, NO_3-, NO_2^-, PO_4^{3-}, TSS and COD concentrations were 29.6 mgN/L, 5.6 mgN/L, 0.79 mgN/L, 0.60 mgP/L, 39 mg/L and 75 mg/L; pH and temperature were 7.1 and 18.8 °C. Finally, parameter prioritization was obtained by the standardized regression coefficient (SRC) method, which is considered relevant for a regression coefficient $R^2 > 0.7$ (Cosenza et al., 2013).

V.2.4 MODEL CALIBRATION

A procedure for “good biofilm reactor modelling practice” (GBRMP) was recently proposed by Rittmann et al. (2018) to provide modellers with clear guidance on how to apply biofilm models for carbon and nitrogen removal. The calibration procedure was divided into four successive steps: (1) calibrating the mass of biomass on carriers, (2) calibrating the degradation of soluble biodegradable COD, (3) calibrating nitrogen removal rates, and (4) calibrating aeration parameters. To evaluate the amount of biomass in each stage of the reactor and the distribution of nitrogen removal rates, the authors suggested collecting biofilm samples to perform experiments, such as the measurement of: VSS concentration, thickness of the biofilm and nitrification rate at different DO setpoints or mixing intensity.

Our approach took some distance from the proposed procedure (Figure V.2-2). First, the sensitivity of N_2O fluxes to oxygen gas/liquid mass transfer led to a preliminary calibration of aeration parameters based on the data from the winter campaign (Chapter IV). Second, given the difficulty to collect representative samples from full-scale BAFs, the experimental protocol did not include *ex situ* analysis of biofilm characteristics and nitrogen removal rates. However, the calibration procedure of the base model of Bernier et al. (2014) included

nutrient gradient data over the media height, which can reflect the distribution of the nitrogen removal rate if oxygen transfer is correctly described. Finally, the soluble biodegradable COD concentration was not included in the daily measurements of nitrifying BAFs. Therefore no calibration step was dedicated to COD removal.

Nitrogen removal was calibrated based on the comparison of model predictions with measured effluent NH_4^+ and NO_3^- concentrations over 643 days, and occasional measurements of NO_2^- concentrations during the summer and winter campaigns. Nitrous oxide production was calibrated in order to describe gaseous and dissolved N_2O fluxes measured during both campaigns.

Model predictions were evaluated based on the values of the mean absolute error (MAE) and the root mean square error (RMSE). Their combination provides information on the global agreement of model predictions with experimental data and on the presence of large errors (Hauduc et al., 2015). Parameters used for manual calibration were identified from the results of the global sensitivity analysis and the prediction of N_2O production pathways during each campaign.

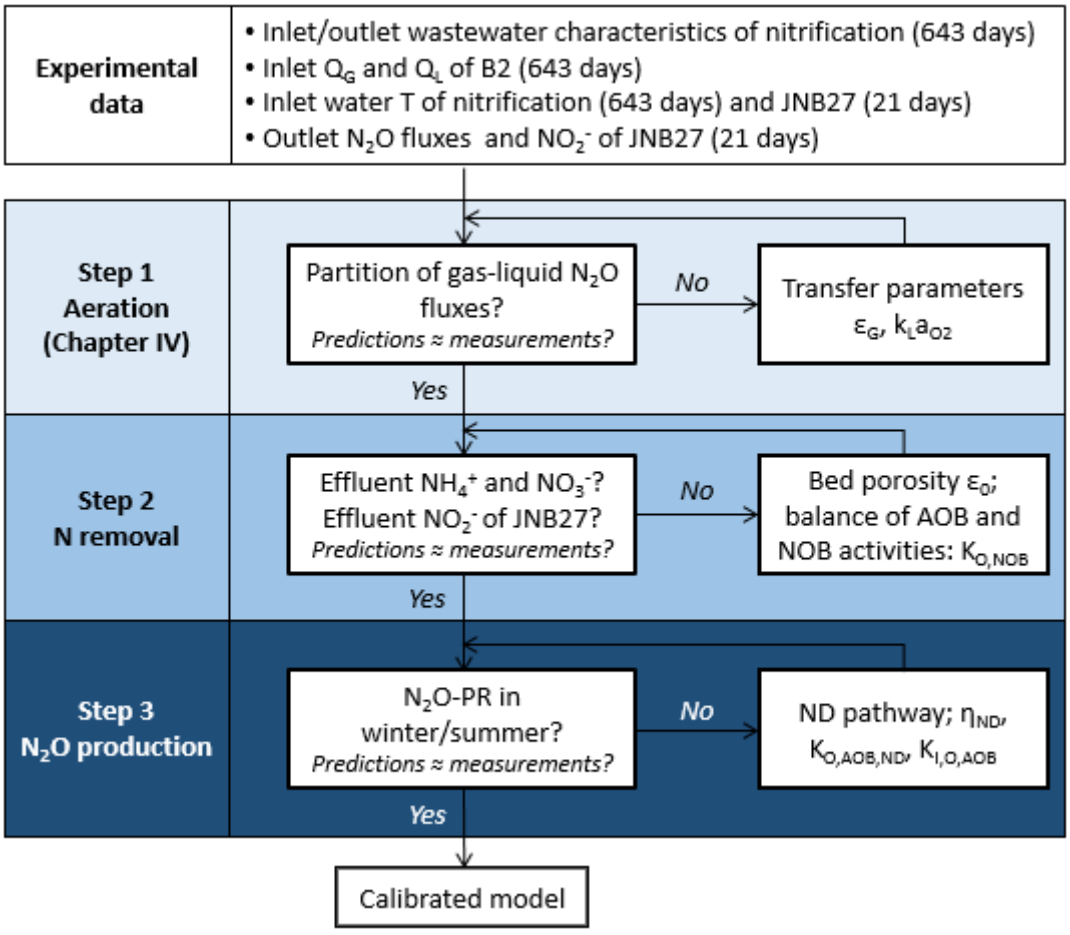

Figure V.2-2. Calibration procedure adapted to the nitrifying BAF model.

V.3 RESULTS

V.3.1 GLOBAL SENSITIVITY ANALYSIS

The results of the global sensitivity analysis are presented in Table V.3-1. Full results, including the parameters with no significant effect on model predictions ($-0.1 < \beta i < 0.1$), can be found in Annex 7.

Table V.3-1. Summary of standardized coefficients βi. Dark orange = high negative effect; medium orange = medium negative effect; light orange = small negative effect; white = no significant effect; light green = small positive effect; medium green = medium positive effect; dark green = high positive effect.

Parameter	Effluent NH_4^+	Effluent NO_3^-	Effluent NO_2^-	Effluent dissolved N_2O	Off-gas N_2O
R^2	0.91	0.86	0.56	0.70	0.69
TKN/NH_4	0.24	-0.01	0.11	0.16	0.15
b_{AOB}	0.07	0.09	-0.13	-0.15	-0.14
b_{NOB}	-0.08	-0.13	0.20	0.17	0.18
η_{ND}	0.02	0.04	-0.24	0.28	0.27
η_{NN}	0.00	-0.03	-0.05	0.14	0.14
$K_{NO,AOB,HAO}$	0.01	0.00	-0.09	0.11	0.11
$K_{NO,AOB,NN}$	0.02	0.06	-0.01	-0.19	-0.18
$K_{O,AOB,1}$	0.16	0.24	-0.26	-0.43	-0.40
$K_{O,AOB,2}$	-0.03	-0.01	-0.08	0.18	0.18
$K_{O,NOB}$	-0.08	-0.21	0.29	0.28	0.26
$\mu_{AOB,max}$	-0.09	-0.14	0.19	0.20	0.20
$\mu_{NOB,max}$	0.02	0.10	-0.13	-0.13	-0.11
ε_0	-0.32	0.29	-0.06	-0.02	0.01
A	-0.38	0.32	-0.07	0.04	0.10
B	-0.61	0.59	-0.25	0.09	0.16
L_f	0.17	-0.17	0.05	0.00	0.00
$\theta_{\mu AOB}$	0.08	0.07	-0.11	-0.15	-0.15
θ_{bAOB}	-0.07	-0.10	0.16	0.11	0.11
A'	0.11	-0.10	0.00	0.06	0.05

The high correlation coefficients for effluent NH_4^+ and NO_3^- concentrations (0.91 and 0.86, respectively) attest the validity of the multiple linear regressions. Lower values for effluent NO_2^-, dissolved and gaseous N_2O concentrations (0.56, 0.70 and 0.69 respectively), can be explained by the low concentrations that were observed. Indeed, many combinations led to concentrations close to zero, especially for NO_2^- (concentrations < 0.2 mgN/L for 26% of the combinations).

V.3.1.1 NITRIFICATION PERFORMANCE

Nitrification, i.e. NH_4^+ conversion to NO_3^-, was found to be mainly impacted by gas-liquid transfer parameters, more specifically by the ones related to the oxygen volumetric transfer coefficient k_La_{O2} (parameters A and B of Eq.IV.3), which logically impacted effluent DO concentrations as well (Annex 7). Nitrification was also negatively correlated to parameter A', which corresponds to the slope of $\varepsilon_G = f(U_G)$. This is consistent with the results in Chapter IV, which showed that, because the media occupies a large fraction of the filter volume (≈60% of the volume), a small augmentation of the gas hold-up highly decreases the liquid volume, thus the hydraulic retention time (HRT) and the mass of bacteria stabilized in the system. For the same reasons, the initial porosity of the bed (ε_0) was found to have a strong positive impact on nitrification.

Nitrification was sensitive to the affinity constant of NH_4^+ oxidation to NH_2OH for oxygen ($K_{O,AOB,1}$). An increase of $K_{O,AOB,1}$ is expected to lower the NH_4^+ oxidation rate, and therefore the O_2 uptake rate by AOB. This would leave more oxygen for the growth of NOB, leading to a higher oxidation rate of NO_2^- (indicated in Table V.3-1 by the high absolute coefficient of $K_{O,AOB,1}$ on effluent NO_2^- and NO_3^- concentrations). On the contrary, the affinity constant for HAO-related steps for O_2 ($K_{O,AOB,2}$) did not have a significant impact on nitrification. Since its reference value is lower than that of $K_{O,AOB,1}$ (0.30 against 0.48 mgO_2/L), it reflects that HAO-related steps were less limited by O_2 than the AMO reaction. In addition, the affinity constant of HAO reactions for NH_2OH (K_{NH2OH}) was not identified as an impacting parameter on nitrification, the first rate (AMO) being the limiting step of the reaction. It should be noted that this analysis was made on a macro-scale, based on the concentrations predicted at the effluent of the BAF.

The effluent NH_4^+ concentration was also positively correlated to the total Kjeldahl nitrogen (TKN) to NH_4^+ ratio in the influent (TKN/NH_4). As explained in the model description (Annex 1), NH_4^+ is a model input, while TKN is deduced from the ratio. A higher TKN/NH_4 at constant influent NH_4^+ concentration leads to a higher influent TKN concentration, which in turns results in a higher particulate organic nitrogen concentration (X_{nd}). With X_{nd} being hydrolysed, it produces soluble organic nitrogen (S_{nd}), itself ammonified into NH_4^+. This result confirms the importance of characterizing particulate (X_{ND}) and soluble (S_{ND}) biodegradable organic nitrogen concentrations in the influent wastewater to avoid hedging the prediction of effluent NH_4^+.

The effluent NO_3^- concentration was influenced by the same parameters as the NH_4^+ concentration, but in the opposite way. It was impacted by additional parameters related to NOB: negatively by their decay rate (b_{NOB}), negatively by their affinity constant for O_2 ($K_{O,NOB}$)

and positively by their maximum growth rate ($\mu_{NOB,max}$). Moreover, it was negatively correlated to the AOB maximum growth rate ($\mu_{AOB,max}$). This is explained by the competition between AOB and NOB for oxygen: higher growth of AOB results in higher consumption of O_2, and therefore a higher limitation of NOB growth.

Finally, the liquid film thickness (L_f) had a negative impact on nitrification, as it results in limitations of substrate diffusion within the biofilm. It showed no effect on effluent NO_2^- and N_2O concentrations, which are presented hereafter.

V.3.1.2 NITRITE AND N_2O PRODUCTION

NO_2^- accumulation results from an imbalance between AOB and NOB reaction rates. It was therefore influenced by parameters affecting AOB and NOB reaction rates (in order of influence: $K_{O,NOB}$, $K_{O,AOB,1}$, $\mu_{AOB,max}$, $\mu_{NOB,max}$, b_{AOB},). At the average temperature of 18.8°C, the Arrhenius coefficients for AOB growth and decay ($\theta_{\mu,AOB}$ and $\theta_{b,AOB}$ respectively) also influenced NO_2^- predictions. Below 20°C, increasing $\theta_{\mu,AOB}$ or $\theta_{b,AOB}$ results in a decrease of $\mu_{AOB,max}$ or b_{AOB} respectively, which explains the negative influence of $\theta_{\mu,AOB}$ and the positive influence of $\theta_{b,AOB}$ on NO_2^-. Parameter B of Eq.25 had a high negative impact on the NO_2^- concentration. Increasing B increased k_La_{O2}, resulting in higher DO levels and thus decreasing the limitation of the NOB growth by O_2. NO_2^- was also negatively influenced by η_{ND}, as the rate at which NO_2^- is being reduced in N_2O by ND is proportional to this parameter. It was the 4th most impacting parameter for NO_2^-, after $K_{O,NOB}$, $K_{O,AOB,1}$ and B.

Results concerning the off-gas and effluent N_2O concentrations were similar. Only parameters related to gas-liquid mass transfer (mainly A and B) had a higher impact on off-gas N_2O concentrations, as they influence N_2O stripping. Most parameters controlling the NO_2^- concentration had a similar effect on N_2O, as N_2O production by ND depends on the NO_2^- concentration. Indeed, N_2O was positively correlated to parameters which increased the NO_2^- concentration (influent TKN/NH_4, b_{NOB}, K_{ONOB}, μ_{AOB}, θ_{bAOB}) and negatively correlated to those which decreased it (b_{AOB}, K_{OAOB1}, μ_{NOB}, $\theta_{\mu AOB}$). The only exception was η_{ND}, since it favours the reduction of NO_2^- to N_2O. The coefficient related to K_{OAOB1} was twice as high on N_2O as on NO_2^- because it had a double effect: it decreased nitrification, therefore N_2O production by NN; and decreased the NO_2^- concentration, therefore N_2O production by ND. N_2O was affected by parameters related to NN to a lower extent, η_{NN} (positively) and $K_{NO,AOB,NN}$ (negatively), and by parameters governing NO oxidation to NO_2^- by AOB, $K_{NO,AOB,HAO}$ and $K_{O,AOB,2}$ (negatively). Finally, parameters related to HD did not appear amongst the most influencing parameters for N_2O. This will be discussed in section V.4.1.

V.3.1.3 SUMMARY

The results led to two main conclusions, which will be further discussed in section :

1. The prediction of nitrification is mainly dependent on oxygen-related parameters, in particular gas-liquid transfer parameters, and on the clean bed porosity;
2. N_2O production is enhanced by parameter combinations which favours an imbalance between nitritation and nitratation, i.e. which lead to NO_2^- accumulation. It is thus mainly dependent on the variations of ND-linked parameters.

V.3.2 SIMULATION WITH THE REFERENCE PARAMETER SET

The long-term prediction of effluent concentrations with the reference parameter set is presented in Table V.3-2 (average data over the 643 days period). Dynamic results can be found in Annex 8.

The effluent NH_4^+ concentration was overestimated by 31%, while NO_3^- and NO_2^- were underestimated by 8 and 14%, respectively. The RMSE and MAE of NH_4^+ were high, indicating limited agreement of model predictions with experimental data. In particular, the model underestimated low NH_4^+ concentrations, and overestimated high ones. On the other hand, the model was able to describe the dynamics of the effluent NO_3^- concentrations, despite its small average underestimation. The AUR was underestimated by 5% on average (562 ± 75 kgN/d simulated against 589 ± 113 kgN/d measured).

These tendencies for effluent NH_4^+ and NO_3^- were similar during the N_2O measuring campaigns. The AUR was underestimated by 12% and 4% in summer and winter periods, respectively (hourly average, n = 168 and 336). Effluent NO_2^- concentrations measured on the studied filter were slightly lower than those measured at the outlet of the nitrification stage (0.25 ± 0.09 against 0.46 ± 0.05 mgN/L in summer, 0.68 ± 0.22 against 0.83 ± 0.12 mgN/L in winter). However, both measurements agreed on an increase of the effluent NO_2^- concentration between summer and winter. This was well captured by the model, which predicted 0.60 ± 0.11 and 0.81 ± 0.22 mgN/L in summer and winter, respectively. These values are consistent with measurements from the nitrification stage, but higher than those from the studied filter. Effluent DO levels were correctly predicted.

Table V.3-2. Average experimental measurements of the 643 day period, the summer and the winter campaigns, and associated model predictions obtained with the reference parameter set: effluent nitrogen concentrations, effluent DO, AUR, and N_2O fluxes.

	Effluent NH_4^+	Effluent NO_3^-	Effluent NO_2^-	Effluent DO	AUR	N_2O-PR	N_2O-EF	Emitted / produced N_2O
	mgN/L	mgN/L	mgN/L	mgO2/L	kgN/d	kgN/h	%	%
Long-term period (643 days)								
Data	4.2 ± 1.8	29.6 ± 5.7	0.65 ± 0.26	-	589 ± 113	-	-	-
Model	5.5 ± 3.3	27.3 ± 5.3	0.56 ± 0.25	6.3 ± 0.7	562 ± 75	1.32 ± 0.46	4.3 ± 1.3	77 ± 5
RMSE	3.0	6.3	0.27	-	166	-	-	-
MAE	2.3	3.8	0.21	-	90	-	-	-
Summer campaign (7 days)								
Data	5.6 ± 2.9	29.2 ± 3.8	0.25 ± 0.09	5.6 ± 0.5	634 ± 119	0.72 ± 0.24	2.3 ± 0.7	83 ± 5
Model	8.9 ± 3.9	26.4 ± 4.2	0.60 ± 0.11	5.7 ± 0.4	560 ± 70	1.43 ± 0.32	4.8 ± 0.6	79 ± 3
RMSE	4.2	5.2	-	1.0	131	0.77	2.7	14
MAE	3.6	3.4	-	0.4	91	0.73	2.6	6
Winter campaign (14 days)								
Data	5.7 ± 2.1	27.7 ± 4.8	0.68 ± 0.22	7.1 ± 0.6	571 ± 98	1.26 ± 0.23	3.6 ± 0.8	66 ± 8
Model	6.9 ± 3.1	26.6 ± 4.5	0.81 ± 0.22	6.5 ± 0.5	546 ± 72	1.81 ± 0.37	5.9 ± 0.8	74 ± 5
RMSE	2.2	2.3	-	0.7	47	0.62	2.5	10
MAE	1.7	1.8	-	0.6	36	0.55	2.3	8

The model was able to describe the main dynamics of the N_2O fluxes: the N_2O-PR typically increased over a filtration cycle, and dropped after a backwash event (Annex 8). The partitioning of N_2O between liquid and gaseous phases was also well captured by the model (-3% in summer and +10% in winter). However, the predicted N_2O-PR was overestimated for both campaigns: +103% in summer, and +44% in winter, resulting in an overestimation of the N_2O production factor (+123% in summer and +47% in winter).

Based on these results, calibration work should be dedicated to (i) increasing the ammonium removal over the long-term period and (ii) decreasing the NO_2^- concentrations and the associated N_2O production, in particular in summer.

V.3.3 CALIBRATION OF NITRIFICATION PERFORMANCES

The objective of this calibration step (step 2 on Figure V.2-2) was double: increasing AUR while slightly decreasing effluent NO_2^- concentrations.

The global sensitivity analysis revealed high impacts of bed porosity, oxygen-related parameters and influent TKN/NH_4 ratio on NH_4^+ removal. It did not appear relevant to increase transfer parameters related to the volumetric oxygen transfer coefficient, as effluent DO concentrations and the liquid/gas partition of N_2O fluxes were correctly described. $K_{O,AOB,1}$ was not decreased either, to avoid further increasing NO_2^- and N_2O concentrations. The influent TKN/NH_4 ratio also remained unchanged, since its reference value was the average one measured during both campaigns (1.1 gN/gN). Finally, the remaining options were to decrease the gas hold-up (A') or increase the initial bed porosity (ε_0), which would both increase the predicted hydraulic retention time. Considering previous efforts on the gas hold-up calibration (chapter IV) and the important modification which would be needed on this parameter, it was chosen to adapt the bed porosity. In the model, the bed height is considered constant, equal to its nominal value of 3.5 m. In functioning BAFs, this height decreases over time, as a fraction of media beads is known to leave the system during backwash events. This means that the bulk volume and therefore the hydraulic retention time are actually higher than the simulated ones. Therefore, nitrification was calibrated by increasing ε_0 to 0.38. This value moves away from the theoretical value (0.34), but remains close to the reference (0.356).

Moreover, NO_2^- accumulation was reduced by increasing the NO_2^- oxidation rate by NOB. To this end, the affinity constant of NOB for O_2 ($K_{O,NOB}$) was decreased from 0.6 to 0.5 mgO_2/L. The long-term prediction of effluent concentrations with this calibrated parameter set is presented in Table V.3-3. Dynamic results can be found in Annex 9.

Table V.3-3. Average experimental measurements of the 643 day period, the summer and the winter campaigns, and associated model predictions obtained with the first-step calibration parameter set: effluent nitrogen concentrations, effluent DO, AUR, and N_2O fluxes.

	Effluent NH_4^+	Effluent NO_3^-	Effluent NO_2^-	Effluent DO	AUR	N_2O-PR	N_2O-EF	Emitted / produced N_2O
	mgN/L	mgN/L	mgN/L	mgO2/L	kgN/d	kgN/h	%	%
Long-term period (643 days)								
Data	4.2 ± 1.8	29.6 ± 5.7	0.65 ± 0.26	-	589 ± 113	-	-	-
Model	4.1 ± 2.9	29.5 ± 5.6	0.32 ± 0.16	6.4 ± 0.8	595 ± 82	0.91 ± 0.35	2.8 ± 0.9	78 ± 5
RMSE	2.3	6.0	0.40	-	169	-	-	-
MAE	1.8	2.7	0.33	-	80	-	-	-
Summer campaign (7 days)								
Data	5.6 ± 2.9	29.2 ± 3.8	0.25 ± 0.09	5.6 ± 0.5	634 ± 119	0.72 ± 0.24	2.3 ± 0.7	83 ± 5
Model	7.5 ± 4.0	28.9 ± 4.4	0.37 ± 0.09	5.7 ± 0.4	589 ± 75	0.99 ± 0.30	3.1 ± 0.7	79 ± 3
RMSE	3.1	4.9	-	1.0	119	0.37	1.2	14
MAE	2.5	2.5	-	0.4	69	0.31	1.0	6
Winter campaign (14 days)								
Data	5.7 ± 2.1	27.7 ± 4.8	0.68 ± 0.22	7.1 ± 0.6	571 ± 98	1.26 ± 0.23	3.6 ± 0.8	66 ± 8
Model	5.3 ± 2.9	29.2 ± 4.9	0.45 ± 0.16	6.5 ± 0.6	577 ± 79	1.29 ± 0.38	3.9 ± 0.8	74 ± 5
RMSE	1.7	2.5	-	0.7	35	0.29	1.1	10
MAE	1.4	2.1	-	0.6	28	0.22	0.9	8

In comparison to the reference, the simulated NH_4^+ and NO_3^- concentrations were closer to the experimental data, as the AUR was better predicted (595 ± 82 against 589 ± 113 kgN/d measured). The effluent NO_2^- concentration was this time underestimated compared to full-scale data measured at the outlet of the nitrification stage (-51%). It was, on the other hand, closer to the measurements made on the studied filter during the summer and winter campaigns (+44% and -34%, respectively). The seasonal fluctuations of the AUR were well captured by the model during the 2-year period, as well as effluent NH_4^+, NO_3^- and NO_2^- concentrations. As the RMSE and MAE pointed out, the model predicted higher fluctuations of NH_4^+ concentrations around the mean. In particular, it was overestimated at high loads, and *vice versa*.

The lower NO_2^- accumulation had a strong influence on the prediction of N_2O fluxes. The N_2O-PR highly decreased, from 1.43 ± 0.32 to 0.99 ± 0.30 kgN/h in summer and from 1.81 ± 0.37 to 1.29 ± 0.38 kgN/h in winter. Simulated emissions were closer to experimental data but still overestimated in summer (+40%), while predicted well in winter (+10%). The fluctuations were, on the other hand, correctly predicted for both campaigns. Except for some peaks of N_2O –which were accompanied by overestimations of the emitted to produced N_2O ratio– the model could describe experimental data in winter.

V.3.4 CALIBRATION OF N_2O PREDICTIONS

This section is dedicated to investigate the differences between model predictions in winter and summer, in order to identify the parameters which can be calibrated to decrease N_2O production in summer, but not in winter. Model predictions in terms of nitrogen removal, biofilm characteristics and N_2O fluxes during both campaigns are presented in Table V.3-4. Model results were averaged over the entire reactor volume, and the whole duration of each campaign, in order to understand the unbalance between N_2O predictions.

The NH_4^+ load was higher in summer (757 against 692 kgN/d) but the air flow rate was lower (49 257 against 51 333 Nm^3/d). The predicted NO_3^- production was therefore higher (+7%). During both campaigns, the fractions of NO_3^- by OHO was low (13% of the produced NO_3^- in summer, 8% in winter). Nevertheless, the predicted mass of OHO was predominant: it represented 70% of the total biomass. This can be explained by: (i) the higher growth yield of OHO, (ii) the input of OHO with the influent entering the nitrification stage (25% of the particulate COD), (iii) the presence of soluble readily biodegradable carbon in the influent (influent soluble COD concentrations were around 30 mgCOD/L), and the growth of OHO on products of AOB decay. The predicted biofilm thickness, DO and NO_2^- concentrations were lower in summer (-18%, -44% and -71%).

Table V.3-4. Mean model predictions during the N_2O campaigns, with the first calibrated parameter set.

		Summer	Winter
Nitrification – denitrification	NH_4^+ conversion to NO_3^-	608 kgN/d	566 kgN/d
	% nitrification	80%	82%
	NO_3^- conversion to N_2	80 kgN/d	46 kgN/d
	% denitrification	13%	8%
Biofilm	Mass heterotrophs / Mass autotrophs	70% / 30%	70% / 30%
	Thickness	83 µm	101 µm
	DO concentration	0.22 mgO_2/L	0.50 mgO_2/L
	NO_2^- concentration	0.49 mgN/L	0.69 mgN/L
	NO concentration	8.7E-4 mgN/L	8.3E-4 mgN/L
	N_2O concentration	0.19 mgN/L	0.28 mgN/L
	NH_2OH concentration	0.029 mgN/L	0.037 mgN/L
N_2O fluxes	NN	1.79 kgN/h	1.29 kgN/h
	ND	1.87 kgN/h	1.80 kgN/h
	AOB production factor	15 %	13 %
	HD NO conversion to N_2O (step 3)	0.21 kgN/h	0.10 kgN/h
	HD N_2O conversion to N_2 (step 4)	2.89 kgN/h	1.90 kgN/h
	HD reduction rate / AOB production rate (%)	73 %	58 %

In these conditions, the predicted N_2O production factor (PF) related to AOB was high: 15 % and 13% of the eliminated NH_4^+ load, while HD consumed 73% and 58% of it in summer and winter, respectively. The small N_2O production by OHO compared to its consumption was related to NO concentrations within the biofilm, which remained low compared to N_2O concentrations, as the net production of NO by AOB was low. Since both affinity constants of OHO growth on NO and N_2O are equal to 0.05 mgN/L, the reduction of NO to N_2O was highly substrate-limited compared to the reduction of N_2O to N_2. The predicted N_2O consumption by HD being already higher in summer, the overestimation of the N_2O-PR during this campaign was believed to be due to an overestimation of the production by AOB.

The predicted N_2O production factor related to NN was higher in summer compared to winter (7% against 5% of the eliminated NH_4^+ load), which was logical considering the higher NH_4^+ load, and the higher maximum specific AOB growth rate (0.97 d^{-1} at 22.5°C against 0.57 d^{-1} at 14.5°C). On the other hand, the predicted N_2O production factor related to ND was similar during both campaigns (8% of the eliminated NH_4^+ load). Considering the lower biofilm NH_2OH, DO and NO_2^- concentrations in summer, the ND production was expected to be lower (reaction rates presented in Annex 1). The evolutions of the Monod term for NO_2^- and the Haldane term for DO on ND are presented in Figure V.3-1, as well as their average values simulated during each campaign. Analysis of the modelling results indicated that the

Monod term for NO_2^- was indeed lower in summer, but the term on DO remained close to its maximum in this DO concentration range, resulting in similar values for both campaigns.

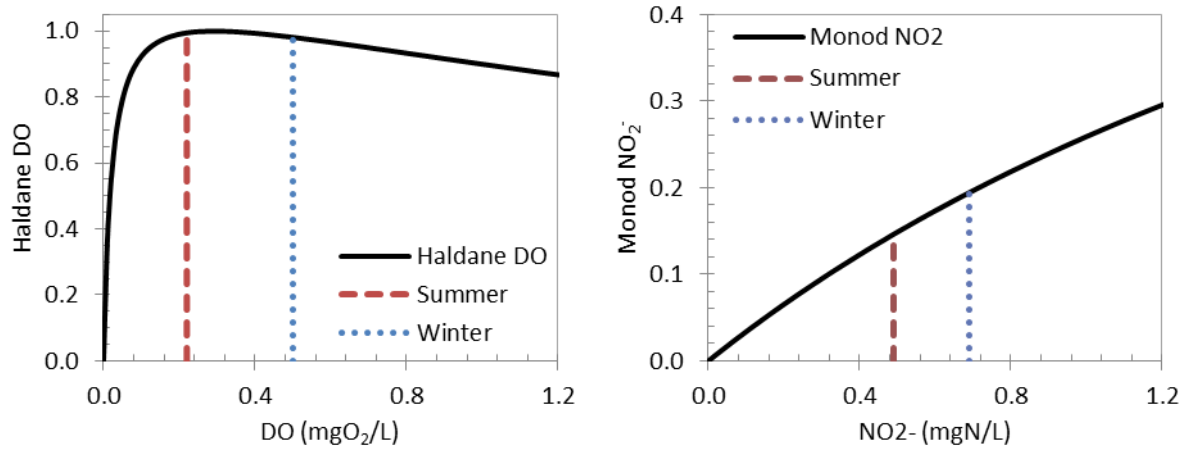

Figure V.3-1. Mean Haldane term of DO and Monod term of NO_2^- on ND for both campaigns.

Since the differences of the N_2O production by NN and HD during the campaigns were consistent with the operational conditions, the calibration of the N_2O-PR was done on the ND path. In order to reduce the N_2O production by ND in summer, without impacting its prediction in winter, parameters related to the Haldane term were modified to move its maximum value towards the average DO concentration predicted in winter (0.50 mgO_2/L, Figure V.3-2). To this end, we used parameters from the original paper (Pocquet et al., 2016) and completed the calibration step by adjusting the value of the reduction factor for ND (η_{ND}). The values of all calibrated parameters are displayed in Table V.3-5.

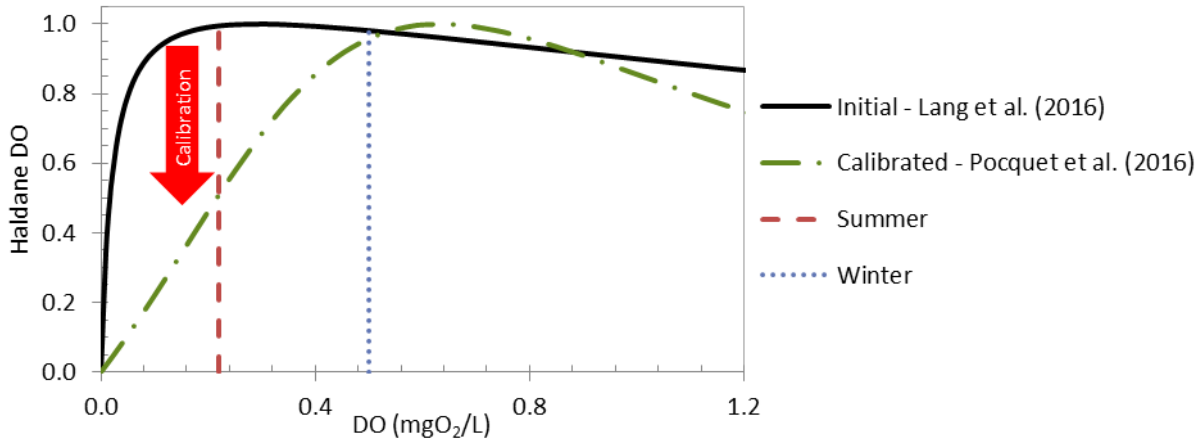

Figure V.3-2. Haldane term of DO for both campaigns with initial and calibrated parameters.

Table V.3-5. Values of reference and calibrated parameters.

	Parameter	Reference value	Calibrated value
Calibration of nitrification (Step 2)	ε_0 (-)	0.356	0.380
	$K_{O,NOB}$ (gO_2/m^3)	0.60	0.50
Calibration of N_2O production (Step 3)	$K_{O,AOB,ND}$ (gO_2/m^3)	0.019	0.500
	$K_{I,O,AOB}$ (gO_2/m^3)	4.5	0.8
	η_{ND} (-)	0.1056	0.1440

The average predictions of the final calibrated model are displayed in Table V.3-6. Dynamic effluent nitrogen concentrations over the 643 days (24h average) and N_2O fluxes (10 min average) during the campaigns are displayed in Figure V.3-3 and Figure V.3-4, respectively.

The calibrated model was still able to catch the seasonal dynamics of the AUR (593 ± 82 against 589 ± 113 kgN/d measured) and effluent nitrogen concentrations (NH_4^+ and NO_3^-). The long-term NO_2^- concentration was underestimated, but was correctly predicted when compared to the occasional measurements made on the studied BAF (0.38 ± 0.09 mgN/L predicted against 0.25 ± 0.09 mgN/L measured in summer; 0.44 ± 0.15 mgN/L predicted against 0.68 ± 0.22 mgN/L measured in winter). It was also able to predict the values and dynamics of the effluent DO concentration.

Table V.3-6. Average experimental measurements of the 643 day period, the summer and the winter campaigns, and associated model predictions obtained with the final calibration parameter set: effluent nitrogen concentrations, effluent DO, AUR, and N_2O fluxes.

	Effluent NH_4^+	Effluent NO_3^-	Effluent NO_2^-	Effluent DO	AUR	N_2O-PR	N_2O-EF	Emitted / produced N_2O
	mgN/L	mgN/L	mgN/L	mgO2/L	kgN/d	kgN/h	%	%
Long-term period (643 days)								
Data	4.2 ± 1.8	29.6 ± 5.7	0.65 ± 0.26	-	589 ± 113	-	-	-
Model	4.2 ± 2.9	29.6 ± 5.6	0.32 ± 0.16	6.4 ± 0.8	593 ± 82	0.81 ± 0.36	2.5 ± 1.0	77 ± 5
RMSE	2.3	6.0	0.39	-	169	-	-	-
MAE	1.8	2.7	0.33	-	81	-	-	-
Summer campaign (7 days)								
Data	5.6 ± 2.9	29.2 ± 3.8	0.25 ± 0.09	5.6 ± 0.5	634 ± 119	0.72 ± 0.24	2.3 ± 0.7	83 ± 5
Model	7.7 ± 3.9	29.2 ± 4.4	0.38 ± 0.09	5.7 ± 0.4	585 ± 76	0.74 ± 0.30	2.3 ± 0.7	79 ± 3
RMSE	3.3	5.0	-	1.0	120	0.24	0.9	14
MAE	2.6	2.5	-	0.4	71	0.18	0.7	6
Winter campaign (14 days)								
Data	5.7 ± 2.1	27.7 ± 4.8	0.68 ± 0.22	7.1 ± 0.6	571 ± 98	1.26 ± 0.23	3.6 ± 0.8	66 ± 8
Model	5.3 ± 2.9	29.2 ± 4.9	0.44 ± 0.15	6.5 ± 0.6	577 ± 79	1.31 ± 0.43	4.0 ± 0.9	74 ± 5
RMSE	1.7	2.5	-	0.7	35	0.34	1.3	10
MAE	1.4	2.2	-	0.6	28	0.26	1.0	8

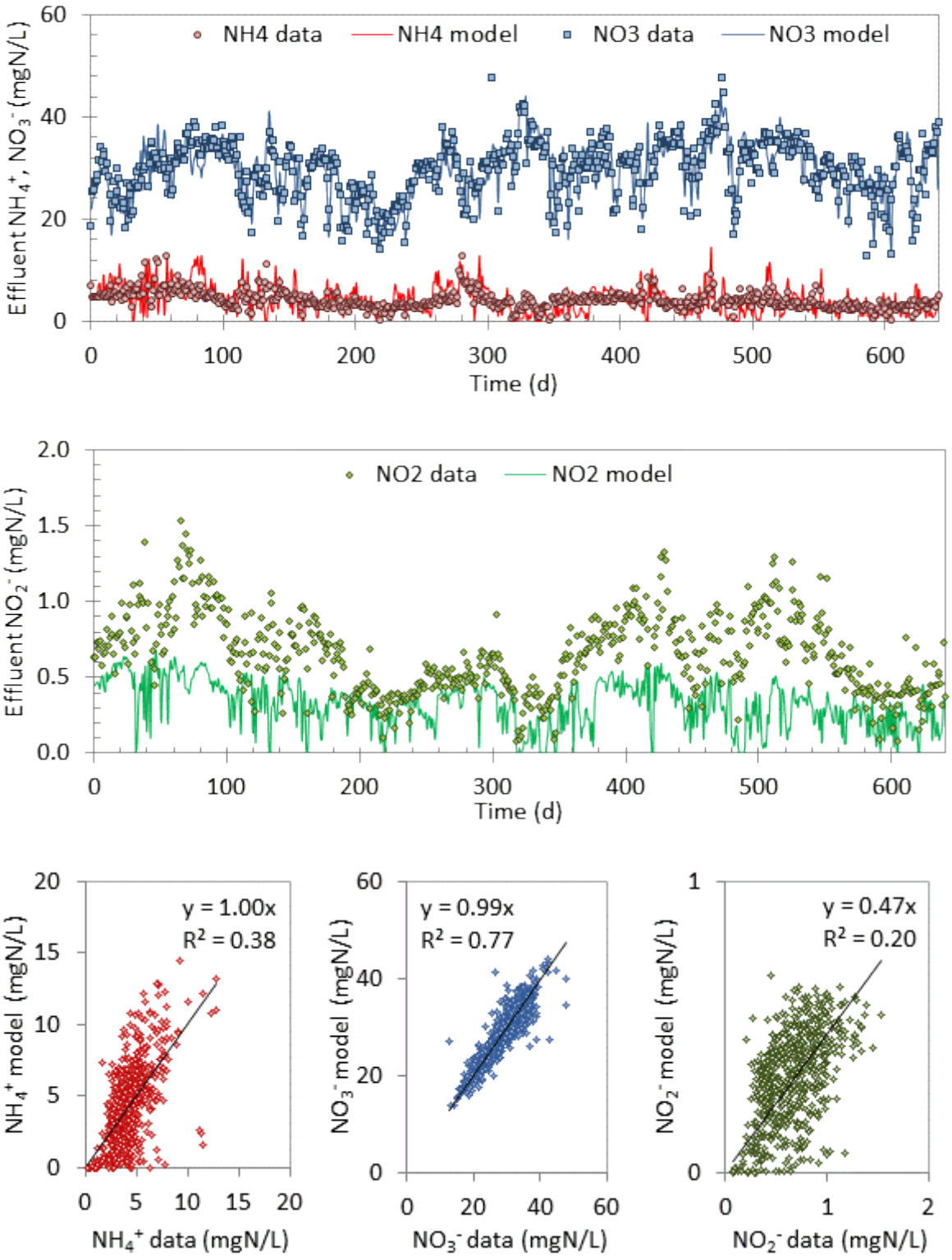

Figure V.3-3. Model predictions with the final calibrated parameter set: daily effluent NH_4^+ and NO_3^- concentrations (top panel); daily effluent NO_2^- (middle panel), and daily predicted against measured effluent nitrogen concentrations (bottom panel).

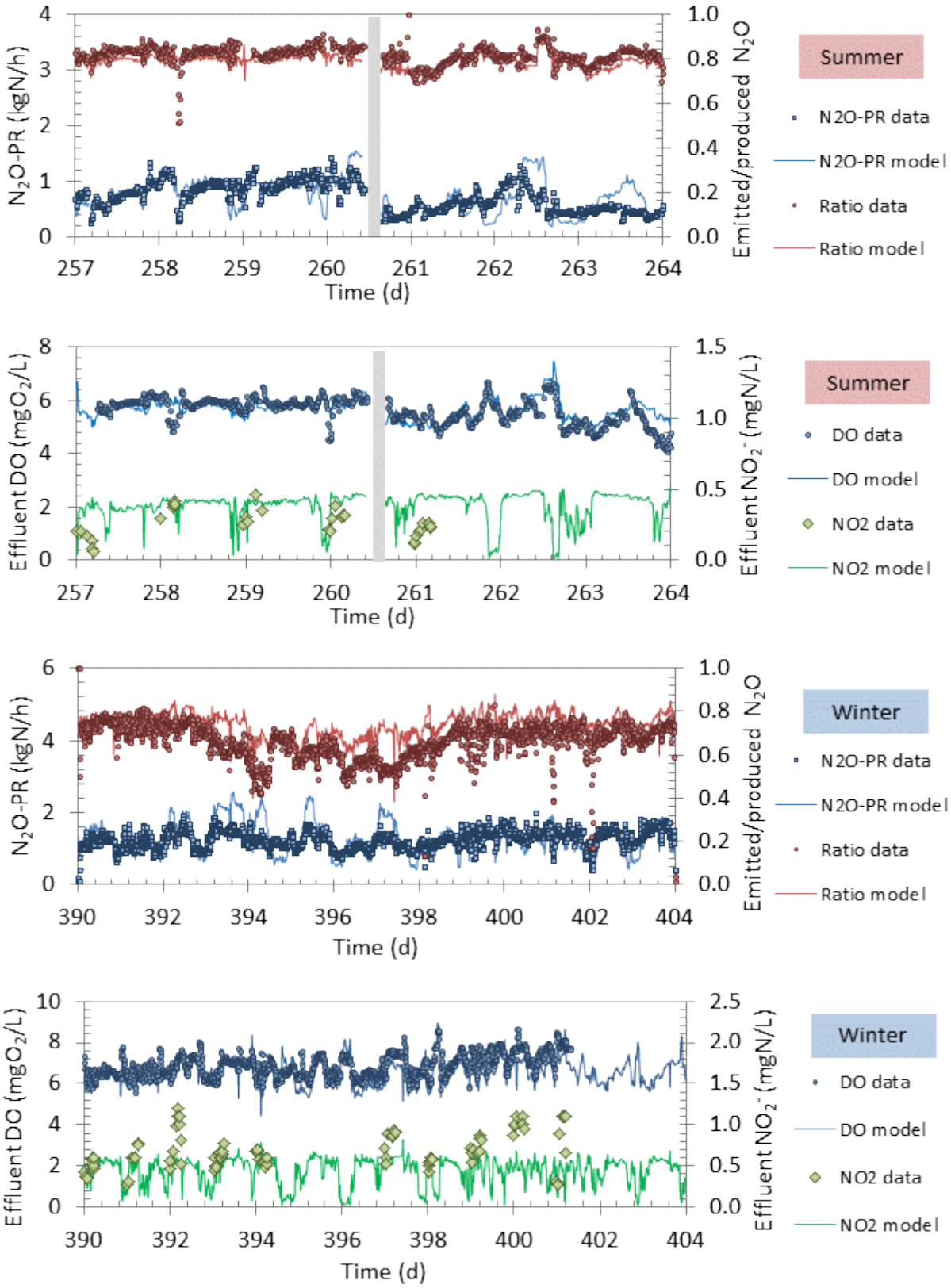

Figure V.3-4. Model predictions with the final calibrated parameter set: 10 min average N_2O fluxes, DO and NO_2^- concentrations in summer (top panels) and winter (bottom panels) in the studied BAF. The grey zone corresponds to a filter stop.

Finally, the calibrated model was able to predict the order of magnitude of the N_2O-PR in winter (1.31 ± 0.43 against 1.26 ± 0.23 kgN/h measured), but also in summer (0.74 ± 0.30 against 0.72 ± 0.24 kgN/h measured). Since the AUR, the N_2O-PR and the ratio between emitted and produced N_2O were all well described, the model was also able to predict the N_2O-EF in summer (2.3 ± 0.7% against 2.3 ± 0.7% measured) and winter (4.0 ± 0.9% against 3.6 ± 1.0% measured).

After calibration, the model predicted different contributions of NN and ND to the AOB-related production of N_2O in summer. While ND was responsible for 58% of the N_2O production by AOB with reference parameters, this contribution dropped to 42% after modification. These results were consistent with the objective of the calibration procedure, which was to decrease N_2O production by ND in summer, while maintaining it similar in winter. The model still predicted a high consumption of N_2O by HD: 77% of the N_2O produced by AOB in summer, and 58% in winter.

V.3.5 VALIDATION: EFFECT OF THE AIRFLOW RATE ON N_2O PRODUCTION

The model was finally evaluated on its capacity to predict the evolution of the ammonium elimination and N_2O production rates during the aeration tests performed during the winter campaign. Evolutions of the AUR, NO_3^- production rate and effluent DO concentration with the air load are presented on Figure V.3-5 (10-min averages).

Similarly to full-scale measurements, the model predicted an increase in the AUR: +29 and +27% measured and simulated respectively, for an increase of the air load from 57 to 131 Nm^3/kgN. The predicted evolution of the NO_3^- production rate was also close to the experimental data. The predicted DO increase with the air load was more pronounced but remained close to the experimental data. Finally, the model predicted a decrease of the effluent NO_2^- concentration with the air load, due to the increase of nitrification efficiency, which was observed experimentally (Figure V.3-6).

Results regarding the N_2O-PR and N_2O-EF are presented on Figure V.3-7. On average, model predictions were similar to the experimental data. In particular, they matched the experimental data in the typical range of air load (70 – 90 Nm^3/d). However, the model did not predict the same trend with increasing air load. While the measured N_2O-PR was found roughly constant, the model predicted an increase. Consequently, the predicted N_2O production factor increased with air load, while experimental data showed a slight decrease.

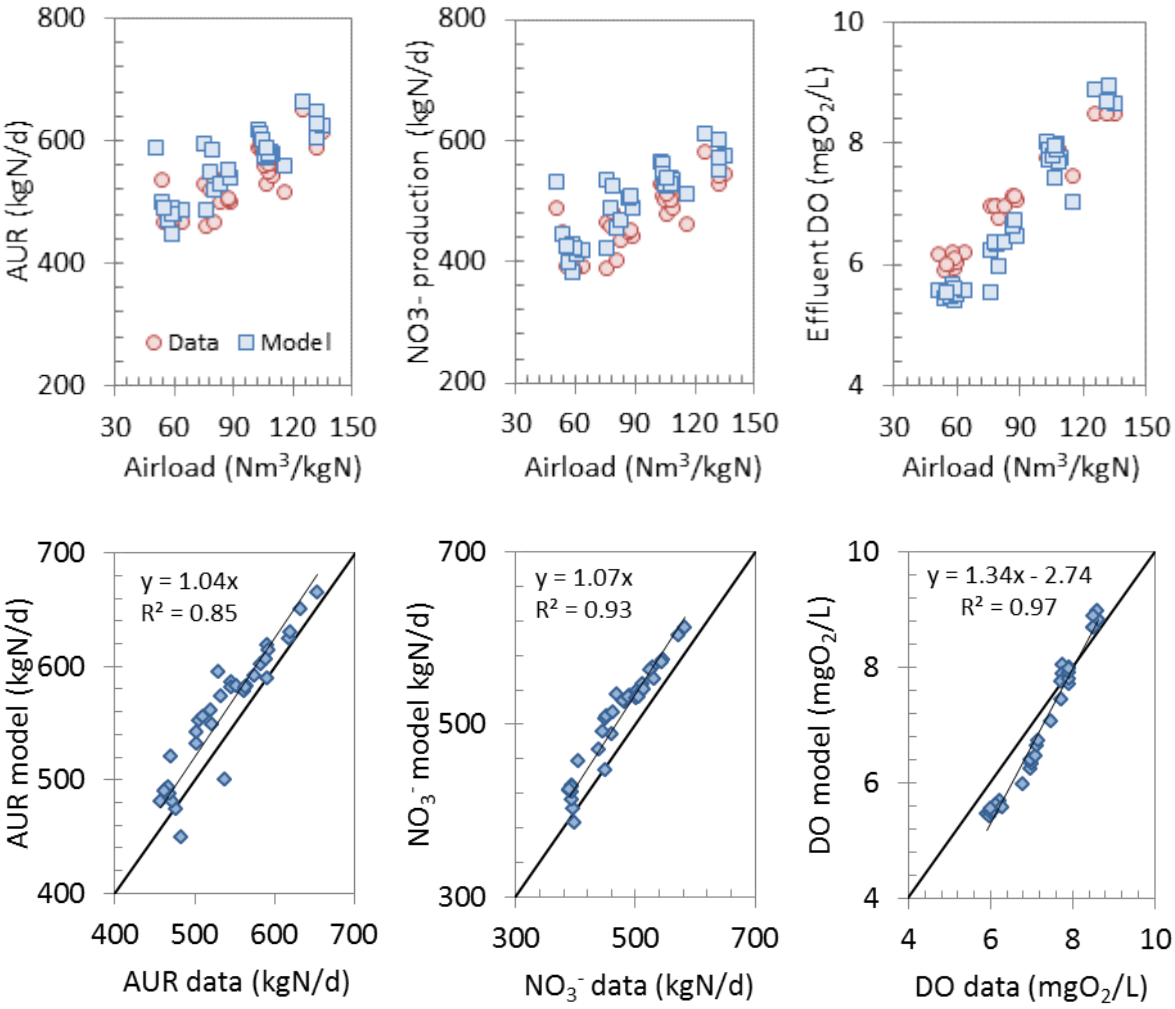

Figure V.3-5. Results of the aeration tests: evolution of the AUR, NO_3^- production rate and effluent DO concentration with the air load (top panels), and model predictions against experimental data (bottom panels).

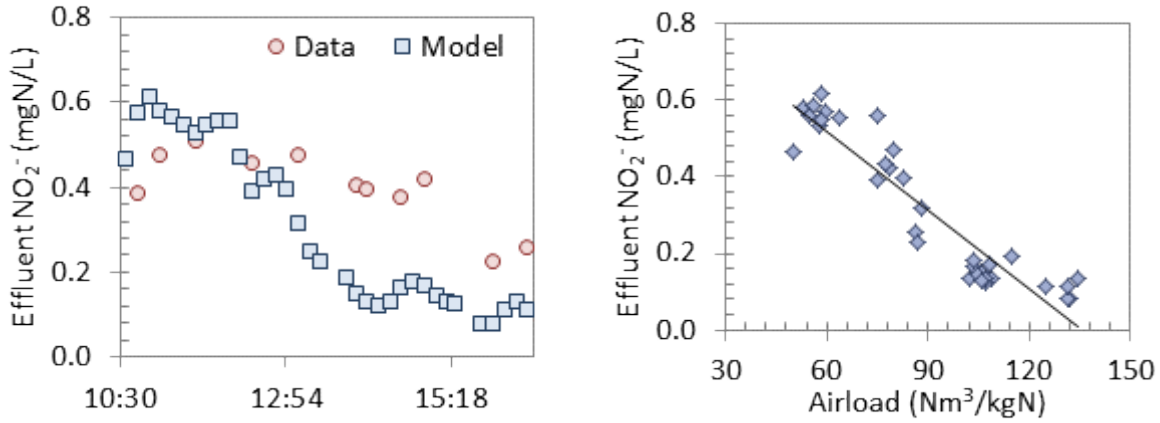

Figure V.3-6. Evolution of effluent NO_2^- concentrations during the aeration test (left panel) and with the air load (right panel).

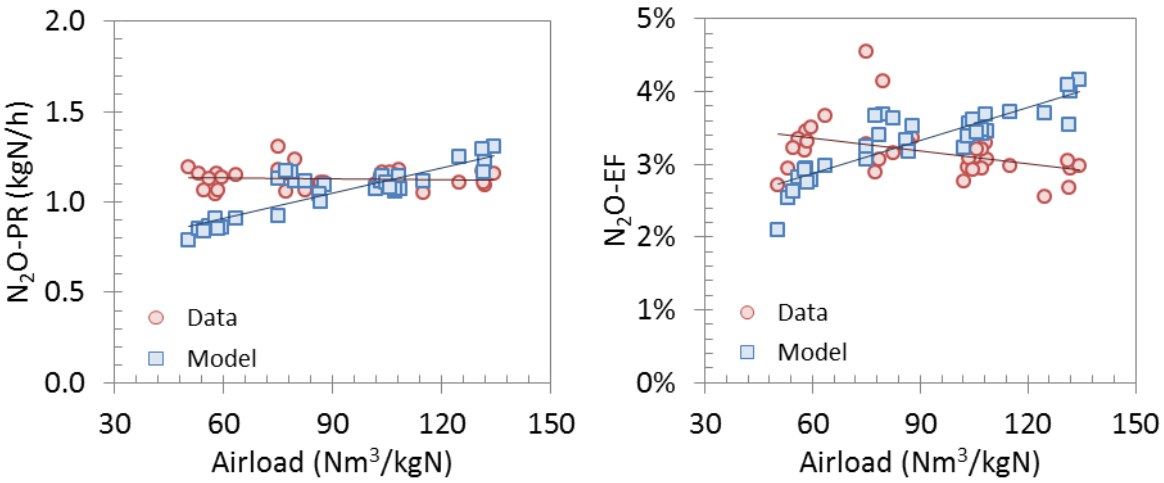

Figure V.3-7. Results of the aeration tests: evolution of the N_2O-PR and N_2O-EF with the air load.

According to the model, the evolution of the N_2O-PR with the air load was related to a decrease of the net consumption by OHO, which was only partly compensated by a decrease of the AOB production (Figure V.3-8). This was explained by higher O_2 transfer rates resulting in higher DO concentrations within the biofilm. The higher DO concentrations inhibited N_2O reduction by HD. In parallel, the N_2O production by the ND pathway (due to a lower nitrite concentration, Figure V.3-6) and the NN pathway was lower, but this did not compensate for the lower heterotroph activity. The higher N_2O-PR predicted by the model, associated to the high airflow rate, resulted in a higher ratio between emitted and produced N_2O.

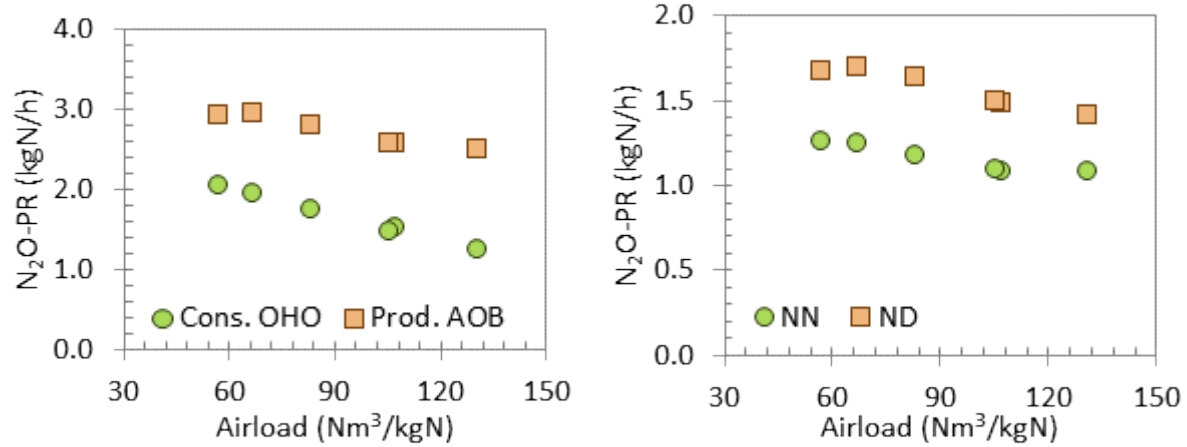

Figure V.3-8. Hourly average prediction of N_2O production and net consumption rates by AOB and OHO during the aeration tests.

These results globally confirm the validity of the gas/liquid transfer model structure, as well as the used biokinetic parameters for average air load values. However, they highlighted remaining improvement points that will be discussed in section V.4.2.

V.4 DISCUSSION

V.4.1 IMPACTING PARAMETERS

Modelling N_2O from biofilm reactors is less advanced than for suspended biomass systems, and was rarely applied at full-scale (Lindblom et al., 2016, Sabba et al., 2018). Very few studies investigated N_2O production from biofilms combining autotrophic and heterotrophic biomass (Sabba et al., 2018). The global sensitivity analysis performed in this work is the first to come with a classification of the parameters impacting N_2O production from tertiary nitrifying BAFs, which combines nitrifiers and denitrifiers. This study highlights the complexity of modelling common intermediate products of nitrification/denitrification, and identifying the parameters that generate their accumulation.

Results of the global sensitivity analysis gave a reliable identification of parameters impacting nitrification (R^2 = 0.91 and 0.86 for NH_4^+ and NO_3^-), but gave less significant results concerning NO_2^- and N_2O (R^2 = 0.56 and 0.70). Similar difficulties were encountered by Mannina et al. (2018), who included N_2O production pathways in a pilot-scale membrane bioreactor model. These authors found a similar regression coefficient for N_2O (R^2 = 0.68) and assumed a non-linear behaviour of the model outputs. In fact, their regression coefficients ranged between 0.27 and 0.79 for all model outputs, which corroborates the fact that parameter identification is more complex in biofilm reactor models, and moreover when multiple reaction intermediates are included in the model. The non-linearity between N_2O emissions and model parameters was already highlighted by Boiocchi et al. (2017) using a plant-wide activate sludge model. Nevertheless, the results can still be used to obtain a classification of the main parameters regulating N_2O production. Absolute standardized coefficients of the parameters most affecting N_2O (β_i > 0.05) are presented on Figure V.4-1.

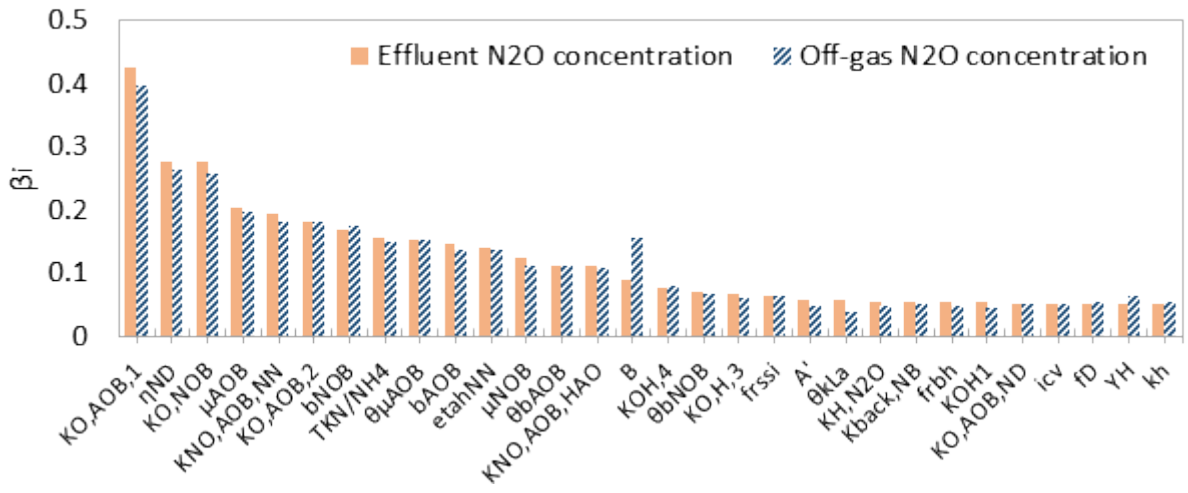

Figure V.4-1. Absolute standardized β_i of the parameters most influencing N_2O predictions.

N_2O predictions were mainly influenced by parameters related to AOB and NOB growth, which govern NO_2^- accumulation. Although NOB are not known to produce N_2O, their activity indirectly affects N_2O production, as it controls NO_2^- accumulation and DO concentrations within the biofilm. Their key role has already been demonstrated in previous studies. Based on a model coupling N_2O production pathways by AOB (Pocquet et al., 2016) and HD (Hiatt and Grady, 2008), and considering NOB growth, Massara et al. (2017b) evaluated the parameters influencing the predicted N_2O-EF *via* local sensitivity analysis. It revealed that, under non-limiting DO conditions in the aerobic tank, the parameters related to NOB were the most influencing (i.e. favoured NOB growth, resulting in lower N_2O-EF), right before AOB parameters. Similarly to our study, these authors related that to the effect of NOB on the accumulation of NO_2^-. Similarly, Kim et al. (2017) were able to describe N_2O production rates measured in sequencing batch reactors, as soon as they included NOB growth in their model (considering the ND path only). It was largely overestimated without considering NOB, as NO_2^- accumulation was overestimated.

On the other hand, Sabba et al. (2017) included N_2O production by AOB (NN + ND) in a one-dimensional 100 µm biofilm model. Their model predicted higher N_2O emissions in a biofilm composed of 70% AOB / 30% NOB compared to a 100% AOB biofilm. Because NOB have a higher specific rate of O_2 consumption, their presence induced limited DO concentrations in a larger part of the biofilm, leading to greater diffusion of NH_2OH into the deeper biofilm where it promoted N_2O production through ND. Their study, which remains theoretical, is the only to demonstrate higher N_2O production rates in presence of NOB in biofilm systems to our knowledge. In the model developed in the present thesis, the biofilm is described by two layers only, which does not allow to observe such concentration gradients, which were found impacting N_2O production according to Sabba et al. (2017).

Parameters related to NN were also highlighted by the sensitivity analysis. While many studies found a predominance of ND on the net N_2O production by AOB (Kim et al., 2010, Wunderlin et al., 2012, Wunderlin et al., 2013, Tumendelger et al., 2014, Peng et al., 2015, Pocquet et al., 2016, Massara et al., 2017b), the contribution of ND was 42% in summer and 58% in winter according to the model. This result can be explained by the high NH_4^+ loads treated by the nitrifying BAFs of Seine Aval (1.0 – 1.5 $kgN/m^3/d$), which led to the accumulation of reaction intermediates, such as NH_2OH, and high associated N_2O production rates by NN. The lower contribution of ND compared to literature values can also come from the fact that NO_2^- did not accumulate that significantly during the measuring campaigns (0.24 and 0.68 mgN/L).

Finally, a debatable result of this sensitivity analysis is the small apparent influence of parameters related to HD ($\beta_i < 0.1$). The denitrified flux was small before the nitrified one (13% in summer, 8% in winter), but HD was found to act as a sink of N_2O during both campaigns, reducing the N_2O-PR drastically. However, these results are dependent on the classification method, since it was arbitrarily decided that only $\beta_i > 0.1$ were significant. In fact, O_2 inhibition constants related to N_2O production and reduction by HD ($K_{I,OH,3}$ and $K_{I,OH,4}$) were slightly below 0.1, and ranked 18th and 16th on 90 parameters (Figure V.4-1).

The most likely explanation is that the effects of the HD parameters were covered by other mechanisms. First, COD remained constant during the simulations (average influent concentrations were used), while the NTK/NH_4 ratio, therefore the nitrogen load, was a variable parameter. Since nitrification was the main source of N_2O, the availability of dissolved N_2O depended on parameters regulating NH_4^+ oxidation, NO_2^- accumulation, and on transfer parameters. Many parameter combinations led to low N_2O concentrations (39% under 0.2 mgN/L), which reduced the opportunities for HD parameters to impact N_2O. The total number of combinations (450) being in the low range of literature recommendations (Cosenza et al., 2013, Vanrolleghem et al., 2015), it may be too limited to assess the real impact of HD parameters. Moreover, the SRC method compels linear relations between model parameters and output, which may not be linear. Finally, it should be recalled that this analysis was performed considering average operating conditions. Boiocchi et al. (2017) studied the sensitivity of N_2O emissions for various conditions of DO and temperature. These authors found that NOB processes impacted N_2O emissions in all conditions, while the effect of parameters related to HD where dependent on the DO level. More specifically, at DO < 2 mgO_2/L, parameters related to the 4th step of HD (N_2O reduction) were predominant, while at 2 mgO_2/L, parameters related to the 1st step (NO_3^- reduction) had a high influence, as O_2 inhibition induced an accumulation of NO_2-, further reduced to N_2O.

To conclude, this global sensitivity analysis provided essential information on the parameters regulating N_2O production from full-scale nitrifying BAFs and helped to choose the parameters to be further calibrated. Additional analysis (or dedicated experiments) could be performed for various NH_4^+ load, temperature and air flow conditions, and various COD feeding, to get a better insight into the conditions regulating N_2O production by AOB and consumption by HD.

V.4.2 THE BAF MODEL CAN PREDICT FULL-SCALE N_2O FLUXES

To the best of our knowledge, this work is the first to calibrate a tertiary nitrifying BAF model including N_2O production pathways, moreover at full-scale. Modifications were made to the

biokinetic model, in order to compose with full-scale constraints. NH_4^+ and NO_2^- were considered the true substrates for AOB and NOB instead of NH_3 and HNO_2, since the latest are estimated based on pH, which is not always reliably measured at full-scale. Additional reactions relative to heterotrophic denitrification were computed, as a significant fraction of heterotrophs is known to enter tertiary nitrifying BAFs (Vigne et al., 2010, Bernier et al., 2014) and can significantly influence the net N_2O production (Sabba et al., 2018).

The high number of parameters and computational time incited to a manual calibration of the model, based on the main parameters revealed by the global sensitivity analysis. Although the procedure proposed by Rittmann et al. (2018) was not strictly followed, physical parameters (bed porosity, diffusion coefficients and gas/liquid transfer) were calibrated before biokinetic parameters. Nitrification performance was calibrated by increasing the initial media bed porosity to 0.38, which remained close to the reference value 0.356 (Bernier et al., 2014). The accumulation of NO_2^- was lowered by decreasing the affinity constant of NOB for O_2 from 0.6 to 0.5 mgO_2/L, which remained within literature ranges: 0.3 – 1.1 mgO_2/L (Sin et al., 2008). At this point, the model was able to predict the main fluctuations of N_2O fluxes, but overestimated the N_2O-PR in summer. The calibration of the N_2O-PR was performed based on the datasets from both campaigns. The predicted production by ND was similar between the two campaigns, while DO levels within the biofilm were significantly different (0.22 mgO_2/L in summer, 0.50 mgO_2/L in winter). Many studies agreed on the fact that N_2O production by ND is inhibited by high DO concentrations (Tallec et al., 2006b, Peng et al., 2014, He et al., 2017b). Maximum N_2O-PR was found for DO concentrations of 0.75 mgO_2/L (Chen et al., 2018) and 0.85 mgO_2/L (Peng et al., 2015) even at low NO_2^- levels in lab-scale reactors operated with nitrifying sludge. In the initial two-pathway model of Pocquet et al. (2016), the effect of DO on ND was represented by a Haldane term, which corresponded to a maximum production at 0.60 – 0.65 mgO_2/L. When the BAF model was extended to include N_2O production pathways, biokinetic parameters were taken from Lang et al. (2016), whose Haldane term reached its maximum value at 0.25 – 0.30 mgO_2/L (Figure V.3-3). The model was calibrated by using the parameters from the initial paper (Pocquet et al., 2016) in order to decrease N_2O production in summer. Only parameters related to ND were finally modified. The predicted N_2O consumption by HD was already high, and no literature data would have justified the modification of HD parameters in order to further decrease N_2O production.

The calibrated model was able to describe long-term nitrification performance and high-frequency variations of N_2O production and emission rates from the studied BAF. Considering the small calibration work (5 parameters changed, close to their reference values), these results highlight the robustness of the original BAF model, and of the

two-pathway biokinetic model. The first was calibrated and validated on data from 2009 (Bernier et al., 2014), and is still able to describe long-term nitrification for 2014-2015 for various conditions, despite the modifications made to its gas-liquid transfer and biokinetic sub-models. The second was only calibrated on activated sludge data (Lang et al., 2016, Pocquet et al., 2016), but was able to describe the order of magnitude and main variations of the N_2O-PR in this full-scale BAF application, even without calibration.

However, the calibrated model slightly overestimated the effect of aeration on NH_4^+ elimination (Figure V.3-5) and on N_2O production (Figure V.3-7). The model predicted higher N_2O-PR at high air loads (> 100 Nm^3/kgN), and lower N_2O-PR at low air loads (< 70 Nm^3/d) than observed during aeration tests. These results explain the overestimation of the N_2O-PR observed between days 393 and 398 of the winter campaign (Figure V.3-4). The peaks of N_2O corresponded to high flowrates, inducing high DO concentrations and more pronounced inhibition of N_2O consumption by HD. In addition to the high N_2O-PR, it resulted in increased N_2O stripping –thus overestimation of the emitted to produced ratio. Such high air loads only concerned some single events, and are not representative of the usual operating conditions of the Seine Aval WRRF. Nevertheless, further calibration could be performed to address this issue. A calibration based on nitrite concentrations could have been done to decrease NO_2^- reduction to N_2O at high flowrates (Figure V.3-6). On-line measurements of NO concentrations would be an asset to further calibrate biokinetic parameters.

To conclude, biological conditions leading to N_2O production in biofilms and suspended biomass systems are similar: in particular low DO, transient NH_4^+ loads, and high NO_2^- concentrations (Sabba et al., 2018). However, biofilms are diffusion-limited, and therefore submitted to substrate and biomass gradients. The ability of the model to accurately simulate the overall N_2O production therefore depends on its capacity to describe the system's hydraulics and substrate diffusion within the biofilm. Results of the present study suggest that, from the moment that the system's hydraulics and mass transfer are correctly described, the biokinetic model –validated on AS data– is relevant to describe N_2O production from a full-scale nitrifying BAF, even with similar parameter values.

V.4.3 HETEROTROPHIC DENITRIFICATION CONTROLS THE N_2O PRODUCTION

This modelling study suggested a strong influence of HD on the net production of N_2O. Despite the nitrifying conditions and the small contribution of denitrification (reducing 8 to 13% of the NO_3^- produced by nitrification), OHO consumed over half of the N_2O produced by AOB. This result is consistent with previous finding from the literature. Using mass balances on the denitrification stage of the Seine Aval plant, Bollon et al. (2016a) showed that HD

could reduce around 93% of the N_2O produced during nitrification, provided that the methanol injection worked properly (influent BOD/N > 3). In a modelling study coupling ND and HD, Guo and Vanrolleghem (2014) showed that HD reduced 2/3 of the N_2O produced by AOB in a full-scale activated sludge WRRF. These results are also consistent with the conclusions of Read-Daily et al. (2016), who investigated denitrification kinetics through batch test experiments. The authors concluded that, in a biofilm system supplied with NH_4^+, DO and COD, the internal anoxic part of the biofilm can act as a sink of N_2O. Finally, recent batch tests on activated sludge from a pre-denitrifying tank reported N_2O reduction rates 2 to 5 times higher than N_2O production rates by HD, even without external carbon supply (Conthe et al., 2019).

HD also explained the difference between measured N_2O-PR in winter and summer. In the original paper, the authors made the assumption that the higher N_2O-PR observed in winter was related to a thicker biofilm, which induced O_2 diffusion limitations, higher accumulation of nitrites, and therefore higher N_2O production by the ND path (Bollon et al., 2016b). The present study only partly corroborates this hypothesis. The model did predict a thicker biofilm in winter (101 µm against 87 µm in summer), and higher NO_2^- concentrations. However, the higher net N_2O-PR was not only related to this higher NO_2^- concentration. The difference mainly came from HD: the higher DO in the biofilm in winter induced a higher inhibition of heterotrophic N_2O reduction, resulting in a lower reduction of N_2O. Although NO reduction is also impacted by DO concentration, its rate remained limited during both periods by NO concentration.

The calibrated model gives us an insight into the effect of operating conditions on N_2O production mechanisms in the Seine Aval tertiary nitrifying BAFs. In particular, it revealed a significant contribution of HD to the net N_2O production, which is conditioned by DO concentrations and the accumulation of reaction intermediates during nitrification (NO, NO_2^-). Supplementary simulations could be performed with a higher number of biofilm compartments, to assess their effect on spatial gradients and N_2O predictions. Moreover, further investigations should be used to evaluate the actual contribution of HD to N_2O production in nitrifying BAFs. Specific experiments on the combined effect of readily biodegradable carbon, DO level and temperature on NO and N_2O production by AOB and OHO, and the associated determination of N_2O production pathways by isotopic analysis, could help in concluding on an optimal operation of nitrifying BAFs to maximize ammonium elimination, while minimizing N_2O production.

V.5 CONCLUSION

Simulation results from a nitrifying BAF model were confronted to full-scale data from the largest European WRRF Seine Aval. The model was evaluated regarding its ability to describe the nitrification performance over two years of data and high-frequency N_2O fluxes during two measuring campaigns performed in contrasted temperature conditions. The mains results are the following:

- N_2O production was due to nitrification through the two main pathways (NN and ND);
- A sensitivity analysis highlighted the dependency of nitrification to oxygen-related parameters, and the dependency of N_2O to oxygen- and nitrite-related parameters;
- With only a few parameter changes (ε_0, $K_{O,NOB}$, η_{ND}, $K_{I,O,AOB}$, and $_{KO,AOB,ND}$), the model could describe long-term nitrification and high-frequency N_2O production data in relation to operating conditions;
- The model predicted a high impact of heterotrophic denitrification on the overall production of N_2O, always acting as a pool of N_2O (consumption of 73% of the N_2O produced by AOB in summer and 58% in winter);
- The higher N_2O production in winter was related to higher inhibition of N_2O reduction by heterotrophic denitrification, due to higher DO levels within the biofilm.

Chapter VI. Model-based evaluation of long-term N_2O emissions in a nitrifying BAF

RESUME

Dans les chapitres précédents, un modèle décrivant la production et les émissions de N_2O par les biofiltres nitrifiants tertiaires de la station Seine Aval a été développé. Les prédictions du modèle sont très sensibles aux paramètres régulant le transfert gaz/liquide et l'accumulation de nitrites. Le modèle a été calé sur les performances de nitrification journalières mesurées en 2014-2015, et sur les moyennes 10 minutes des émissions de N_2O observées pendant deux campagnes de mesure courtes. En modifiant quelques paramètres seulement, le modèle est capable de prédire l'ordre de grandeur et les principales dynamiques des émissions de N_2O pour les deux campagnes. Dans ce chapitre, les prédictions sont extrapolées pour étudier les flux de N_2O en 2014-2015, et proposer un outil simplifié d'estimation du facteur d'émission (FE) associé à la nitrification tertiaire de Seine Aval.

Les deux jeux de données utilisés pour caler les paramètres du modèle N_2O sont considérés représentatifs de la période d'étude, couvrant 81% et 43% des conditions de charge en ammonium et d'aération observées en 2014-2015. De plus, avec un unique jeu de paramètres, le modèle est capable de décrire les flux de N_2O des deux campagnes, pourtant réalisées à des températures différentes (14,5 et 22,5 °C en moyenne). Le modèle a donc été utilisé pour évaluer les émissions de N_2O sur cette période. Le facteur d'émission (FE) prédit est en moyenne de 2,0 ± 0,7 % de la charge en azote appliquée, représentant 56 fois le facteur préconisé par le GIEC. Ses variations sont en outre très importantes, allant de 0,2 à 4,0 % de la charge en azote. Une matrice de corrélation révèle qu'elles sont principalement influencées par la concentration en ammonium (+), le débit d'air (+), et la température (-). Un effet seuil de la charge en ammonium est observé sur les émissions de N_2O : au-delà de 0,87 $kgN/m^3/j$, l'abattement de l'ammonium diminue, favourisant l'accumulation d'intermédiaires réactionnels précurseurs du N_2O. A charge constante, la baisse du FE avec la température est liée à une baisse de la concentration en nitrite et à celle de la concentration en oxygène dissous. Les résultats de simulation ont finalement été utilisés pour proposer un modèle de régression linéaire multiple décrivant le FE journalier à partir des trois conditions opératoires susmentionnées. Ce modèle statistique est capable de décrire très correctement l'évolution du facteur d'émission de N_2O journalier en fonction des conditions opératoires appliquées. Il constitue donc une meilleure alternative à la méthode de quantification des émissions de N_2O recommandée par le GIEC.

Mots-clés : biofilm, dénitrification hétérotrophe, nitrification, N_2O, statistiques

ABSTRACT

In previous chapters, a model describing N_2O production and emissions from tertiary nitrifying BAFs of the Seine Aval WRRF was developed. Model predictions were found highly sensitive to parameters related to gas-liquid transfer and to those regulating the accumulation of nitrites. The model was calibrated on daily average nitrification performance monitored in 2014-2015, and 10-min average N_2O emissions observed during two short measuring campaigns. By modifying only a few parameters, the model was able to predict the order of magnitude and main fluctuations of N_2O emissions from both campaigns. In the present chapter, model predictions will be extrapolated to investigate N_2O variations over 2014-2015, and propose a simplified tool to estimate the emission factor (EF) from the full-scale tertiary nitrifying BAFs of the Seine Aval WRRF.

The two datasets used to calibrate the N_2O model parameters were found to be representative of the entire studied period, as they covered 81% of the daily ammonium load and 43% of the airflow conditions observed in 2014-2015. Moreover, with a single calibrated parameter set, the model could describe N_2O emissions from both campaigns, which were performed at contrasted temperatures (14.5 and 22.5 °C on average). The model was therefore used to investigate N_2O emissions for this long-term period. The simulated N_2O-EF was 2.0 ± 0.7% of the applied nitrogen load on average, which is 56 times the factor used by the IPCC. Moreover, its fluctuations were high, ranging from 0.2 to 4.0% of the influent nitrogen load. A correlation matrix revealed that these fluctuations were mostly governed by the influent ammonium concentration (+), the airflow (+) and the influent temperature (-). A threshold effect of the ammonium load on the N_2O emissions was observed: above 0.87 $kgN/m^3/d$, ammonium removal decreased, leading to an accumulation of reaction intermediates, precursors to N_2O. For a given ammonium load, the decrease of the N_2O-EF with temperature was related to a decrease of the nitrite concentrations and to a decrease of dissolved oxygen. Simulation results were finally used to propose a multiple linear regression model describing the daily N_2O-EF based on the three identified operating conditions only. The statistical model was able to describe dynamics of daily average N_2O-EF according to operating conditions. It constitutes a better alternative to the IPCC's methodology.

Keywords: biofilm, heterotrophic denitrification, nitrification, N_2O, statistics

VI.1 INTRODUCTION

During the last decade, increasing attention has been paid to nitrous oxide (N_2O) emissions from wastewater resource recovery facilities (WRRF) due to its detrimental environmental effect (potent greenhouse gas –GHG– and ozone depleting substance) and high impact on the carbon footprint of WRRFs (Daelman et al., 2013, Kosonen et al., 2016). Although N_2O can be produced and emitted at different locations of a WRRF, it is generally agreed that the biological nitrogen removal (BNR) stage is the main source (Kampschreur et al., 2009).

Several measuring campaigns, mainly on conventional activated sludge processes (CAS), have been performed to evaluate the extent of N_2O emission variability in connection with the WRRF design and operating parameters. Contrasted emission factor values (N_2O-EF, percentage of influent nitrogen load emitted as N_2O-N) were reported, ranging from 0 to 25% (Law et al., 2012b, Massara et al., 2017a). To account for the high temporal variability of N_2O emissions (daily and seasonal), efforts were recently dedicated to perform long-term monitoring, usually over several months. They ended up to lower average N_2O-EF values: 0.036 % in the UK (Aboobakar et al., 2013), 0.016% in Spain (Rodriguez-Caballero et al., 2014), 1.9% in Finland (Kosonen et al., 2016) and 2.8% in the Netherlands (Daelman et al., 2013). Conversely, emission data from biological aerated filters (BAF) are limited. Wang et al. (2016) investigated seasonal variations of N_2O emissions from tertiary nitrifying BAFs over 12 months. The N_2O-EF varied from 0.02 to 1.26% (0.26% on average). Based on two short campaigns, Bollon et al. (2016b) reported N_2O emissions twice as high in winter (3.11% of the removal nitrogen load) compared to summer (1.77%).

Several parameters affecting N_2O production were identified and reviewed by Law et al. (2012b) and Massara et al. (2017a). During nitrification, it has been observed that low dissolved oxygen (DO) concentrations, nitrite (NO_2^-, or nitrous acid, HNO_2) accumulation and increased nitrogen load were usually associated to high emissions (Ahn et al., 2010, Foley et al., 2010, Aboobakar et al., 2013, Daelman et al., 2015). Several studies reported a positive correlation between daily variations of the influent nitrogen load and the N_2O-EF (Daelman et al., 2015, Bollon et al., 2016b, Kosonen et al., 2016). An increased nitrogen load is suspected to promote a shift in metabolism from a low hydroxylamine (NH_2OH) oxidation activity towards the maximum activity (Chandran et al., 2011). It could also lead to a buildup of N_2O production pathways intermediates such as ammonium (NH_4^+), NH_2OH, NO or NO_2^- (Chandran et al., 2011, Law et al., 2012b). A low DO concentration is likely to cause NO_2^- accumulation and promote N_2O production through nitrifier denitrification (Colliver and Stephenson, 2000, Tallec et al., 2006a, Kampschreur et al., 2008a). Wang et al. (2016) correlated the seasonal fluctuations of N_2O emissions from BAFs to the influent NO_2^-

concentration, which is the precursor of N_2O production *via* nitrifier denitrification. The temperature effect on seasonal N_2O fluctuations was evaluated in a few cases and results are rather controversial. Whereas some studies did not show a strong correlation between N_2O emissions and mixed liquor or effluent temperatures (Daelman et al., 2015, Kosonen et al., 2016, Wang et al., 2016), other studies reported increased emissions in cold periods (STOWA, 2010, Bollon et al., 2016b). On the opposite, the benchmark model based study of Guo and Vanrolleghem (2014) suggested increased N_2O emissions with water temperature. This was mainly related to an increased N_2O production rate from AOB (nitrifier denitrification) while the net production rate by heterotrophs remained stable.

Since 2011, GHG surveys became mandatory for French territorial municipalities with over 50 000 inhabitants. The current method to quantify direct N_2O emissions from WRRFs is based on the use of a fixed emission factor of 0.0032 kgN_2O/person/year (Eyring et al., 2007), corresponding to 0.035% of the nitrogen load for developed countries (Kampschreur et al., 2009). This factor is based on the results of a single study on a secondary treatment plant in the USA (Czepiel et al., 1995), and is usually applied as a reference factor in GHG surveys. Based on previous investigations, this factor appears to be irrelevant to quantify N_2O emissions, as they are highly fluctuating and generally much higher. Consequently, several authors have called for an alternative estimation method (Ahn et al., 2010, Foley et al., 2010, Daelman et al., 2013). Performing measuring campaigns to assess the dynamics of N_2O emissions is time and money consuming, and is generally performed on short periods, while long-term data are required. Mathematical models, calibrated on full-scale data, can therefore be used to generate long-term data, and further propose simplified estimation tools for WRRF operators. To this end, a deeper understanding of the triggers of N_2O emissions from BNR systems is required, in particular the effect of operating conditions.

The model previously developed to describe N_2O emissions from a full-scale tertiary nitrifying BAF of Seine Aval WRRF was used to this aim. This model was calibrated on nitrification performance data collected over two years, and on N_2O emission data from two short periods (September 2014 and January/February 2015). Those were characterized by contrasted N_2O-EF, twice as high in winter compared to summer. In this work, simulations were performed to investigate N_2O emissions over a two-year period (2014-2015). The objectives were: (1) to quantify long-term N_2O emission rates and EF, (2) to investigate the variations of N_2O emissions in relation to operating conditions, and (3) to propose a practical tool to predict the N_2O-EF of full-scale tertiary nitrifying BAFs based on operating data.

VI.2 MATERIAL AND METHODS

VI.2.1 MODEL AND EXPERIMENTAL DATA

The functioning of a nitrifying Biostyr® of Seine Aval WRRF was previously simulated over 643 days (January 1st 2014 – October 10th 2015) with the calibrated BAF model. Its description is given in Annex 1. As a reminder, the biokinetic model includes NH_4^+ oxidation to nitrite NO_2^- *via* NH_2OH and NO by ammonium oxidizing bacteria (AOB), NO_2^- oxidation to nitrate (NO_3^-) by nitrite oxidizing bacteria (NOB), and NO_3^- reduction to nitrogen gas (N_2) *via* NO_2^-, NO and N_2O by heterotrophs (OHO). N_2O is a by-product of nitrification by nitrifier nitrification (NN) and nitrifier denitrification (ND), and a reaction intermediate of heterotrophic denitrification (HD). The long-term simulation results presented in Chapter V are further investigated here. Model outputs were logged in a Matlab file each 10 minutes. Then, they were averaged over 24 hours and extracted in Excel Files.

VI.2.2 ANALYSIS OF MODEL RESULTS

VI.2.2.1 CALCULATION OF N_2O PRODUCTION RATES

In the BAF model, biological reactions were computed within the two biofilm layers of each of the seven reactors in series. The N_2O production rates by NN (NN-PR), ND (ND-PR) and HD (HD-PR) were averaged on the overall BAF. Calculations are detailed for NN-PR, but are similar for ND and HD-PR. The daily NN-PR was calculated as the sum of NN production rates in both biofilm layers (Eq.38). The production in a biofilm layer j was calculated as the sum of productions in this layer of each reactor n (Eq.39). The stoichiometric coefficients can be found in Annex 1 (Table A.1 and A.3). The net HD-PR was calculated as the difference between the NO reduction rate to N_2O and the N_2O reduction rate to N_2. Finally, the N_2O-PR was calculated as the sum of NN, ND and HD production rates.

Eq.38
$$\mathrm{NN-PR} = \sum_{j=1}^{2} (\mathrm{NN-PR})_j$$

Eq.39
$$(\mathrm{NN-PR})_j = \sum_{n=1}^{7} \nu_{NN} r_{NN,n} V_{max,j}$$

Where $(NN\text{-}PR)_j$ is the N_2O production rate by NN (kgN/h), ν_{NN} the stoichiometric coefficient of NO reduction to N_2O by AOB, r_{NN} the associated reduction rate, and V_{max} the maximum biofilm volume (m^3).

VI.2.2.2 STATISTICAL ANALYSIS

Analysis of the model inputs (influent NH_4^+, NO_3^-, NO_2^-, TSS, COD, PO_4^{3-} concentrations, liquid and airflow rates, water temperature) and main predictions (AUR, N_2O fluxes, NO_2^-, DO, NH_2OH and NO concentrations in the biofilm) was performed on daily averages (n = 643), using R software. A matrix of Pearson's coefficients was built to assess the correlation between each pair of input and/or output (function *rcorr*). For clarity, and because of the elevated number of variables considered (19), a color code was arbitrarily associated to Pearson's coefficients r: dark blue for r > 0.6, medium blue for 0.6 > r > 0.4, light blue for 0.4 > r > 0.2, white for 0.2 > r > -0.2, light red for -0.2 > r > -0.4, medium red for -0.4 > r > -0.6 and dark red for r < -0.6. Each variable was standardized, i.e. centered around zero and of standard deviation 1. This method is classically used to compare variables of distinct orders of magnitude and units to each other. Finally, a multiple linear regression was performed to correlate standardized N_2O-EF to model inputs (function *lm*).

VI.3 RESULTS AND DISCUSSION

VI.3.1 DATA FROM N_2O MEASURING CAMPAIGNS VERSUS LONG-TERM DATA

This section aims at comparing the operating conditions prevailing during the summer and winter campaigns to the ones of the two-year dataset from the Seine Aval WRRF (2014-2015). The objective was to evaluate the relevance of using the model – calibrated on short term datasets for N_2O – to extrapolate production and emission rates over the two-year period. Long-term simulations were performed on daily average inputs, while summer and winter campaigns were simulated based on 10-min averages (see Chapter V). Therefore, model inputs and predictions from 2014-2015 and from the campaigns are presented as daily averages and 10-min averages, respectively. Long-term and campaign data are, however, compared based on the same time step, i.e. 24 h averages.

VI.3.1.1 DISTRIBUTION OF MODEL INPUTS (EXPERIMENTAL DATA)

The distributions of influent NH_4^+ load, aeration intensity and water temperature over 2014-2015 (daily averages, n = 643), summer 2014 and winter 2015 (10-min averages, n = 1008 and 2016, respectively) are presented on Figure VI.3-1. Other model inputs are presented in Annex 10. Data are presented using boxplots: bars (from bottom to top) represent the minimum value, 1st quartile, median, 3rd quartile, and maximum value, respectively. The median value is indicated by a dash on each boxplot.

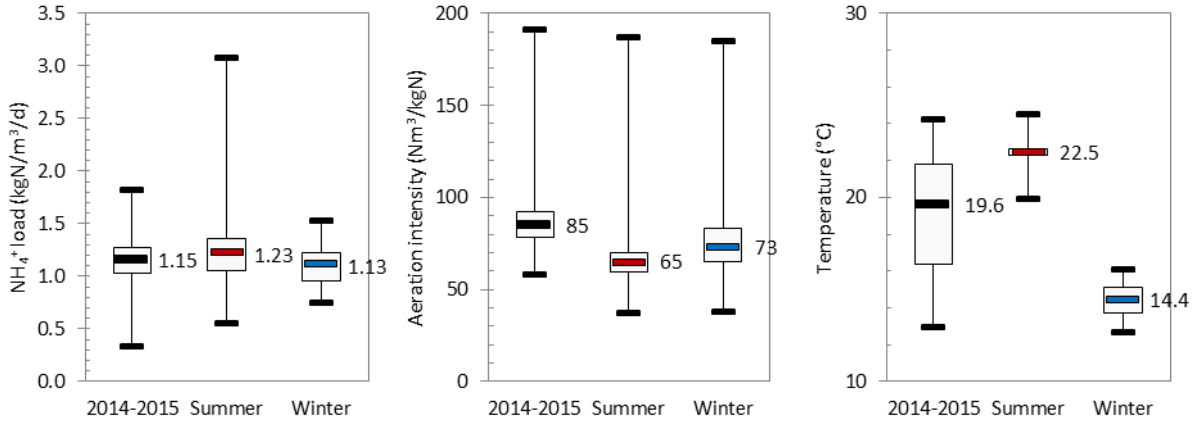

Figure VI.3-1. Distribution of the ammonium load, aeration intensity and water temperature used to simulate the nitrifying BAFs of the Seine Aval WRRF in 2014-2015 (n = 643), in summer 2014 (n = 1008) and winter 2015 (n = 2016).

The average values of the NH_4^+ load, aeration intensity and temperature were 1.15 ± 0.22 kgN/m^3/d, 87 ± 15 Nm^3/kgNH_4-$N_{applied}$ and 19.2 ± 2.9 °C, respectively. As presented on the boxplots, 50% of the NH_4^+ load values remained around ± 10% of the median value (1.03 to 1.27 kgN/m^3/d). The 25% lower and 25% higher values were due to low and high values of both the influent NH_4^+ concentration and flow rate (Figures A.19 and A.21). Median NH_4^+ loads measured in summer and winter campaigns were close to the third quartile (1.23 kgN/m^3/d) and to the average value over 2014-2015 (1.13 kgN/m^3/d), respectively. High values measured in summer were related to high influent flow rates (up to + 128% of the median value, Figure A21), while NH_4^+ concentrations remained close to the median value (± 24%, Figure A19). Based on daily averages, the NH_4^+ loads measured during the campaigns covered 81% of the range observed in 2014-2015: 0.96 to 1.49 kgN/m^3/d.

Although aeration is controlled by influent/effluent NH_4^+ concentrations on the Seine Aval WRRF (Figure A22), the aeration intensity was dispersed in 2014-2015. Half of the values remained close to the median (78 to 92 Nm^3/kgNH_4-$N_{applied}$), but high intensities were observed. These were mainly related to high air flow rates (Q_G, Figure A21). Similar trends were observed in summer and winter. The median Q_G measured during the campaigns was close to the first quartile of 2014-2015 (48 479 and 46 448 Nm^3/d, respectively). The aeration intensity was therefore lower during the campaigns (65 and 73 Nm^3/kgNH_4-$N_{applied}$, respectively), in particular in summer (higher NH_4^+ load at similar Q_G). Both lay below the first quartile, i.e. within the 25% lower values. All in all, aeration intensities and Q_G measured during the campaigns covered 43% of the ranges observed in 2014-2015: 62 to 83 Nm^3/kgNH_4-$N_{applied}$.

Finally, the temperature ranged between 12.9 and 24.2 °C, with a median value of 19.6 °C. Summer and winter campaigns were performed under contrasted temperature conditions. Their median temperature values (22.5 and 14.4 °C, respectively) lay above the third and below the first quartile, respectively. Temperatures measured during the campaigns covered 30% of the range observed in 2014-2015: 22.2 to 22.7 and 13.1 to 15.8 °C.

VI.3.1.2 MODEL PREDICTIONS IN TERMS OF NITROGEN REMOVAL

Daily average predictions of nitrogen removal over 2014-2015 are recalled in Table VI.3-1. As stated in Chapter V, the calibrated model was able to describe ammonium removal and nitrate production satisfactorily (order of magnitude and variations likewise). The effluent nitrite concentration was slightly underestimated (0.32 ± 0.16 against 0.65 ± 0.26 mgN/L), which resulted in an underestimation of the nitrite production rate. However, as observed experimentally, the model did predict a net consumption of nitrite in the BAF unit over 2014-2015.

Table VI.3-1. Ammonium removal, NO_3^- and NO_2^- evolution rates measured in 2014-2015 and predicted by the calibrated model (n = 643).

n = 643	AUR (kgN/m^3/d)	NO_3^- evolution rate (kgN/m^3/d)	NO_2^- evolution rate (kgN/m^3/d)
Experimental data	0.98 ± 0.17	0.91 ± 0.15	-0.01 ± 0.03
Model predictions	0.98 ± 0.13	0.90 ± 0.11	-0.02 ± 0.02

Distributions of the AUR, NO_3^- and NO_2^- production rates are presented on Figure VI.3-2 (effluent NH_4^+, NO_3^- and NO_2^- concentrations in Annex 10, Figure A23). The AUR was on average 0.98 ± 0.13 kgN/m^3/d, which represents 87 ± 8% of the influent ammonium load, and varied between ± 7% of the median value (0.92 to 1.07 kgN/m^3/d). Median predictions of the AUR in summer and winter lay between the first quartile and the median values (0.98 and 0.94 kgN/m^3/d, respectively). The AUR predicted in summer was slightly higher to that predicted in winter, despite the lower aeration intensity. This can be explained by the higher applied NH_4^+ load and the higher water temperature, which are suspected to induce higher oxygen uptake rates. Finally, predictions in summer and winter covered 72% of the data observed in 2014-2015: 0.77 to 1.17 kgN/m^3/d.

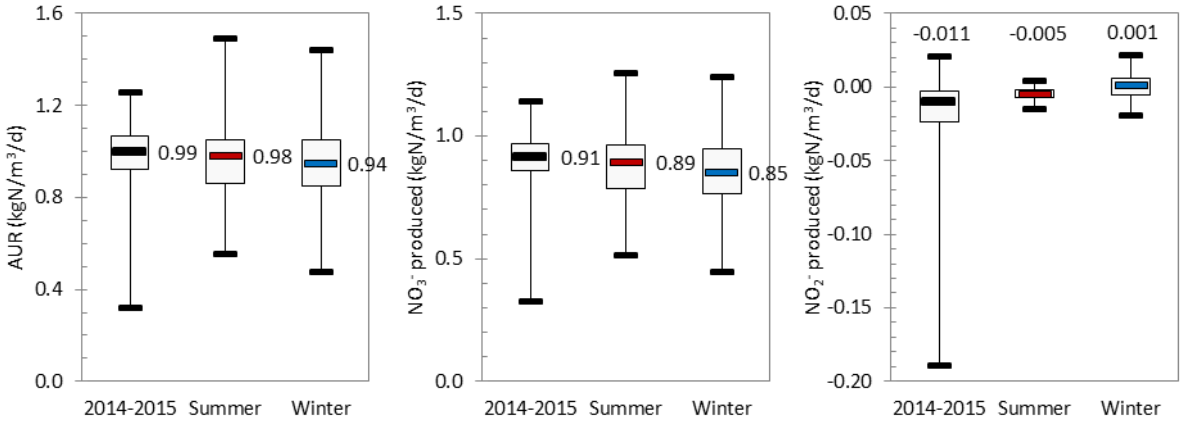

Figure VI.3-2. Distribution of the AUR, NO_3^- and NO_2^- evolution rates predicted by the model in 2014-2015 (n = 643), in summer 2014 (n = 1008) and winter 2015 (n = 2016).

The NO_3^- evolution rate mainly depends on the AUR, and therefore varied in a similar range (0.86 to 0.97 kgN/m³/d), while the NO_2^- evolution rate showed noticeable tendencies. It was on average -10 ± 14 kgN/d and 50% of the values lied between -14 and -2 kgN/d which indicated that NO_2^- was generally consumed in the BAF. The extremely low values corresponded to occasional events, in particular on days 367 and 592 (Figure A24).

A mass balance was performed on NO_2^- to understand its general consumption and the extreme values observed on days 367 and 592 (Table VI.3-2). On average, NO_2^- consumption by NOB was larger than its production by AOB (net nitrifiers = -0.004 kgN/m³/d), while OHO produced more than they consumed (net denitrifiers = 0.017 kgN/m³/d). The net NO_2^- consumption in the BAF was therefore due to its reduction to N_2O (0.030 kgN/m³/d).

Table VI.3-2. Mass balance on NO_2^- in 2014-2015 (n = 643) and during high NO_2^- consumption peaks.

	Concentrations		NO_2^- volumic loads						
	NH_4. IN mgN/L	NO_2. IN mgN/L	Inlet kgN/m³/d	Outlet kgN/m³/d	AOB production kgN/m³/d	AOB reduction to N_2O kgN/m³/d	NOB consumption kgN/m³/d	Net OHO kgN/m³/d	Total kgN/m³/d
2014-2015	30	0.75	0.030	0.013	1.016	0.030	1.020	0.017	-0.017
d = 367	23	2.62	0.122	0.008	1.008	0.036	1.088	0.003	-0.113
d = 592	17	3.53	0.199	0.009	0.951	0.030	1.119	0.009	-0.190

The extremely low values observed on days 367 and 592 were related to high NO_2^- input concentrations (2.62 and 3.53 mgN/L against 0.75 mgN/L on average), associated to lower influent NH_4^+ concentrations than usual (23 and 17 mgN/L against 30 mgN/L on average). This combination indicates incomplete nitrification in the former stage. During these events,

AOB activity was limited by the NH_4^+ concentration, inducing lower competition for O_2 between AOB and NOB. Therefore, the NOB activity was less limited by O_2 and NO_2^-. Interestingly, these peaks of influent NO_2^- concentration did not trigger N_2O production by ND. This was due to the concentration gradients over the filter height (Figure A25): the high influent NO_2^- induced high N_2O production by ND at the bottom of the BAF, but also a higher NOB activity, which resulted in a sharper decrease of NO_2^- concentration over the filter height, leading to a decrease of ND.

Finally, NO_2^- production rates predicted in summer and winter were close to the third quartile of 2014-2015. Low consumption rates predicted during these campaigns were due to low influent NO_2^- concentrations measured for these periods (0.27 to 0.92 mgN/L).

VI.3.1.3 DISCUSSION ON THE MODEL VALIDITY FOR THE 2014-2015 PERIOD

This BAF model was developed, among other reasons, to investigate the main factors determining N_2O production and emissions in a full-scale nitrifying BAF. “Good Modelling Practice” states that a model should be validated before being used to answer its original objective, when the necessary data are available (Rieger et al., 2013). Nitrification performances were calibrated on 643 days, and validated on the data from the N_2O campaigns. On the other hand, N_2O data were only available during these campaigns, and were thus used to calibrate the N_2O predictions. Consequently, the prediction of N_2O fluxes could not be validated on supplementary data. However, based on the present investigation, the BAF model was nevertheless used to investigate N_2O production and emission rates over 2014-2015 for the following reasons:

- The calibrated model is able to predict daily nitrogen removal observed over the entire period of study (2014-2015);
- Applied and removed ammonium loads measured during the campaigns were representative to those observed in 2014-2015 on the Seine Aval WRRF, and their average values were close to the median of the long-term period.
- As stated in Chapter V, the model presented a tendency to underestimate nitrification, and therefore N_2O fluxes, at ammonium loads higher that 1.5 $kgN/m^3/d$ and overestimate them at values lower than 0.8 $kgN/m^3/d$, which represented only 10% of the values in 2014-2015;
- The model predictions of the N_2O fluxes were closer to the observed values at aeration conditions between 70 and 100 $Nm^3/kgNH_4\text{-}N_{applied}$ (Chapter V), which represented 80% of the values in 2014-2015;

- The model was able to predict N_2O fluxes measured during both campaigns with the same parameter set, although they were performed at temperatures close to the minimum and maximum observed in 2014-2015.

VI.3.2 MODEL PREDICTIONS IN TERMS OF N_2O

The predicted N_2O-PR, the emitted to produced ratio and the N_2O-EF (% of NH_4-N eliminated) are presented on Figure VI.3-3.

The N_2O-PR was on average 0.81 ± 0.35 kgN/h, which corresponds to 3.2 ± 1.2% of the eliminated NH_4^+ load. Overall, 77 ± 5% of the produced N_2O was emitted, which resulted in an emission factor of 2.5 ± 1.0% of the eliminated NH_4^+ load, or 2.0 ± 0.7% of the applied TKN load (considering an average TKN to NH_4^+ ratio of 1.1). Observations from the summer campaign were close to the prediction during the entire period of study, in terms of N_2O production and emission. On the other hand, the N_2O-PR and N_2O-EF observed in the winter campaign lay above the third quartile of 2014-2015, i.e. within the 25% highest values. Low values of the emitted to produced ratio were related to the low values of Q_G observed in winter (Annex 10, Figure A21), which reduced the stripping of N_2O.

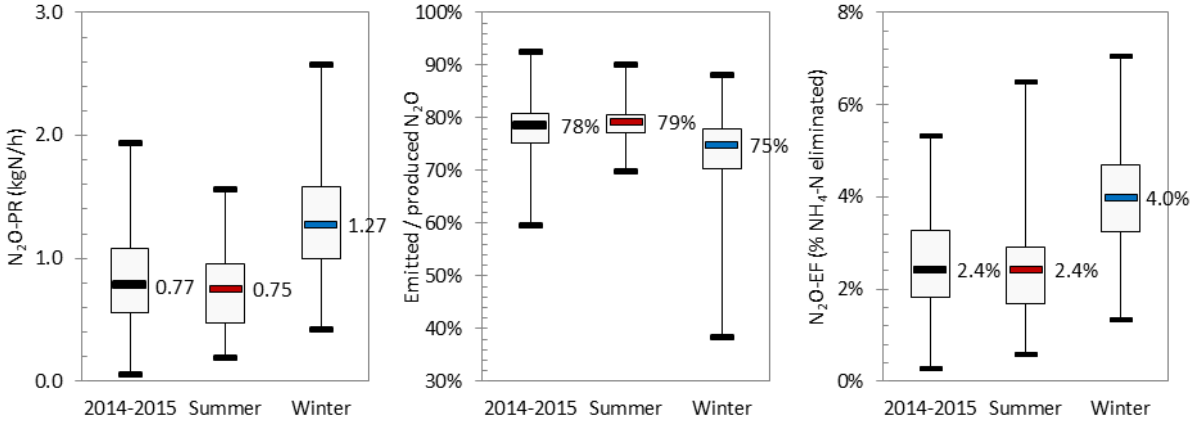

Figure VI.3-3. Distribution of the N_2O-PR, emitted / produced ratio, and N_2O-EF predicted by the model in 2014-2015 (n = 643), in summer 2014 (n = 1008) and winter 2015 (n = 2016).

The N_2O-EF predicted in this study was 56 times the factor used by the IPCC (0.035%). It fluctuated between 0.2 to 4.0% of the influent NH_4^+ load, which corresponded to 7 - 115 times the reference value. Such large ranges of N_2O emissions were already reported in the literature: from 0 to 25% of the influent nitrogen load, based on a review of over 30 studies at various scales (Massara et al., 2017a). Full-scale data ranged between 0.1 and 6.8% of the influent nitrogen load. Recent full-scale studies, reported N_2O-EF of 2.3 and 4.9% (Bollon et

al., 2016b) and 0.3% in BAFs (Wang et al., 2016), 1.9% (Kosonen et al., 2016) and 2.8% in CAS (Daelman, 2014), which is consistent with the present results. Moreover, these authors agreed on the high temporal variability of N_2O emissions and EF, which can also be observed on the presented daily averages. The N_2O-EF reported in this study are much higher than the N_2O-EF reported in French low loaded CAS processes (Filali et al., 2017). Although BAFs are used in fewer plants than CAS, they receive 20% of the load in France (60% in the Parisian area). Their contribution to the overall carbon footprint of wastewater management is therefore suspected to be large.

These results support two messages: (1) actions should be taken to mitigate N_2O emissions from nitrifying BAFs, (2) the current accounting method based on a generic (same value for all BNR technologies) and fixed N_2O-EF is not realistic, and an alternative approach should be proposed. To this end, a better understanding of the triggers of N_2O emissions from such systems is necessary. In the next section, the effect of operating conditions on N_2O production and emission rates is investigated, based on long-term predictions.

VI.3.3 EFFECT OF OPERATING CONDITIONS ON N_2O PRODUCTION

VI.3.3.1 ANALYSIS OF THE CORRELATION MATRIX

Table VI.3-3 presents the correlation matrix between model inputs and/or predictions. The objective was to identify the main factors controlling N_2O emissions and the relative contributions of the different N_2O production pathways in full-scale nitrifying BAFs. Results revealed the main impact of four parameters: influent NH_4^+ and COD concentrations, airflow and water temperature.

The **influent NH_4^+ concentration** is highly and positively correlated to the AUR and N_2O-PR and EF. In fact, the NH_4^+ concentration is positively correlated to reaction intermediates concentrations in the biofilm (NO_2^-, NO and NH_2OH), induced by NH_4^+ oxidation. These intermediates trigger the production of N_2O, which explain the high and positive correlation between influent NH_4^+ (and AUR) and N_2O production rates by AOB. Conversely, the NH_4^+ concentration, therefore the AUR, negatively impacts the DO concentration in the biofilm. This reduces the inhibition of N_2O reduction, which explains the negative correlation between influent NH_4^+ concentration and the net production of N_2O by HD.

The **airflow** is highly and positively correlated to AUR. This result is expected as air is injected proportionally to the NH_4^+ load (Figure A.22) in order to ensure efficient nitrification. Consequently, its effect on N_2O fluxes is similar to that of the AUR: it is positively correlated to the N_2O-PR and production by AOB, and negatively to the HD-PR. It is less correlated to

NO concentration within the biofilm, since aeration favours the stripping of NO, which reduces the residual dissolved NO concentration. Moreover, the airflow rate is highly and positively correlated to the emitted to produced N_2O ratio (data not shown), as it induces higher gas-liquid mass transfer rates.

The **influent COD concentration** shows similar correlations to model outputs as the NH_4^+ concentration, to a lower extent (lower absolute Pearson's coefficients). It should be noted, that COD and NH_4^+ concentrations are themselves significantly correlated (r = 0.48), since their concentrations are both dependent on the performance of the previous stage (activated sludge lines). Influent COD concentration is positively correlated to NO_2^- concentrations in the biofilm, which favours ND-PR. This effect of COD on NO_2^- comes from: (1) the positive correlation between influent COD and NH_4^+ concentrations, (2) the positive correlation between influent NH_4^+ and NO_2^- concentrations in the biofilm. On the contrary, the influent COD favours the reduction of NO_2^- by denitrifiers.

Temperature presents contrasted effects on N_2O pathways. On the one hand, it is positively correlated to NN-PR, since temperature increases the ammonium oxidization rate. On the other hand, it is negatively correlated to ND-PR and HD-PR. In fact, temperature is negatively correlated to DO and NO_2^- concentrations within the biofilm. Consequently, a temperature increase results in a lower inhibition of N_2O reduction to N_2 by O_2, resulting in higher net N_2O consumption. In parallel, N_2O production by ND becomes more limited, since ND-PR is strongly and positively correlated to the NO_2^- concentration, and negatively to DO.

Table VI.3-3. Matrix of Pearson's coefficients between model inputs and predictions (based on daily averages, n = 643).

	NH_4.IN	NO_3.IN	NO_2.IN	COD.IN	TSS.IN	PO_4.IN	Q_L	Q_G	T	AUR	N_2O-PR	N_2O-EF	NN-PR	ND-PR	HD-PR	DO Biofilm	NO_2 Biofilm	NH_2OH Biofilm	NO Biofilm
NH_4.IN	1	-0.09	-0.24	0.48	0.19	-0.13	-0.66	0.31	-0.20	0.52	0.71	0.75	0.36	0.67	-0.25	-0.28	0.53	0.51	0.41
NO_3.IN		1	0.00	-0.17	-0.14	0.06	-0.06	0.11	0.16	0.07	-0.18	-0.18	0.03	-0.09	-0.08	-0.01	-0.21	-0.25	-0.30
NO_2.IN			1	-0.30	-0.28	0.11	0.13	-0.16	0.14	-0.11	-0.14	-0.14	-0.11	-0.16	0.10	0.06	-0.09	-0.22	-0.18
COD.IN				1	0.77	-0.25	-0.25	0.39	-0.35	0.21	0.41	0.45	0.14	0.46	-0.15	-0.03	0.44	0.35	0.26
TSS.IN					1	-0.41	-0.05	0.30	-0.37	0.04	0.24	0.27	-0.04	0.34	-0.04	0.02	0.36	0.28	0.22
PO_4.IN						1	0.16	-0.16	0.46	0.07	-0.30	-0.35	0.18	-0.35	-0.09	-0.15	-0.38	-0.12	-0.03
Q_L							1	0.17	0.32	0.14	-0.27	-0.44	0.24	-0.12	-0.27	-0.27	-0.14	0.14	0.13
Q_G								1	0.01	0.67	0.45	0.37	0.52	0.57	-0.47	-0.17	0.29	0.41	0.14
T									1	0.19	-0.51	-0.60	0.56	-0.42	-0.46	-0.26	-0.60	-0.22	-0.29
AUR										1	0.61	0.46	0.74	0.69	-0.61	-0.73	0.42	0.59	0.44
N_2O-PR											1	0.97	0.14	0.82	0.00	-0.24	0.69	0.65	0.55
N_2O-EF												1	0.01	0.77	0.12	-0.09	0.67	0.55	0.47
NN-PR													1	0.43	-0.94	-0.69	0.23	0.53	0.38
ND-PR														1	-0.46	-0.51	0.91	0.78	0.67
HD-PR															1	0.70	-0.33	-0.49	-0.37
DO biofilm																1	-0.46	-0.53	-0.56
NO_2 biofilm																	1	0.74	0.73
NH_2OH biofilm																		1	0.94
NO biofilm																			1

VI.3.3.2 FURTHER ANALYSIS OF NH_4^+ AND TEMPERATURE EFFECTS

To get a better insight into the relative effects of the NH_4^+ concentration (or NH_4^+ load) and temperature on N_2O emissions, daily predictions are plotted against the NH_4^+ load, by distinguishing values obtained at water temperatures above (red points) and below (blue points) its median value (T median = 19.6 °C).

Figure VI.3-4 presents the evolution of AUR and N_2O-EF according to the NH_4^+ load. Whatever the temperature, ammonium removal was most efficient (> 95%) at NH_4^+ loads below 0.87 kgN/m^3/d. This trend is consistent with previous studies on the performances of the Seine Aval and Seine Centre nitrifying Biostyr® units (Rocher et al., 2012). The authors reported ammonium removal close to 100% for a NH_4^+ load lower than 1.1 – 1.2 kgN/m^3/d and applied aeration between 100 and 150 Nm^3/kgNH_4-$N_{applied}$. Similarly to the present model predictions, a decrease was observed for higher NH_4^+ loads.

Based on experimental data from the Seine Aval WRRF in 2014-2015, which are characterized by lower aeration intensities (typically 78 to 92 Nm^3/kgNH_4-$N_{applied}$), a decrease of ammonium removal was observed from 0.60 – 0.65 kgN/m^3/d. The higher value at which predicted ammonium removal starts decreasing relates to the fact that the model presented a tendency to overestimate nitrification performances at low NH_4^+ loads (Chapter V).

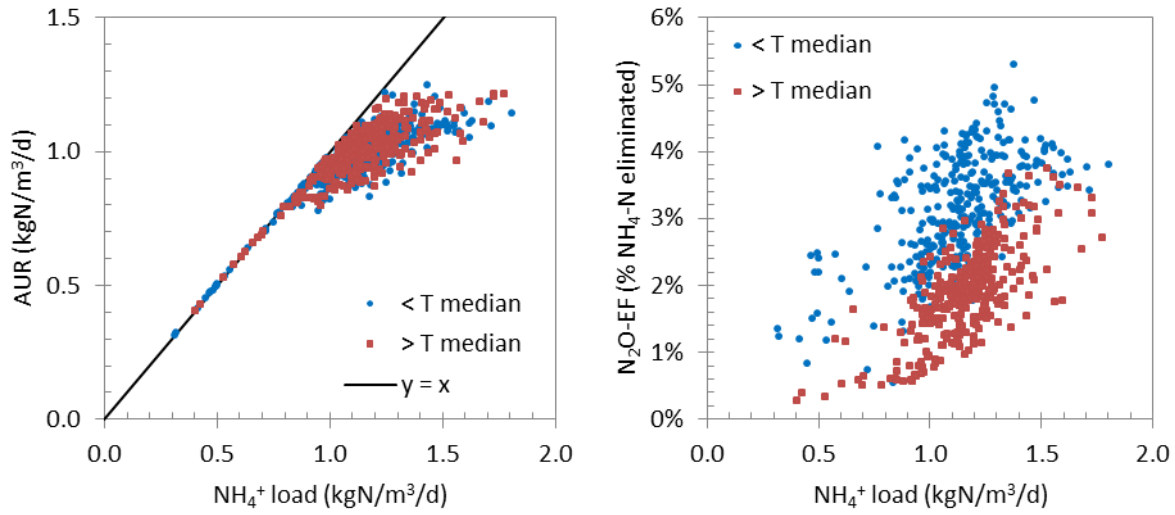

Figure VI.3-4. Evolution of the AUR and N_2O-PR predicted by the model in 2014-2015 with the applied NH_4^+ load (n = 643).

An increase of the N_2O-EF with the NH_4^+ load was observed at all temperature conditions. However, for a given NH_4^+ load, the value of the N_2O-EF was significantly higher at low temperatures compared to high temperatures. On average, the N_2O-EF was 1.9% at

temperatures > 19.6 °C, and 3.1% at T < 19.6 °C, i.e. 1.7 times as high. The threshold value of the NH_4^+ load at which ammonium removal decreased significantly was associated to the increase of the N_2O-EF. Then, the question can be asked: which production pathway was triggered by the NH_4^+ load, and how did temperature affect them? To answer these questions, the different N_2O production rates are represented against the NH_4^+ load on Figure VI.3-5.

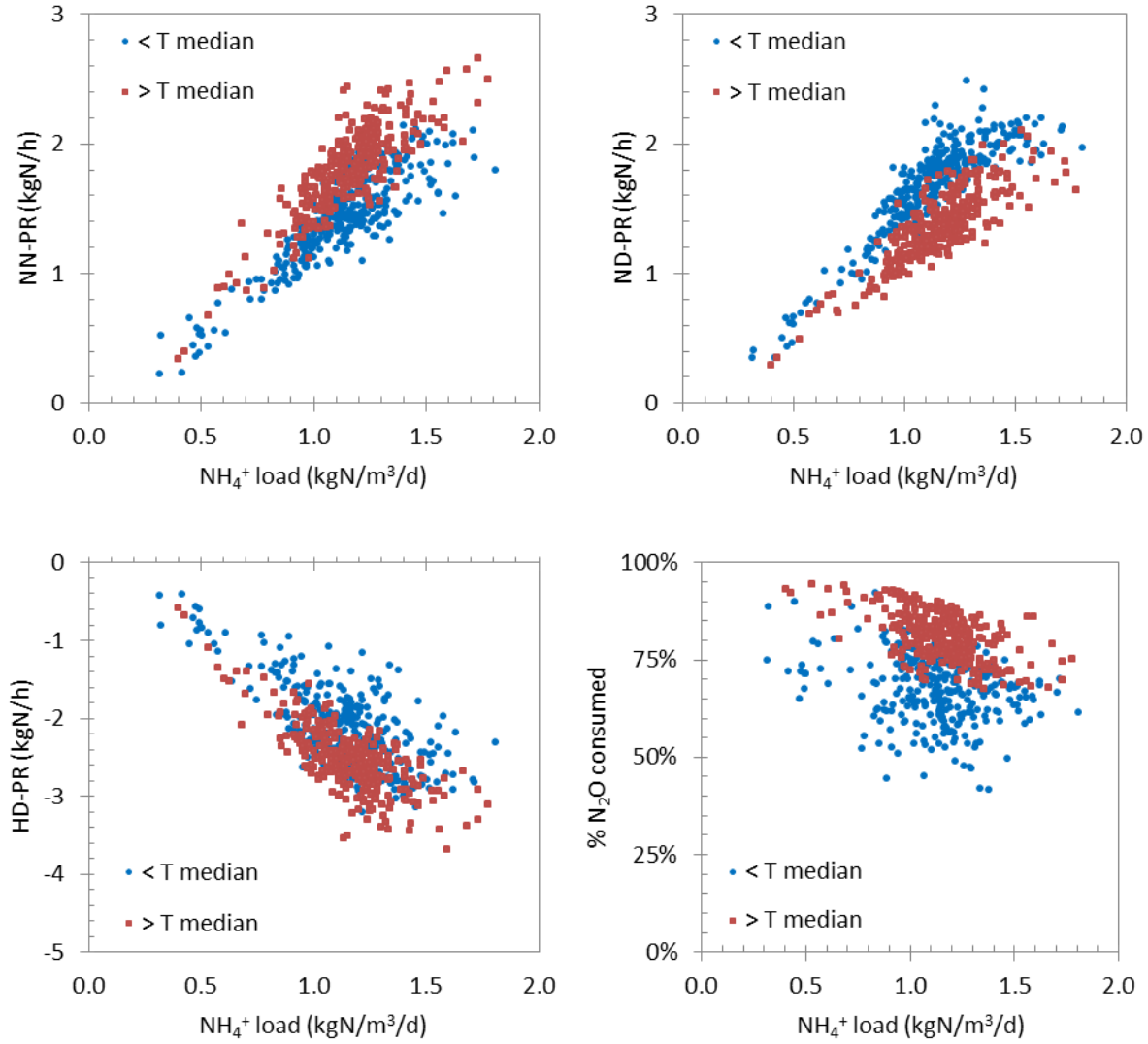

Figure VI.3-5. Evolution of N_2O production rate related to each pathway predicted by the model in 2014-2015 with the applied NH_4^+ load (n = 643).

Both NN and ND production rates increased linearly with the NH_4^+ load (R^2 ranged between 0.70 and 0.78). The consumption of N_2O by heterotrophs also increased with the NH_4^+ load. Again, a clear influence of temperature on each production rate is highlighted, and allows stating HD to be the origin of the difference in terms of net N_2O production. Indeed, the lower NN-PR observed at low temperatures was compensated by a higher ND-PR, resulting

in similar overall N_2O production rates during nitrification (3.11 and 3.16 kgN/h at low and high temperatures, respectively). On the other hand, the fraction of N_2O consumed by HD was lower at low temperature (68% on average against 81%). This confirms the results obtained for short-term data from summer and winter campaigns (Chapter V). These results differ from the CAS modelling study of Guo and Vanrolleghem (2014), who predicted higher net N_2O production rates during the warmest periods. On the one hand, temperature increased NO reduction to N_2O but HD, but also N_2O reduction to N_2, resulting in similar net N_2O production by HD. On the other hand, N_2O production by AOB only increased with temperature. In the present work, the dependency of N_2O production to temperature is related to its effect on the concentration of reaction intermediates, in particular oxygen. These are represented on Figure VI.3-6 to explain these evolutions of N_2O production rates.

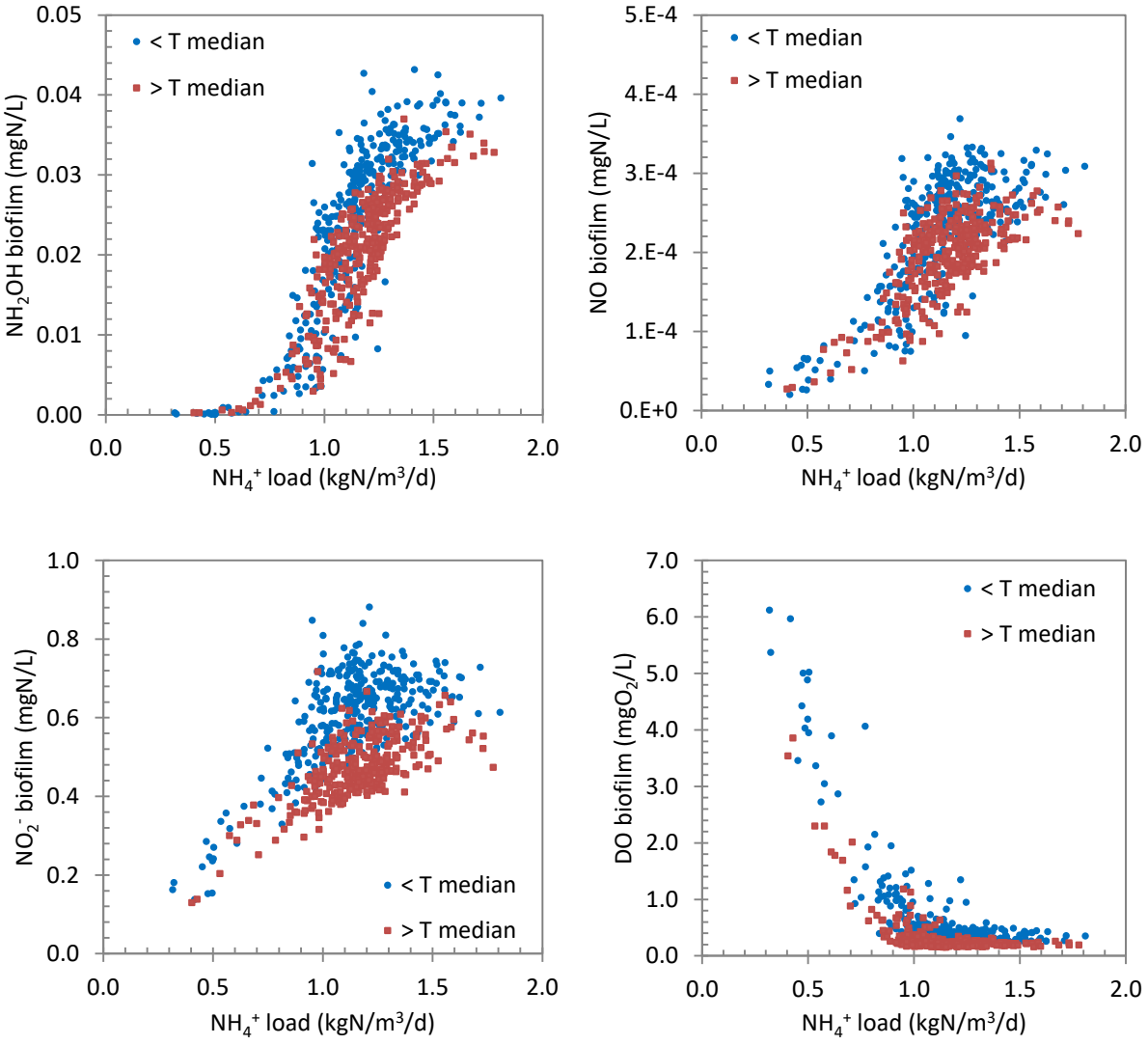

Figure VI.3-6. Evolution of average concentrations in the biofilm predicted by the model in 2014-2015 with the applied NH_4^+ load (n = 643).

A threshold effect of NH_4^+ load can be observed on the accumulation of reaction intermediates in the biofilm, especially for NH_2OH and NO, which explains a similar effect noticed on the N_2O-EF. This was explained by the decrease of the ammonium removal efficiency, i.e. incomplete nitrification, which led to the accumulation of reaction intermediates. The DO concentration in the biofilm remained low (< 2.0 mgO_2/L) at high ammonium loads (> 0.87 $kgN/m^3/d$). In fact, it was observe that a limited DO concentration in the biofilm and incomplete nitrification are associated to a significant increase of the NH_2OH concentration, NH_2OH being an obligatory intermediate for N_2O production by NN and ND. In a pure autotrophic biofilm modelling study, Sabba et al. (2015) observed that NH_2OH produced in aerobic zones of the biofilm could diffuse to anoxic zones in which NO_2^- becomes the main electron acceptor, producing high amounts of N_2O *via* ND. Although the distribution of N_2O production within the biofilm was not investigated, our results confirm that N_2O production is triggered when high NH_2OH concentrations (up to 0.04 mgN/L, while K_{NH2OH} = 0.0147 mgN/L) are associated to low DO conditions. I should be noted that the NH_2OH concentration was never measured in the biofilm.

The effect of temperature was most apparent on DO and NO_2^- concentrations, which were respectively twice as high (0.68 against 0.32 mgO_2/L) and 1.3 times as high (0.60 against 0.47 mgO_2/L) at low temperatures. Lower DO concentrations predicted at high temperatures were related to increased conversion rates and oxygen uptake rates. It was not related to gas-liquid O_2 transfer rate, which was found to vary with the NH_4^+ load (or applied air flow rate) but in the same proportion at high and low temperatures (Annex 10, Figure A27). Higher DO at winter time inhibited N_2O reduction to N_2 by HD, which explained the higher net N_2O production by HD, while NO_2^- favoured N_2O production by ND. This is consistent with results obtained on data from summer and winter campaigns (Chapter V). Likewise, higher N_2O emissions were reported in a full-scale plant operating CAS during cold periods, which were also associated to higher NO_2^- concentrations (STOWA, 2010).

VI.3.3.3 DISCUSSION ON THE TEMPERATURE EFFECT ON NO_2^- AND N_2O

In the base model (Bernier et al., 2014), the coefficient related to the influence of temperature on NOB ($\theta_{\mu NOB}$ = 1.090) and AOB ($\theta_{\mu AOB}$ = 1.078) growth were calibrated to meet the seasonal variation of effluent NO_2^- concentrations in the Seine Aval WRRF (θ_b was considered the same for AOB and NOB). Consequently, the higher the temperature, the higher the net NOB to AOB growth rate ratio is (Figure VI.3-7). As indicated in Figure VI.3-7, this ratio regulated the accumulation of NO_2^-, and thus the N_2O production by ND. This representation is, however, opposite to literature studies. Indeed, NOB are likely to be

washed-out at high temperatures, which is the basic concept of some partial nitrification processes (for example the SHARON process).

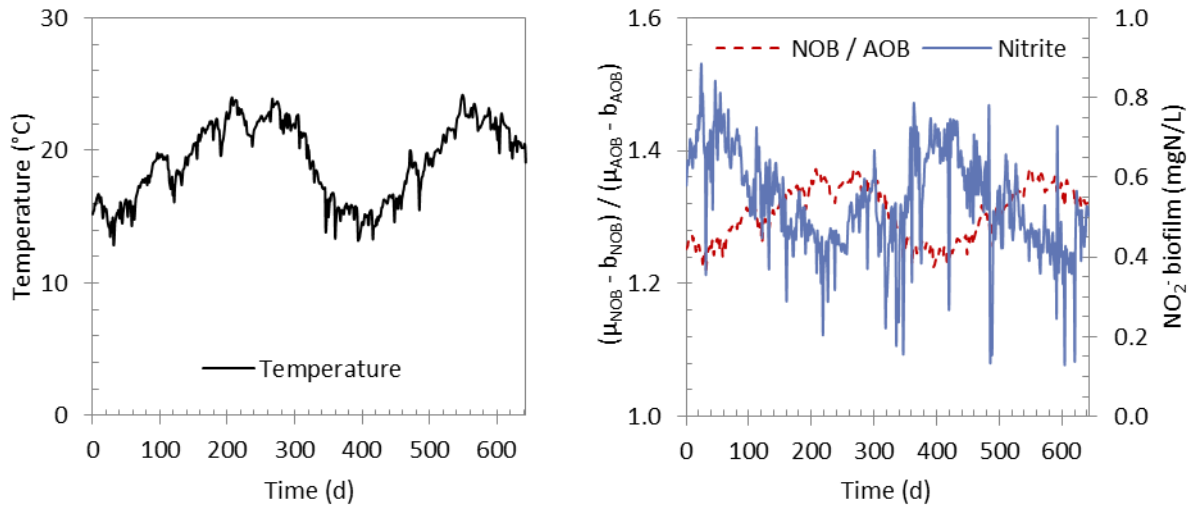

Figure VI.3-7. Evolution of influent temperature, net NOB to AOB maximum growth rate ratio and predicted NO_2^- concentration in the biofilm in 2014-2015 (n = 643).

In fact, the effect of temperature on NO_2^- accumulation and associated N_2O production is poorly documented. Bao et al. (2018) and Reino et al. (2017) investigated N_2O emissions from partial nitrification reactors in various temperature conditions (10 to 30°C). Both studies reported an increase of the N_2O-EF with increasing temperature from 10 to 20°C. However, these studies were performed on AOB-enriched cultures (80% to 90% of the biomass composed of AOB). Nitrification therefore induced direct accumulation of NO_2^- and further production of N_2O, while NO_2^- was essentially consumed by NOB in our study.

VI.3.3.4 SUMMARY AND IDENTIFICATION OF MITIGATION POSSIBILITIES

This analysis of N_2O production and emission with respect to operating conditions provided the following main conclusions:

- Whatever the influent temperature, the NH_4^+ load is the main trigger to N_2O emissions in the Seine Aval WRRF. Increasing the NH_4^+ load induces an increase of reaction intermediates (NH_2OH, NO, NO_2^-), which triggers N_2O production by AOB;
- As observed during two campaigns on the Seine Aval WRRF, for a given NH_4^+ load, N_2O emissions are much higher at low temperatures. This is mainly due to the higher residual DO concentrations in the biofilm, which inhibit N_2O reduction to N_2 by HD.

Based on these conclusions, maintaining the NH_4^+ load in the Seine Aval WRRF below 0.87 $kgN/m^3/d$ would allow efficient ammonium removal (> 95%). This would also induce lower

accumulation of reaction intermediates, and therefore lower N_2O production (maximum N_2O-EF of 1.5 to 2.3% of the NH_4-N eliminated, depending on water temperature). This is consistent with previous studies that recommended to reach complete nitrification to mitigate N_2O emissions (Kampschreur et al., 2009, Ahn et al., 2010, Desloover et al., 2012, Law et al., 2012b). Moreover, as long as aeration control is based on NH_4^+, reducing NH_4^+ load would reduce the airflow, inducing lower N_2O stripping. This is particularly interesting for nitrifying BAFs that are followed by a post-denitrification stage, as the latter can consume residual dissolved N_2O (Bollon et al., 2016a). For future BNR stages operating nitrifying BAFs, this threshold effect of NH_4^+ load could be included as a design criterion, in order to target maximum ammonium removal and minimum N_2O emissions.

For existing BAFs, strategies could be envisaged to reduce the influent NH_4^+ concentration, such as recirculating the effluent of the nitrification stage to dilute the influent. The Seine Aval WRRF is actually under redesign: a pre-denitrification BAF stage will be added, and effluent NO_3^- from the nitrifying BAFs will be recirculated at the inlet of the pre-denitrification reactors. This should have a double effect on N_2O production: influent NH_4^+ concentration will be lower and residual N_2O will enter pre-denitrification, where it may be reduced under optimum C/N conditions. A measuring campaign on nitrifying BAFs of the Seine Aval WRRF after redesign would give further information on the potential of such solutions to reduce N_2O emissions.

It should be noted that the threshold NH_4^+ load value also depends on aeration conditions and on influent characteristics. On the Seine Aval WRRF, a previous carbon removal treatment by CAS provides a fraction of OHO and soluble carbon at the inlet of tertiary nitrifying BAFs. These conditions, coupled with a low average aeration intensity (85 $Nm^3/kgNH_4\text{-}N_{applied}$), induce a large contribution of HD to the net production of N_2O, reducing 42 to 94% of the N_2O produced during nitrification (according to the present model). Exploratory simulations could be performed to assess the specific effects of influent COD concentration and fractionation as well as aeration intensity on N_2O production.

Finally, reducing N_2O emissions during winter time seems complicated as it would require lowering the aeration rate in order to favour N_2O consumption through HD, which could affect nitrification performance and further promote NO_2^- accumulation. Here again, simulations could provide insights into how to control aeration in order to balance removal performance and N_2O emissions.

VI.3.4 PROPOSAL OF A SIMPLIFIED TOOL TO PREDICT FULL-SCALE EMISSIONS

Even though the previously developed BAF model has many practical outcomes, it may not be easy-to-use for prediction of the EF. Model results were therefore used to propose a simplified model for predicting the daily N_2O-EF, based on operating parameters of the Seine Aval WRRF. A multiple linear regression model was proposed, based on the main influencing variables identified in the previous section: influent NH_4^+ concentration, airflow and influent temperature. Influent liquid flow rate and COD were not considered in this simplified statistical model, as they were highly correlated to NH_4^+ (Table VI.3-3). A linear regression based on the entire operating data (all model inputs) was also performed, to compare the respective relevance of these models. Estimates of both regressions are reported in Table VI.3-4, with statistical relevance parameters (standard error, p-value).

Table VI.3-4. Standardized estimated coefficients of the multiple linear regressions to predict N_2O-EF.

	Estimated coefficients	Standard Error	Pr (>|t|)
Complete model (R^2 = 0.85)			
NH_4.IN	0.791	0.0273	< 2E-16
Q_L	0.217	0.0265	1.43E-15
Q_G	0.145	0.0210	1.45E-11
NO_2.IN	0.092	0.0161	1.85E-08
NO_3.IN	-0.041	0.0167	1.46E-02
COD.IN	-0.046	0.0294	1.19E-01
PO_4.IN	-0.070	0.0184	1.61E-04
TSS.IN	-0.088	0.0275	1.49E-03
T	-0.541	0.0188	< 2E-16
Simplified model (R^2 = 0.81)			
NH_4.IN	0.596	0.0184	< 2E-16
Q_G	0.191	0.0181	< 2E-16
T	-0.487	0.0175	< 2E-16

Both complete and simplified statistical models were able to predict the daily average N_2O-EF based (R^2 = 0.85 and 0.81, respectively, all p-values < 0.05). Only little differences could be observed between both models, which confirmed the relevance of using only a few variables to predict the N_2O emissions from full-scale nitrifying BAFs. For practical use, the model variables were expressed in their conventional units. The associated linear regression is given in Eq.40.

Eq.40 $$N_2O - EF = 0.021 + 8.85E-4 * NH_{4,in}^{+} + 1.37E-7 * Q_G - 1.62E-3 * T$$

where N_2O-EF is the emission factor (gN_2O-N/gNH_4-N eliminated), $NH_{4,in}^{+}$ the influent NH_4^+ concentration (mgN/L), Q_G the airflow (Nm^3/d) and T the influent temperature (°C).

The simplified model was applied to the daily average functioning conditions of the nitrifying BAFs of Seine Aval WRRFs in 2014-2015, and to hourly average data measured during the summer and winter campaigns (Figure VI.3-8). The statistical model gives similar N_2O emissions to the ones predicted using the BAF model over two years. It was therefore considered as appropriate to estimate daily N_2O emissions in the operating conditions prevailing during the two-year scrutinized period. On the other hand, the statistical model allows predicting the order of magnitude of the N_2O-EF measured during the summer and winter campaigns, but failed to describe their variations at this refined timescale. Such results were expected, for two reasons: (1) the statistical model was built on daily averages, i.e. on lower variation ranges compared to those measured during the campaigns at a shorter time step, (2) such regression describes non-linear evolutions as linear ones.

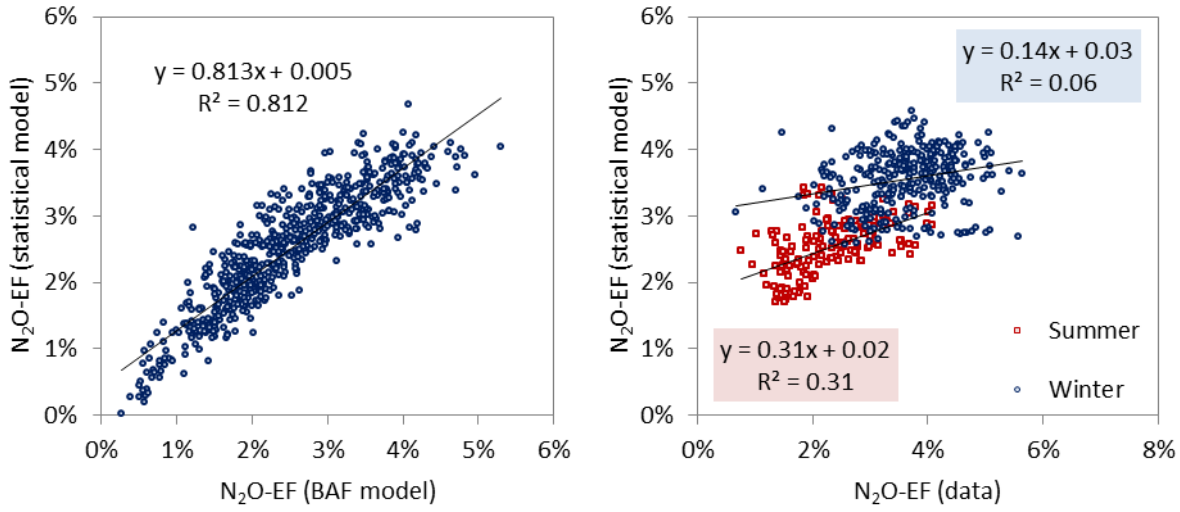

Figure VI.3-8. N_2O-EF predicted by the statistical model against BAF model predictions in 2014-2015 (daily averages) and N_2O-EF predicted by the statistical model on the summer and winter campaign.

This estimation method has its limits: its parameters are specific to the Seine Aval WRRF in the simulated operating condition ranges, and is therefore not applicable to another plant; if the operating conditions of Seine Aval nitrifying BAFs were to change significantly (higher amplitudes, addition of a pre-denitrification stage), the regression parameters may have to be re-evaluated. Nevertheless, it could be relatively simple to extrapolate the results from a complex mechanistic model to develop a simplified tool for estimating daily N_2O emissions, which remains far more appropriate than the IPCC's fixed EF. It could therefore help estimating N_2O emissions from full-scale BAFs and refining the CO_2 balance of WRRFs.

VI.4 CONCLUSION

Predictions of N_2O fluxes were calibrated on operating conditions which covered most of those observed over two years (2014-2015). The calibrated BAF model was therefore used to extrapolate N_2O predictions from the Seine Aval WRRF on this long-term period.

- The average N_2O-EF was 2.0 ± 0.7% of the applied nitrogen load, which is 56 times the value used by the IPCC. Moreover, it fluctuates over a large range: 0.2 to 4.0% of the applied nitrogen load;
- These fluctuations were mainly induced by three operating variables: influent NH_4^+ concentration (positive effect), airflow (positive effect), and influent temperature (negative effect);
- A threshold effect of the NH_4^+ load on the N_2O-EF was observed: above 0.87 $kgN/m^3/d$, ammonium removal starts decreasing, triggering an accumulation of reaction intermediates, among which N_2O. This supports the message that complete nitrification should be achieved to avoid an excessive increase of N_2O emissions;
- The negative effect of temperature on the N_2O emissions was related to its negative correlation to NO_2^- and DO concentrations within the biofilm, which impacts N_2O production by nitrifier denitrification and N_2O reduction by heterotrophs;
- A multiple linear regression based on only three variables was proposed to estimate daily N_2O-EF from the full-scale nitrifying BAF of Seine Aval. Comparison with both simulated N_2O-EF and experimentally observed values showed the high accuracy of the model on daily averages, but its limits to describe N_2O emissions measured at an hourly time step.

Chapter VII. N_2O emissions from a nitrifying BAF: a lab-scale study

RESUME

Dans les précédents chapitres, un modèle de biofiltration été calé pour représenter le fonctionnement des biofiltres nitrifiants de Seine Aval et les émissions de N_2O associées. Le modèle a montré une corrélation positive entre la charge azotée et les émissions de N_2O, et négative entre ces émissions et la température. Dans les conditions classiques de fonctionnement des biofiltres nitrifiants, le modèle suggère une contribution équivalente des deux voies de production de N_2O par les bactéries autotrophes, mais aussi une forte consommation de N_2O par les bactéries hétérotrophes.

Dans ce chapitre, les émissions de N_2O sont analysées à échelle laboratoire, l'objectif par rapport aux chapitres précédents étant d'analyser l'effet individuel des principaux paramètres opératoires sur la production de N_2O et sur la contribution des voies par analyses isotopiques. Ces résultats sont ainsi confrontés aux résultats obtenus par l'outil de modélisation développé à pleine échelle. Pour cela, des billes colonisées, collectées en sortie des biofiltres nitrifiants de la station Seine Centre, ont été introduites dans un réacteur de petite taille. Les conditions d'alimentation ont été simplifiées par rapport aux conditions réelles pour se placer dans des conditions nitrifiantes : alimentation synthétique ne contenant ni carbone exogène ni bactéries hétérotrophes. Les performances ont été mesurées pour différentes charges en ammonium, différentes fraction d'oxygène dans le gaz insufflé, et différentes températures de l'influent. Ces expériences ont mis en évidence un effet dominant et positif de la charge en ammonium sur les performances de nitrification et les émissions de N_2O, ce qui corrobore les résultats obtenus à pleine échelle. A petite échelle, une hausse du facteur d'émission a été mesurée avec la température. Cependant, la baisse parallèle de la concentration en oxygène suppose un effet combiné de la température et de l'oxygène sur l'activité des bactéries oxydant l'ammonium et les nitrites. Enfin, les analyses isotopiques ont montré une forte contribution de la voie de réduction des nitrites à la production de N_2O, de provenance autotrophe et/ou hétérotrophe. L'activité dénitrifiante mesurée par l'évolution des nitrates produits conforte les résultats obtenus à pleine échelle, qui suggèrent un rôle important des hétérotrophes à la réduction du N_2O produit pendant la nitrification, malgré un faible taux de dénitrification. Ces résultats, complémentaires aux travaux de modélisation, demandent à être confirmés par des études futures et par des simulations de ces expériences à petite échelle pour déterminer plus précisément les contributions respectives des voies de production.

Mots-clés : biofilm, laboratoire, nitrification, N_2O, oxygène, température

ABSTRACT

In previous chapters, a model was calibrated to represent the functioning of tertiary nitrifying BAFs of the Seine Aval WRRF and the associated N_2O emissions. The model demonstrated a positive correlation between the nitrogen load and N_2O emissions and a negative correlation between these emissions and the influent temperature. Under conventional operating conditions of the Seine Aval WRRF, the model suggested a similar contribution of the two biological N_2O production pathways by autotrophic bacteria, but also a high N_2O consumption by heterotrophic denitrifiers.

In this chapter, N_2O emissions are analysed at laboratory scale, the objective –compared to previous chapters– being to characterize the individual effects of the main operating conditions on N_2O emissions and the contributions of N_2O production pathways *via* isotopic analyses. The results are then confronted to modelling results on full-scale data. To this end, colonized media beads, sampled at the outlet of the Seine Centre nitrifying Biostyr® units were introduced in a lab-scale reactor. Influent conditions were simplified compared to full-scale ones, to remain in nitrifying conditions: synthetic water without exogenous carbon or heterotrophic bacteria supply. The reactor performance was evaluated for different ammonium load conditions, different fractions of oxygen in the supplied gas and different influent temperatures. These experiments highlighted a dominant and positive effect of the ammonium load on nitrification performance and N_2O emission, which corroborates the full-scale results. At lab-scale, an increase of the N_2O emission factor was measured with increasing temperature. However, a parallel decrease of the DO concentration suggested a combined effect of temperature and DO on ammonium and nitrite oxidizing bacteria. Finally, isotopic analyses revealed a high contribution of nitrite reduction to N_2O production, from autotrophic and/or heterotrophic origin. The heterotrophic activity, identified by the evolution of nitrate production, supports the full-scale results, which suggested an essential role of heterotrophic denitrification to the reduction of N_2O produced during nitrification. These results, which are complementary to the full-scale modelling findings, should be confirmed by future work, and by simulations of the laboratory reactor, to refine the contributions of N_2O production pathways.

Keywords: biofilm, lab-scale, nitrification, N_2O, oxygen, temperature

VII.1 INTRODUCTION

Modelling full-scale nitrifying biological active filters (BAFs) of the Seine Aval wastewater resource recovery facility (WRRF) highlighted the main influence of three operating conditions on nitrous oxide (N_2O) emissions: ammonium (NH_4^+) load, airflow and water temperature. The model suggested a similar contribution of nitrifier nitrification (NN) and nitrifier denitrification (ND) to N_2O production by ammonia oxidizing bacteria (AOB) and a high consumption of N_2O by heterotrophic denitrification (HD).

Assessing the effect of a single operating condition on N_2O emissions based on full-scale monitoring data only is delicate, since some conditions vary concomitantly. This is the case of the airflow and NH_4^+ load in the Seine Aval nitrifying BAFs as the airflow is controlled by the NH_4^+ load to maintain sufficient oxygen supply for nitrification. Seasonal fluctuations of the biofilm composition, in relation to water temperature changes, were found to significantly affect the magnitude of N_2O emissions. Finally, uncertainties remain regarding the identification of kinetic parameters related to N_2O, since nitrification and HD share many reaction intermediates (Schreiber et al., 2012). The calibration of N_2O parameters was based on the data of two measuring campaigns performed at low and high temperatures. As the model predicted higher dissolved oxygen (DO) and nitrite (NO_2^-) concentrations in the biofilm at low temperatures, N_2O production was calibrated by modifying the effect of DO on ND, to reduce N_2O production at high temperature / low DO. In fact, such calibration choices may condition the prediction of N_2O production pathway contributions (Domingo-Felez et al., 2017) and call for further information on their actual contribution in nitrifying BAFs. Isotopic analysis, such as site-preference measurement, can be used to quantify the production of N_2O by biological pathways, and get an insight into the “black boxes” that BNR processes are (Duan et al., 2017).

Lab-scale experiments were performed on colonized media beads from Seine Centre nitrifying BAFs (the Seine Aval WRRF was in redesign). The objective was to evaluate the impact of operating conditions (NH_4^+ load, aeration and temperature) on nitrogen removal, N_2O emissions and respective contributions of the N_2O pathways, as individually as possible. Experimental constraints linked to air distribution led to a counter-current operation of the reactor, which is different from full-scale conditions in the Seine Centre and Seine Aval nitrifying Biostyr® reactors that are co-current. Heterotrophic activity was limited by feeding the reactor with a synthetic ammonium solution, with no addition of organic carbon. Results related to operating condition effects on nitrogen removal and N_2O emissions will be presented, and discussed with modelling results. Isotopic analyses were performed by iEES-Paris and Ecobio, and will therefore not be presented in detail (upcoming publication).

VII.2 MATERIAL AND METHODS

VII.2.1 OPERATING CONDITIONS BEFORE MEDIA SAMPLING

The colonized media (clean diameter 3 mm) used in this work was sampled from the nitrification stage of the Seine Centre WRRF (France, 240 000 m^3/d). As described in Chapter III, the scheme of the Seine Centre WRRF is similar to the Seine Aval WRRF, except that carbon removal is not performed by a conventional activated sludge (CAS) system but in BAF units. Consequently, the effluent entering the nitrification stage of the Seine Centre WRRF was less concentrated in terms of suspended solids (9 ± 4 mg/L) in comparison to the Seine Aval WRRF (39 ± 16 mg/L in 2014-2015). Tertiary nitrifying BAFs of the Seine Centre WRRF are designed to treat 0.7 $kgN/m^3/d$ and have a unitary section 111 m^2 and a filter bed height of 3 m.

Sample collection was performed on January 29th 2018 in the water tarp of the nitrification stage, where backwash water is collected. Unfortunately, the plant stopped functioning three days before sampling (for more details see Section III.3.1). Prior to media sampling and filter stop (from January 1st to 25th 2018), the daily average operating conditions were the following: influent NH_4^+ concentration 13.0 ± 4.3 mgN/L, applied NH_4^+ load 0.37 ± 0.11 $kgN/m^3/d$, NH_4^+ removal 99 ± 1%, aeration intensity 212 ± 96 $Nm^3/kgNH_4\text{-}N_{applied}$ and influent water temperature 14.9 ± 0.8 °C. The colonized media was introduced in the reactor, supplied in tap water and air, on January 30th 2018, i.e. the day following its sampling. The feeding solution was supplied starting from February 1st.

VII.2.2 REACTOR SET-UP

The reactor was filled with colonized media, retained by a metal grid. Its working volume was 11.4 L, composed of a 9.4 L media bed (colonized media + interstitial water) and a 1.4 L water lamina on top of the metal grid, where DO, pH and temperature sensors were located. It was operated in continuous down-flow counter-current mode during the eight weeks of experiments. For 12 days before the beginning of the experiments, the reactor was fed by an ammonium-rich solution and operated in a recirculation mode (i.e. the effluent was reinjected into the feeding tank).

Mass flow meters maintained the gas flow rate (compressed air / N_2 mix) at 0.5 L/min. A peristaltic pump fed the synthetic solution from a feeding tank into the reactor at 0.2 L/min (regularly checked), to maintain the hydraulic retention time (HRT) in the active zone at 20.1 ± 0.5 min, which is close to the estimated value in the Seine Centre nitrifying BAFs (19 min, considering a theoretical bed porosity of 0.34). Except for experiments dedicated to study

the temperature effect, the temperature in the reactor was maintained at 19.5 ± 0.4 °C using a cryogenic regulator and a water jacket. The synthetic solution was made of ammonium chloride (NH_4Cl) as substrate, monobasic potassium phosphate (KH_2PO_4) as phosphorus source for bacterial growth (5 mg PO_4^-/L), and sodium bicarbonate ($NaHCO_3$) as pH buffer and inorganic carbon source (2.5 mol HCO_3^-/mol N) in tap water dechlorinated overnight.

VII.2.3 OPERATING CONDITIONS TESTED

The effect of three main operating conditions was tested in a series of experiments: NH_4^+ load, oxygenation and temperature. Each condition was tested in two series of experiments. To avoid modifying the reactor hydraulics, the NH_4^+ load effect was tested by modifying the influent NH_4^+ concentration only, and the oxygenation was tested by modifying the fraction of oxygen in the influent gas. Temperature was modified by adjusting the temperature of the solution in the feeding tank and was maintained stable in the reactor using the cryogenic regulator and the water jacket. On average, pH was 7.8 ± 0.3 over the 21 experiments. Those were all conducted for more than one HRT, in order to reach a steady-state functioning. The timeline of the experiments is given on Figure VII.2-1, with experimental conditions in Table VII.2-1. Experiments were performed by three partners of the N_2OTrack project: Longqi LANG (INSA of Toulouse), Guillaume HUMBERT (iEES-Paris/Ecobio) and my-self. I more specifically designed the experimental plan, performed the first NH_4^+ experiments, and performed all data treatment and results analyses.

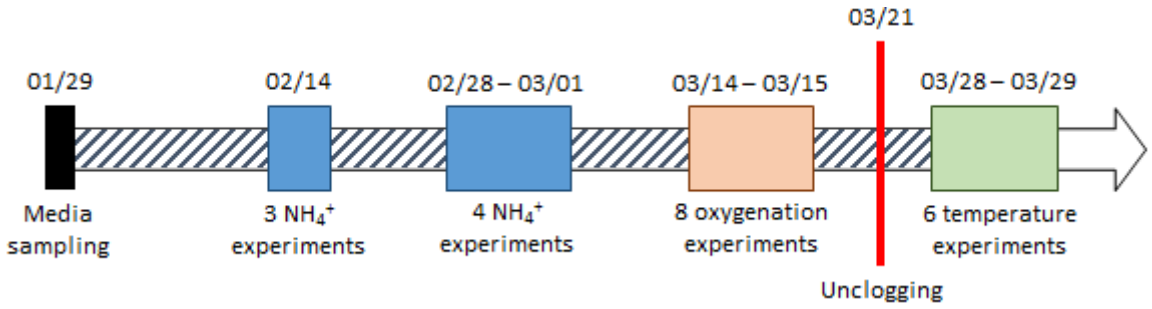

Figure VII.2-1. Timeline of lab-scale experiments.

- Seven NH_4^+ load tests were performed: three by increasing the NH_4^+ concentration in the influent over one day (6.2, 28.6 and 62.1 mgN/L, February 14th), and four by decreasing it over two days (56.1, 42.9, 42.7 and 20.2 mgN/L, February 28th and March 1st);
- Eight oxygenation tests were performed by mixing compressed air and pure nitrogen gas to reach 0 (pure N_2) to 100% air (i.e. 21% O_2) in the gas mix. Five air fractions were tested over a single day (100%, 0%, 20%, 50% and 80%, March 14th), which resulted in short experiments; three oxygenation levels were tested the day after (20%, 50% and 80%, March 15th);

- At this point, a clogging of the media bed was visually observed. The reactor was therefore emptied and the media bed cleaned on March 21st. From March 21st to 27th, the reactor was fed with various NH_4^+ loads in order to verify that nitrification was recovered; Recovery tests were performed either at higher Q_G or lower Q_L (not shown) and can therefore not be interpreted. The temperature test at 18.2 °C and 20.1 mgN/L in the influent showed moderately lower NH_4^+ removal than the NH_4^+ load test at 19.6 °C and 20.2 mgN/L in the influent, at similar DO and pH in the top water zone: 36 against 43 % of the applied load. It was therefore assumed that nitrifying activity was recovered;
- Six temperature tests were finally conducted by decreasing the temperature over two days (20.3, 16.4 and 15.5 °C on March 28th and 22.3, 18.2 and 13.4 °C on March 29th).

Table VII.2-1. Operating condition ranges during the 21 experiments.

Experiments	$[NH_4^+]$ in mgN/L	NH_4^+ load kgN/m^3/d	Q_G L/min	Aeration Nm^3/kgN	Air fraction %	Temperature °C
NH_4^+ load (7)	6.2 – 62.1	0.17 – 1.63	0.50	44 – 420	100	19.4 ± 0.3
Oxygenation (8)	24.7 ± 0.7	0.66 ± 0.02	0.51 ± 0.05	0 – 119	0 – 100	19.6 ± 0.4
Temperature (6)	20.5 ± 0.3	0.57 ± 0.01	0.50	128 ± 3	100	13.4 – 22.3

VII.2.4 REACTOR MONITORING

On-line sensors were present in the top water zone of the reactor to measure the pH (H8481 HD, SI Analytics), DO concentration and temperature (VisifermTM, Hamilton). The off-gas N_2O concentration was continuously analysed (X-STREAM X2GP, Emerson) with a temporal resolution ranging from 10 sec to 1 min. Minute averages were used for data analysis. For each condition tested, the synthetic solution was characterized in 1 to 5 samples collected directly in the feeding tank and the effluent (immediate outlet of the reactor) from 1 to 14 samples. Liquid samples were immediately filtered through a 0.2 µm syringe filter (polyamide) and stored at 4 °C until their analysis within five days. Ammonium was analysed photometrically according to the Nessler method (AFNOR NFT 90-015). Nitrite and nitrate were determined by ion chromatography (DIONEX) during NH_4^+ load experiments and by spectrophotometry during aeration and temperature experiments (Smartchem 200, AMS).

Gas samples were taken to determine N_2O isotopic signatures by outlet gas pipe derivation into a sealed glass vial of 20 mL. The vial was first flushed with the sampling gas for > 45 sec prior to 1 to 5 min sampling. Gas samples were then stored in the dark at room temperature until analysis. Analysis and interpretation of nitrogen and oxygen isotope ratios were performed by N_2OTrack project partners (iEES-Paris and ECOBIO Rennes).

VII.3 RESULTS

VII.3.1 REACTOR PERFORMANCE

On Figure VII.3-1, ammonium uptake rates (AUR) calculated over the 21 lab-scale experiments are plotted against the applied NH_4^+ loads. Ammonium removal was on average 32 ± 11% of the applied load and did not exceed 81% at the lowest applied NH_4^+ load. Similarly to full-scale observations (discussed in section VII.4.1), a decrease of NH_4^+ removal percentage was observed with increasing applied NH_4^+ loads. This was expected since the NH_4^+ loads were increased without modifying the airflow rates, resulting in decreasing aeration intensities (in $Nm^3/kgNH_4\text{-}N_{applied}$). During oxygenation tests, the total gas flow rate remained the one used during all experiments (0.50 L/min except for one point discussed thereafter), while the air fraction varied from 0 to 100%. Consequently, oxygen transfer rates were always lower than those applied during NH_4^+ and temperature experiments, which explains the low NH_4^+ removal efficiencies. On the other hand, the NH_4^+ removal measured during the temperature tests remained consistent with those observed during the NH_4^+ loading tests.

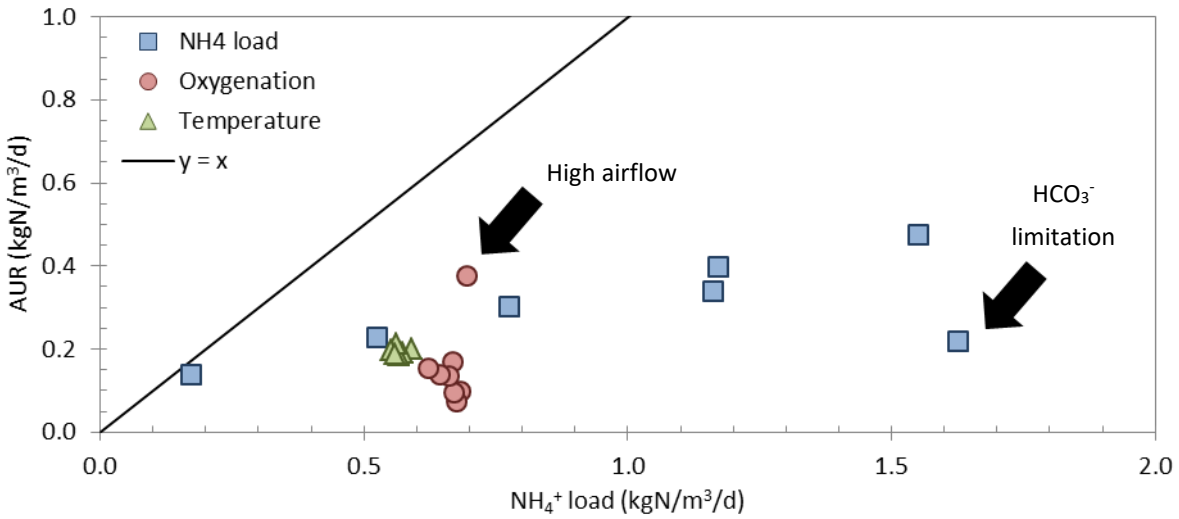

Figure VII.3-1. Removed against applied ammonium load during lab-scale.

Remark on two points

The low AUR measured at the highest applied NH_4^+ load was explained by an inorganic carbon limitation (addition of $NaHCO_3$ forgotten). No stabilization of N_2O emissions could be observed during this experiment (Annex 11). It was therefore not considered in the following discussions. For the other experiments, the HCO_3^-/N ratio remained at 2.5 $gHCO_3^-/gN$, which is above the ratio measured on the Seine Centre BAFs during campaigns performed by Irstea

(1.7 $gHCO_3^-$/gN, not published). The high ammonium removal observed during one oxygenation test was due to a higher gas flow rate (0.57 against 0.50 L/min), at 100% of air in the gas mix, which induced a higher oxygen supply compared to the other experiments. Nevertheless, this experiment was kept in the following discussions, because of its interesting effect on N_2O emissions.

VII.3.2 EFFECT OF APPLIED CONDITIONS ON NITRIFICATION AND N_2O EMISSIONS

VII.3.2.1 GLOBAL OVERVIEW

Figure VII.3-2 displays the effects of the applied NH_4^+ load, air fraction in the gas mix and temperature on the AUR, N_2O emission rate (ER) and emission factor (EF). For each condition tested, important fluctuations of the N_2O-EF could be observed with or without a significant evolution of the AUR.

The main variations of the AUR were related to the NH_4^+ load (0.14 to 0.48 kgN/m^3/d against 0.07 to 0.38 and 0.19 to 0.21 kgN/m^3/d during oxygenation and temperature tests, respectively). It was also associated to the highest variations of the N_2O-ER (8.7 10^{-5} to 4.8 10^{-3} mgN/min, against 3.4 10^{-4} to 1.4 10^{-3} and 8.5 10^{-4} to 2.4 10^{-3} mgN/min). The AUR did not vary significantly during the temperature tests; it remained close to the AUR measured during the NH_4^+ test performed at a similar applied NH_4^+ load (0.23 kgN/m^3/d eliminated at 0.52 kgN/m^3/d applied) confirming that nitrification activity was maintained during this period. Despite these low AUR variations, the N_2O-ER varied significantly, reaching half of the maximum value obtained during NH_4^+ tests. Consequently, the maximum N_2O-EF was in the same order of magnitude (0.16 against 0.15% during NH_4^+ experiments). Its minimum value was, however, higher compared to other tests: 0.07 against 0.01 and 0.04%). Similarly, the N_2O-EF was in the same order of magnitude during oxygenation experiments, owing to significant variations of the N_2O-ER and low variations of the AUR.

The specific effect of each condition on N_2O emissions and the possible N_2O production pathways will be discussed in the next section. To support the discussion, the results of the isotopic analyses (not presented since they have not been published yet) were as follows:

- A major contribution of NO_2^- reduction to N_2O (either by nitrifiers or denitrifiers) was identified during all experiments;
- An increase of the NN pathway contribution to N_2O production with increased NH_4^+ load was observed;
- The evolution of the NN and NO_2^- reduction contribution (by HD and/or ND) during oxygenation and temperature tests were not clearly identified.

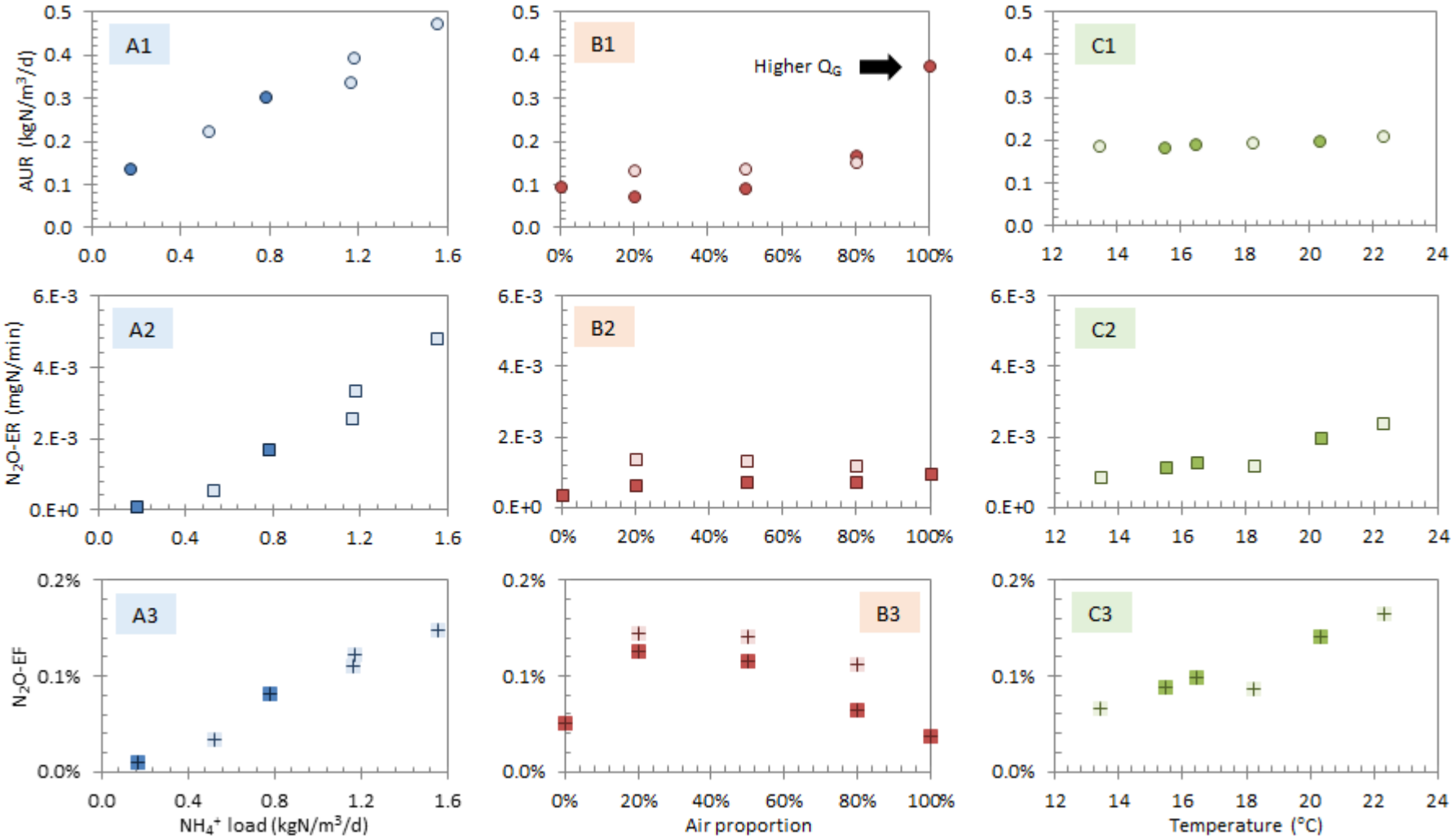

Figure VII.3-2. AUR (A1, B1 and C1), N_2O-ER (A2, B2 and C2) and N_2O-EF (A3, B3 and C3) against NH_4^+ load (A1-3), air proportion (B1-3), and temperature (C1-3). Dark and light colors corresponded to the first and second series of experiments for each parameter tested.

VII.3.2.2 EFFECT OF THE NH_4^+ LOAD

A dominant and positive effect of the NH_4^+ load was observed on the AUR, N_2O-ER and EF, which all increased with the applied load (Figure VII.3-2, panels A1 to A3). A ten-time increase in the applied NH_4^+ load (0.17 to 1.55 $kgN/m^3/d$) induced increases by a factor 3 (from 0.14 to 0.48 $kgN/m^3/d$) and 55 (from 8.7 10^{-5} to 4.8 10^{-3} mgN/min) of the AUR and N_2O-ER, respectively. The N_2O-EF thus increased from 0.01 to 0.15% of the eliminated NH_4^+ load.

The evolution of the N_2O-ER could not be related to the effluent NO_2^- concentration, as the latter did not present any clear correlation with the NH_4^+ load (Figure VII.3-3, left panel). On the other hand, the ratio between produced NOx (NO_2^- + NO_3^-) and AUR increased with NH_4^+ load (Figure VII.3-3, right panel). This suggests that the percentage of NO_3^- reduced by HD decreased, i.e. that the denitrifiers activity decreased compared to the nitrifier one.

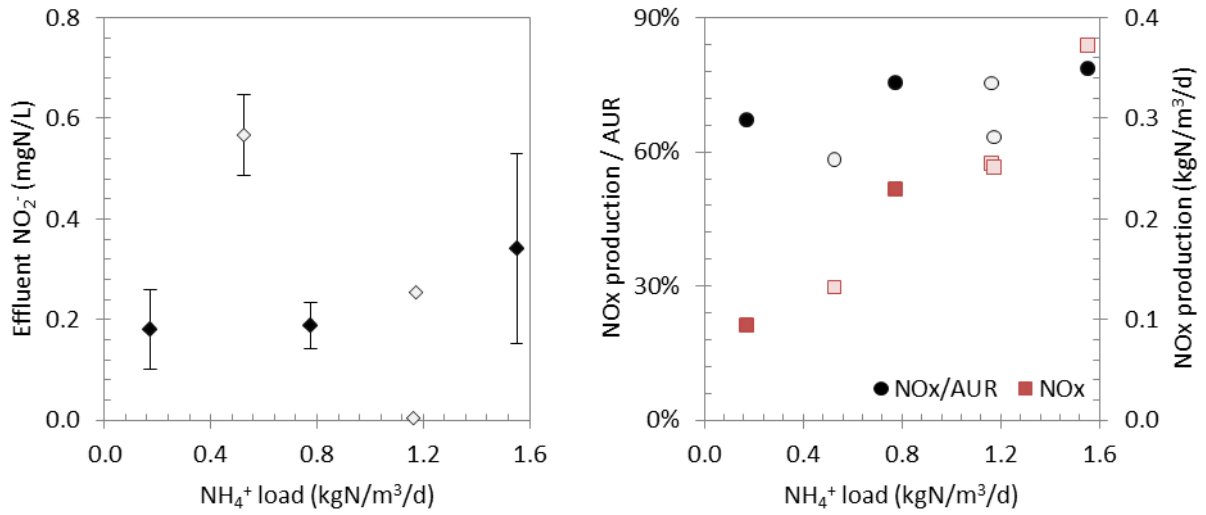

Figure VII.3-3. Evolution of the effluent NO_2^- concentration (left) and NOx production to AUR ratio (right) with NH_4^+ load. Black bars correspond to standard deviations of concentrations measured for a single experiment. Dark and light colours corresponded to the first and second series of experiments.

VII.3.2.3 EFFECT OF OXYGENATION

The AUR increased from 0.07 to 0.17 $kgN/m^3/d$ for oxygenation ranging between 0 and 80% air fractions. It was not zero at 0%, because oxygen was also supplied with the influent (saturation concentration estimated to 9.2 mgO_2/L at 19.2 °C), which maintained a low nitrification activity. Moreover, the test at 0% was performed directly after the one at 100%; residual DO may thus have been present in the biofilm (not measured). A strong increase in the AUR was observed between 80 and 100% (0.17 to 0.38 $kgN/m^3/d$), but this also

corresponded to an increase of the gas flow rate. In fact, the test at 100% of air was performed at significantly higher oxygen transfer rate compared to the others. In contrast to the NH_4^+ load experiment, the evolutions of N_2O-ER and N_2O-EF were not linear. The N_2O-ER increased from 0 to 20% of air in the gas mix, and remained quite stable from 20 to 100%. Consequently, the N_2O-EF first increased (0.05 to 0.14%) and then decreased with the air fraction (0.14 to 0.04%).

When the two series of experiments are analysed separately, an effect of the air fraction on N_2O emissions and effluent NO_2^- concentration appears (Figure VII.3-4). During the first series, a decrease of effluent NO_2^- concentrations was observed, from 0.33 to 0.11 mgN/L. On the other hand, an increase from 0.17 to 0.35 mgN/L was observed in the second series. Surprisingly, they corresponded to a small increase and decrease of the N_2O-ER during the first and second series of experiments, respectively (N_2O-ER zoomed on the right panel).

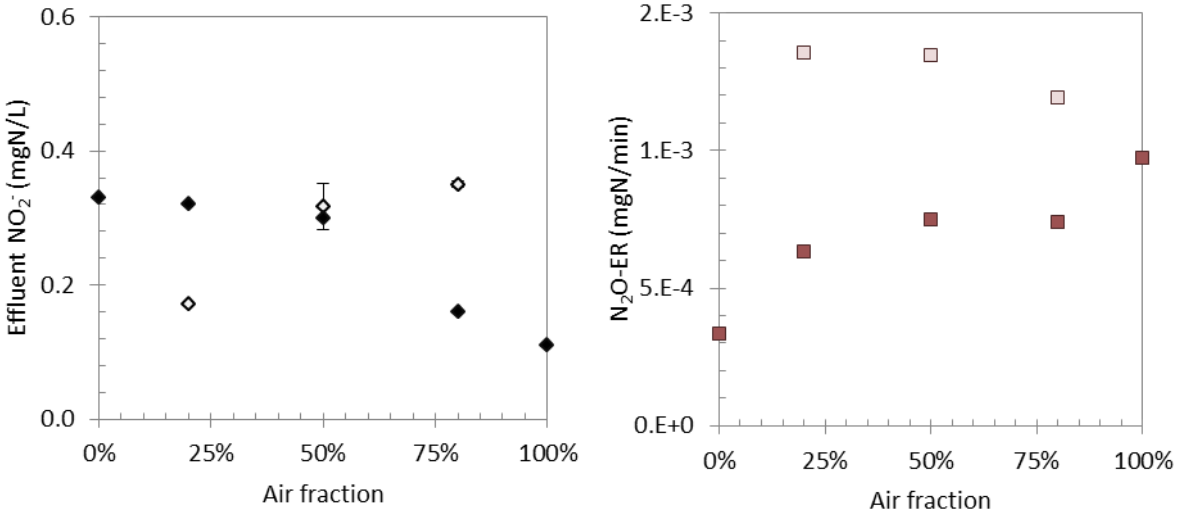

Figure VII.3-4. Evolution of effluent NO_2^- concentration (left) and N_2O-ER (right) with the air fraction in the gas mix. Dark and light colors correspond to the first and second series of experiments.

The evolution of the NOx production from both series of experiments is presented on Figure VII.3-5. NOx production increased with the air fraction, which is consistent with the evolution of AUR. Except for the value at 100% of air, the NOx production to AUR ratio increased with air fraction, which indicates a decrease of the denitrifiers' activity compared to the nitrifiers' activity. The extremely low ratio at 0% of air (29%) indicates that in those low-DO conditions, most of the NO_3^- production by nitrification was reduced by denitrification. However, the low ratio at 100% could not be explained and is attributed to a measurement error of the NO_3^- concentration.

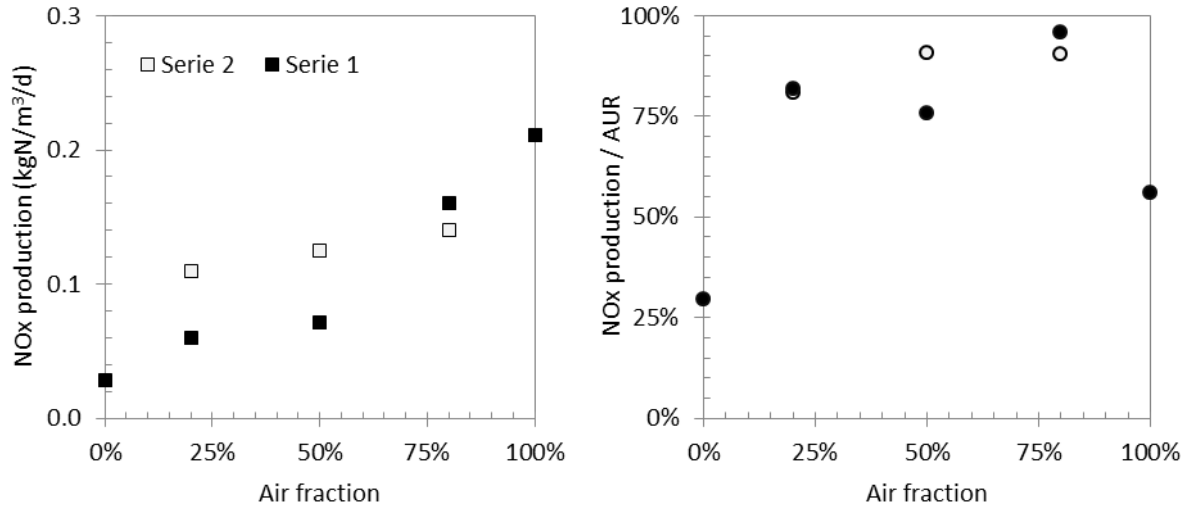

Figure VII.3-5. Evolution of the NOx production to AUR ratio with the air fraction. Dark and light colors correspond to the first and second series of experiments.

The specific effect of the air supply was compared to results from experiments of the NH_4^+ load performed under close influent NH_4^+ concentrations. To this end, the AUR and N_2O-EF were plotted against the aeration intensity (air fraction in the supplied gas x Q_G / NH_4^+ load) on Figure VII.3-6.

Oxygenation tests were performed at 23.8 and 25.1 mgN/L in the influent, which is close to the conditions during the two NH_4^+ tests (20.2 and 28.6 mgN/L, average 24.4 mgN/L). Results from these tests were therefore averaged, and added on Figure VII.3-6. The average value from the NH_4^+ load experiments fitted well within the evolution observed between AUR and aeration intensity during oxygenation experiments. This was also observed on the evolution of N_2O-EF.

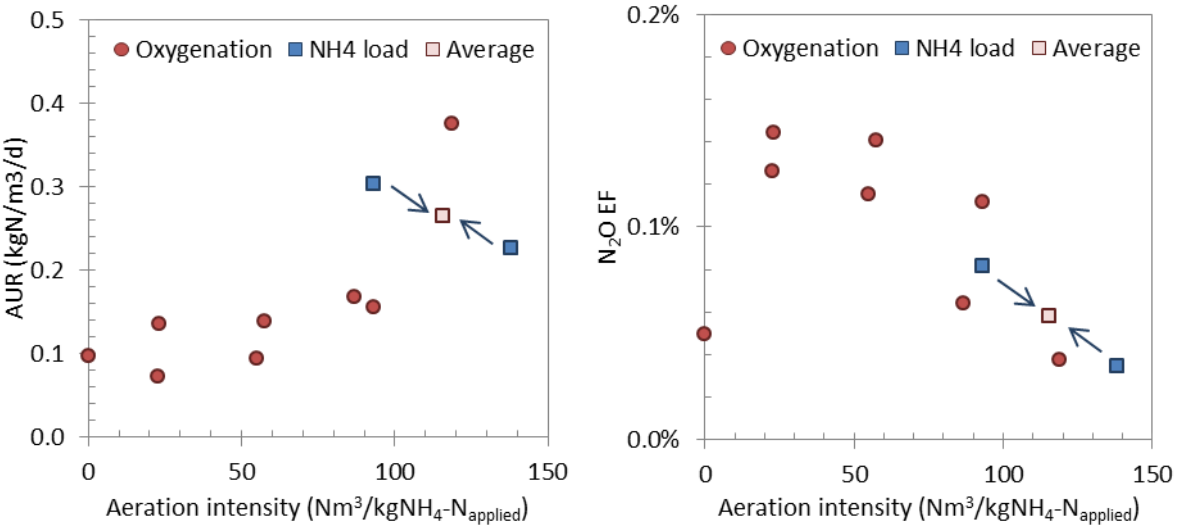

Figure VII.3-6. Evolution of the AUR and N_2O-EF with aeration intensity.

These results indicate that the lower NH_4^+ removal observed during oxygenation tests were only due to the lower oxygen supplied and not to a decrease of nitrifiers activity over the weeks.

VII.3.2.4 EFFECT OF THE INFLUENT TEMPERATURE

A small and linear increase of the AUR, from 0.19 to 0.21 kgN/m^3/d, was observed with increasing temperature from 13.4 to 22.3 °C (R^2 = 0.91). An associated increase of N_2O-ER was observed, which induced a significant increase of the N_2O-EF, from 0.07 to 0.16% of the NH_4-N eliminated.

The evolutions of the effluent NO_2^- concentration, DO concentration in the top water zone and NOx production with temperature are presented on Figure VII.3-7. A linear increase of the effluent NO_2^- concentration was observed with influent temperature. The increase of N_2O emissions was highly correlated to that of the effluent NO_2^- concentration (R^2 = 0.95), although these remained low (< 0.2 mgN/L). The DO concentration in the top water zone decreased with increasing temperature, which was due to the lower saturation concentration at high temperature. The differences in terms of DO levels between the two series could not be explained. All conditions were similar: the gas flow rate (0.50 L/min), the air fraction (100%) and the AUR (0.19 ± 0.01 and 0.20 ± 0.01 kgN/m^3/d). It was thus suspected to be due to different DO concentrations in the feeding tank, which was not explained or verified. This decrease of DO concentrations could explain the increase in NO_2^- concentrations. Finally, no effect of temperature could be observed on the NOx production to AUR ratio.

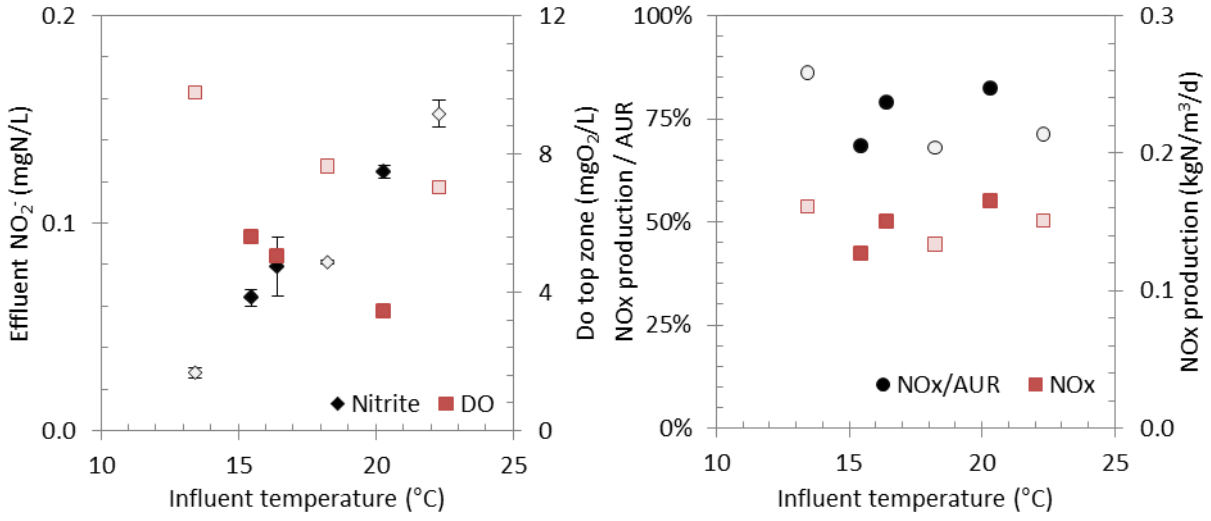

Figure VII.3-7. Evolution of effluent NO_2^- concentration and DO concentration in the top water zone (left) and NOx production to AUR ratio (right) with influent water temperature. Dark and light colors correspond to the first and second series of experiments.

VII.4 DISCUSSION

VII.4.1 LOW NITRIFICATION PERFORMANCES AND ASSOCIATED N_2O EMISSIONS

Due to the conditions applied in this study, the nitrification performance was low compared to those measured in the Seine Centre and Seine Aval nitrifying BAFs, which exhibited lower N_2O emissions. These results are discussed hereafter.

On Figure VII.4-1, the calculated AUR is plotted against the applied NH_4^+ load based on average data of the Seine Centre and Seine Aval Biostyr® units and measured in this study. The applied NH_4^+ load was lower in the Seine Centre than the Seine Aval BAFs (0.44 ± 0.18 against 1.14 ± 0.21 kgN/m^3/d on average). The ammonium removal was consequently higher (97 ± 8% against 86 ± 6% of the applied load on average). In this study, the ammonium removal was only 32 ± 11%, while the applied load varied in the same range as the full-scale conditions. Beyond the fact that the reactor was functioning in counter-current mode and full-scale Biostyr units run in co-current mode, which was expected to result in different concentration gradients within the filter bed, these differences were attributed to the NH_4^+ load and aeration conditions.

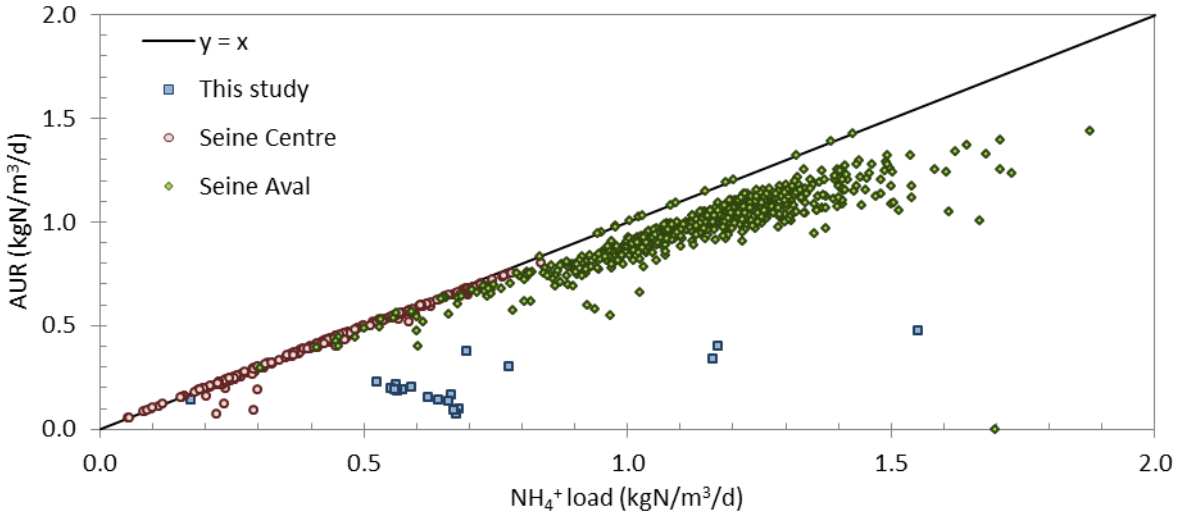

Figure VII.4-1. Removed against applied ammonium load during lab-scale experiments and monitored in the Seine Centre (2017-2018) and Seine Aval (2014-2015) nitrifying BAFs.

The average applied load chosen for the experiments was based on the design of the Seine Centre nitrifying BAFs (0.7 kgN/m^3/d). However, they were operated at significantly lower loads and these were, moreover, decreasing since November 2017, reaching 0.21 kgN/m^3/d before sampling. Since the nitrification rate depends on the received ammonia load, the mass of nitrifying bacteria stabilized in nitrifying Biostyr® must have been low at the period

of sampling. It can therefore be supposed that the nitrifying activity in the lab-scale reactor was low due to an insufficient concentration of nitrifying bacteria. This would explain the high NH_4^+ removal efficiency at the lowest applied NH_4^+ load (81% at 0.17 kgN/m^3/d applied), which was close to full-scale conditions (100% at 0.21 kgN/m^3/d applied) and its drop at higher applied loads.

Another reason for this low performance is the aeration conditions. First, the aeration intensity applied in this study (0 – 138 $Nm^3/kgNH_4\text{-}N_{applied}$ excluding the lowest NH_4^+ load) was always lower than those applied on Seine Centre nitrifying BAF before sampling (212 ± 96 $Nm^3/kgNH_4\text{-}N_{applied}$). Then, the oxygen transfer efficiency (OTE) was expected to be different in this study, as it increases with the diffuser immersion depth and decreases with the gas velocity (Harris et al., 1996, Stenstrom et al., 2008). Considering the small bed height in this study and based on the relation found in a Biostyr pilot study by Amiel (2002) during his PhD, the estimated OTE was 18%, against 60 and 66% in the Seine Centre and Seine Aval nitrifying BAFs (Table VII.4-1). This was confirmed by effluent DO concentrations measured occasionally at the effluent of the reactor (during only 4 NH_4^+ load tests), which were low compared to full-scale measurements on the Seine Aval WRRF (3.8 – 4.5 mgO_2/L against 5.5 – 7.5 mgN/L). Finally, a heterogeneous distribution of the gas was visually observed, which could be responsible for low-DO zones, where the nitrifying activity was limited.

Table VII.4-1. Estimated OTE in this study and in full-scale Biostyr® units.

	This study	Seine Centre	Seine Aval
Immersion depth (m)	0.4	3.0	3.5
Gas velocity (m/h)	1	7	12
Estimated SOTE (% m^{-1})	42	20	16
Estimated OTE (%)	18	60	66

All in all, the highest N_2O-EF was 0.16% of the eliminated NH_4-N load at lab-scale, which is 11 and 19 times lower than values measured during summer and winter campaigns on Seine Aval nitrifying BAFs (Bollon et al., 2016b), and 4 times lower than the value measured on Seine Centre in June 2017 (0.7% at AUR 0.4 kgN/m^3/d, not published). The limitations of nitrification were held accountable for the low N_2O-EF measured during the experiments. Previous modelling results suggested that the accumulation of intermediates and associated N_2O production were triggered at AUR above 0.87 kgN/m^3/d (see Chapter VI), which is twice the maximum value reached during the lab-scale experiments. Moreover, oxygen limitation may have induced N_2O reduction by HD. This was already observed by modelling study on

the Seine Aval WRRF, more than half of the AOB-produced N_2O being reduced by HD, despite the low C/N ratio (see chapters V and VI).

VII.4.2 EFFECT OF OPERATING CONDITIONS ON N_2O EMISSIONS

Thanks to these experiments, it was possible to identify the effects of three applied conditions on ammonium removal and N_2O emissions (Table VII.4-2), although a grey area remains with respect to temperature. The main observations were a dominant / positive impact of the applied load on nitrification and N_2O emissions but also a strong / positive impact of temperature on the N_2O emissions. On the contrary, the N_2O-EF decreased with the oxygenation level and remained low.

Table VII.4-2. Summary of operating condition effects on N_2O emissions and production pathways observed at full- and lab-scales.

	AUR		N_2O-ER		N_2O-EF	
	Lab-scale	Full-scale	Lab-scale	Full-scale	Lab-scale	Full-scale
NH_4^+ load	+	+	+	+	+	+
Aeration intensity	+	+	/	/	-	-
Temperature	/	+	+	-	+	-

The dominant and positive effect of the NH_4^+ load on the N_2O emissions is in agreement with model predictions and consistent with other studies (Ali et al., 2014; Chandran et al., 2011; Law et al., 2012a; Yu et al., 2010). Isotopic analyses suggested an increase of the NN contribution to N_2O production, triggered by NH_2OH and NO, which seems fair considering there was no significant increase of the nitrite concentration during the experiment (Figure VII.3-3). However, the contribution of nitrite reduction remained dominant, which can be explained by ND and/or HD. On the one hand, even low nitrite concentrations can trigger ND, in particular given the suspected limitations of oxygen (Peng et al., 2015). On the other hand, a decrease of the HD activity was identified by the increase of the NOx production to AUR ratio (Figure VII.3-3). According to the BAF model (Chapter V), HD acted like a sink of N_2O in the Seine Aval nitrifying BAFs. If this was also the case in this reactor, we can imagine that this decreasing HD activity resulted in a decrease of the net N_2O consumption by denitrifiers.

Finally, except for the point at 0% of air in the gas mix, increasing the air fraction, i.e. aeration intensity (from 29 to 119 $Nm^3/kgNH_4\text{-}N_{applied}$), induced an increase of NH_4^+ removal at roughly constant N_2O-ER, therefore leading to a decrease of the N_2O-EF. The inhibition of denitrifiers' activity by DO increased with aeration intensity (increased NOx to AUR ratio). It

can therefore be imagined that the constant N_2O-ER was related to (i) a decrease of N_2O production by ND at higher DO and (ii) an increase of the net N_2O production by HD (or decrease of the net consumption). This would be in total agreement with model predictions (Chapter V) and is also consistent with full-scale observations on the Seine Aval nitrifying BAFs. During specific experiments, Bollon et al. (2016) increased the airflow, while the ammonium load remained fairly constant. An increase of the aeration intensity from 60 to 130 $Nm^3/kgNH_4\text{-}N_{applied}$ induced a decrease of the N_2O production factor (total N_2O production rate divided by the AUR) from 5.5 to 4.5%. It should be reminded that during the lab-scale experiments, Q_G remained unchanged (only the O_2 fraction changed). Therefore, increased oxygen transfer rates were due to increased O_2 partial pressures but not to the transfer coefficient, which remained constant.

To our knowledge, this is the first attempt to study the single influence of temperature on N_2O emissions in a nitrifying BAF. What we observed is an increase of the N_2O-EF, up to 0.15%, when increasing the influent temperature from 13.4 to 22.3°C. In fact, N_2O-ER remained low (8.5 10^{-4} to 2.4 10^{-3} mgN/min) but the AUR was roughly stable (0.19 to 0.21 $kgN/m^3/d$), which induced an increase of the N_2O-EF. A parallel increase of the NO_2^- concentration was observed, at low concentrations though (below 0.2 mgN/L). In fact, a combined effect of temperature and DO concentration was suspected, as a significant decrease of the DO concentration in the top water zone was observed with increasing temperature. Since NOB have a lower affinity for oxygen than AOB (Blackburne et al. 2008), the accumulation of NO_2^- was likely to be related to oxygen limitation, which is supported by the low evolution of AUR during these tests. However, model predictions were contradictory with the present study: increasing the temperature resulted in a decrease of the effluent NO_2^- concentrations, which was transcribed in the model by a higher NOB activity compared to AOB activity, and in a decrease of the N_2O-EF.

Isotopic analysis revealed a dominant contribution of NO_2^- reduction to N_2O production. This is consistent with the fact that oxygen limitation was suspected during the lab-scale experiments, since low DO concentrations promote N_2O production by ND and HD activity. Full-scale modelling results suggested a similar contribution of NN and ND, coupled to a strong reduction of N_2O by HD. At both lab- and full-scales, NO_2^- accumulation remained low, suggesting that the high contribution of NO_2^- reduction during lab-scale experiments were mostly due to (i) oxygen limitations and (ii) low AUR, which did not favour a high contribution of the NN pathway.

Considering the absence of exogenous carbon in the synthetic influent, one can suppose that carbon originating from bacteria decay was sufficient to sustain heterotrophic activity. This

was already observed by Felez et al. (2017). By modelling batch experiments on aerated activated sludge submitted to NH_4^+ spike additions, these authors revealed a major contribution of HD to N_2O production. This result is essential, since a significant contribution of HD to the net N_2O production from full-sale nitrifying BAFs was predicted by the BAF model, despite the small denitrified flux (about 10% of the produced NO_3^- was reduced, Chapter V). These lab-scale results therefore corroborate the message that HD can contribute significantly to the N_2O balance from nitrifying BAFs. In this study, isotopic analysis did not allow to determine their producing or reducing potential, which should be assessed in future work.

Because the nitrifying activity was limited by the aeration conditions, interpreting the results from these experiments is challenging, in particular the temperature tests. The oxygen transfer was not characterized in this study, as the O_2 concentrations were only measured in the top water zone. Further experiments should be performed, preferably in a full-depth reactor to be in similar aeration efficiency conditions as full-scale BAFs. Moreover, the O_2 transfer should be characterized through measurements of DO concentration over the bed height (in addition to the inlet / outlet measurements). Applying fully aerobic or anaerobic conditions would moreover help discriminating N_2O production pathways. In particular, the effect of temperature could be further studied without limitation of NOB growth due to O_2. Finally, feeding the reactor with real influent water of different compositions, like wastewater from the Seine Centre WRRF, would allow assessing the effect of influent carbon on HD activity and N_2O emissions. Indeed, this remains another question.

VII.5 CONCLUSION

A lab-scale reactor, filled with colonized media beads from the Seine Centre nitrifying BAFs, was submitted to various NH_4^+ loads, the oxygenation and temperature conditions. Despite limited nitrification rates, low N_2O emissions were observed compared to full-scale observations. Their main effects on nitrogen removal and N_2O emissions were assessed.

- A dominant and positive effect of the applied NH_4^+ load on N_2O emissions and on the N_2O-EF was demonstrated. The increase of N_2O emissions with NH_4^+ load was related to a higher contribution of the NN pathway to N_2O production;
- Temperature was the second parameter most affecting N_2O emissions. An increase of temperature from 13.4 to 22.3 °C increased the N_2O-EF by a factor 2.5. The difference was partially attributed to low DO concentrations at the high temperatures, which limited NOB activity. This is not in accordance with the seasonal variations observed at full scale which suggests more complex phenomena than a direct temperature effect;
- The N_2O emission rate remained quite stable with increasing aeration intensity, while the AUR increased, which finally led to decrease the N_2O-EF, similarly to full-scale observations;
- NO_2^- reduction, by nitrifier or/and denitrifiers, was found to be the main contributor of N_2O production during all experiments, which was expected considering the low AUR and DO levels.

Chapter VIII. Conclusion & perspectives

VIII.1 CONCLUSIONS

The main focus of this PhD thesis was to investigate nitrous oxide (N_2O) emissions from full-scale nitrifying biological aerated filters (BAFs). Better understanding the triggers of this potent greenhouse gas and ozone depleting substance is mandatory to reduce environmental impacts of water resource recovery facilities (WRRF).

The approach adopted included the development of a dynamic model based on data from Seine Aval nitrifying BAFs and its use to identify the biological pathways responsible for N_2O production, and the main conditions controlling them. The model was also used to propose mitigation strategies and to refine the quantification of N_2O emissions, poorly estimated by current methods including IPCC approaches. Finally, dedicated lab-scale experiments under controlled conditions were performed to better identify N_2O production pathways and to confront the findings to simulation results.

VIII.1.1 DEVELOPMENT OF A TERTIARY NITRIFYING BAF MODEL AT FULL-SCALE

In this work, N_2O emissions were included in a nitrifying BAF model calibrated on full-scale data for the first time. To this end, an existing BAF model (called base) calibrated and validated on long-term nitrification performances of Seine Aval tertiary nitrifying BAF was extended to include two N_2O production pathways by ammonium oxidizing bacteria (AOB): nitrifier nitrification (NN) and denitrification (ND) according to Pocquet et al. (2016); and four-step heterotrophic denitrification (HD) according to Hiatt and Grady (2008).

As highlighted in the literature review of Chapter IV, full-scale BAF models usually describe oxygen gas-liquid mass transfer considering strong simplifications which are inappropriate for N_2O prediction. Besides, a good prediction of off-gas N_2O concentration is as important as that of dissolved N_2O, the latter being potentially reduced by heterotrophs. Consequently, the first major modification to the base model structure was to include a gas phase as a compartment of the model and describe it as plug-flow; whereas, it was initially considered as perfectly mixed. To assess the relevance of the new model structure, simulation results were confronted to experimental data from the winter campaign.

- The base model was found able to describe nitrification and the order of magnitude of N_2O production rate. However, It was unable to predict the N_2O gas-liquid partition, highly overestimating the emitted to produced N_2O ratio (over 90%, against 65%).
- Including the mass balance on the gaseous phase had limited impact on oxygen mass transfer, but significantly improved the description of the N_2O gas-liquid partition (emitted to produced N_2O ratio was closer to experimental results, 75%).

- The volumetric oxygen transfer coefficient and gas hold up were both found to highly impact nitrification performances. The impact of gas hold up (on average 3.5%) was linked to a substantial reduction of the hydraulic retention time (-13%) due to the low fraction of the working volume in BAFs in comparison with suspended growth systems.
- The value of the volumetric oxygen transfer coefficient was adjusted (117 h^{-1}) to successfully predict both nitrification and N_2O gas-liquid partition.

Then, the predictions of nitrification performances were calibrated on daily characteristics of Seine Aval nitrifying BAFs monitored over two years (2014-2015). N_2O fluxes were calibrated on the data from the two measuring campaigns performed on a given filter unit, which were included in the long-term dataset.

- A global sensitivity analysis highlighted the dependency of nitrification to oxygen-related parameters and to clean media bed porosity. Nitrous oxide production was enhanced by parameter combinations which favoured an imbalance between nitritation and nitratation, i.e. which led to NO_2^- accumulation. It was thus mainly dependent on the variations of ND-linked parameters.
- After modification of five parameters only (out of 90), the model was able to predict nitrification performances on a daily basis, but also on a 10-min basis during the campaigns. Nitrous oxide production rate was successfully predicted on a 10-min basis during both campaigns (average error of 25% and 21% in winter and summer periods, respectively). It showed, however, a tendency to underestimate ammonium removal and to overestimate N_2O fluxes at high air loads (> 100 $Nm^3/kgNH_4\text{-}N_{applied}$), which represented 13% of the experimental dataset.
- Model predictions were extrapolated to estimate the emission factor over the two-year period. It was on average 2.0 ± 0.7% of the applied nitrogen load, which is 56 times the value preconized by the IPCC. Proposing an alternative to the current quantification method is therefore necessary and mitigation strategies should be investigated.

VIII.1.2 PATHWAYS CONTRIBUTING TO N_2O PRODUCTION IN A NITRIFYING BAF

The calibrated model was used to get insights in the contribution of each production pathway on N_2O production over two years (Figure VIII.1-1).

- Based on the results of the sensitivity analysis, a high contribution of the ND pathway was expected. Indeed, NN and ND contributed almost equally to N_2O production during nitrification (51/49 % on average), but the contribution of ND significantly increased with NO_2^- concentration in the biofilm. The concentration of NO_2^- was mainly controlled by

autotrophic reactions (i.e, low contribution of HD), therefore impacted by the regulation between AOB and NOB activities.

- The most surprising result was the contribution of HD. Its net N_2O production (NO reduction to N_2O – N_2O reduction to N_2) was on average -2.3 kgN/h and remained negative in all conditions, reflecting a net consumption of N_2O by heterotrophs. Despite the small denitrified flux (only 12% of the produced NO_3^-), HD highly impacted the net production of N_2O, reducing 74% of the N_2O produced during nitrification.
- According to the model, the accumulation of NO during nitrification remained low, which limited NO reduction to N_2O by HD. On the other hand, N_2O is an end-product of nitrification and was produced in excess, which triggered N_2O consumption by HD. This was possible because of the influent characteristics of the nitrification stage of Seine Aval WRRF, preceded by a CAS which provided exogenous carbon and a significant fraction of heterotrophs (estimated at 25% of the particulate COD in a previous study).

The respective contributions of N_2O production pathways were partially identified by isotopic analyses during the lab-scale experiments on colonized media from Seine Centre nitrifying BAFs (performed by iEES-Paris and Ecobio).

- For all NH_4^+ load (from 0.17 to 1.63 kgN/m^3/d), oxygenation conditions (from 0 to 420 $Nm^3/kgNH_4\text{-}N_{applied}$) and temperature (from 13.4 to 22.3 °C) tested, N_2O production mainly originated from nitrite reduction by heterotrophs and/or autotrophs. This confirmed the results of the sensitivity analysis, which revealed that N_2O production was mainly influenced by parameters regulating NO_2^- accumulation. Unfortunately, the specific contribution of ND and HD could not be identified, which should be done in further work to validate the model predictions (section VIII.2.1).

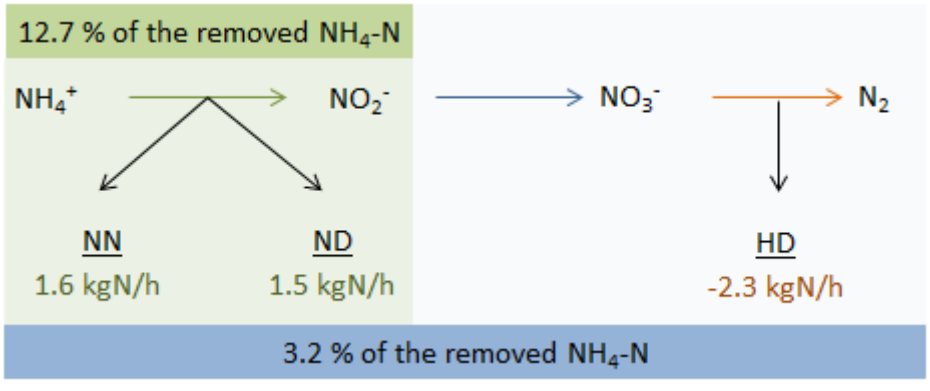

Figure VIII.1-1. Average N_2O production rates in 2014-2015 and associated production factor.

VIII.1.3 TRIGGERS OF N_2O EMISSIONS AND MITIGATION STRATEGIES

Finally, the model was used to identify the conditions inducing high and low amounts of N_2O. Based on a statistical analysis, three main impacting conditions were identified: the influent NH_4^+ concentration, the airflow rate and influent temperature. Their influence on N_2O production was investigated through the daily average predictions of the calibrated model in 2014-2015 and through lab-scale experiments.

- Both agreed on the dominant impact of NH_4^+ concentration on the N_2O emissions factor (EF). The model suggested a threshold value, 0.87 kgN/m^3/d, above which ammonium removal decreased and the concentration of reaction intermediates increased substantially, in particular NH_2OH and NO_2^-, triggering N_2O production by NN and ND. Lab-scale results suggested an increase of NN contribution to N_2O production, which explained the increase of N_2O-EF with the applied NH_4^+ concentration (or load). Maintaining the applied NH_4^+ load below this threshold value should maintain the N_2O-EF under 1% (above 20 °C) – 2% (below 20 °C). Moreover, as far as aeration is controlled by NH_4^+ load in Seine Aval WRRF, reducing the applied NH_4^+ load would allow reducing the airflow rate, therefore energy consumption (indirect CO_2 emissions) and N_2O stripping. This is expected to allow a larger fraction of N_2O to remain dissolved and possibly reduced in the post-denitrification stage.
- Full-scale experiments and lab-scale results agreed on a decrease of the N_2O-EF with increasing oxygen supply. The effect of oxygenation was investigated during the winter campaign. At fairly constant NH_4^+ load, the airflow rate was increased in order to increase the aeration intensity. The measured N_2O production rate remained constant, while NH_4^+ removal increased, which resulted in a decrease of the EF. At lab-scale, the effect of oxygen was studied in a different way: at constant NH_4^+ load and gas flow rate, the fraction of oxygen in the gas was increased, from 0 to 100%. While ammonium removal increased slightly, N_2O emissions remained fairly constant, which resulted in a decrease of the EF. The BAF model, however, suggested a decrease of N_2O consumption by HD, therefore an increase of N_2O production. No clear tendency could be observed *via* isotopic analyses, which did not allow calibrating model predictions during these experiments. In relation to the effect of the applied NH_4^+ load, a proper control of aeration should be operated to maintain sufficient oxygen supply for complete nitrification (around 100 $Nm^3/kgNH_4$-Napplied) and reduce N_2O production, while reducing the proportion of N_2O directly emitted.
- Finally, temperature showed contrasted effect on N_2O production between full-scale (long term time-scale) and lab-scale experiments (short term time-scale). In lab-scale experiments, increasing temperature increased N_2O emissions, while NH_4^+ removal

remained constant, resulting in higher EF. A parallel increase of NO_2^- concentration (which remained < 0.2 mgN/L) and decrease of DO concentration in the top water zone were observed. Since NOB have lower affinity to oxygen than AOB, it was impossible to state on the specific effect of temperature on NO_2^- accumulation and N_2O production, as a limitation of NOB growth by DO was suspected. At the opposite, full-scale monitoring campaigns reported higher N_2O production rates and effluent nitrite concentrations in winter time compared to summer. According to the model, this was mainly related to a lower consumption rate of N_2O by HD due to a higher DO concentration in the biofilm during winter.

VIII.2 PERSPECTIVES

Because there is undeniably a difference between operating conditions at small and industrial scales, we choose to model N_2O emissions from a full-scale BAF in order to evaluate its triggers in representative and dynamic operating conditions. Moreover, the objective was to develop an operational tool that could ultimately serve to evaluate extend of N_2O emissions and evaluate its impact on the climate footprint of the process. These objectives were answered in this work.

Nevertheless, the development and utilization of such model raises interrogations, in particular regarding the contribution of N_2O production pathways. Answering those questions at full-scale is challenging because of the high number of common reaction intermediates and possible interactions between biomasses (AOB, NOB and OHO). Getting information on a smaller scale, in controlled conditions, would have allowed a proper calibration of biokinetic rates, allowing a better estimation of respective N_2O production rates by ND and HD. Moreover, modelling full-scale reactors implicates simplifications of the system representation. In this work, the biofilm wad divided into two layers only, which is debatable considering previous research on N_2O gradients in a nitrifying biofilm.

Two complementary approaches could be proposed to answer these issues. The first would be to confront model predictions to other datasets, preferably WRRFs operated in contrasted conditions. The second would be to work at pilot-scale, to answer specific questions related to contribution of N_2O production pathways and test mitigation strategies. In regards with the uncertainties highlighted in Chapter VII, a pre-requisite for such experiments would be to characterize hydraulic conditions and gas/liquid transfer in the pilot, before investigating biological mechanisms.

VIII.2.1 TOWARDS A BETTER MICRO AND MACRO DESCRIPTION OF THE STRATIFICATION OF BACTERIAL ACTIVITIES

The biofilm thickness and composition was reported to affect significantly N_2O production (Eldyasti et al., 2014, Sabba et al., 2017). In the developed model, the spatial distribution of substrate concentrations and N_2O production rate is mostly described over the BAF height; whereas, it is poorly described in the biofilm compartment as it divided into two layers. This low number of layers may not allow a proper description of microbial activities stratification and its impact on N_2O production mechanisms. Indeed, it is believed that the higher effluent NO_2^- concentration observed in winter compared to summer is not due to a higher growth rate of AOB over NOB at low effluent temperatures (hypothesis of the base model). Since biofilm was found (both experimentally and numerically) to be thicker in winter, it is likely that low DO conditions would have been present in deeper zones of the biofilm, which could have promoted NO_2^- accumulation. However, these mechanisms could not be evidenced using a two layers biofilm model.

To verify this assumption, a first approach would be to compare simulation results obtained with a more discretized description of the biofilm against that of the current model. If significant differences were obtained, then increasing complexity of the model would have been justified and accepted. This assumption could also be verified experimentally and preferably at pilot-scale to limit axial gradients. The distribution of substrate concentrations (DO, nitrogen species) and N_2O concentrations could be measured at various heights of the media bed. Owing to micro-sensors, their distribution in the biofilm could be measured in different locations of the bed, as recently done by Wang et al. () in a partial nitrification reactor. Finally, as discussed in Chapter IV, an experimental evaluation of the evolution of the biofilm compartment (biofilm thickness, bed's porosity over a filtration cycle) along with oxygen mass transfer measurements (static and dynamic retention times, k_La_{O2}, bubble's size and shape) should also help better understanding the parameters affecting mass transfer parameters.

VIII.2.2 FURTHER UTILIZATION AND ANALYSIS OF THE FULL-SCALE MODEL PREDICTIONS

Whereas NN and ND pathways were estimated to contribute almost equally to AOB related N_2O production from the full-scale BAF, HD was found to be a major source of N_2O reduction. Results from chapter V highlighted that extend of N_2O reduction from HD was limited by the content of readily biodegradable organic substrate (Ss) in the effluent entering the nitrification stage. In the present study, influent fractionation from the base model was

used. However, it should be evaluated and analysed on site in regards with performances of upstream processes. In the meantime, a model-based sensitivity analysis on effluent characteristics (concentrations and COD fractionation) could help defining specific ranges of Ss and X_{BH} fractions (against NH_4^+ concentration) inducing contrasted N_2O production rates, which could be experimentally tested at pilot-scale. As COD content was found to be correlated to alpha factor, a better characterization of influent composition is expected to provide useful information on gas/liquid transfer and its spatial evolution within reactors.

In view of better describing the distribution of biomass activities in the reactor, we could collect biomass samples as suggested by the GBRMP (Rittmann et al., 2018). This would help assessing the biofilm characteristics (dry density, thickness), nitritation, nitratation and denitrification rates *via* ex-situ experiments. Other experiments could be performed under various DO levels, representative of gradients in full-scale reactors. Measuring NO emissions could also provide additional information to calibrate biokinetic parameters.

Finally, the model could be used to test mitigation strategies proposed in Chapter VI: minimizing the ammonium load and controlling the aeration rate for biomass distributions stabilized at different temperatures. It could be used to investigate additional operating condition reported to be correlated to N_2O production (Bollon et al., 2016b), but not studied in this work: the filtration time and associated backwash frequency.

VIII.2.3 EXTRAPOLATION TO ANOTHER PLANT OPERATING NITRIFYING BAFS

Finally, the calibrated model should be confronted to the data from another plan operating nitrifying BAF, preferably on long-term data. In particular, it could be applied to the data from Seine Centre WRRF in order to (i) verify the robustness of the biokinetic and gas/liquid transfer models, (ii) assess the respective contributions of N_2O pathways, (iii) compare model predictions with lab-scale observations at the period of the colonized media sampling and (iv) propose mitigation strategies specific to Seine Centre WRRF, which is not operated similarly to Seine Aval (higher aeration intensity and lower applied loads). This study highlighted some additional parameters (influent fractionation, gas/liquid transfer) to evaluate in order to facilitate the full-scale modelling work.

Applying this model –after calibration and potentially further on site measurements– would allow estimating N_2O emissions from these plants and refining the quantification of N_2O contribution to the carbon footprint of WRRFs, first in the Parisian area (only few WRRFs operating BAFs) and possibly on the national scale.

References

ABOOBAKAR, A., CARTMELL, E., STEPHENSON, T., JONES, M., VALE, P. & DOTRO, G. 2013. Nitrous oxide emissions and dissolved oxygen profiling in a full-scale nitrifying activated sludge treatment plant. *Water Research,* 47**,** 524-534.

ADEME, A. 2013. Guide méthodologique d'évaluation des émissions de GES des services de l'eau et de l'assainissement.

ADOUANI, N., LIMOUSY, L., LENDORMI, T. & SIRE, O. 2015. N2O and NO emissions during wastewater denitrification step: Influence of temperature on the biological process. *Comptes Rendus Chimie,* 18**,** 15-22.

AHN, J. H., KIM, S., PARK, H., RAHM, B., PAGILLA, K. & CHANDRAN, K. 2010. N2O Emissions from Activated Sludge Processes, 2008-2009: Results of a National Monitoring Survey in the United States. *Environmental Science & Technology,* 44**,** 4505-4511.

AHN, Y. H. 2006. Sustainable nitrogen elimination biotechnologies: A review. *Process Biochemistry,* 41**,** 1709-1721.

ALI, T. U., AHMED, Z. & KIM, D. J. 2014. Estimation of N2O emission during wastewater nitrification with activated sludge: Effect of ammonium and nitrite concentration by regression analysis. *Journal of Industrial and Engineering Chemistry,* 20**,** 2574-2579.

AMIEL, C. 2002. *Mise au point d'une méthodologie de détermination du transfert d'oxygène application aux biofiltres.* PhD thesis, Institut National des Sciences Appliquées.

AVALAKKI, U., STRONG, W. & SAFFIGNA, P. 1995. Measurement of gaseous emissions from denitrification of applied N-15 .2. Effects of temperature and added straw. *Soil Research,* 33**,** 89-99.

AZIMI, S., FERREIRA, P., ROCHER, V., PAFFONI, C. & GONCALVES, A. 2010. Vieillissement des unités de biofiltration des eaux usées : bilan après 10 années de fonctionnement. *L'eau, l'Industrie, les Nuisances,* 339**,** 58-66.

BAO, Z. Y., RIBERA-GUARDIA, A., SPINELLI, M., SUN, D. Z. & PIJUAN, M. 2018. The effect of temperature shifts on N2O and NO emissions from a partial nitritation reactor treating reject wastewater. *Chemosphere,* 212**,** 162-169.

BEAUMONT, H. J. E., HOMMES, N. G., SAYAVEDRA-SOTO, L. A., ARP, D. J., ARCIERO, D. M., HOOPER, A. B., WESTERHOFF, H. V. & VAN SPANNING, R. J. M. 2002. Nitrite reductase of Nitrosomonas europaea is not essential for production of gaseous nitrogen oxides and confers tolerance to nitrite. *Journal of Bacteriology,* 184**,** 2557-+.

BEHRENDT, J. 1999. Modeling of aerated upflow fixed bed reactors for nitrification. *Water Science and Technology,* 39**,** 85-92.

BERNIER, J. 2013. *Modélisation simultanée de l'enlèvement des nutriments et de l'évolution de la perte de charge en biofiltration des eaux usées.*

BERNIER, J., ROCHER, V., GUERIN, S. & LESSARD, P. 2014. Modelling the nitrification in a full-scale tertiary biological aerated filter unit. *Bioprocess and Biosystems Engineering,* 37**,** 289-300.

BERNIER, J., ROCHER, V. & LESSARD, P. 2016. Initial and hourly headloss modelling on a tertiary nitrifying wastewater biofiltration plant. *Environmental Technology,* 37**,** 1188-1196.

BOCK, E., SCHMIDT, I., STUVEN, R. & ZART, D. 1995. NITROGEN LOSS CAUSED BY DENITRIFYING NITROSOMONAS CELLS USING AMMONIUM OR HYDROGEN AS ELECTRON-DONORS AND NITRITE AS ELECTRON-ACCEPTOR. *Archives of Microbiology,* 163**,** 16-20.

BOIOCCHI, R., GERNAEY, K. V. & SIN, G. 2017. Understanding N2O formation mechanisms through sensitivity analyses using a plant-wide benchmark simulation model. *Chemical Engineering Journal,* 317**,** 935-951.

BOLLON, J., FILALI, A., FAYOLLE, Y., GUERIN, S., ROCHER, V. & GILLOT, S. 2016a. Full-scale post denitrifying biofilters: Sinks of dissolved N2O? *Science of the Total Environment,* 563-564**,** 320-328.

BOLLON, J., FILALI, A., FAYOLLE, Y., GUERIN, S., ROCHER, V. & GILLOT, S. 2016b. N2O emissions from full-scale nitrifying biofilters. *Water Research,* 102**,** 41-51.

BOLTZ, J. P. & DAIGGER, G. T. 2010. Uncertainty in bulk-liquid hydrodynamics and biofilm dynamics creates uncertainties in biofilm reactor design. *Water Science and Technology,* 61**,** 307-316.

BOLTZ, J. P., MORGENROTH, E., BROCKMANN, D., BOTT, C., GELLNER, W. J. & VANROLLEGHEM, P. 2011. Systematic evaluation of biofilm models for engineering practice: components and critical assumptions. *Water Science & Technology*.

BOLTZ, J. P., MORGENROTH, E. & SEN, D. 2010. Mathematical modelling of biofilms and biofilm reactors for engineering design. *Water Science and Technology,* 62**,** 1821-1836.

BOLTZ, J. P., SMETS, B. F., RITTMANN, B. E., VAN LOOSDRECHT, M. C. M., MORGENROTH, E. & DAIGGER, G. T. 2017. From biofilm ecology to reactors: a focused review. *Water Science and Technology,* 75**,** 1753-1760.

BORDAS, M.-L., CARTELLIER, A., SÉCHET, P. & BOYER, C. 2006. Bubbly flow through fixed beds: micro-scale experiments in the dilute regime and modelling. *AICHE J,* 52**,** 3722-3743.

BROCKMANN, D., ROSENWINKEL, K. H. & MORGENROTH, E. 2008. Practical identifiability of biokinetic parameters of a model describing two-step nitrification in biofilms. *Biotechnology and Bioengineering,* 101**,** 497-514.

CASCIOTTI, K. L. & WARD, B. B. 2005. Phylogenetic analysis of nitric oxide reductase gene homologues from aerobic ammonia-oxidizing bacteria. *Fems Microbiology Ecology,* 52**,** 197-205.

CASTRO-BARROS, C. M., RODRIGUEZ-CABALLERO, A., VOLCKE, E. I. P. & PIJUAN, M. 2016. Effect of nitrite on the N2O and NO production on the nitrification of low-strength ammonium wastewater. *Chemical Engineering Journal,* 287**,** 269-276.

CHANDRAN, K., STEIN, L. Y., KLOTZ, M. G. & VAN LOOSDRECHT, M. C. M. 2011. Nitrous oxide production by lithotrophic ammonia-oxidizing bacteria and implications for engineered nitrogen-removal systems. *Biochemical Society Transactions,* 39**,** 1832-1837.

CHEN, X., YUAN, Z. & NI, B.-J. 2018. Nitrite accumulation inside sludge flocs significantly influencing nitrous oxide production by ammonium-oxidizing bacteria. *Water Research,* 143**,** 99-108.

CHEN, Z., YANG, J., LING, D., LIU, P., ILANKOON, I. M. S. K., HUANG, Z. & CHENG, Z. 2017. Packing Size Effect on the Mean Bubble Diameter in a Fixed Bed under Gas–Liquid Concurrent Upflow. *Industrial & Engineering Chemistry Research,* 56**,** 13490-13496.

COLLINS, J. H. P., SEDERMAN, A. J., GLADDEN, L. F., AFEWORKI, M., KUSHNERICK, J. D. & THOMANN, H. 2017. Characterising gas behaviour during gas-liquid co-current up-flow in packed beds using magnetic resonance imaging. *Chemical Engineering Science,* 157**,** 2-14.

COLLIVER, B. B. & STEPHENSON, T. 2000. Production of nitrogen oxide and dinitrogen oxide by autotrophic nitrifiers. *Biotechnology Advances,* 18**,** 219-232.

CONTHE, M., LYCUS, P., ARNTZEN, M. Ø., RAMOS DA SILVA, A., FROSTEGÅRD, Å., BAKKEN, L. R., KLEEREBEZEM, R. & VAN LOOSDRECHT, M. C. M. 2019. Denitrification as an N2O sink. *Water Research,* 151**,** 381-387.

COSENZA, A., MANNINA, G., VANROLLEGHEM, P. A. & NEUMANN, M. B. 2013. Global sensitivity analysis in wastewater applications: A comprehensive comparison of different methods. *Environmental Modelling & Software,* 49**,** 40-52.

CRUVELLIER, N., POUGHON, L., CREULY, C., DUSSAP, C. G. & LASSEUR, C. 2017. High ammonium loading and nitrification modelling in a fixed-bed bioreactor. *Journal of Water Process Engineering,* 20**,** 90-96.

CZEPIEL, P., CRILL, P. & HARRISS, R. 1995. Nitrous Oxide Emissions from Municipal Wastewater Treatment. *Environmental Science & Technology,* 29**,** 2352-2356.

DAELMAN, M. R. J. 2014. *Emissions of methane and nitrous oxide from full-scale municipal wastewater treatment plants.*

DAELMAN, M. R. J., VAN VOORTHUIZEN, E. M., VAN DONGEN, L., VOLCKE, E. I. P. & VAN LOOSDRECHT, M. C. M. 2013. Methane and nitrous oxide emissions from municipal wastewater treatment - results from a long-term study. *Water Science and Technology,* 67**,** 2350-2355.

DAELMAN, M. R. J., VAN VOORTHUIZEN, E. M., VAN DONGEN, U., VOLCKE, E. I. P. & VAN LOOSDRECHT, M. C. M. 2015. Seasonal and diurnal variability of N2O emissions from a full-scale municipal wastewater treatment plant. *Science of the Total Environment,* 536**,** 1-11.

DERLON, N. 2008. *Analyse de la compétition microbienne entre bactéries autotrophes et hétérotrophes au sein d'un biofilm éliminant l'azote.* Institut National des Sciences Appliquées de Toulouse.

DERONT, M., SAMB, F. M., ADLER, N. & PÉRINGER, P. 1998. Volumetric oxygen mass transfer coefficient in an upflow cocurrent packed-bed bioreactor. *Chemical Engineering Science,* 53**,** 1321-1330.

DESHPANDE, S. S., WALKER, J., PRESSLER, J. & HICKMAN, D. 2018. Effect of packing size on packed bubble column hydrodynamics. *Chemical Engineering Science,* 186**,** 199-208.

DESLOOVER, J., VLAEMINCK, S. E., CLAUWAERT, P., VERSTRAETE, W. & BOON, N. 2012. Strategies to mitigate N2O emissions from biological nitrogen removal systems. *Current Opinion in Biotechnology,* 23**,** 474-482.

DOMINGO-FÉLEZ, C., CALDERÓ-PASCUAL, M., SIN, G., PLÓSZ, B. G. & SMETS, B. F. 2017. Calibration of the comprehensive NDHA-N2O dynamics model for nitrifier-enriched biomass using targeted respirometric assays. *Water Research*.

DOMINGO-FELEZ, C., PELLICER-NACHER, C., PETERSEN, M. S., JENSEN, M. M., PLOSZ, B. G. & SMETS, B. F. 2017. Heterotrophs Are Key Contributors to Nitrous Oxide Production in Activated Sludge Under Low C-to-N Ratios During Nitrification-Batch Experiments and Modeling. *Biotechnology and Bioengineering,* 114**,** 132-140.

DOMINGO-FELEZ, C. & SMETS, B. F. 2016. A consilience model to describe N2O production during biological N removal. *Environmental Science-Water Research & Technology,* 2**,** 923-930.

DUAN, H., YE, L., ERLER, D., NI, B.-J. & YUAN, Z. 2017. Quantifying nitrous oxide production pathways in wastewater treatment systems using isotope technology – a critical review. *Water Research*.

ELDYASTI, A., NAKHLA, G. & ZHU, J. 2014. Influence of biofilm thickness on nitrous oxide (N2O) emissions from denitrifying fluidized bed bioreactors (DFBBRs). *Journal of Biotechnology,* 192, Part A**,** 281-290.

EYRING, V., WAUGH, D. W., BODEKER, G. E., CORDERO, E., AKIYOSHI, H., AUSTIN, J., BEAGLEY, S. R., BOVILLE, B. A., BRAESICKE, P., BRUHL, C., BUTCHART, N., CHIPPERFIELD, M. P., DAMERIS, M., DECKERT, R., DEUSHI, M., FRITH, S. M., GARCIA, R. R., GETTELMAN, A., GIORGETTA, M. A., KINNISON, D. E., MANCINI, E., MANZINI, E., MARSH, D. R., MATTHES, S., NAGASHIMA, T., NEWMAN, P. A., NIELSEN, J. E., PAWSON, S., PITARI, G., PLUMMER, D. A., ROZANOV, E., SCHRANER, M., SCINOCCA, J. F., SEMENIUK, K., SHEPHERD, T. G., SHIBATA, K., STEIL, B., STOLARSKI, R. S., TIAN, W. & YOSHIKI, M. 2007. Multimodel projections of stratospheric ozone in the 21st century. *Journal of Geophysical Research-Atmospheres,* 112.

FIAT, J., FILALI, A., FAYOLLE, Y., BERNIER, J., ROCHER, V., SPERANDIO, M. & GILLOT, S. 2019. Considering the plug-flow behavior of the gas phase in nitrifying BAF models significantly improves the prediction of N2O emissions. *Water Res,* 156**,** 337-346.

FILALI, A., BOLLON, J., FAYOLLE, Y., GUERIN, S., ROCHER, V. & GILLOT, S. Nitrous oxide emissions from full-scale nitrifying and denitrifying BAF reactors. 10th Internation Conference on Biofilm Reactors, 2017 Dublin.

FLORES-ALSINA, X., AMELL, M., ARNERLINCK, Y., COROMINAS, L., GERNAEY, K. V., GUO, L., LINDBLOM, E., NOPENS, I., PORRO, J., SHAW, A., SNIP, L., VANROLLEGHEM, P. A. & JEPPSSON, U. 2014. Balancing effluent quality, economic cost and greenhouse gas emissions during the evaluation of (plant-wide) control/operational strategies in WWTPs. *Science of the Total Environment,* 466**,** 616-624.

FOLEY, J., DE HAAS, D., YUAN, Z. G. & LANT, P. 2010. Nitrous oxide generation in full-scale biological nutrient removal wastewater treatment plants. *Water Research,* 44**,** 831-844.

FUJIE, K., HU, H.-Y., IKEDA, Y. & URANO, K. 1992. Gas-liquid oxygen transfer characteristics in an aerobic submerged biofilter for the wastewater treatment. *Chemical Engineering Science,* 47**,** 3745-3752.

GILLOT, S., KIES, F., AMIEL, C., ROUSTAN, M. & HEDUIT, A. 2005. Application of the off-gas method to the measurement of oxygen transfer in biofilters. *Chemical Engineering Science,* 60**,** 6336-6345.

GRIFFITH, D. R., BARNES, R. T. & RAYMOND, P. A. 2009. Inputs of Fossil Carbon from Wastewater Treatment Plants to U.S. Rivers and Oceans. *Environmental Science & Technology,* 43**,** 5647-5651.

GUNDE, R., DAWES, M., HARTLAND, S. & KOCH, M. 1992. Surface tension of wastewater samples measured by the drop volume method. *Environmental Science & Technology,* 26**,** 1036-1040.

GUO, L. S. 2014. *Greenhouse gas emissions from and storm impacts on wastewater treatment plants: Process modelling and control.* Ph.D, Université Laval.

GUO, L. S. & VANROLLEGHEM, P. A. 2014. Calibration and validation of an activated sludge model for greenhouse gases no. 1 (ASMG1): prediction of temperature-dependent N2O emission dynamics. *Bioprocess and Biosystems Engineering,* 37**,** 151-163.

HANAKI, K., HONG, Z. & MATSUO, T. 1992. PRODUCTION OF NITROUS-OXIDE GAS DURING DENITRIFICATION OF WASTE-WATER. *Water Science and Technology,* 26**,** 1027-1036.

HARPER, W. F., TAKEUCHI, Y., RIYA, S., HOSOMI, M. & TERADA, A. 2015. Novel abiotic reactions increase nitrous oxide production during partial nitrification: Modeling and experiments. *Chemical Engineering Journal,* 281**,** 1017-1023.

HARRIS, S. L., STEPHENSON, T. & PEARCE, P. 1996. Aeration investigation of biological aerated filters using off-gas analysis. *Water Science and Technology,* 34**,** 307-314.

HAUDUC, H., NEUMANN, M. B., MUSCHALLA, D., GAMERITH, V., GILLOT, S. & VANROLLEGHEM, P. A. 2015. Efficiency criteria for environmental model quality assessment: A review and its application to wastewater treatment. *Environmental Modelling & Software,* 68**,** 196-204.

HE, Q., ZHU, Y. Y., FAN, L. L., AI, H. N., HUANGFU, X. L. & CHEN, M. 2017a. Effects of C/N ratio on nitrous oxide production from nitrification in a laboratory-scale biological aerated filter reactor. *Water Science and Technology,* 75**,** 1270-1280.

HE, Q., ZHU, Y. Y., LI, G., FAN, L. L., AI, H. N., HUANGFU, X. L. & LI, H. 2017b. Impact of dissolved oxygen on the production of nitrous oxide in biological aerated filters. *Frontiers of Environmental Science & Engineering,* 11.

HENZE, M., GRADY JR, L., GUJER, W., V. R MARAIS, G. & MATSUO, T. 1987. *Activated Sludge Model No 1*.

HENZE, M., VAN LOOSDRECHT, M., EKAMA, G. & BRDJANOVIC, D. 2008. *Biological Wastewater Treatment: Principles, Modelling and Design*, IWA Publishing.

HIATT, W. C. & GRADY, C. P. L. 2008. An Updated Process Model for Carbon Oxidation, Nitrification, and Denitrification. *Water Environment Research,* 80**,** 2145-2156.

HIDAKA, T. & TSUNO, H. 2004. Development of a biological filtration model applied for advanced treatment of sewage. *Water Research,* 38**,** 335-346.

HIGBIE, R. 1935. The rate of absorption of a pure gas into still liquid during short periods of exposure. *Trans. Am. Inst. Chem. Eng.,* 31**,** 365-389.

HOLTAN-HARTWIG, L., DÖRSCH, P. & BAKKEN, L. R. 2002. Low temperature control of soil denitrifying communities: kinetics of N2O production and reduction. *Soil Biology and Biochemistry,* 34**,** 1797-1806.

HU, Z., ZHANG, J., XIE, H., LI, S., WANG, J. & ZHANG, T. 2011. Effect of anoxic/aerobic phase fraction on N2O emission in a sequencing batch reactor under low temperature. *Bioresource Technology,* 102**,** 5486-5491.

IPCC 2013. Climate change 2013: the physical science basis. In: Stocker, T.F. (Ed.), Contribution of Working Group I to the Fifth Assessment Report of the Intergouvernmental Panel on Climate Change. USA, Cambridge University Press, Cambridge, United Kingdom and New York 1535 p.

IPCC 2014. Climate Change 2014: Mitigation of Climate Change. Contribution of Working Group III to the Fifth Assessment Report of the Intergovernmental Panel on Climate Change.

ITOKAWA, H., HANAKI, K. & MATSUO, T. 2001. Nitrous oxide production in high-loading biological nitrogen removal process under low COD/N ratio condition. *Water Research,* 35**,** 657-664.

JIANG, Q. Q. & BAKKEN, L. R. 1999. Nitrous oxide production and methane oxidation by different ammonia-oxidizing bacteria. *Applied and Environmental Microbiology,* 65**,** 2679-2684.

JONES, C. M., GRAF, D. R. H., BRU, D., PHILIPPOT, L. & HALLIN, S. 2012. The unaccounted yet abundant nitrous oxide-reducing microbial community: a potential nitrous oxide sink. *The Isme Journal,* 7**,** 417.

KAMPSCHREUR, M. J., TAN, N. C. G., KLEEREBEZEM, R., PICIOREANU, C., JETTEN, M. S. M. & LOOSDRECHT, M. C. M. 2008a. Effect of dynamic process conditions on nitrogen oxides emission from a nitrifying culture. *Environmental Science & Technology,* 42**,** 429-435.

KAMPSCHREUR, M. J., TEMMINK, H., KLEEREBEZEM, R., JETTEN, M. S. M. & VAN LOOSDRECHT, M. C. M. 2009. Nitrous oxide emission during wastewater treatment. *Water Research,* 43**,** 4093-4103.

KAMPSCHREUR, M. J., VAN DER STAR, W. R. L., WIELDERS, H. A., MULDER, J. W., JETTEN, M. S. M. & VAN LOOSDRECHT, M. C. M. 2008b. Dynamics of nitric oxide and nitrous oxide emission during full-scale reject water treatment. *Water Research,* 42**,** 812-826.

KHERBECHE, A., MILNES, J., JIMENEZ, M., DIETRICH, N., HEBRARD, G. & LEKHLIF, B. 2013. Multi-scale analysis of the influence of physicochemical parameters on the hydrodynamic and gas-liquid mass transfer in gas/liquid/solid reactors. *Chemical Engineering Science,* 100**,** 515-528.

KIES, F., GILLOT, S. & HEDUIT, A. 2005. Paramètres influençant le transfert d'oxygène en biofiltres. *10ème congrès de la SFGP : Récents progrès en génie des procédés.* Toulouse.

KIM, D. J., LEE, D. I. & KELLER, J. 2006. Effect of temperature and free ammonia on nitrification and nitrite accumulation in landfill leachate and analysis of its nitrifying bacterial community by FISH. *Bioresour Technol,* 97**,** 459-68.

KIM, M., WU, G. & YOO, C. 2017. Quantification of nitrous oxide (N2O) emissions and soluble microbial product (SMP) production by a modified AOB-NOB-N2O-SMP model. *Bioresource Technology,* 227**,** 227-238.

KIM, S. W., MIYAHARA, M., FUSHINOBU, S., WAKAGI, T. & SHOUN, H. 2010. Nitrous oxide emission from nitrifying activated sludge dependent on denitrification by ammonia-oxidizing bacteria. *Bioresource Technology,* 101**,** 3958-3963.

KINDAICHI, T., ITO, T. & OKABE, S. 2004. Ecophysiological Interaction between Nitrifying Bacteria and Heterotrophic Bacteria in Autotrophic Nitrifying Biofilms as Determined by Microautoradiography-Fluorescence In Situ Hybridization. *Applied and Environmental Microbiology,* 70**,** 1641-1650.

KNOWLES, R. 1982. DENITRIFICATION. *Microbiological Reviews,* 46**,** 43-70.

KOSONEN, H., HEINONEN, M., MIKOLA, A., HAIMI, H., MULAS, M., CORONA, F. & VAHALA, R. 2016. Nitrous Oxide Production at a Fully Covered Wastewater Treatment Plant: Results of a Long-Term Online Monitoring Campaign. *Environmental Science & Technology,* 50**,** 5547-5554.

LANG, L., POCQUET, M., NI, B., YUAN, Z. & SPERANDIO, M. 2016. Comparison of different 2-pathway models for describing the combined effect of DO and nitrite on the nitrous oxide production by ammonia-oxidizing bacteria. *Water Science & Technology*.

LAW, Y., LANT, P. & YUAN, Z. G. 2013. The Confounding Effect of Nitrite on N2O Production by an Enriched Ammonia-Oxidizing Culture. *Environmental Science & Technology,* 47**,** 7186-7194.

LAW, Y., NI, B. J., LANT, P. & YUAN, Z. G. 2012a. N2O production rate of an enriched ammonia-oxidising bacteria culture exponentially correlates to its ammonia oxidation rate. *Water Research,* 46**,** 3409-3419.

LAW, Y. Y., YE, L., PAN, Y. T. & YUAN, Z. G. 2012b. Nitrous oxide emissions from wastewater treatment processes. *Philosophical Transactions of the Royal Society B-Biological Sciences,* 367**,** 1265-1277.

LE TALLEC, X., VIDAL, A. & THORNBERG, D. 1999. Upflow biological filter: Modeling and simulation of filtration. *Water Science and Technology,* 39**,** 79-84.

LEUNG, S. M., LITTLE, J. C., HOLST, T. & LOVE, N. G. 2006. Air/water oxygen transfer in a biological aerated filter. *Journal of Environmental Engineering-Asce,* 132**,** 181-189.

LINDBLOM, E., ARNELL, M., FLORES-ALSINA, X., STENSTROM, F., GUSTAVSSON, D. J. I., YANG, J. & JEPPSSON, U. 2016. Dynamic modelling of nitrous oxide emissions from three Swedish sludge liquor treatment systems. *Water science and technology : a journal of the International Association on Water Pollution Research,* 73**,** 798-806.

LIZARRALDE, I., FERNANDEZ-AREVALO, T., BELTRAN, S., AYESA, E. & GRAU, P. 2018. Validation of a multi-phase plant-wide model for the description of the aeration process in a WWTP. *Water Research,* 129**,** 305-318.

MALDONADO, J. G. G., BASTOUL, D., BAIG, S., ROUSTAN, M. & HEBRARD, G. 2008. Effect of solid characteristics on hydrodynamic and mass transfer in a fixed bed reactor operating in co-current gas-liquid up flow. *Chemical Engineering and Processing,* 47**,** 1190-1200.

MAMPAEY, K. E., BEUCKELS, B., KAMPSCHREUR, M. J., KLEEREBEZEM, R., VAN LOOSDRECHT, M. C. M. & VOLCKE, E. I. P. 2013. Modelling nitrous and nitric oxide emissions by autotrophic ammonia-oxidizing bacteria. *Environmental Technology,* 34**,** 1555-1566.

MANNINA, G., COSENZA, A. & EKAMA, G. A. 2018. A comprehensive integrated membrane bioreactor model for greenhouse gas emissions. *Chemical Engineering Journal,* 334**,** 1563-1572.

MASSARA, T. M., MALAMIS, S., GUISASOLA, A., BAEZA, J. A., NOUTSOPOULOS, C. & KATSOU, E. 2017a. A review on nitrous oxide (N2O) emissions during biological nutrient removal from municipal wastewater and sludge reject water. *Science of The Total Environment,* 596–597**,** 106-123.

MASSARA, T. M., SOLÍS, B., GUISASOLA, A., KATSOU, E. & BAEZA, J. A. 2017b. Development of an ASM2d-N2O model to describe nitrous oxide emissions in municipal WWTPs under dynamic conditions. *Chemical Engineering Journal*.

MENDOZA-ESPINOSA, L. & STEPHENSON, T. 1999a. A review of biological aerated filters (BAFs) for wastewater treatment. *Environmental Engineering Science,* 16**,** 201-216.

MENDOZA-ESPINOSA, L. & STEPHENSON, T. 1999b. *A Review of Biological Aerated Filters (BAFs) for Wastewater Treatment*.

MORGENROTH, E. 2008. Biofilm reactors. *Biological Wastewater Treatment.* IWA Publishing.

MORGENROTH, E. & WILDERER, P. A. 2000. Influence of detachment mechanisms on competition in biofilms. *Water Research,* 34**,** 417-426.

NFEN-12255-15 2004. European Standard: Wastewater treatment plants - Part 15: Measurement of the oxygen transfer in clean water in aeration tanks of activated sludge plants.

NI, B.-J., PAN, Y., GUO, J., VIRDIS, B., HU, S., CHEN, X. & YUAN, Z. 2016. Denitrification Processes for Wastewater Treatment.

NI, B.-J., PAN, Y., VAN DEN AKKER, B., YE, L. & YUAN, Z. 2015. Full-Scale Modeling Explaining Large Spatial Variations of Nitrous Oxide Fluxes in a Step-Feed Plug-Flow Wastewater Treatment Reactor. *Environmental Science & Technology,* 49**,** 9176-9184.

NI, B. J., PENG, L., LAW, Y. Y., GUO, J. H. & YUAN, Z. G. 2014. Modeling of Nitrous Oxide Production by Autotrophic Ammonia-Oxidizing Bacteria with Multiple Production Pathways. *Environmental Science & Technology,* 48**,** 3916-3924.

NI, B. J., RUSCALLEDA, M., PELLICER-NACHER, C. & SMETS, B. F. 2011. Modeling Nitrous Oxide Production during Biological Nitrogen Removal via Nitrification and Denitrification: Extensions to the General ASM Models. *Environmental Science & Technology,* 45**,** 7768-7776.

NI, B. J., YE, L., LAW, Y. Y., BYERS, C. & YUAN, Z. G. 2013. Mathematical Modeling of Nitrous Oxide (N2O) Emissions from Full-Scale Wastewater Treatment Plants. *Environmental Science & Technology,* 47**,** 7795-7803.

NI, B. J. & YUAN, Z. G. 2015. Recent advances in mathematical modeling of nitrous oxides emissions from wastewater treatment processes. *Water Research,* 87**,** 336-346.

OTTE, S., GROBBEN, N. G., ROBERTSON, L. A., JETTEN, M. S. M. & KUENEN, J. G. 1996. Nitrous oxide production by Alcaligenes faecalis under transient and dynamic aerobic and anaerobic conditions. *Applied and Environmental Microbiology,* 62**,** 2421-2426.

PAN, Y. T., NI, B. J., BOND, P. L., YE, L. & YUAN, Z. G. 2013a. Electron competition among nitrogen oxides reduction during methanol-utilizing denitrification in wastewater treatment. *Water Research,* 47**,** 3273-3281.

PAN, Y. T., NI, B. J. & YUAN, Z. G. 2013b. Modeling Electron Competition among Nitrogen Oxides Reduction and N2O Accumulation in Denitrification. *Environmental Science & Technology,* 47**,** 11083-11091.

PENG, L., NI, B. J., ERLER, D., YE, L. & YUAN, Z. G. 2014. The effect of dissolved oxygen on N2O production by ammonia-oxidizing bacteria in an enriched nitrifying sludge. *Water Research,* 66**,** 12-21.

PENG, L., NI, B. J., YE, L. & YUAN, Z. G. 2015. The combined effect of dissolved oxygen and nitrite on N2O production by ammonia oxidizing bacteria in an enriched nitrifying sludge. *Water Research,* 73**,** 29-36.

PÉREZ, J., MONTESINOS, J. L. & GÒDIA, F. 2006. Gas–liquid mass transfer in an up-flow cocurrent packed-bed biofilm reactor. *Biochemical Engineering Journal,* 31**,** 188-196.

POCQUET, M., WU, Z., QUEINNEC, I. & SPERANDIO, M. 2016. A two pathway model for N2O emissions by ammonium oxidizing bacteria supported by the NO/N2O variation. *Water Research,* 88**,** 948-959.

POH, L. S., JIANG, X., ZHANG, Z. B., LIU, Y., NG, W. J. & ZHOU, Y. 2015. N2O accumulation from denitrification under different temperatures. *Applied Microbiology and Biotechnology,* 99**,** 9215-9226.

POUGHON, L., DUSSAP, C. G. & GROS, J. B. 1999. Dynamic model of a nitrifying fixed bed column: Simulation of the biomass distribution of Nitrosomonas and Nitrobacter and of transient behaviour of the column. *Bioprocess Engineering,* 20**,** 209-221.

POUGHON, L., DUSSAP, C. G. & GROS, J. B. 2001. Energy model and metabolic flux analysis for autotrophic nitrifiers. *Biotechnology and Bioengineering,* 72**,** 416-433.

RASSAMEE, V., SATTAYATEWA, C., PAGILLA, K. & CHANDRAN, K. 2011. Effect of Oxic and Anoxic Conditions on Nitrous Oxide Emissions from Nitrification and Denitrification Processes. *Biotechnology and Bioengineering,* 108**,** 2036-2045.

RAVISHANKARA, A. R., DANIEL, J. S. & PORTMANN, R. W. 2009. Nitrous Oxide (N2O): The Dominant Ozone-Depleting Substance Emitted in the 21st Century. *Science,* 326**,** 123-125.

READ-DAILY, B. L., SABBA, F., PAVISSICH, J. P. & NERENBERG, R. 2016. Kinetics of nitrous oxide (N2O) formation and reduction by Paracoccus pantotrophus. *AMB Express,* 6**,** 85.

REIBER, S. & STENSEL, D. 1985. Biologically Enhanced Oxygen Transfer in a Fixed-Film System. *Journal (Water Pollution Control Federation),* 57**,** 135-142.

REINO, C., VAN LOOSDRECHT, M. C. M., CARRERA, J. & PÉREZ, J. 2017. Effect of temperature on N2O emissions from a highly enriched nitrifying granular sludge performing partial nitritation of a low-strength wastewater. *Chemosphere*.

RIEGER, L., GILLOT, S., LANGERGRABER, G., OHTSUKI, T., SHAW, A., TAKÃ¡CS, I. & WINKLER, S. 2013. *Guidelines for using activated sludge models*, IWA Publishing.

RITTMANN, B. E., BOLTZ, J. P., BROCKMANN, D., DAIGGER, G. T., MORGENROTH, E., SORENSEN, K. H., TAKACS, I., VAN LOOSDRECHT, M. & VANROLLEGHEM, P. A. 2018. A framework for good biofilm reactor modeling practice (GBRMP). *Water Sci Technol,* 77**,** 1149-1164.

ROCHER, V., PAFFONI, C., GONCALVES, A., GUERIN, S., AZIMI, S., GASPERI, J., MOILLERON, R. & PAUSS, A. 2012. Municipal wastewater treatment by biofiltration: comparisons of various treatment layouts. Part 1: assessment of carbon and nitrogen removal. *Water Science and Technology,* 65**,** 1705-1712.

RODRIGUEZ-CABALLERO, A., AYMERICH, I., POCH, M. & PIJUAN, M. 2014. Evaluation of process conditions triggering emissions of green-house gases from a biological wastewater treatment system. *Science of the Total Environment,* 493**,** 384-391.

SABBA, F., PICIOREANU, C., BOLTZ, J. P. & NERENBERG, R. 2017. Predicting N2O emissions from nitrifying and denitrifying biofilms: a modeling study. *Water Sci Technol,* 75**,** 530-538.

SABBA, F., PICIOREANU, C., PEREZ, J. & NERENBERG, R. 2015. Hydroxylamine Diffusion Can Enhance N2O Emissions in Nitrifying Biofilms: A Modeling Study. *Environmental Science & Technology,* 49**,** 1486-1494.

SABBA, F., TERADA, A., WELLS, G., SMETS, B. F. & NERENBERG, R. 2018. Nitrous oxide emissions from biofilm processes for wastewater treatment. *Appl Microbiol Biotechnol*.

SALTELLI, A., RATTO, M., ANDRES, T., CAMPOLONGO, F., CARIBONI, J., GATELLI, D., SAISANA, M. & TARANTOLA, S. 2008. Global Sensitivity Analysis: the Primer. Sensitivity Analysis: From Theory to Practice. *Global Sensitivity Analysis. The Primer.* John Wiley & Sons, Ltd.

SAMIE, G., BERNIER, J., ROCHER, V. & LESSARD, P. 2011. Modeling nitrogen removal for a denitrification biofilter. *Bioprocess and Biosystems Engineering,* 34**,** 747-755.

SANDER, R. 2015. Compilation of Henry's law constants (version 4.0) for water as solvent. *Atmospheric Chemistry and Physics,* 15**,** 4399-4981.

SCHMIDT, I., VAN SPANNING, R. J. M. & JETTEN, M. S. M. 2004. Denitrification and ammonia oxidation by Nitrosomonas europaea wild-type, and NirK- and NorB-deficient mutants. *Microbiology-Sgm,* 150**,** 4107-4114.

SCHREIBER, F., WUNDERLIN, P., UDERT, K. M. & WELLS, G. F. 2012. Nitric oxide and nitrous oxide turnover in natural and engineered microbial communities: biological pathways, chemical reactions, and novel technologies. *Frontiers in Microbiology,* 3.

SHAW, L. J., NICOL, G. W., SMITH, Z., FEAR, J., PROSSER, J. I. & BAGGS, E. M. 2006. Nitrosospira spp. can produce nitrous oxide via a nitrifier denitrification pathway. *Environmental Microbiology,* 8**,** 214-222.

SHISKOWSKI, D. M. & MAVINIC, D. S. 2006. The influence of nitrite and pH (nitrous acid) on aerobic-phase, autotrophic N2O generation in a wastewater treatment bioreactor. *Journal of Environmental Engineering and Science,* 5**,** 273-283.

SHISKOWSKI, D. M., SIMM, R. A. & MAVINIC, D. S. 2004. An experimental procedure for identifying the aerobic-phase biological source of nitrous oxide in anoxic-aerobic wastewater treatment systems. *Journal of Environmental Engineering and Science,* 3**,** 549-553.

SIN, G., GERNAEY, K. V., NEUMANN, M. B., VAN LOOSDRECHT, M. C. M. & GUJER, W. 2011. Global sensitivity analysis in wastewater treatment plant model applications: Prioritizing sources of uncertainty. *Water Research,* 45**,** 639-651.

SIN, G., KAELIN, D., KAMPSCHREUR, M. J., TAKÁCS, I., WETT, B., GERNAEY, K. V., RIEGER, L., SIEGRIST, H. & VAN LOOSDRECHT, M. C. M. 2008. Modelling nitrite in wastewater treatment systems: a discussion of different modelling concepts. *Water Science and Technology,* 58**,** 1155-1171.

SOLER-JOFRA, A., STEVENS, B., HOEKSTRA, M., PICIOREANU, C., SOROKIN, D., VAN LOOSDRECHT, M. C. M. & PEREZ, J. 2016. Importance of abiotic hydroxylamine conversion on nitrous oxide emissions during nitritation of reject water. *Chemical Engineering Journal,* 287**,** 720-726.

SPERANDIO, M. & PAUL, E. 1997. Determination of carbon dioxide evolution rate using on-line gas analysis during dynamic biodegradation experiments. *Biotechnology and Bioengineering,* 53**,** 243-252.

SPÉRANDIO, M., POCQUET, M., GUO, L., NI, B.-J., VANROLLEGHEM, P. A. & YUAN, Z. 2016. Evaluation of different nitrous oxide production models with four continuous long-term wastewater treatment process data series. *Bioprocess and Biosystems Engineering,* 39**,** 493-510.

SRIDHAR, M. K. C. & RAMI REDDY, C. 1984. Surface tension of polluted waters and treated wastewater. *Environmental Pollution Series B, Chemical and Physical,* 7**,** 49-69.

STENSTROM, M. K., ROSSO, D., MELCER, H., APPLETON, R., OCCIANO, V., LANGWORTHY, A. & WONG, P. 2008. Oxygen Transfer in a Full-Depth Biological Aerated Filter. *Water Environment Research,* 80**,** 663-671.

STOWA 2010. Emissies van broeikasgassen van RWZI's, Amersfoort, the Netherlands.

SUZUKI, I., DULAR, U. & KWOK, S. C. 1974. Ammonia or ammonium ion as substrate for oxidation by Nitrosomonas europaea cells and extracts. *J Bacteriol,* 120**,** 556-8.

TALLEC, G., GARNIER, J., BILLEN, G. & GOUSAILLES, M. 2006a. Nitrous oxide emissions from secondary activated sludge in nitrifying conditions of urban wastewater treatment plants: Effect of oxygenation level. *Water Research,* 40**,** 2972-2980.

TALLEC, G., GARNIER, J., BILLEN, G. & GOUSAILLES, M. 2008. Nitrous oxide emissions from denitrifying activated sludge of urban wastewater treatment plants, under anoxia and low oxygenation. *Bioresource Technology,* 99**,** 2200-2209.

TALLEC, G., GARNIER, J. & GOUSAILLES, M. 2006b. Nitrogen removal in a wastewater treatment plant through biofilters: nitrous oxide emissions during nitrification and denitrification. *Bioprocess and Biosystems Engineering,* 29**,** 323-333.

TODT, D. & DORSCH, P. 2016. Mechanism leading to N2O production in wastewater treating biofilm systems. *Reviews in Environmental Science and Bio-Technology,* 15**,** 355-378.

TOYODA, S., YANO, M., NISHIMURA, S.-I., AKIYAMA, H., HAYAKAWA, A., KOBA, K., SUDO, S., YAGI, K., MAKABE, A., TOBARI, Y., OGAWA, N. & OHKOUCHI, N. 2011. *Characterization and production and consumption processes of N2O emitted from temperate agricultural soils determined via isotopomer ratio analysis*.

TUMENDELGER, A., TOYODA, S. & YOSHIDA, N. 2014. Isotopic analysis of N2O produced in a conventional wastewater treatment system operated under different aeration conditions. *Rapid Communications in Mass Spectrometry,* 28**,** 1883-1892.

VANEECKHAUTE, C., CLAEYS, F. H. A., TACK, F. M. G., MEERS, E., BELIA, E. & VANROLLEGHEM, P. A. 2018. Development, implementation, and validation of a generic nutrient recovery model (NRM) library. *Environmental Modelling & Software,* 99**,** 170-209.

VANROLLEGHEM, P. A., MANNINA, G., COSENZA, A. & NEUMANN, M. B. 2015. Global sensitivity analysis for urban water quality modelling: Terminology, convergence and comparison of different methods. *Journal of Hydrology,* 522**,** 339-352.

VIEIRA, A., GALINHA, C. F., OEHMEN, A. & CARVALHO, G. 2019. The link between nitrous oxide emissions, microbial community profile and function from three full-scale WWTPs. *Science of The Total Environment,* 651**,** 2460-2472.

VIGNE, E. 2007. *Etude et modélisation dynamique d'un procédé par biofiltration en nitrification tertiaire.* PhD thesis, Département de Génie Civil, Université Laval.

VIGNE, E., CHOUBERT, J.-M., CANLER, J.-P., HEDUIT, A., SØRENSEN, K. H. & LESSARD, P. 2011. The role of loading rate, backwashing, water and air velocities in an up-flow nitrifying tertiary filter. *Bioresource Technology,* 102**,** 904-912.

VIGNE, E., CHOUBERT, J. M., CANLER, J. P., HEDUIT, A. & LESSARD, P. 2007. Toward an operational dynamic model for tertiary nitrification by submerged biofiltration. *Water Science and Technology,* 55**,** 301-308.

VIGNE, E., CHOUBERT, J. M., CANLER, J. P., HEDUIT, A., SORENSEN, K. & LESSARD, P. 2010. A biofiltration model for tertiary nitrification of municipal wastewaters. *Water Research,* 44**,** 4399-4410.

VIOTTI, P., ERAMO, B., BONI, M. R., CARUCCI, A., LECCESE, M. & SBAFFONI, S. 2002. Development and calibration of a mathematical model for the simulation of the biofiltration process. *Advances in Environmental Research,* 7**,** 11-33.

VON SCHULTHESS, R. & GUJER, W. 1996. Release of nitrous oxide (N2O) from denitrifying activated sludge: Verification and application of a mathematical model. *Water Research,* 30**,** 521-530.

VON SCHULTHESS, R., KUHNI, M. & GUJER, W. 1995. RELEASE OF NITRIC AND NITROUS OXIDES FROM DENITRIFYING ACTIVATED-SLUDGE. *Water Research,* 29**,** 215-226.

VON SCHULTHESS, R., WILD, D. & GUJER, W. 1994. NITRIC AND NITROUS OXIDES FROM DENITRIFYING ACTIVATED-SLUDGE AT LOW-OXYGEN CONCENTRATION. *Water Science and Technology,* 30**,** 123-132.

WANG, X.-X., FANG, F., CHEN, Y.-P., GUO, J.-S., LI, K. & WANG, H. 2017. N2O micro-profiles in biofilm from a one-stage autotrophic nitrogen removal system by microelectrode. *Chemosphere*.

WANG, Y., FANG, H., ZHOU, D., HAN, H. & CHEN, J. 2016. Characterization of nitrous oxide and nitric oxide emissions from a full-scale biological aerated filter for secondary nitrification. *Chemical Engineering Journal,* 299**,** 304-313.

WICHT, H. 1996. A model for predicting nitrous oxide production during denitrification in activated sludge. *Water Science and Technology,* 34**,** 99-106.

WRAGE, N., VELTHOF, G. L., VAN BEUSICHEM, M. L. & OENEMA, O. 2001. Role of nitrifier denitrification in the production of nitrous oxide. *Soil Biology & Biochemistry,* 33**,** 1723-1732.

WUNDERLIN, P., LEHMANN, M. F., SIEGRIST, H., TUZSON, B., JOSS, A., EMMENEGGER, L. & MOHN, J. 2013. Isotope Signatures of N2O in a Mixed Microbial Population System: Constraints on N2O Producing Pathways in Wastewater Treatment. *Environmental Science & Technology,* 47**,** 1339-1348.

WUNDERLIN, P., MOHN, J., JOSS, A., EMMENEGGER, L. & SIEGRIST, H. 2012. Mechanisms of N2O production in biological wastewater treatment under nitrifying and denitrifying conditions. *Water Research,* 46**,** 1027-1037.

YU, R., KAMPSCHREUR, M. J., VAN LOOSDRECHT, M. C. M. & CHANDRAN, K. 2010. Mechanisms and Specific Directionality of Autotrophic Nitrous Oxide and Nitric Oxide Generation during Transient Anoxia. *Environmental Science & Technology,* 44**,** 1313-1319.

ZENG, R. J., LEMAIRE, R., YUAN, Z. & KELLER, J. 2003. Simultaneous nitrification, denitrification, and phosphorus removal in a lab-scale sequencing batch reactor. *Biotechnology and Bioengineering,* 84**,** 170-178.

ZHANG, T. C., FU, Y. C. & BISHOP, P. L. 1995. Competition for substrate and space in biofilms. *Water Environment Research,* 67**,** 992-1003.

ZHANG, Y., JI, G. & WANG, R. 2016. Drivers of nitrous oxide accumulation in denitrification biofilters with low carbon:nitrogen ratios. *Water Research,* 106**,** 79-85.

Annexes

ANNEX 1. DESCRIPTION OF THE EXTENDED BAF MODEL

1. GENERAL PRESENTATION

The particle and soluble fluxes computed in the model are represented on Figure A.1 and described in the following sections. The gas-liquid fluxes are not included, as they are described in details in Chapter IV. The compartments are not true to scale, for better clarity.

The model used in this paper was extended from a BAF model proposed by Bernier et al. (2014). It describes the functioning of a tertiary nitrifying upflow co-current Biostyr® reactor. The 3.5 meters filter bed is represented as seven reactors in series of equal height, to mimic a plug-flow reactor. This number was chosen as a compromise between correct flow representation and reasonable calculation time. Each reactor is composed of four compartments: the liquid phase that is considered biologically inactive – biomass concentrations being negligible compared to those in the biofilm, – the gas phase, the inert media, and two biofilm layers: the basal layer (close to the media), and the surface one (in contact with water). These compartments are modelled as completely stirred tank reactors (CSTR). An additional CSTR is modelled to represent the 1.5 meter overflow. Finally, the system is represented by height reactors in series. Effluent concentrations refer to the concentrations simulated in the overflow (reactor 8).

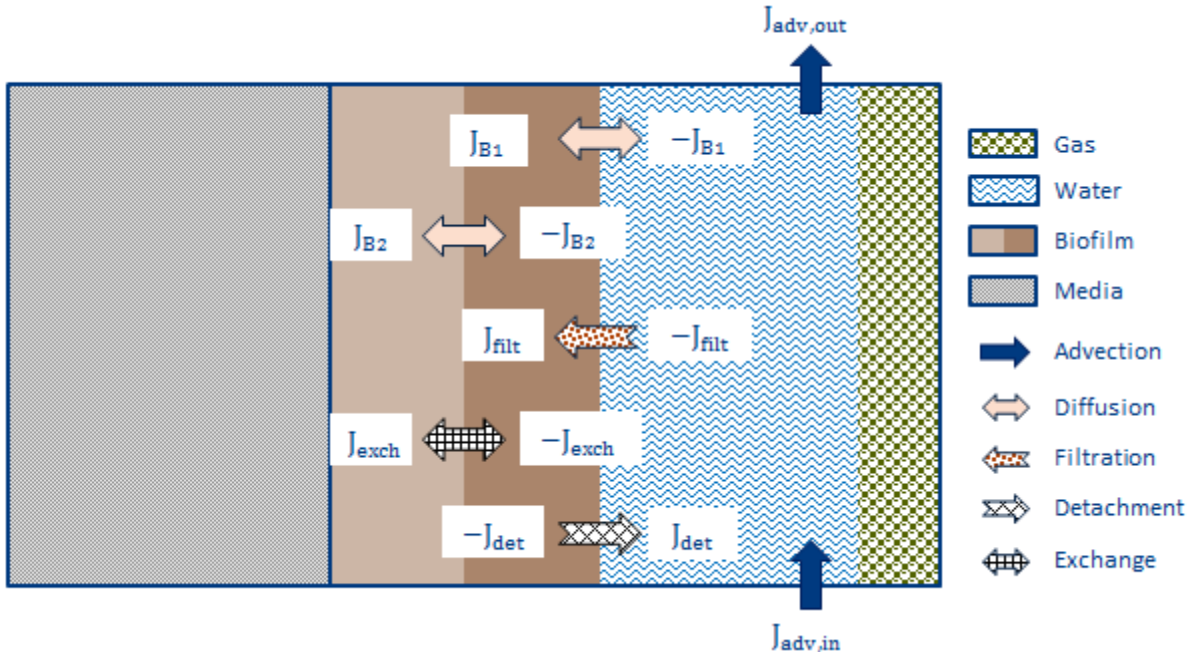

Figure A.1. Schematic representation of one of the seven reactors in the series and the associated fluxes (except fluxes related to the gas phase).

2. BIOFILM REPRESENTATION

The media and the expansion of the biofilm reduce the volume accessible to the water flow. The media fraction is constant (64% of the active zone), while the biofilm fraction is variable and can be calculated from the biofilm thickness, and the media specific area (Eq.A.1). The biofilm thickness in a given reactor n is equal to the sum of all biofilm layer thicknesses (Eq.A.2, in this work, k = 2). The biofilm thickness varies with the filtration of particles (attachment), detachment and net biomass growth. It is estimated based on the density of the dry biofilm, the maximum biofilm thickness and the local TSS concentration (Eq.A.3). The factor ICV is used to convert the sum of particle concentrations from COD to TSS. In other words, a biofilm layer is considered as full when the concentration of particles reaches its maximal value (which corresponds to the density of the dry biofilm). This maximum thickness is calculated from the constant maximum deposit fraction on the media (Eq.A.4).

Eq.A.1 $$\varepsilon_{B,n} = Z_n a_a$$

Eq.A.2 $$Z_n = \sum_{j=1}^{k} Z_{j,n}$$

Eq.A.3 $$Z_{j,n} = \frac{\sum X_{j,n} / ICV}{\rho_B} Z_{max,j}$$

Eq.A.4 $$Z_{max,j} = \frac{Z_{max}}{k}$$

where ε_B is the biofilm fraction, Z and Z_j (m) respectively the total biofilm thickness in reactor, and the biofilm thickness in a given biofilm layer, Z_{max} and $Z_{max,j}$ (m) their respective maximum values, ΣX_j the sum of particle concentrations in a biofilm layer (gCOD/m^3), ICV the conversion factor from COD to TSS (1.5 gCOD/gTSS), ρ_B, the dry biofilm density (g/m^3) and k the number of biofilm layers. n stands for the reactor number, and j for the biofilm layer.

3. FATE OF PARTICLES

The mass balances of a particulate compound X_i in the liquid, the surface biofilm layer (B1) and the basal biofilm layer (B2) of a reactor n are given in Eq.A.5, Eq.A.6 and Eq.A.7, respectively. Particles can be filtered, detached, or exchanged.

Eq.A.5 $$V_{L,n} \frac{\partial X_{i,L,n}}{\partial t} = J_{Xi,adv,in,n} - J_{Xi,adv,out,n} - J_{Xi,filt,n} + J_{Xi,det,n}$$

Eq.A.6 $$V_{B1,n} \frac{\partial X_{i,B1,n}}{\partial t} = J_{Xi,filt,n} - J_{Xi,det,n} - J_{Xi,exch,n} + V_{B1,n} r_{i,B1,n}$$

Eq.A.7 $$V_{B2,n}\frac{\partial X_{i,B2,n}}{\partial t} = J_{Xi,exch,n} + V_{B2,n}r_{i,B2,n}$$

Where X (g/m^3) is the concentration of a given particulate compound, V_{B1} and V_{B2} (m^3) are the surface and basal biofilm layer volumes respectively. For simplification, they were considered equal to their maximum value (7.35 m^3). The terms r_{B1} and r_{B2} (g/m^3/d) stand for the sum of reaction rates involving a given X_i. J_{adv} (g/d) is the flux entering (in) or leaving (out) the reactor. J_{filt} (g/d) is the flux retained in the surface biofilm layer by filtration (Eq.A.8). The filtration coefficient is calculated from an empirical relation (Eq.A.9), which involves the deposit fraction on the media (Eq.A.10), J_{det} (g/d) is the flux detached from the surface layer to the bulk (Eq.A.11). J_{exch} (g/d) is the flux leaving the surface for the basal layer (Eq.A.12). i and n stand for the component and the reactor respectively.

Eq.A.8 $$J_{Xi,filt,n} = \frac{\lambda U_L X_{i,L,n} V_{R,n}}{1 - \sum X_{bulk,n}/\rho_B}$$

Eq.A.9 $$\lambda = \lambda_0 \left(1 + \frac{\beta\sigma}{\varepsilon_0}\right)^y \left(1 - \frac{\sigma}{\varepsilon_0}\right)^z \left(1 - \frac{\sigma}{\sigma_{max}}\right)^x$$

Eq.A.10 $$\sigma = a_a Z_n$$

Eq.A.11 $$J_{Xi,det,n} = k_{det} a_a V_{R,n} \frac{X_{i,B1,n}}{\sum X_{B1,n}}$$

Eq.A.12 $$J_{Xi,exch,n} = k_{exc} a_a V_{R,n} (\Sigma X_{B1,n} - \Sigma X_{B2,n})$$

where λ and λ_0 are the filtration and the clean filtration coefficients, U_L (m^3/m^2/d) the surface liquid flowrate, x, y and z empirical constants calibrated in a previous work (Bernier et al., 2014), σ the biofilm deposit fraction, a_a the media specific area (1000 m^2/m^3 of empty reactor), k_{det} (g/m^2/d) the detachment coefficient, and k_{exc} (m/d) the exchange coefficient.

4. FATE OF SOLUBLE COMPONENTS

The mass balances of a soluble component S_i in the liquid, the surface biofilm layer and the basal biofilm layer of a reactor n are given in Eq.A.13, Eq.A.14 and Eq.A.15, respectively. A soluble can enter or leave a reactor by advection, and diffuse between compartments.

Eq.A.13 $$V_{L,n}\frac{\partial S_{i,L,n}}{\partial t} = J_{Si,adv,in,n} - J_{Si,adv,out,n} - J_{Si,B1,n}$$

Eq.A.14 $$V_{B1,n}\frac{\partial S_{i,B1,n}}{\partial t} = J_{Si,B1,n} - J_{Si,B2,n} + V_{B1,n}r_{i,B1,n}$$

Eq.A.15 $$V_{B2,n}\frac{\partial S_{i,B2,n}}{\partial t} = J_{Si,B2,n} + V_{B1}r_{i,B2,n}$$

where S (g/m^3) is the concentration of a given soluble compound, J_{B1} (g/d) the flux diffused from the liquid to the surface layer (Eq.A.16), and J_{B2} (g/d) the flux diffused from the surface to the basal biofilm layer (Eq.A.17). The resistance to transfer is modelled by a constant thickness liquid film. A reduction factor is included to better describe the diffusion into the biofilm compared to water.

Eq.A.16 $$J_{Si,B1,n} = \frac{D_i f_D}{L_f} a_a V_{R,n} \left(S_{i,bulk,n} - S_{B1,n}\right)$$

Eq.A.17 $$J_{Si,B2,n} = \frac{D_i f_D}{Z_{1,n}} a_a V_{R,n} \left(S_{B1,n} - S_{B2,n}\right)$$

where D (m^2/d) is the diffusion coefficient in water, f_D the reduction factor of diffusion in the biofilm compared to water, L_f (m) the thickness of the liquid film.

5. INFLUENT FRACTIONATION

The fractionation of carbon oxygen demand (COD) and nitrogen (N) is presented on Figure A.2. Parameters were not modified from the base model proposed by Bernier et al. (2014).

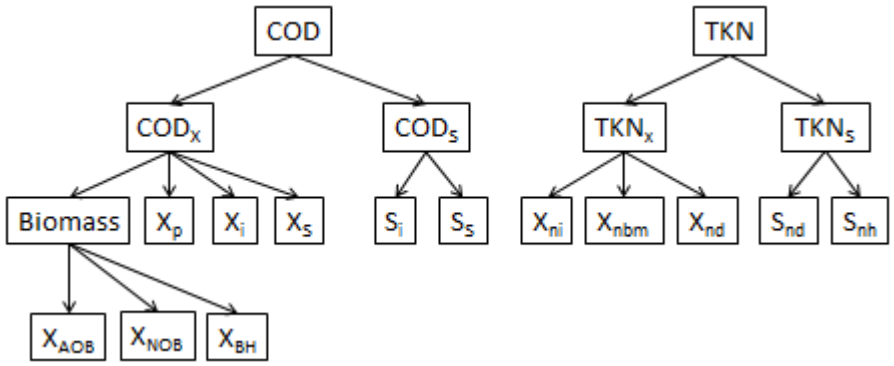

Figure A.2. Influent COD and N fractionation computed in the BAF model.

Classically, COD (model input) was divided into particular and soluble COD. Particular COD was calculated from the TSS concentration (model input), multiplied by the VSS to TSS and particular COD to VSS fractions (model parameters). Soluble COD was then deduced from total and particular COD. Influent TKN (total Kjeldahl nitrogen) was calculated from the influent NH_4^+ concentration (model input). It was divided into particular and soluble TKN. Particular TKN was calculated by deducing NH_4^+ concentration to total TKN, multiplied by the particular fraction of organic nitrogen (model parameter). Soluble TKN was deduced from total and particulate nitrogen. The subsequent fractions were calculated based on model parameters listed in Table A.5.

6. BACKWASH EVENTS

Backwash activation and deactivation is an input of the model (0 and 1 signal), and impacts each reactor in series independently. To maintain enough biomass for pollution elimination, lower extraction efficiency is implemented for biomass than for non-biomass particles (1% against 20%). For simplification, the model does not consider a homogenization of biomass concentrations in the biofilter during a backwash cycle. During the summer and winter N_2O measuring campaigns, the activity of the filter is available. It allowed us to know and input the exact backwash hour during these two periods. When simulating the long-term functioning of the filter based on exploitation data of the nitrification stage, a backwash event is imposed every 24 hours for 30 minutes.

7. BIOKINETIC MODEL

The main biological reactions are recalled on Figure A.3. The Gujer matrix and reaction rates of heterotrophic denitrification and nitrification are given in Table A.1 to Table A.4. The parameters of the calibrated model are given in Table A.5.

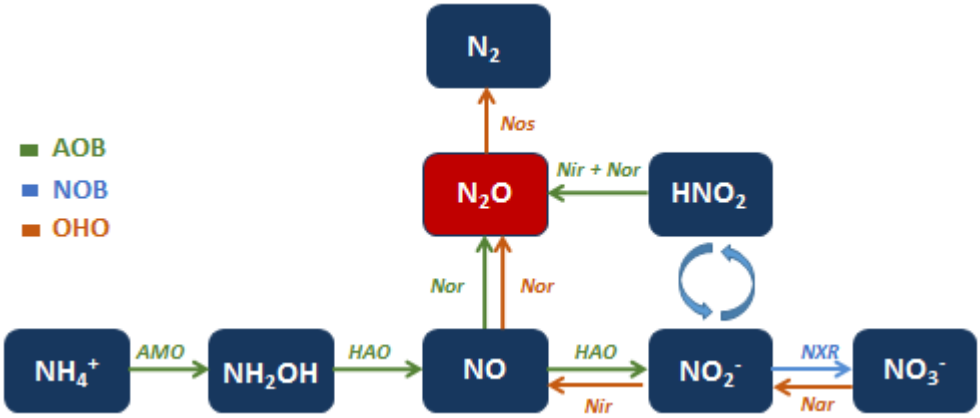

Figure A.3. Schematic representation of the N_2O biological pathways included in the modified BAF model. AMO, HAO, NXR, Nar, Nir, Nor and Nos stand for the enzymes ammonium monooxygenase, hydroxylamine oxidoreductase, nitrite oxidoreductase, nitrate reductase, nitrite reductase, and NO reductase and N_2 synthase.

Table A.1. Gujer matrix of the heterotrophic denitrification model.

Process	S_S	X_S	X_{BH}	X_P	S_O	S_{NH4}	S_{NO}	S_{NO2}	S_{N2O}	S_{NO3}	S_{N2}	S_{PO}	S_{ALK}
R1	$-\frac{1}{Y_h}$		1		$-\frac{(1-Y_h)}{Y_h}$	$-ixbn$						$-ixbp$	$-\frac{ixbn}{14}$
R2	$-\frac{1}{\eta_Y Y_h}$		1			$-ixbn$		B		$-B$		$-ixbp$	$-\frac{ixbn}{14}$
R3	$-\frac{1}{\eta_Y Y_h}$		1			$-ixbn$	A	$-A$				$-ixbp$	$\frac{(1-\eta yYh)}{(14*4/7*\eta yYh)}-\frac{ixbn}{14}$
R4	$-\frac{1}{\eta_Y Y_h}$		1			$-ixbn$	$-A$		A			$-ixbp$	$-\frac{ixbn}{14}$
R5	$-\frac{1}{\eta_Y Y_h}$		1			$-ixbn$			$-A$		A	$-ixbp$	$-\frac{ixbn}{14}$
R6		$1-f_p$	-1	f_p								$-ixbp$	

$A=\frac{(1-\eta yYh)}{(4/7*\eta yYh)}$; $B=\frac{(1-\eta yYh)}{(8/7*\eta yYh)}$

Table A.2. Kinetic rates of the heterotrophic denitrification model.

Process	Kinetic rate
R1 = Aerobic growth heterotrophs	$\mu_{H,max}\left(\frac{S_S}{S_S+K_S}\right)\left(\frac{S_O}{S_O+K_{O,H}}\right)\left(\frac{S_{PO}}{S_{PO}+K_{PO}}\right)X_{BH}$
R2 = Anoxic growth heterotrophs (NO_3^-)	$\eta_{H1}\mu_{H,max}\left(\frac{S_S}{S_S+K_{S,1}}\right)\left(\frac{K_{I,O,H,1}}{S_O+K_{I,O,H,1}}\right)\left(\frac{S_{NO3}}{S_{NO3}+K_{H,NO3}}\right)\left(\frac{S_{PO}}{S_{PO}+K_{PO}}\right)X_{BH}$
R3 = Anoxic growth of heterotrophs (NO_2^-)	$\eta_{H2}\mu_{H,max}\left(\frac{S_S}{S_S+K_{S,2}}\right)\left(\frac{K_{I,O,H,2}}{S_O+K_{I,O,H,2}}\right)\left(\frac{S_{NO2}}{S_{NO2}+K_{H,NO2}}\right)\left(\frac{K_{I,NO,2}}{S_{NO}+K_{I,NO,2}}\right)\left(\frac{S_{PO}}{S_{PO}+K_{PO}}\right)X_{BH}$
R4 = Anoxic growth of heterotrophs (NO)	$\eta_{H3}\mu_{H,max}\left(\frac{S_S}{S_S+K_{S,3}}\right)\left(\frac{K_{I,O,H,3}}{S_O+K_{I,O,H,3}}\right)\left(\frac{S_{NO}}{S_{NO}+K_{H,NO}+S_{NO}^2/K_{I,NO,3}}\right)\left(\frac{S_{PO}}{S_{PO}+K_{PO}}\right)X_{BH}$
R5 = Anoxic growth of heterotrophs (N_2O)	$\eta_{H4}\mu_{H,max}\left(\frac{S_S}{S_S+K_{S,4}}\right)\left(\frac{K_{I,O,H,4}}{S_O+K_{I,O,H,4}}\right)\left(\frac{S_{N2O}}{S_{N2O}+K_{H,N2O}}\right)\left(\frac{K_{I,NO,4}}{S_{NO}+K_{I,NO,4}}\right)\left(\frac{S_{PO}}{S_{PO}+K_{PO}}\right)X_{BH}$
R6 = Decay of heterotrophs	$b_H X_{BH}$

Table A.3. Gujer matrix of the nitrification model.

Process	S_S	X_S	X_{AOB}	X_{NOB}	X_P	S_O	S_{NH4}	S_{NH2OH}	S_{NO}	S_{NO2}	S_{N2O}	S_{NO3}	S_{ND}	X_{ND}	S_{PO}	S_{ALK}
R7						$-8/7$	-1	1								$-\frac{1}{14}$
R8			1			$-\frac{(12/7-\mathrm{Yaob})}{\mathrm{Yaob}}$	$-\mathrm{ixbn}$	$-\frac{1}{\mathrm{Yaob}}$	$\frac{1}{\mathrm{Yaob}}$						$-\mathrm{ixbp}$	$-\frac{\mathrm{ixbn}}{14}$
R9						$-4/7$			-1	1						$-\frac{1}{14}$
R10								-1	-4	1	4					$-\frac{1}{14}$
R11								-1		-1	2					$\frac{1}{14}$
R12				1		$-\frac{(16/14-\mathrm{Ynob})}{\mathrm{Ynob}}$	$-\mathrm{ixbn}$			$-\frac{1}{\mathrm{Ynob}}$		$\frac{1}{\mathrm{Ynob}}$			$-\mathrm{ixbp}$	$-\frac{\mathrm{ixbn}}{14}$
R13		$1-f_p$	-1		f_p									$\mathrm{ixbn}-\mathrm{fp}*\mathrm{ixun}$	$\mathrm{ixbp}-\mathrm{fp}*\mathrm{ixup}$	
R14		$1-f_p$		-1	f_p									$\mathrm{ixbn}-\mathrm{fp}*\mathrm{ixun}$	$\mathrm{ixbp}-\mathrm{fp}*\mathrm{ixup}$	
R15							1						-1			$\frac{1}{14}$
R16	1	-1														
R17													1	-1		

Table A.4. Kinetic rates of the nitrification model.

Process	Kinetic rate
R7 = Oxidation of NH_4 to NH_2OH	$\left(\frac{\mu_{AOB}}{Y_{AOB}}\right)\left(\frac{S_O}{S_O + K_{O,AOB,1}}\right)\left(\frac{S_{NH4}}{S_{NH4} + K_{NH4,AOB}}\right)X_{AOB}$
R8 = Growth of AOB	$\mu_{AOB}\left(\frac{S_O}{S_O + K_{O,AOB,2}}\right)\left(\frac{S_{NH4}}{S_{NH4} + 10^{-12}}\right)\left(\frac{S_{NH2OH}}{S_{NH2OH} + K_{NH2OH}}\right)\left(\frac{S_{PO}}{S_{PO} + K_{PO}}\right)X_{AOB}$
R9 = Oxidation of NO to NO_2^-	$\left(\frac{\mu_{AOB}}{Y_{AOB}}\right)\left(\frac{S_O}{S_O + K_{O,AOB,2}}\right)\left(\frac{S_{NO}}{S_{NO} + K_{NO,AOB,HAO}}\right)X_{AOB}$
R10 = Reduction of NO to N_2O	$\eta_{NN}\left(\frac{\mu_{AOB}}{Y_{AOB}}\right)\left(\frac{S_{NH2OH}}{S_{NH2OH} + K_{NH2OH}}\right)\left(\frac{S_{NO}}{S_{NO} + K_{NO,AOB,NN}}\right)X_{AOB}$
R11 = Reduction of NO_2 to N_2O	$\eta_{ND}\left(\frac{\mu_{AOB}}{Y_{AOB}}\right)\left(\frac{S_{NH2OH}}{S_{NH2OH} + K_{NH2OH}}\right)\left(\frac{S_{NO2}}{S_{NO2} + K_{NO2,AOB}}\right)DO_{Haldane}X_{AOB}$
R12 = Growth of NOB	$\mu_{NOB,max}\left(\frac{S_O}{S_O + K_{O,NOB}}\right)\left(\frac{S_{NO2}}{S_{NO2} + K_{NO2,NOB}}\right)\left(\frac{S_{PO}}{S_{PO} + K_{PO}}\right)X_{NOB}$
R13 = Decay of AOB	$b_{AOB}X_{AOB}$
R14 = Decay of NOB	$b_{NOB}X_{NOB}$
R15 = Ammonification	$k_a S_{ND} X_{BH}$
R16 = Hydrolysis	$k_H\left(\frac{X_S/X_{BH}}{K_X + X_S/X_{BH}}\right)\left[\left(\frac{S_O}{S_O + K_{O,H}}\right) + \eta_h\left(\frac{K_{O,H}}{S_O + K_{O,H}}\right)\left(\frac{\sum S_{NOX}}{H_{H,NO3} + \sum S_{NOX}}\right)\right]X_{BH}$
R17 = N hydrolysis	$k_H\left(\frac{X_{ND}}{X_S}\right)\left(\frac{X_S/X_{BH}}{K_X + X_S/X_{BH}}\right)\left[\left(\frac{S_O}{S_O + K_{O,H}}\right) + \eta_h\left(\frac{K_{O,H}}{S_O + K_{O,H}}\right)\left(\frac{\sum S_{NOX}}{H_{H,NO3} + \sum S_{NOX}}\right)\right]X_{BH}$

8. LIST OF PARAMETERS USED IN THE CALIBRATED MODEL

Table A.5. List of parameters defined in the modified BAF model. [a] Bernier et al. (2014), [b] Hiatt and Grady (2008), [c] Lang et al. (2016), [d] Sander (2015), [e] Pocquet et al. (2016), [f] Vigne et al. (2010), [g] Sabba et al. (2017), [h] Gillot et al. (2005), * modified from original publication.

Parameter	Description	Value	Source
Influent fractionation (10)			
DCO_X/MVS	Particular COD to VSS ratio	1.5 gCOD/gVSS	[a]
MVS/MES	VSS to TSS ratio	0.75 gVSS/gTSS	[a]
TKN/NH4	TKN to NH4 ratio	1.1 gN/gN	[a]
frssi	Inert fraction of soluble COD	0.65 gCOD/gCOD	[a]
frxxi	Inert fraction of particular COD	0.65 gCOD/gCOD	[a]
frxu	Inactive biomass fraction of particular COD	0 gCOD/gCOD	[a]
frbh	Heterotrophic biomass fraction of particular COD	0.25 gCOD/gCOD	[a]
frbai	AOB fraction of particular COD	0 gCOD/gCOD	[a]
frbaa	NOB fraction of particular COD	0 gCOD/gCOD	[a]
frxnd	Particular fraction of organic N	0.45 gCOD/gCOD	[a]
Biokinetic model (62)			
b_{AOB}	Decay coefficient, AOB	0.17 d^{-1}	[a]
b_{NOB}	Decay coefficient, NOB	0.17 d^{-1}	[a]
b_H	Decay coefficient, heterotrophs	0.62 d^{-1}	[a]
η_H	Anoxic hydrolysis factor	0.4	[a]
η_{H1}	Anoxic growth factor for heterotrophs, NO_3^-	0.28	[b]
η_{H2}	Anoxic growth factor for heterotrophs, NO_2^-	0.16	[b]
η_{H3}	Anoxic growth factor for heterotrophs, NO	0.35	[b]
η_{H4}	Anoxic growth factor for heterotrophs, N_2O	0.35	[b]
η_{ND}	Reduction factor for the ND pathway	0.144	Calibrated
η_{NN}	Reduction factor for the NN pathway	0.07693	[c]
η_Y	Anoxic yield factor	0.75	[a]
ixbn	Mass of nitrogen per mass of COD in active biomass	0.086 gN/gCOD	[a] [b]
ixun	Mass of nitrogen per mass of COD in biomass debris	0.06 gN/gCOD	[a] [b]
ixbp	Mass of phosphorus per mass of COD in active biomass	0.015 gP/gCOD	[a]
ixup	Mass of phosphorus per mass of COD in biomass debris	0.015 gP/gCOD	[a]
f_p	Fraction of active biomass contributing to biomass debris	0.08 gN/gCOD	[a] [b]
k_a	Ammonification rate coefficient	0.08 m^3/(gCOD.d)	[a]
k_h	Hydrolysis coefficient	3 gCOD/(gCOD.d)	[a]
$K_{H,NO3}$	Half-saturation coefficient for NO_3^-, heterotrophs (gN/m^3)	0.2 gN/m^3	[a] [b]
$K_{H,NO2}$	Half-saturation coefficient for NO_2^-, heterotrophs (gN/m^3)	0.2 gN/m^3	[a] [b]
$K_{H,NO}$	Half-saturation coefficient for NO, heterotrophs	0.05 gN/m^3	[b]

$K_{H,N2O}$	Half-saturation coefficient for N_2O, heterotrophs	0.05 gN/m^3	[b]
$K_{NO2,AOB}$	AOB affinity constant for NO_2 (ND path)	2.86 gN/m^3	Calculated
$K_{I,NO,2}$	NO inhibition coefficient, NO_2^-	0.5 gN/m^3	[a] [b]
$K_{I,NO,3}$	NO inhibition coefficient, NO	0.3 gN/m^3	[a] [b]
$K_{I,NO,4}$	NO inhibition coefficient, N_2O	0.075 gN/m^3	[a] [b]
$K_{I,O,AOB}$	Inhibition constant by O_2 on N_2O production	0.8 gO_2/m^3	[e]
K_{NH2OH}	AOB affinity constant for NH_2OH	0.0147 gN/m^3	Calculated
$K_{NH4,AOB}$	AOB affinity constant for NH_4	1 gN/m^3	[a]
$K_{NO,AOB,HAO}$	AOB affinity constant for NO from HAO	0.0003 gN/m^3	[c]
$K_{NO,AOB,NN}$	AOB affinity constant for NO from NirK	0.008 gN/m^3	[c]
$K_{NO2,NOB}$	Half-saturation coefficient for NO_2^-, NOB	0.2 gN/m^3	[a]
$K_{O,AOB,1}$	AOB affinity constant for O_2 (AMO reaction)	0.48 gO_2/m^3	[a]
$K_{O,AOB,2}$	AOB affinity constant for O_2 (HAO reactions)	0.3 gO_2/m^3	[c]
$K_{O,AOB,ND}$	AOB constant for O_2 effect on the ND pathway	0.5 gO_2/m^3	[e]
$K_{O,H}$	Half-saturation coefficient for O_2, heterotrophs	0.1 gO_2/m^3	[a] [b]
$K_{I,OH,1}$	Inhibition coefficient for O_2, heterotrophs, NO_3^-	0.1 gO_2/m^3	[a] [b]
$K_{I,OH,2}$	Inhibition coefficient for O_2, heterotrophs, NO_2^-	0.1 gO_2/m^3	[b]
$K_{I,OH,3}$	Inhibition coefficient for O_2, heterotrophs, NO	0.1 gO_2/m^3	[b]
$K_{I,OH,4}$	Inhibition coefficient for O_2, heterotrophs, N_2O	0.1 gO_2/m^3	[b]
$K_{O,NOB}$	NOB affinity constant for O_2	0.5 gO_2/m^3	Calibrated
K_{PO}	Half-saturation coefficient for orthophosphate	0.01 gP/m^3	[a]
K_S	Half-saturation coefficient for substrate, heterotrophs	20 $gCOD/m^3$	[b]
K_{S1}	Half-saturation coefficient for substrate, heterotrophs, NO_3^-	20 $gCOD/m^3$	[b]
K_{S2}	Half-saturation coefficient for substrate, heterotrophs, NO_2^-	20 $gCOD/m^3$	[b]
K_{S3}	Half-saturation coefficient for substrate, heterotrophs, NO	20 $gCOD/m^3$	[b]
K_{S4}	Half-saturation coefficient for substrate, heterotrophs, N_2O	40 $gCOD/m^3$	[b]
K_x	Half-saturation coefficient for hydrolysis	0.03 gCOD/gCOD	[a]
$\mu_{AOB,max}$	Maximum specific growth rate for AOB	0.8 d^{-1}	[a]
$\mu_{NOB,max}$	Maximum specific growth rate for NOB	1 d^{-1}	[a]
$\mu_{H,max}$	Maximum specific growth rate for heterotrophs	6 d^{-1}	[a]
Y_{AOB}	Autotrophic yield, AOB	0.21 gCOD/gN	[a]
Y_{NOB}	Autotrophic yield, NOB	0.06 gCOD/gN	[a] [b]
Y_H	Heterotrophic yield	0.666 gCOD/gN	[a]
$\theta_{\mu H}$	Temperature effect on heterotroph growth	1.072	[a]
θ_{bH}	Temperature effect on heterotroph decay	1.029	[a]
$\theta_{\mu AOB}$	Temperature effect on AOB growth	1.078	[a]
θ_{bAOB}	Temperature effect on AOB decay	1.029	[a]
$\theta_{\mu NOB}$	Temperature effect on NOB growth	1,09	[a]
θ_{bNOB}	Temperature effect on NOB decay	1.029	[a]

θ_{ka}	Temperature effect on ammonification	1.072	[a]
θ_{kH}	Temperature effect on hydrolysis	1.072	[a]
Reactor and fixed-bed properties (11)			
a_a	Media specific area	1000 m^2/m^3	[a]
ε_0	Media initial porosity	0.38	Calibrated
S	Media bed area	173 m^2	[a]
H_{media}	Media bed height	3.5 m	[a]
$H_{surverse}$	Water height above media	1.5 m	[a]
$H_{sousverse}$	Water height under media	1.6 m	[a]
D_p	Media particles mean diameter	0.004 m	[a]
icv	COD to TSS ratio in biofilm	1.5 gCOD/gTSS	[a]
k_{det}	Biofilm detachment level	1 $g/(m^2.d)$	[a]
ρ_B	Biofilm dry density	100200 g/m^3	[a]
σ_u	Max specific deposit around media	0.17	[a]
Backwash model (2)			
$k_{back,B}$	Extraction efficiency for biomass, backwash	0.01 d^{-1}	[a]
$k_{back,NB}$	Extraction efficiency for non-biomass, backwash	0.2 d^{-1}	[a]
Filtration model (5)			
β	Media packing factor	1.95	[a]
λ_0	Clean filter filtration coefficient	0.0006	[a]
x	x filter constant	1	[a]
y	y filter constant	3	[a]
z	z filter constant	0.375	[a]
Gas/liquid transfer model (17)			
A	Slope of the k_La_{O2} to U_G's correlation	28	Calibrated
B	Power constant of the k_La_{O2} to U_G's correlation	0.63	[h]
A'	Slope of the gas hold-up to U_G's correlation	0.0163	[h]
B'	Power constant of the gas hold-up to U_G's correlation	0.3503	[h]
F	Fouling factor for aeration	1	[a]
F_R	Transfer reduction in the overflow	0.032	[a]
α	Efficiency factor for aeration in wastewater	0.95	[a]
β_0	Factor for oxygen solubility	0.95	[a]
KH_{O2}	Henry's law constant for O_2 at 20°C	41.6 $gO_2/m^3/atm$	[d]
KH_{NO}	Henry's law constant for NO at 20°C	26.6 $gN/m^3/atm$	[d]
KH_{N2O}	Henry's law constant for N_2O at 20°C	700 $gN/m^3/atm$	[d]
KH_{N2}	Henry's law constant for N_2 at 20°C	16.8 $gN/m^3/atm$	[d]
ρ_O	Partial pressure of O_2	0.21 atm	Calculated
ρ_{NO}	Partial pressure of NO	0 atm	Calculated
ρ_{N2O}	Partial pressure of N_2O	3.3E-07 atm	Calculated

ρ_{N2}	Partial pressure of N_2	0.78 atm	Calculated
θ_{kLa}	Temperature effect on k_La	1.024	[h]
Biofilm model (16)			
DS_{alk}	Alkalinity diffusion coefficient	1.73E-04 m^2/d	[f]
DS_s	Soluble substrate diffusion coefficient	8.64E-05 m^2/d	[f]
DS_i	Inert diffusion coefficient	8.64E-05 m^2/d	[f]
DS_{no3}	NO_3^- diffusion coefficient	1.73E-04 m^2/d	[f]
DS_{n2}	N_2 diffusion coefficient	1.64E-04 m^2/d	[f]
DS_{nd}	Soluble nitrogen diffusion coefficient	8.64E-05 m^2/d	[f]
DS_{nh}	Ammonia diffusion coefficient	2.16E-04 m^2/d	[f]
DS_{po}	Orthophosphates diffusion coefficient	2.16E-04 m^2/d	[a]*
DS_{no2}	NO_2^- diffusion coefficient	1.81E-04 m^2/d	[a]*
DS_o	Dissolved oxygen diffusion coefficient	2.16E-04 m^2/d	[f]
DS_{nh2oh}	Hydroxylamine diffusion coefficient	1.87E-04 m^2/d	[g]
DS_{no}	NO diffusion coefficient	1.91E-04 m^2/d	[g]
DS_{n2o}	Nitrous oxide diffusion coefficient	2.22E-04 m^2/d	[g]
f_D	Diffusion reduction factor in biofilm	0.7	[a]
L_f	Liquid film thickness	100 µm	Calculated
k_{exc}	Particular matter exchange coefficient	0.00002 m/d	[a]

ANNEX 2. PARAMETER VALUES AND RANGES FOR THE SENSITIVITY ANALYSIS

Table A.6. Reference values and variation ranges of parameters used in the global sensitivity analysis. Parameters in pink are different from Table A.5 because this is their values before calibration.

Parameter	Reference value	Variation	Parameter	Reference value	Variation
Influent fractionation (7)			**Reactor and fixed-bed properties (6)**		
DCO_X/MVS	1.5 gCOD/gVSS	± 20%	a_a	1000 m^2/m^3	± 20%
MVS/MES	0.75 gVSS/gTSS		ε_0	0.356	
TKN/NH4	1.3 gN/gN		icv	1.5 gCOD/gTSS	
frssi	0.65 gCOD/gCOD		k_{det}	1 g/(m^2.d)	
frxxi	0.65 gCOD/gCOD		ρ_B	100200 g/m^3	
frbh	0.25 gCOD/gCOD		σ_u	0.17	
frxnd	0.45 gCOD/gCOD		**Backwash model (2)**		
Biokinetic model (62)			$k_{back,B}$	0.01 d^{-1}	± 20%
b_{AOB}	0.17 d^{-1}	± 20%	$k_{back,NB}$	0.2 d^{-1}	
b_{NOB}	0.17 d^{-1}		**Filtration model (4)**		
b_H	0.62 d^{-1}		λ_0	0.0006	± 20%
η_H	0.4		x	1	
η_{H1}	0.28		y	3	
η_{H2}	0.16		z	0.375	
η_{H3}	0.35		**Gas/liquid transfer model (6)**		
η_{H4}	0.35		A	28	± 50%
η_{ND}	0.1056	± 100%	B	0.63	
η_{NN}	0.07693		A’	0.0163	
η_Y	0.75	± 20%	B’	0.3503	
ixbn	0.086 gN/gCOD	± 10%	F_R	0.032	± 20%
ixun	0.06 gN/gCOD		θ_{kLa}	1.024	± 10%
ixbp	0.015 gP/gCOD		**Biofilm model (3)**		
ixup	0.015 gP/gCOD		f_D	0.7	± 20%
f_p	0.08 gN/gCOD		L_f	100 µm	± 50%
k_a	0.08 m^3/(gCOD.d)		k_{exc}	0.00002 m/d	
k_h	3 gCOD/(gCOD.d)				
$K_{H,NO3}$	0.2 gN/m^3	± 20%			
$K_{H,NO2}$	0.2 gN/m^3				
$K_{H,NO}$	0.05 gN/m^3				
$K_{H,N2O}$	0.05 gN/m^3				
$K_{HNO2,AOB}$	0.00073 gN/m^3	± 50%			
$K_{I,NO,2}$	0.5 gN/m^3				
$K_{I,NO,3}$	0.3 gN/m^3				

$K_{I,NO,4}$	0.075 gN/m^3	
$K_{I,O,AOB}$	4.5 gO_2/m^3	± 100%
K_{NH2OH}	0.0147 gN/m^3	
$K_{NH4,AOB}$	1 gN/m^3	± 50%
$K_{NO,AOB,HAO}$	0.0003 gN/m^3	± 100%
$K_{NO,AOB,NN}$	0.008 gN/m^3	
$K_{NO2,NOB}$	0.2 gN/m^3	± 50%
$K_{O,AOB,1}$	0.48 gO_2/m^3	
$K_{O,AOB,2}$	0.3 gO_2/m^3	
$K_{O,AOB,ND}$	0.019 gO_2/m^3	± 100%
$K_{O,H}$	0.1 gO_2/m^3	± 20%
$K_{I,OH,1}$	0.1 gO_2/m^3	
$K_{I,OH,2}$	0.1 gO_2/m^3	
$K_{I,OH,3}$	0.1 gO_2/m^3	
$K_{I,OH,4}$	0.1 gO_2/m^3	
$K_{O,NOB}$	0.6 gO_2/m^3	± 50%
K_{PO}	0.01 gP/m^3	± 20%
K_S	20 $gCOD/m^3$	
K_{S1}	20 $gCOD/m^3$	
K_{S2}	20 $gCOD/m^3$	
K_{S3}	20 $gCOD/m^3$	
K_{S4}	40 $gCOD/m^3$	
K_x	0.03 gCOD/gCOD	
$\mu_{AOB,max}$	0.8 d^{-1}	
$\mu_{NOB,max}$	1 d^{-1}	
$\mu_{H,max}$	6 d^{-1}	
Y_{AOB}	0.21 gCOD/gN	
Y_{NOB}	0.06 gCOD/gN	
Y_H	0.666 gCOD/gN	
$\theta_{\mu H}$	1.072	± 10%
θ_{bH}	1.029	
$\theta_{\mu AOB}$	1.078	
θ_{bAOB}	1.029	
$\theta_{\mu NOB}$	1,09	
θ_{bNOB}	1.029	
θ_{ka}	1.072	
θ_{kH}	1.072	
k_{exc}	0.00002 m/d	

ANNEX 3. ADDITIONAL EXPERIMENTS PERFORMED AT LAB-SCALE

1. RECIRCULATION TESTS

Between the colonized media sampling on Seine Centre WRRF (January 29th 2018) and the experiments presented in Chapter III, preliminary tests have been conducted. The reactor was initially operating in recirculation mode: the outlet pipe of the reactor was directly positioned in the feeding tank, which was constantly stirred (mechanic arm, low rotation rate). In a first test, the feeding tank was filled with 20 L of synthetic water at 30 mgN/L. The tap water, which composed most of the feeding solution, was drawn just before the test. The influent and gas (100% air) flow rates were respectively 0.43 and 0.42 L/min. The hydraulic retention time (HRT) was thus low: 8.9 min. NH_4^+ concentration in the feeding tank was analysed regularly (Nessler method). The evolutions of influent DO, water temperature and pH, off-gas N_2O and NH_4^+ concentration over the day are presented on Figure A.4.

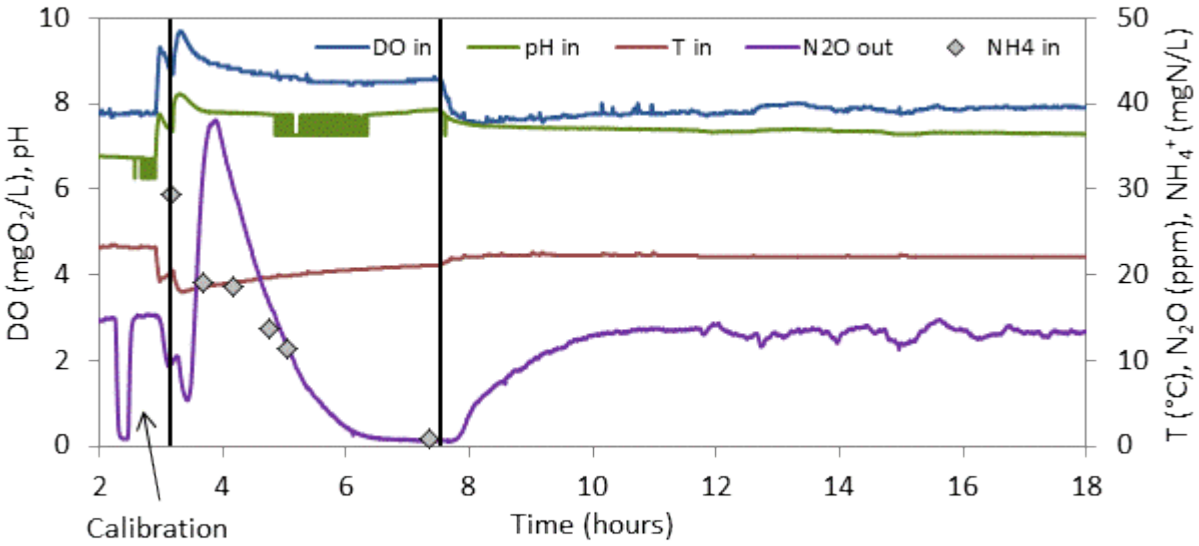

Figure A.4. Reactor monitoring during the first recirculation test.

N_2O analyser was calibrated before the experiment started. Air and liquid alimentation were launched at 2.9 and 3.2 h respectively, which explained the signal perturbations. NH_4^+ concentration in the tank decreased from 29.5 to 0.8 mgN/L in 251 minutes, which corresponded to a NH_4^+ degradation rate of 2.3 mgN/min. About 15 min after recirculation was activated, N_2O concentration increased from 5 to 38 ppm in 25 min. It was follow by a decrease to below 1 ppm in 2.5 h. At 7.5 h, liquid alimentation stopped, while aeration remained. Interestingly, the off-gas N_2O concentration increased regularly in absence of liquid alimentation, and reached a stable value of 13 – 14 ppm. In fact, before air and liquid alimentation were started, the off-gas N_2O concentration stable around 15 ppm. This test therefore indicated a possible production of N_2O by heterotrophic denitrification.

In a second test, the feeding tank was filled with 50 L of synthetic water at 20 mgN/L. This time, NO_3^- and NO_2^- concentrations in the tank were also analysed. The activation of recirculation (t = 0.5 h) was followed by a decrease of NH_4^+ concentration in the tank, with an average degradation rate of 2.0 mgN/L. Again, a spike of N_2O was rapidly observed, but at a lower maximum concentration (15 ppm, Figure A.5). Analyses revealed a gradual increase of NO_3^- concentration in the tank, from 3.5 mgN/L already present in tap water to 19 mgN/L. NO_2^- concentration at the end of the experiment was 0.21 mgN/L, which represented a small accumulation. Higher NO_2^- concentrations observed at 0.40 mgN/L where attributed to the measurement, since no pick of N_2O was associated. A small decrease of total nitrogen concentration was observed during the experiment (22.7 to 21.4 mgN/L, R^2 = 0.64), which could be attributed to a small heterotrophic activity. However, the concentration difference remained close to the measure uncertainty, which make it difficult to conclude on a possible consumption of NO_3^-/NO_2^- by heterotrophic denitrification.

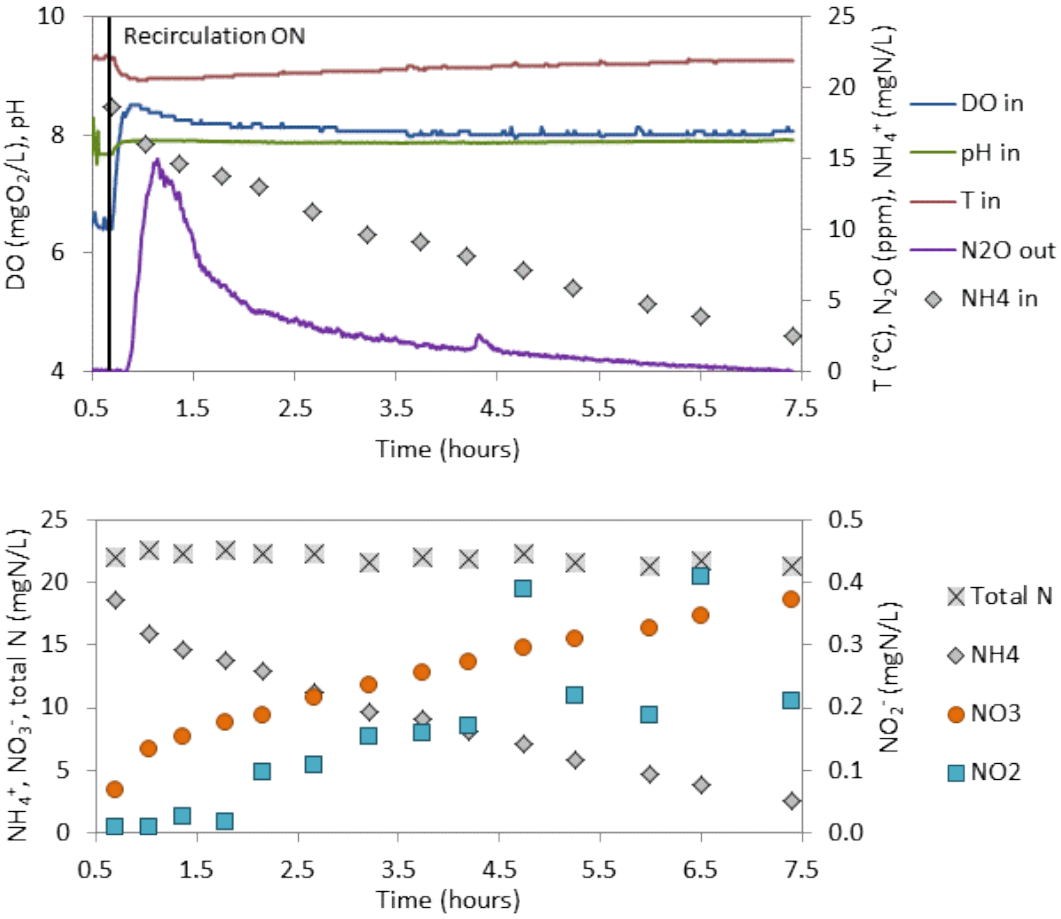

Figure A.5. Reactor and tank monitoring during the second recirculation test.

2. INVESTIGATION OF N_2O PICKS: EFFECT OF CHLORINE

In order to assess the origin of the N_2O picks observed during both recirculation tests, specific tests were conducted. This time, the reactor was alimented in continuous mode. Successive NH_4^+ loads were applied to the reactor: 6.3, 1.4, 2.1, 3.0, 3.6, 3.3 mgN/L. Except during the first level (2 to 5 h) which was done at 0.33 L/min, the influent flow rate remained at 0.07 L/min (HRT = 54 ± 1 min). The first four influent were diluted in tap water (directly drawn before the tests), while the last two were diluted in distilled water. The reactor monitoring, including off-gas N_2O concentration, is presented on Figure A.6. The difference was clear: the N_2O picks were systematic when adding tap water, while a gradual increase of N_2O concentration was observed with distilled water.

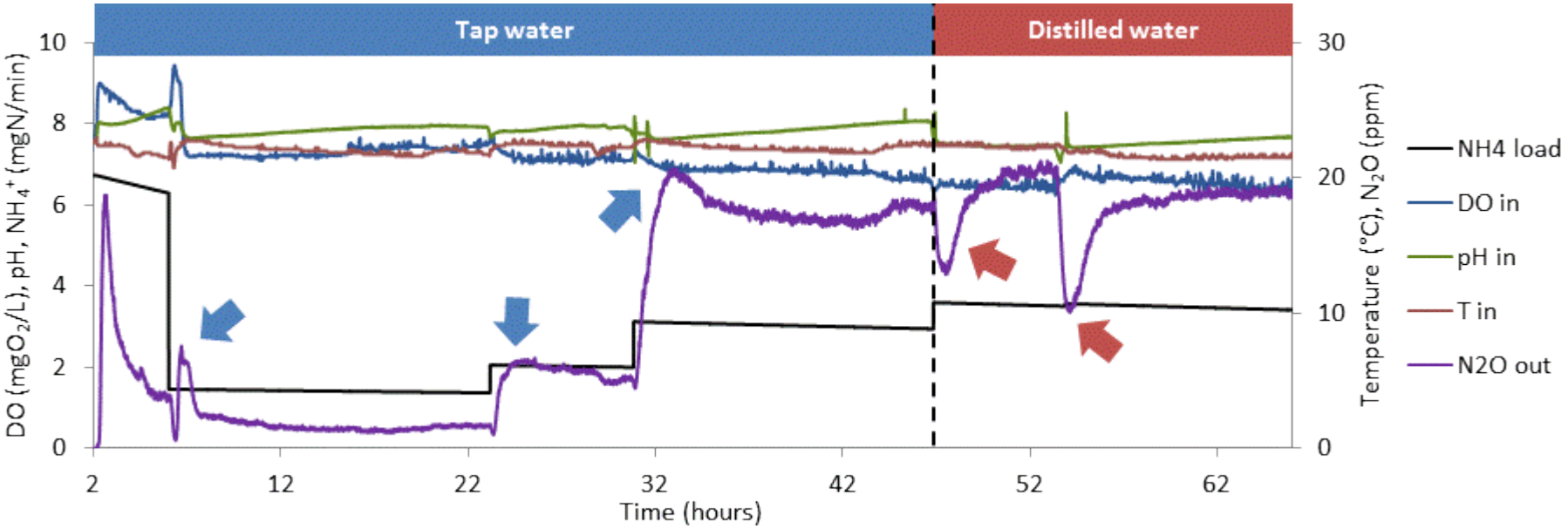

Figure A.6. Reactor monitoring during different NH4+ load tests with tap or distilled water.

After this observation, we investigated the origin this pick of N_2O. The pick observed at t = 6.6 was less pronounced than the others. In fact, all experiments were performed with 100 L of water, except this one. Only 50 L of tap water were added in the tank, which was not empty (26 L remained). This led us to the hypothesis that chlorine was activating these N_2O picks. This hypothesis was confirmed with the experiments presented in Chapter III. They were conducted with tap water left in open sky over the night preceding the experiment. In these conditions, no picks of N_2O were observed, as chlorine evaporated.

ANNEX 4. INITIAL PREDICTIONS OF THE EXTENDED BAF MODEL (#0)

Predictions of the extended BAF model #0 (biokinetics, gas stripping, diffusion parameters, initialization method) were confronted to full-scale data from the winter campaign (hourly averages, n = 338, except for nitrites). Dynamic predictions of N_2O production rates – dissolved and emitted– are presented on Figure A.7. Model predictions against experimental production rates are presented on Figure A.8.

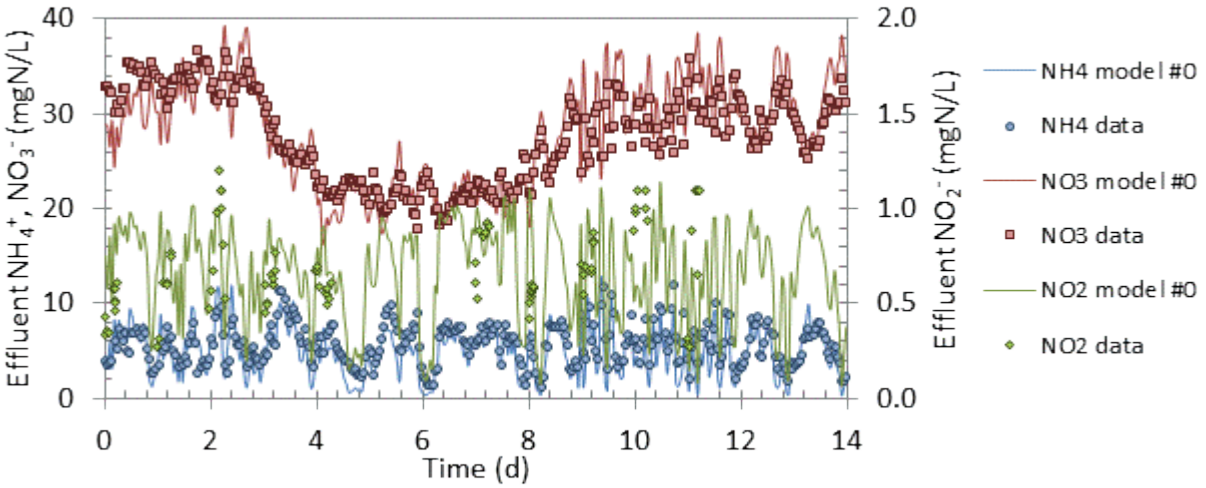

Figure A.7. Effluent NH4+, NO3- and NO2- concentrations measured and predicted with the initial extended model (#0 in Chapter IV).

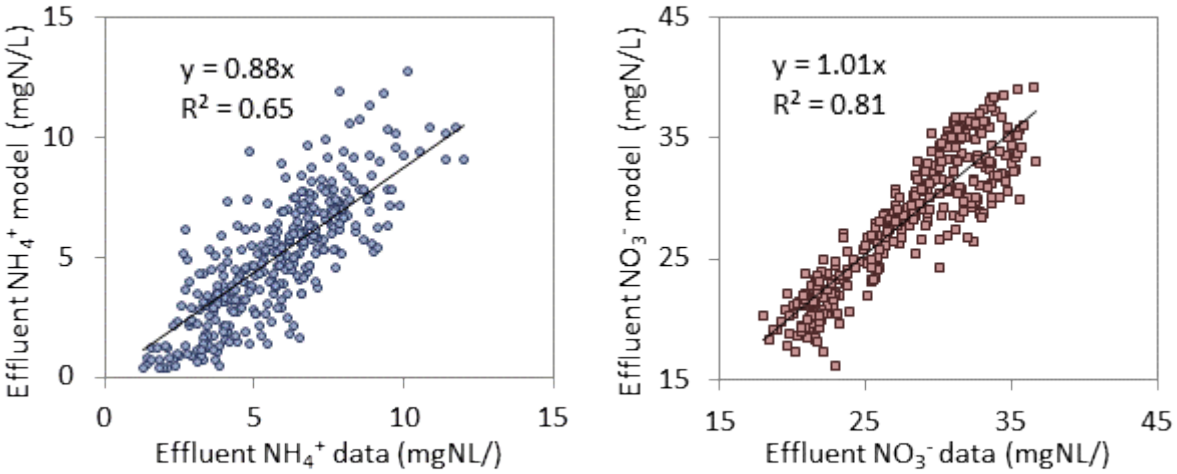

Figure A.8. Predicted versus measured effluent NH_4^+ and NO_3^- (model #0, Chapter IV).

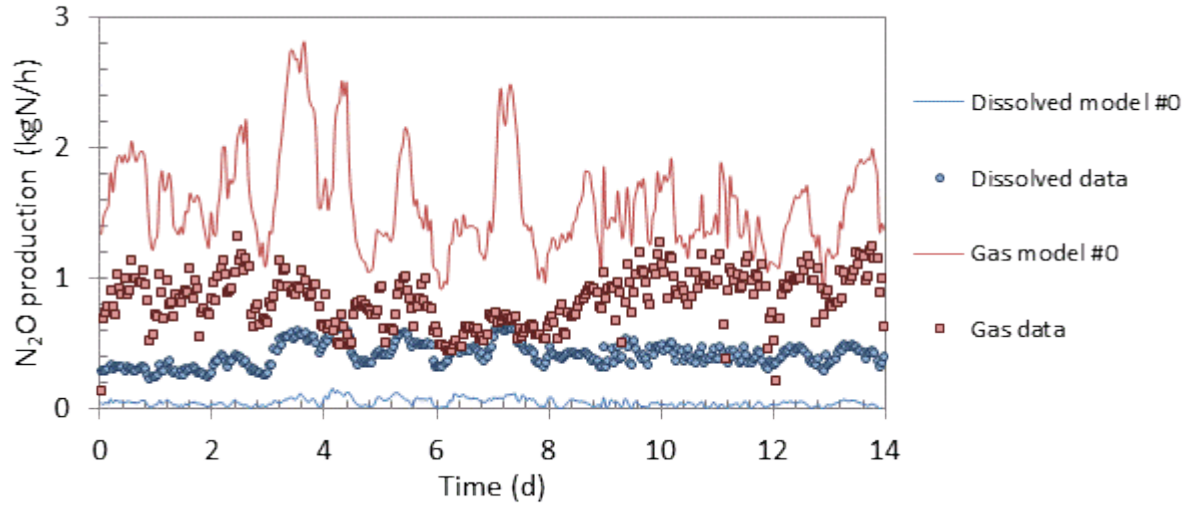

Figure A.9. Gas and dissolved N_2O production rates measured and predicted with the initial extended model (#0 in Chapter IV).

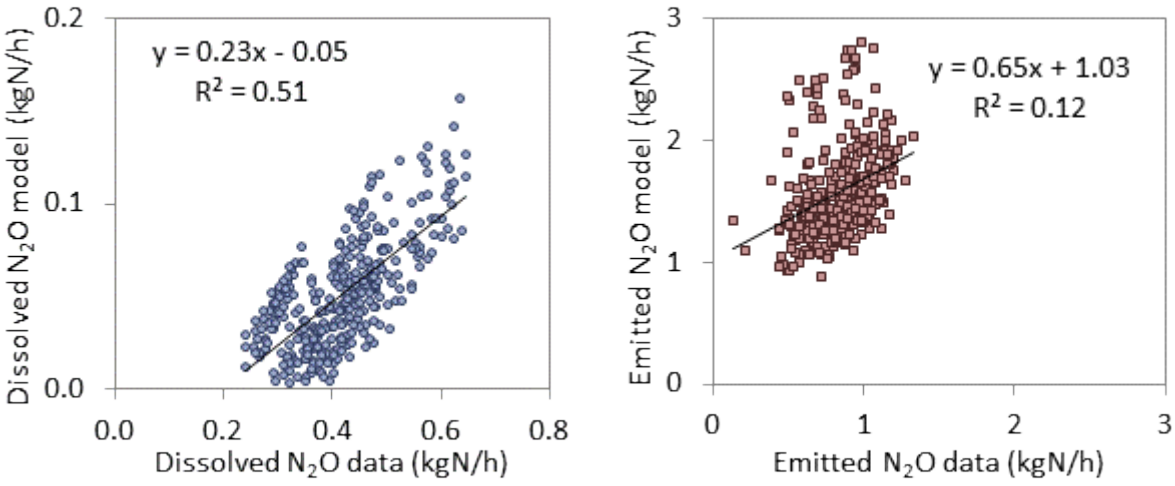

Figure A.10. Predicted versus measured emitted and dissolved N_2O (model #0, Chapter IV).

ANNEX 5. PREDICTIONS WITH INPUT DATA FROM NITRIFICATION AND FROM B2

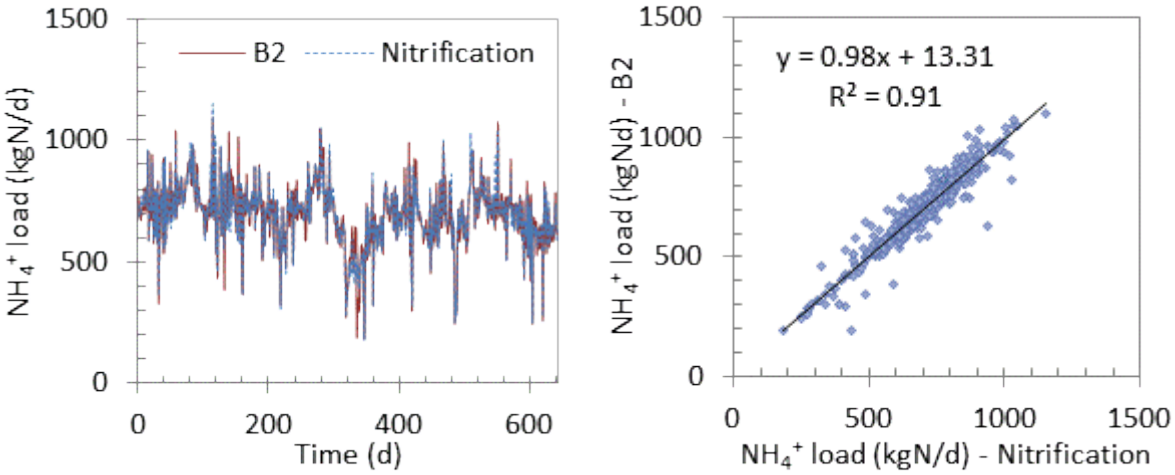

Figure A.11. Applied NH_4^+ load based on input data from nitrification and from B2 (n = 643).

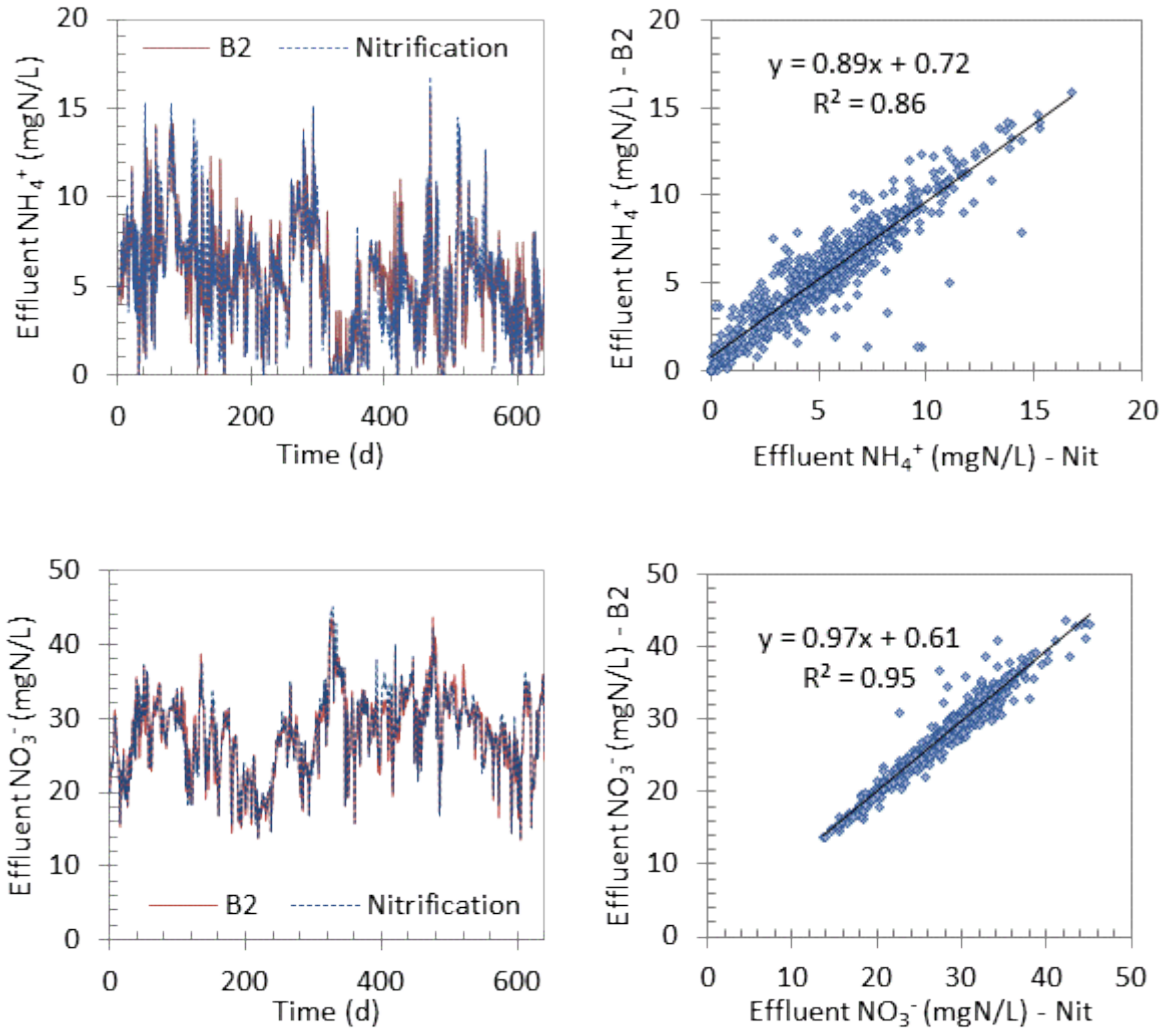

Figure A.12. Predicted effluent NH_4^+ and NO_3^- concentrations based on input data from nitrification and from B2 (n = 643).

ANNEX 6. EFFECT OF HNO_2/NO_2^- ON THE PREDICTION OF ND

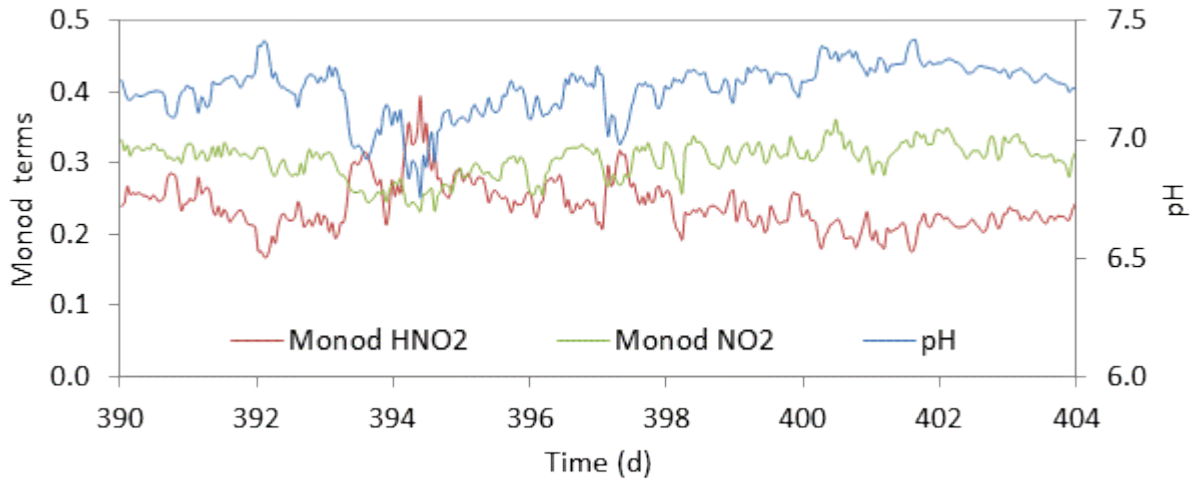

Figure A.13. Evolution of the Monod term of HNO_2 on ND and pH in winter (1 h average).

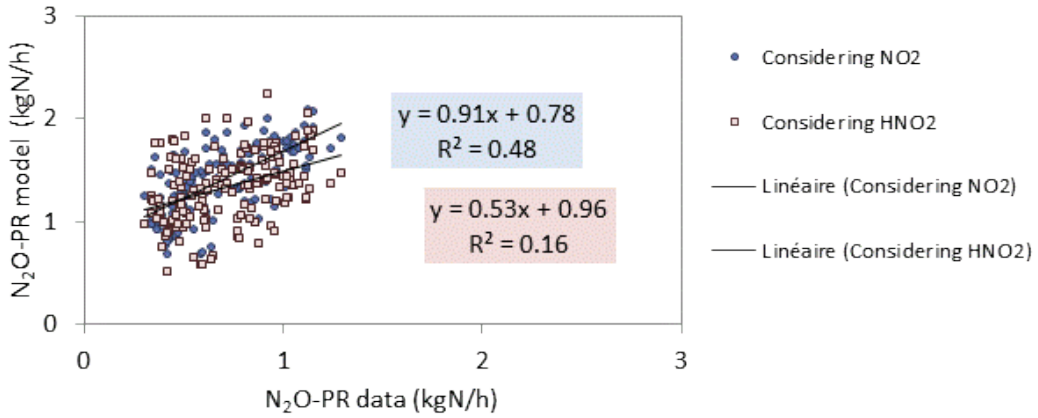

Figure A.14. Predicted against measured N_2O-PR in summer, when NO_2^- or HNO_2 are considered the rue substrates of nitrifier denitrification (n = 172).

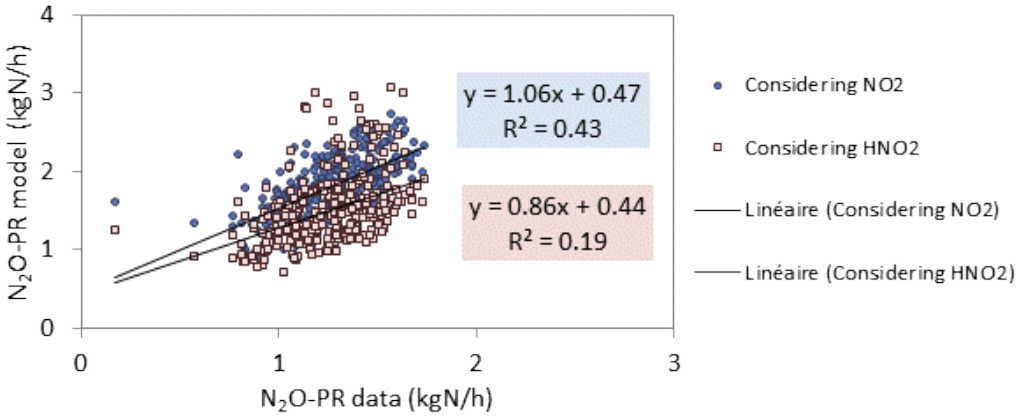

Figure A.15. Predicted against measured N_2O-PR in winter, when NO_2^- or HNO_2 are considered the rue substrates of nitrifier denitrification (n = 336).

ANNEX 7. COMPLETE RESULTS OF THE SENSITIVITY ANALYSIS

Table A.7. Summary of standardized coefficients βi. Dark orange = high negative effect (βi < -0.3); medium orange = medium negative effect (-0.3 < βi < -0.3); light orange = small negative effect (-0.2 < βi < -0.1); white = no significant effect (-0.1 < βi < 0.1); light green = small positive effect (0.1 < βi < 0.2); medium green = medium positive effect (0.2 < βi < 0.3); dark green = high positive effect (0.3 < βi).

Parameter	Effluent NH_4^+	Effluent NO_3^-	Effluent NO_2^-	Effluent DO	Effluent dissolved N_2O	Off-gas N_2O
R^2	0.91	0.86	0.56	0.92	0.70	0.69
DCOX/MVS	0.03	-0.07	0.06	-0.02	0.04	0.02
MVS/MES	-0.05	0.04	-0.04	0.00	0.04	0.06
TKN/NH4	0.24	-0.01	0.11	-0.10	0.16	0.15
frssi	-0.07	0.05	0.01	0.01	0.06	0.07
frxxi	-0.01	0.04	-0.06	-0.02	0.04	0.04
frbh	0.01	0.03	-0.03	-0.02	-0.05	-0.05
frxnd	-0.04	-0.01	0.06	-0.02	-0.01	0.00
b_{AOB}	0.07	0.09	-0.13	0.01	-0.15	-0.14
b_{NOB}	-0.08	-0.13	0.20	0.01	0.17	0.18
b_H	0.00	0.00	0.02	0.03	-0.03	-0.03
η_H	0.01	0.02	-0.02	0.00	-0.02	-0.02
η_{H1}	0.00	-0.05	0.07	0.05	0.01	0.02
η_{H2}	0.01	0.00	-0.01	0.03	0.01	0.02
η_{H3}	-0.02	0.00	0.02	-0.02	0.01	0.01
η_{H4}	-0.03	-0.03	0.09	0.01	-0.04	-0.05
η_{ND}	0.02	0.04	-0.24	0.04	0.28	0.27
η_{NN}	0.00	-0.03	-0.05	0.02	0.14	0.14
η_Y	0.00	0.03	0.01	-0.02	0.00	-0.02
ixbn	0.00	-0.01	0.03	0.02	0.00	-0.01
ixun	-0.02	0.00	0.03	-0.01	-0.01	-0.02
ixbp	-0.01	0.00	0.00	0.00	0.00	0.00
ixup	0.00	0.01	-0.05	0.02	0.04	0.05
f_p	0.02	-0.02	-0.03	-0.03	0.03	0.04
k_a	0.00	0.00	0.01	-0.01	0.01	0.00
k_h	-0.01	0.00	-0.01	0.02	0.05	0.06
K_{HNO3}	0.02	-0.01	0.00	0.00	-0.02	-0.01
K_{HNO2}	-0.01	0.00	0.04	0.02	-0.05	-0.05
K_{HNO}	0.04	-0.02	-0.02	0.03	-0.01	-0.01
K_{HN2O}	-0.03	-0.04	0.08	0.01	0.06	0.05
$K_{HNO2AOB}$	0.01	0.00	0.00	0.01	-0.03	-0.03
K_{INO2}	0.02	0.02	-0.06	0.01	0.00	0.00
K_{INO3}	0.02	0.03	-0.07	0.00	-0.01	0.01

$K_{INO,4}$	0.02	-0.02	-0.01	0.02	0.01	0.01
K_{IOAOB}	-0.01	0.01	-0.03	0.00	0.03	0.02
K_{NH2OH}	-0.01	0.00	0.03	-0.03	-0.03	-0.04
K_{NH4AOB}	0.00	0.01	0.02	-0.02	-0.04	-0.03
$K_{NOAOBHAO}$	0.01	0.00	-0.09	-0.01	0.11	0.11
$K_{NOAOBNN}$	0.02	0.06	-0.01	-0.01	-0.19	-0.18
K_{NO2NOB}	-0.01	-0.04	0.08	-0.03	0.00	0.00
K_{OAOB1}	0.16	0.24	-0.26	-0.02	-0.43	-0.40
K_{OAOB2}	-0.03	-0.01	-0.08	0.03	0.18	0.18
K_{OAOBND}	-0.02	0.01	0.03	-0.04	-0.05	-0.05
K_{OH}	0.04	0.03	-0.07	0.00	-0.05	-0.05
K_{IOH1}	-0.03	-0.02	0.06	0.00	0.05	0.05
K_{IOH2}	-0.03	0.00	0.03	-0.03	0.02	0.01
K_{IOH3}	0.00	0.02	0.00	-0.01	-0.07	-0.06
K_{IOH4}	0.02	-0.01	0.01	0.00	-0.08	-0.08
K_{ONOB}	-0.08	-0.21	0.29	0.04	0.28	0.26
K_{PO}	0.01	-0.04	0.03	-0.01	0.04	0.03
K_S	-0.04	-0.02	0.05	0.01	0.00	0.00
K_{S1}	0.01	-0.03	0.05	-0.02	-0.03	-0.03
K_{S2}	-0.02	0.02	0.00	0.00	-0.03	-0.03
K_{S3}	-0.01	0.05	-0.08	0.02	0.01	0.02
K_{S4}	0.03	0.01	-0.03	-0.01	0.02	0.01
K_x	0.00	-0.01	0.01	-0.01	0.00	0.00
$\mu_{AOB,max}$	-0.09	-0.14	0.19	-0.01	0.20	0.20
$\mu_{NOB,max}$	0.02	0.10	-0.13	0.00	-0.13	-0.11
$\mu_{H,max}$	0.03	-0.01	-0.04	-0.02	0.01	0.00
Y_{AOB}	-0.02	-0.03	0.08	-0.02	-0.03	-0.03
Y_{NOB}	0.02	-0.04	0.06	0.01	-0.02	-0.03
Y_H	0.04	0.02	-0.04	-0.01	-0.05	-0.07
a_a	-0.06	0.05	-0.01	-0.06	-0.01	-0.01
ε_0	-0.32	0.29	-0.06	0.14	-0.02	0.01
icv	-0.03	0.06	-0.08	0.03	0.05	0.05
K_{det}	-0.04	-0.02	0.10	0.01	-0.01	-0.01
ρ_{Bsec}	-0.02	0.04	-0.02	0.02	-0.05	-0.06
σ_u	0.07	-0.07	0.03	0.02	-0.02	-0.02
K_{backB}	0.00	0.00	-0.01	0.02	0.04	0.04
K_{backNB}	-0.01	0.07	-0.07	0.05	-0.06	-0.05
λ_0	0.03	-0.06	0.05	-0.01	0.02	0.02
x	-0.03	0.02	0.02	-0.01	0.01	0.00
y	0.09	-0.02	-0.07	0.02	0.01	0.01
z	-0.03	0.03	-0.01	-0.01	0.00	0.00
A	-0.38	0.32	-0.07	0.47	0.04	0.10

B	-0.61	0.59	-0.25	0.78	0.09	0.16
f_D	-0.09	0.02	0.05	-0.04	0.05	0.06
L_f	0.17	-0.17	0.05	0.13	0.00	0.00
k_{exc}	0.00	-0.04	0.04	-0.01	0.02	0.03
$\theta_{\mu H}$	-0.01	0.00	-0.01	-0.02	0.03	0.04
θ_{bH}	0.02	-0.02	0.02	0.02	-0.01	0.00
$\theta_{\mu AOB}$	0.08	0.07	-0.11	0.01	-0.15	-0.15
θ_{bAOB}	-0.07	-0.10	0.16	0.00	0.11	0.11
$\theta_{\mu NOB}$	0.00	-0.08	0.10	0.01	0.05	0.04
θ_{bNOB}	0.00	0.06	-0.06	0.00	-0.07	-0.07
θ_{ka}	-0.04	-0.02	0.03	-0.01	0.04	0.04
θ_{kh}	0.00	0.04	-0.05	-0.01	-0.01	-0.02
θ_{kLa}	0.08	-0.08	0.01	-0.10	0.06	0.04
A’	0.11	-0.10	0.00	-0.06	0.06	0.05
B’	0.07	-0.08	0.05	-0.04	-0.01	-0.01
F_R	0.00	0.00	0.02	0.09	-0.02	-0.02

ANNEX 8. DYNAMIC PREDICTIONS WITH THE REFERENCE PARAMETER SET

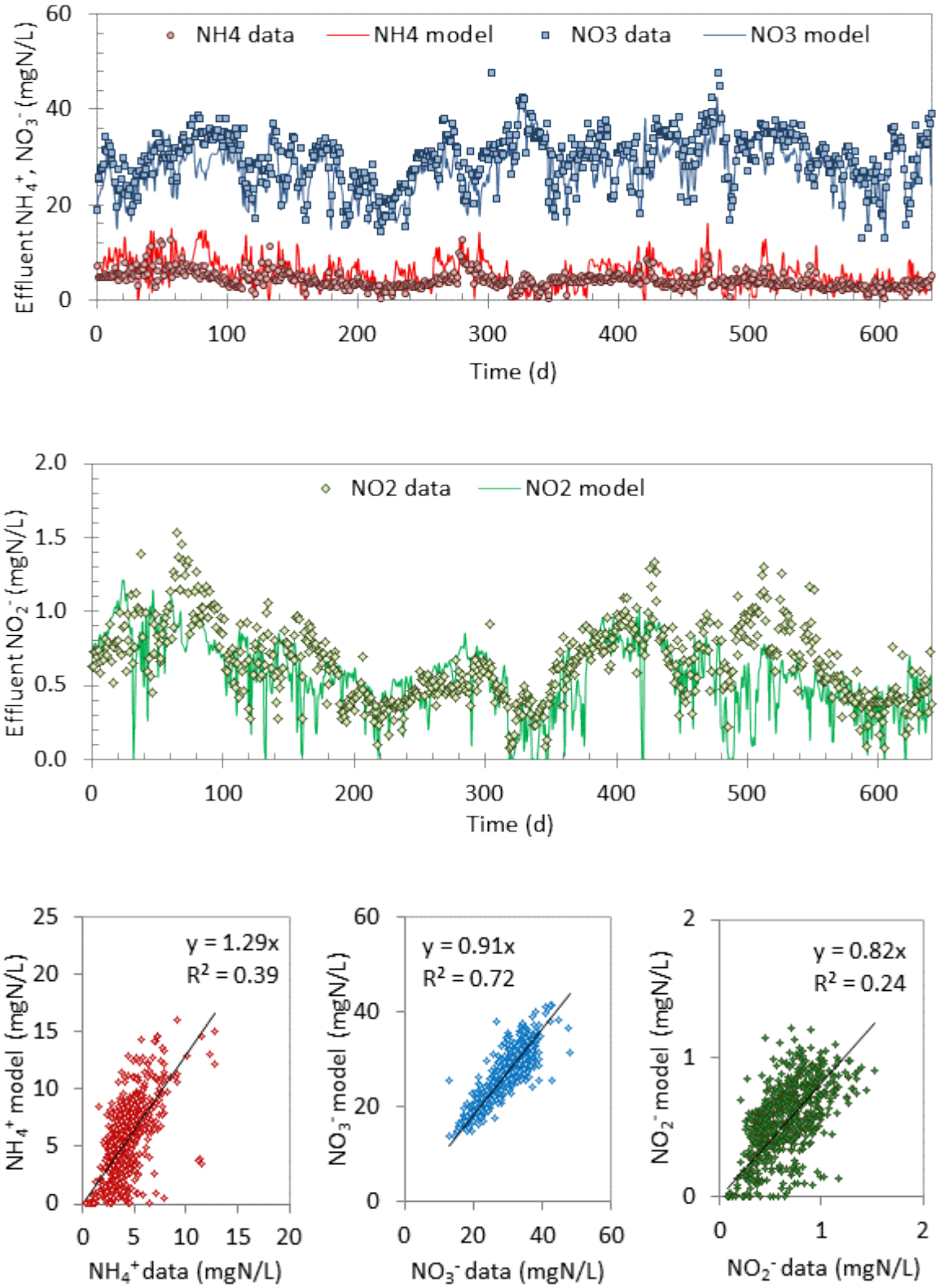

Figure A.16. Model predictions with the reference parameter set: daily effluent NH_4^+ and NO_3^- concentrations (top panel); daily effluent NO_2^- (middle panel), and daily predicted against measured effluent nitrogen concentrations (bottom panel).

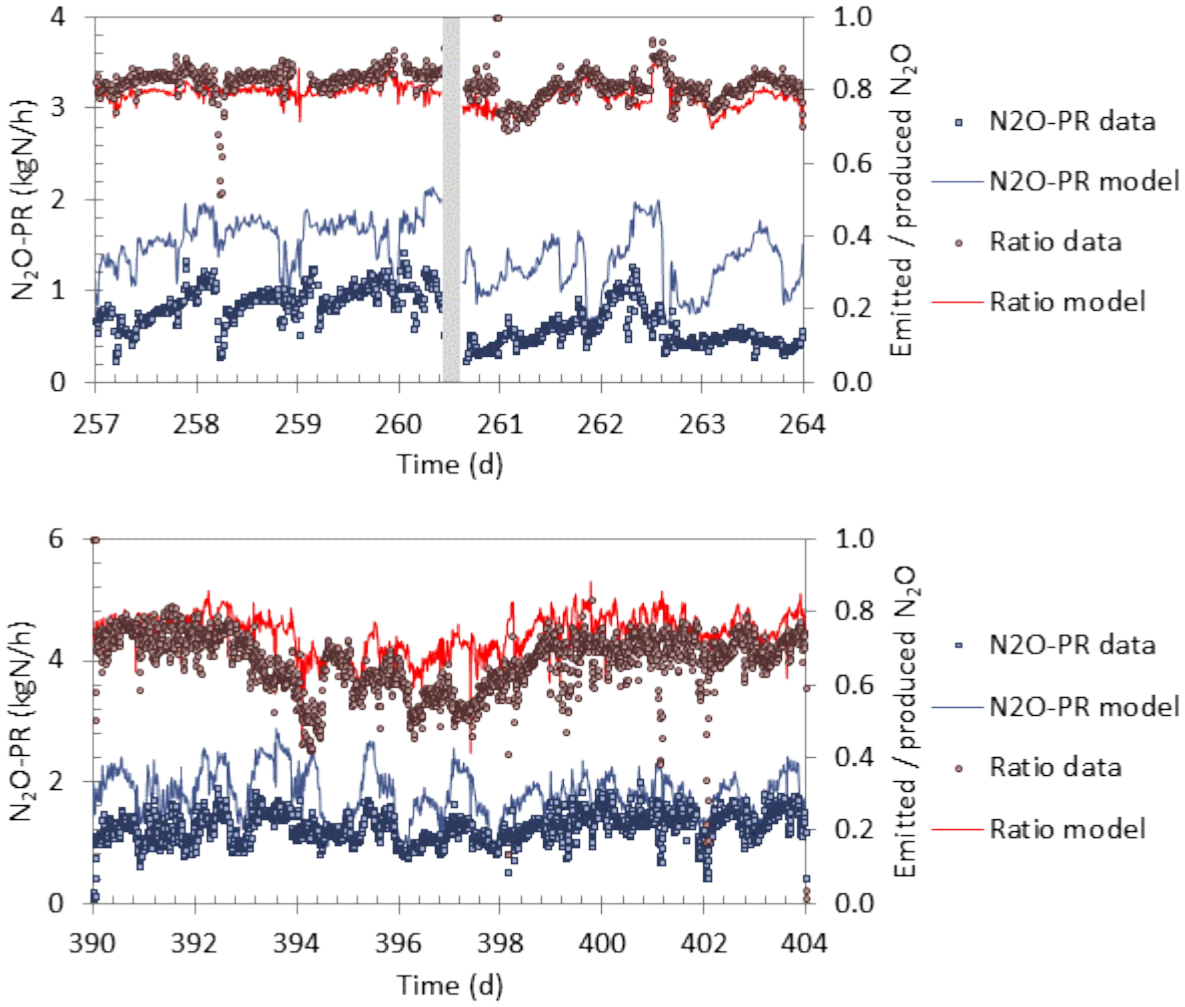

Figure A.17. Model predictions with the reference parameter set: 10 min average N_2O-PR and emitted / produced N_2O ratio in summer (top panel) and winter (bottom panel) in the studied BAF. The grey zone corresponds to a filter stop.

ANNEX 9. DYNAMIC PREDICTIONS AFTER CALIBRATION STEP 2

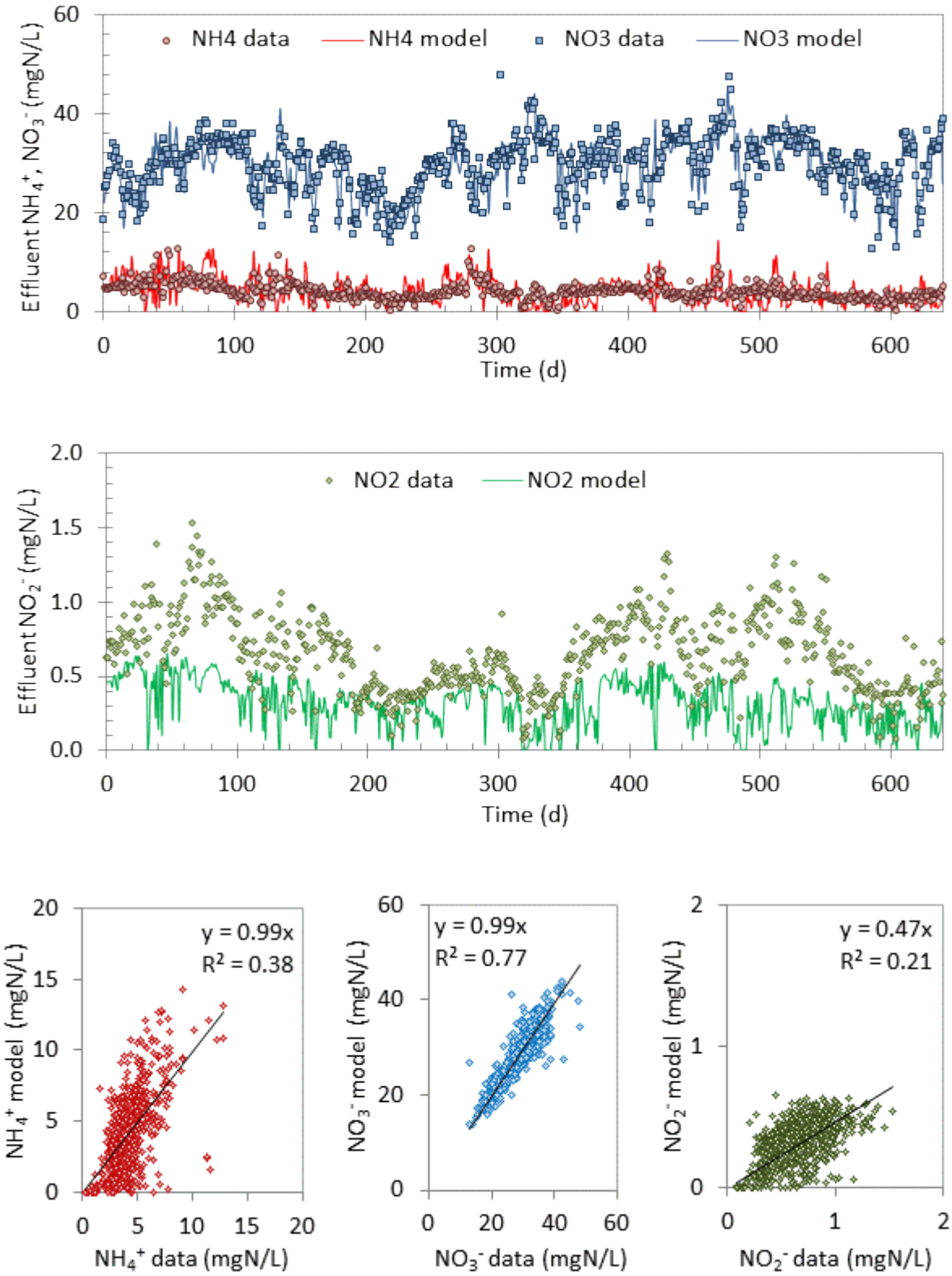

Figure A.18. Model predictions with the first-step calibrated parameter set: daily effluent NH_4^+ and NO_3^- concentrations (top panel); daily effluent NO_2^- (middle panel), and daily predicted against measured effluent nitrogen concentrations (bottom panel).

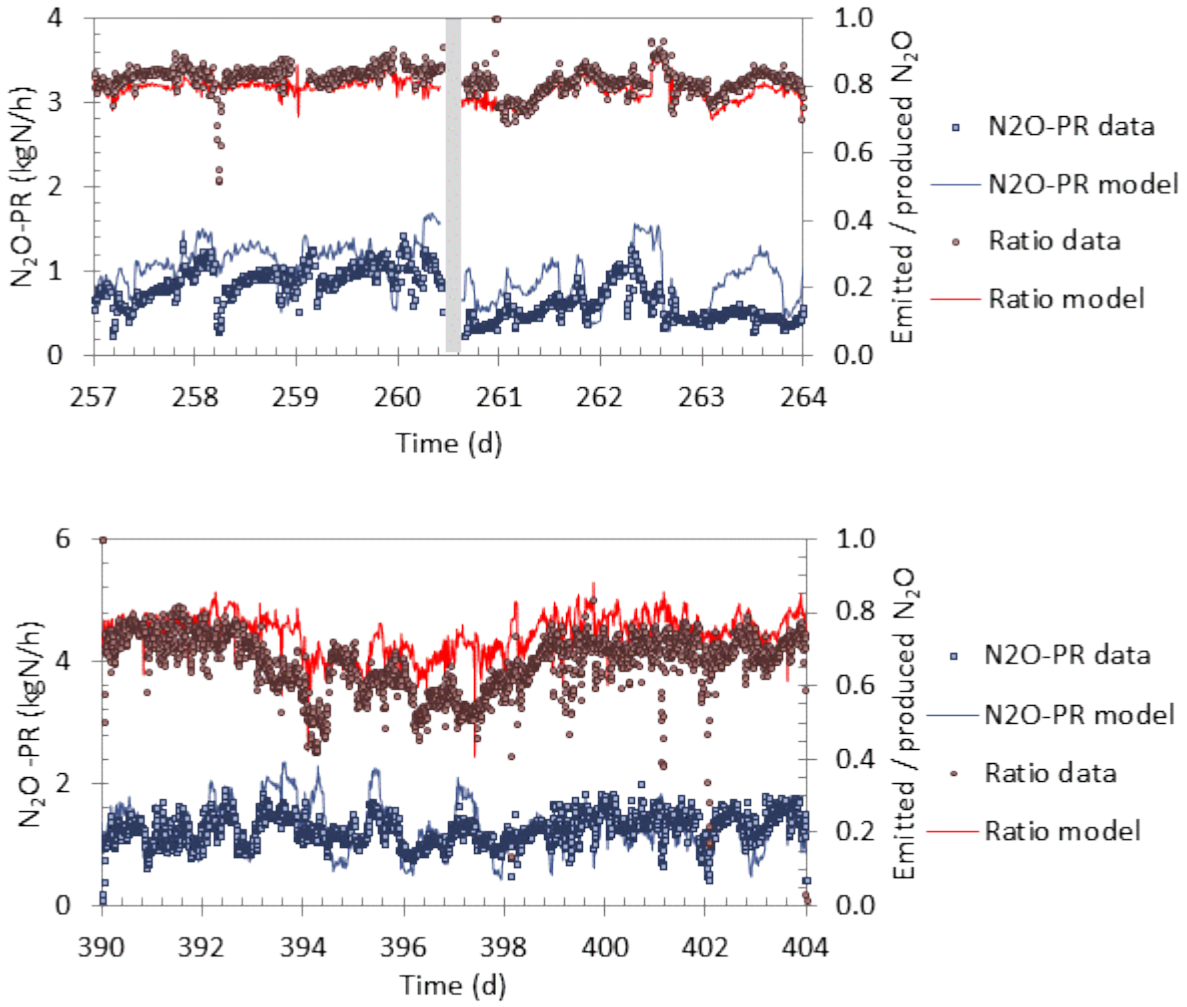

Figure A.19. Model predictions with the first-step calibrated parameter set: 10 min average N_2O-PR and emitted / produced N_2O ratio in summer (top panel) and winter (bottom panel) in the studied BAF. The grey zone corresponds to a filter stop.

ANNEX 10. MODEL INPUTS AND PREDICTIONS IN 2014-2015

1. DISTRIBUTION OF MODEL INPUTS

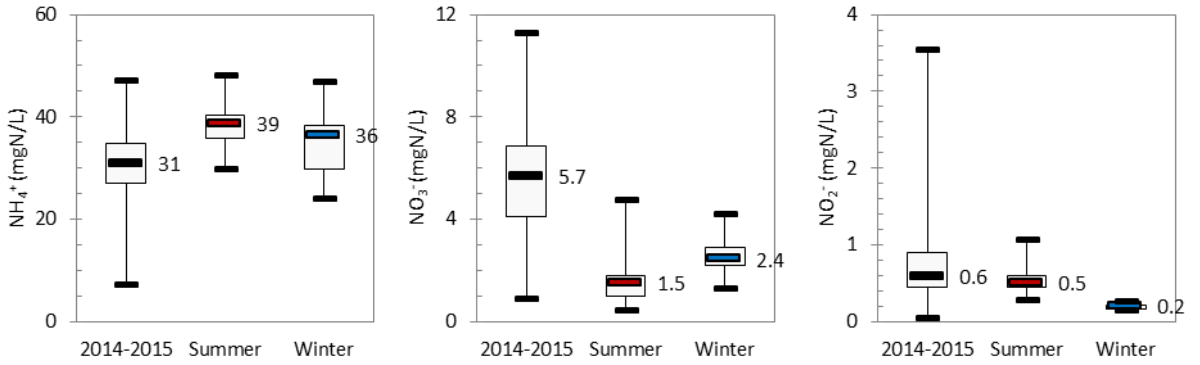

Figure A.20. Distribution of influent NH_4^+, NO_3^- and NO_2^- concentrations used to simulate the nitrifying BAFs of Seine Aval WRRF in 2014-2015 (n = 643), in summer 2014 (n = 1008) and winter 2015 (n = 2016).

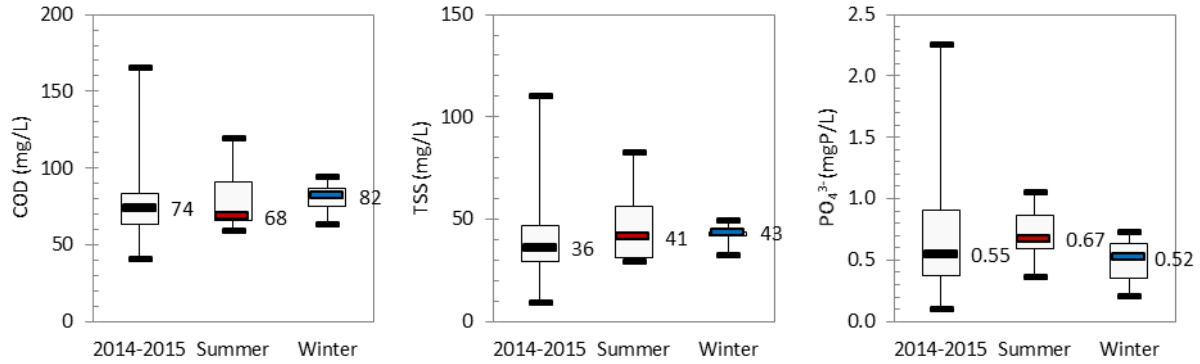

Figure A.21. Distribution of influent COD, TSS and PO_4^{3-} concentrations used to simulate the nitrifying BAFs of Seine Aval WRRF in 2014-2015 (n = 643), in summer 2014 (n = 1008) and winter 2015 (n = 2016).

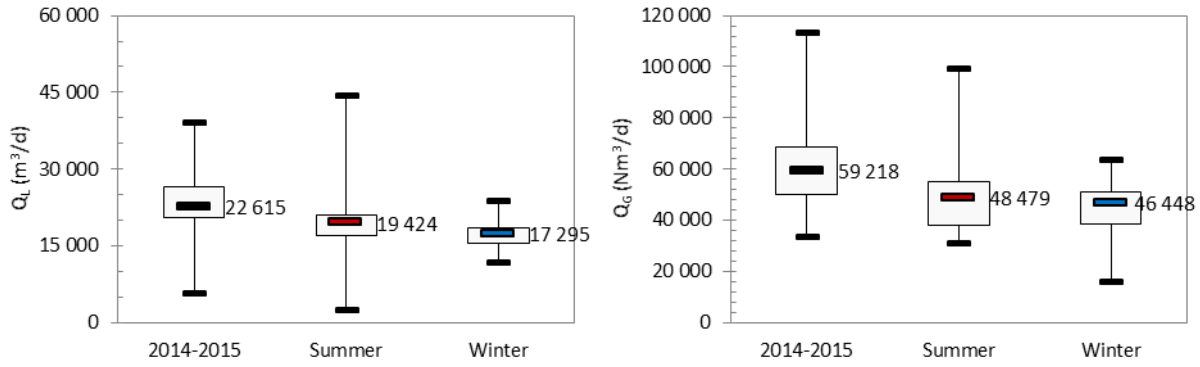

Figure A.22. Distribution of influent and air flow rates used to simulate the nitrifying BAFs of Seine Aval WRRF in 2014-2015 (n = 643), in summer 2014 (n = 1008) and winter 2015 (n = 2016).

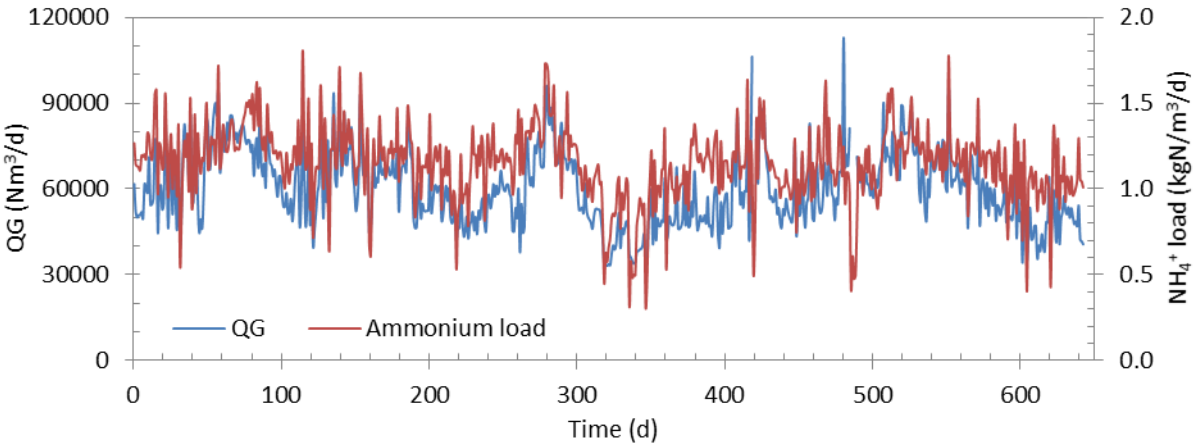

Figure A.23. Evolution of the air flow and NH_4^+ load in 2014-2015 (n = 643).

2. DISTRIBUTION OF MODEL PREDICTIONS

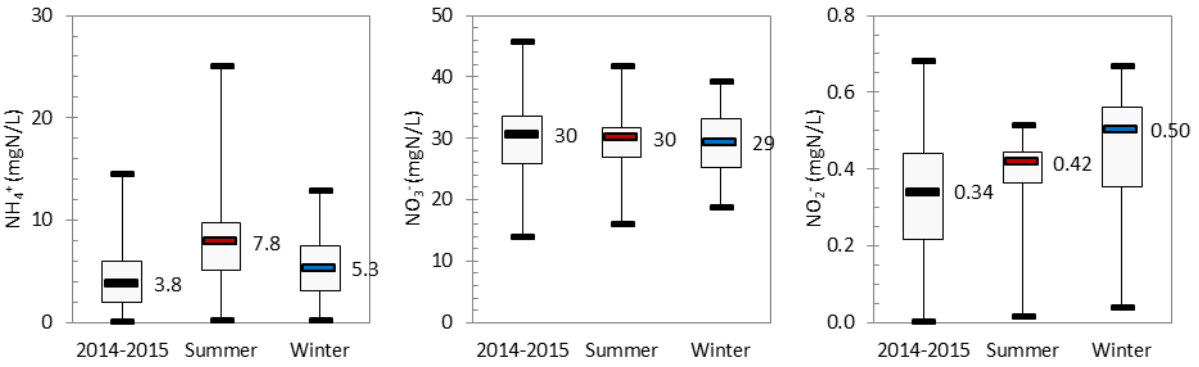

Figure A.24. Distribution of effluent NH_4^+, NO_3^- and NO_2^- concentrations predicted by the model in 2014-2015 (n = 643), in summer 2014 (n = 1008) and winter 2015 (n = 2016).

3. BALANCE ON NITRITE PRODUCTION RATE

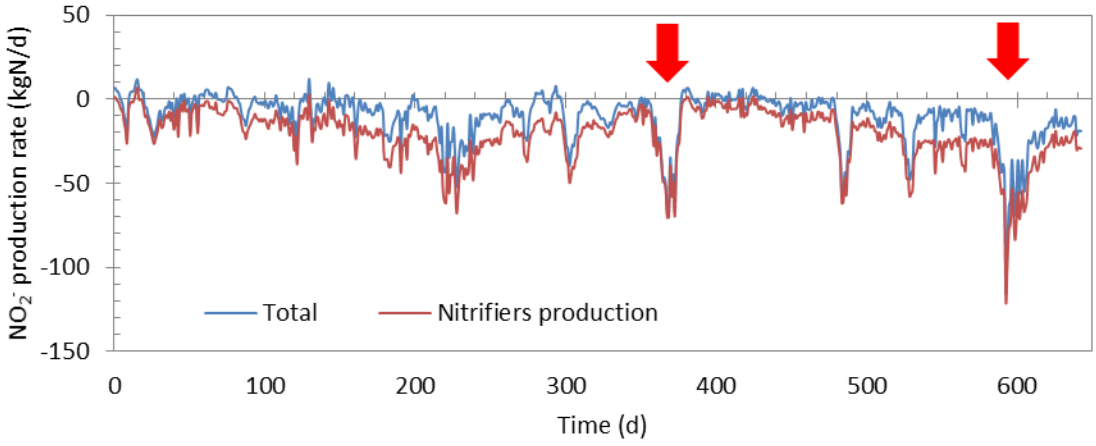

Figure A.25. Evolution of the total NO_2^- production rate, and net NO_2^- production rate by nitrifiers predicted by the model in 2014-2015 (n = 643).

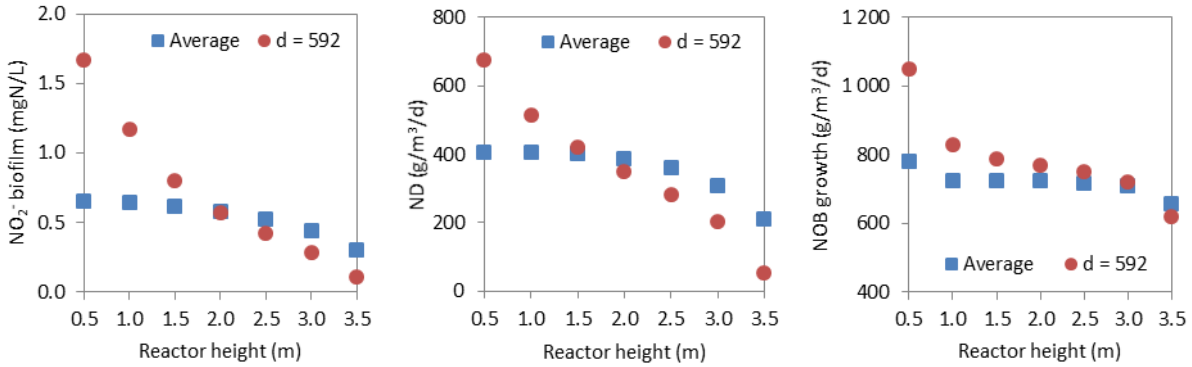

Figure A.26. Predicted evolution of the NO_2^- concentration in the biofilm, the NO_2^- reduction rate to N_2O (ND) rate and the NOB growth rate over the BAF height, averaged in 2014-2015 (n = 643) and at day 592 (corresponding to a peak of influent NO_2^-).

5. OXYGEN TRANSFERRED WITH NH_4^+ LOAD AND WATER TEMPERATURE

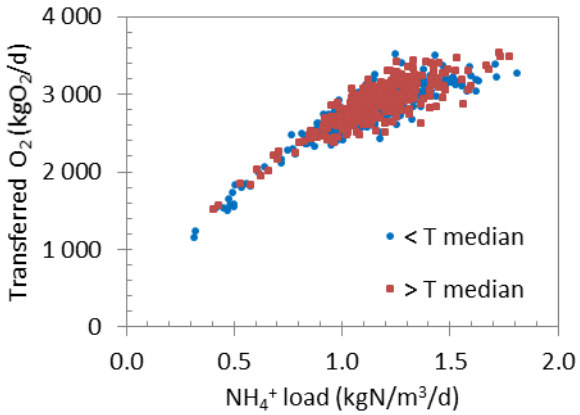

Figure A.27. Evolution of the O_2 transferred flux and its percentage consumed by biological reactions predicted by the model in 2014-2015 with the applied NH_4^+ load (n = 643).

ANNEX 11. FIRST SERIES OF NH_4^+ EXPERIMENTS

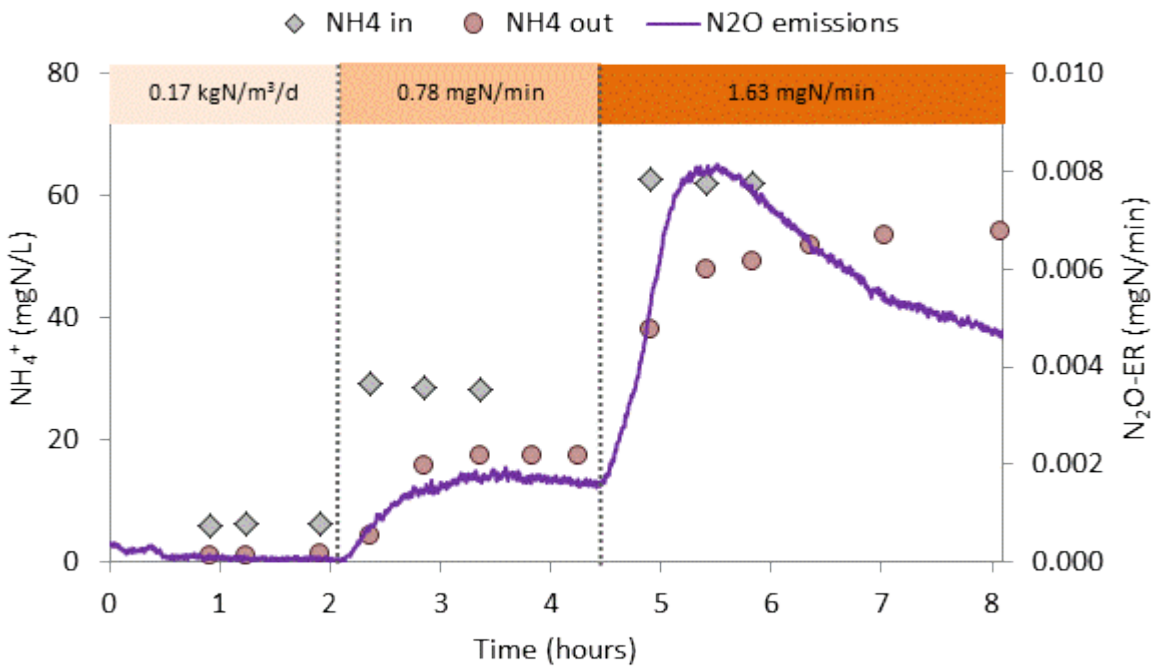

Figure A.28. Evolution of effluent NH_4^+ concentration and N_2O-ER during the first three NH_4^+ load experiments. The third corresponded to the highest load applied during the seven tests.

Résumé

Le protoxyde d'azote (N_2O) est un puissant gaz à effet de serre (GES) jouant un rôle clé dans la destruction de la couche d'ozone. Principalement d'origine naturelle, il est également émis par les procédés de traitement des eaux résiduaires lors du traitement biologique de l'azote par nitrification et dénitrification. Dû à son fort pouvoir de réchauffement global, équivalent à 300 fois celui du dioxyde de carbone, le N_2O contribue significativement au bilan carbone des stations d'épuration. Depuis une dizaine d'années, des efforts ont été consacrés à la compréhension des mécanismes de production du N_2O et à l'évaluation *in situ* de ces émissions, ce qui a conduit au développement de modèles mécanistes. Ces derniers ont, pour l'instant, principalement été appliqués aux procédés à biomasse libre et très peu aux procédés à biomasse fixée. Or, de récentes mesures réalisées sur les unités de biofiltration de la station Seine Aval (~ 5 millions d'équivalents-habitants) indiquent des taux d'émission du N_2O élevés, bien supérieurs à ceux des procédés conventionnels à boues activées. L'objectif de cette thèse était d'approfondir la compréhension des mécanismes sous-jacents aux émissions de N_2O par les unités de biofiltration en nitrification tertiaire. A cette fin, un modèle de biofiltration représentant le fonctionnement des biofiltres nitrifiants de la station de Seine Aval a été étendu pour y inclure les principales voies biologiques de production de N_2O. L'évaluation de l'influence de la représentation du transfert gaz/liquide sur les performances de traitement de l'azote et la répartition des flux de N_2O entre les phases gazeuse et liquide a montré que la prise en compte d'un bilan matière sur la phase gazeuse avait un impact relativement faible sur le transfert de matière de l'oxygène. A contrario, celle-ci s'avère indispensable à la représentation des échanges gaz/liquide du monoxyde d'azote (NO) et du N_2O. Afin d'étudier les mécanismes à l'origine de la production de N_2O, le modèle biocinétique a par ailleurs été calé sur un jeu de données comprenant deux ans de fonctionnement des biofiltres et incluant deux périodes pour lesquelles les flux de N_2O ont été mesurés expérimentalement. Une analyse de sensibilité globale a permis d'identifier l'effet dominant des paramètres affectant l'accumulation de nitrites, un précurseur de la production de N_2O, sur les concentrations de N_2O. Avec une modification de seulement 7 paramètres (sur plus de 90), le modèle s'avère capable de prédire les performances de traitement de l'azote ainsi que l'ordre de grandeur et les principales dynamiques des flux de N_2O mesurés lors de deux campagnes. Le modèle calé a par la suite été employé pour extrapoler les émissions sur l'ensemble de la période d'étude et analyser l'effet des conditions opératoires sur les mécanismes de production. Le facteur d'émission de N_2O (FE), qui correspond à la proportion d'ammonium appliquée émise en N_2O, était en moyenne de 2,2%, soit plus de 60 fois le FE usuellement employé pour l'établissement des bilans d'émission de GES des stations d'épuration. Ce facteur varie de 0,3 en 4,4%, en lien avec la charge ammoniacale appliquée, les débits d'air, et la température. Sur la base de ces résultats, des leviers de réduction des émissions ont été identifiés et un modèle statistique a été établi afin de proposer une nouvelle méthodologie de quantification des émissions.

Abstract

Nitrous oxide (N_2O) is a powerful greenhouse gas (GHG), playing a major role in the ozone layer depletion. Mainly from natural origin, it is also emitted by wastewater treatment processes, during biological nitrogen removal through nitrification and denitrification. Because of its high global warming potential, about 300 times the one of carbon dioxide, N_2O contributes significantly to the carbon footprint of wastewater resource recovery facilities (WRRF). For the last decade, considerable efforts have been made to understand the mechanisms of N_2O production and evaluate *in situ* emissions, which led to the development of mechanistic models. The latter have been mainly applied to suspended biomass systems, and rarely to fixed biomass processes. Yet, recent measurements performed on biologically active filters (BAF) of Seine Aval WRRF (~ 5 million people equivalents) indicated high N_2O emissions, much higher than those measured on conventional activated sludge systems. The objective of this PhD thesis was to increase knowledge on the comprehension of N_2O production mechanisms in tertiary nitrifying BAFs. To this end, a BAF model describing the functioning of Seine Aval tertiary nitrification units was extended to include the main biological N_2O production pathways. Studying the influence of the gas/liquid transfer representation on the prediction of nitrification performances and the gas/liquid partition of N_2O fluxes showed that considering a mass balance on the gas phase did not significantly affect oxygen transfer. In contrast, including a mass balance was found essential to represent gas/liquid exchanges of nitric oxide (NO) and N_2O. To investigate the triggers of N_2O production, the biokinetic model was calibrated on a dataset including two years of functioning of the nitrification stage and two periods during which N_2O fluxes were measured. A sensitivity analysis highlighted the major effect of parameters controlling the accumulation of nitrite, a precursor to N_2O production, on the prediction of N_2O concentrations. By modifying 7 parameters only (on over 90), the model was able to predict nitrification performances and the order of magnitude and main dynamics of N_2O fluxes measured during both measuring campaigns. The calibrated model was then used to extrapolate the predictions on the entire period of study, and analyze the effect of operating conditions on N_2O production mechanisms. The N_2O emissions factor (EF), which corresponds to the proportion of influent ammonium emitted as N_2O, was on average 2.2%, which is over 60 times the factor generally applied to estimate the GES balance of WRRFs. This factor fluctuates from 0.3 to 4.4%, mainly in correlation to the applied ammonium load, airflow rates, and temperature. Based on these results, mitigation levers were identified, and a statistical model was proposed as an alternative methodology to quantify N_2O emissions.